Durham E-Theses

The role of gamma-ray sources in relation to the observed diffuse emission and the cosmic ray origin problem

Houston, Brian P.

THE ROLE OF GAMMA-RAY SOURCES IN RELATION

TO THE OBSERVED DIFFUSE EMISSION AND

THE COSMIC RAY ORIGIN PROBLEM

by

Brian P. Houston, B.Sc.

A Thesis submitted to the University of Durham

for the

Degree of Doctor of Philosophy

February, 1985.

Galilei :   Und was wir heute finden, werden wir morgen

von der Tafel streichen und erst wieder

anschreiben, wenn wir es noch einmal gefunden

haben.

Leben des Galilei, Bertolt Brecht (1955).

Hamm :   J'aime les vieilles questions. (Avec élan).

Ah les vieilles questions, les vieilles

réponses, il n'y a que ca!

Fin de Partie, Samuel Beckett (1957)

Galileo :   *And what we find today, we will strike*

from the blackboard tomorrow and write

down once more, when we have found it

yet again.

Hamm :   *I love the old questions. (With fervour).*

Ah the old questions, the old answers,

there's nothing like them!

ABSTRACT

Interpretation of the present gamma-ray data above 100 MeV is discussed in relation to cosmic ray interactions with the atomic and molecular hydrogen in the Galactic plane.

The SAS II gamma-ray data are analysed for supportive evidence on the 2CG candidate sources identified from the COS B observations. The strongest sources are confirmed. There is good evidence to suggest that many of the weaker sources are not truly discrete.

A Monte-Carlo analysis of the discrete source detection efficiencies suggests that many 2CG sources are unresolved giant molecular clouds, irradiated by the ambient cosmic ray flux. An attempt is made to define a genuine source catalogue. Taking account of the detection efficiencies the net source flux (from both resolved and unresolved sources) is estimated to be 11-23% of the Galactic plane emission.

Cosmic ray interactions with the Orion molecular cloud complex are investigated through an analysis of the gamma-ray emission above 100 MeV. There is no evidence for cosmic ray exclusion from the clouds. A new derivation of the CO/H_2 ratio is obtained.

$$N_{H_2} / \int T(^{12}CO)dv = (3.7 \pm 0.6) \times 10^{20} \text{ at } cm^{-2}(K \text{ } kms^{-1})^{-1}.$$

Contributions to the extragalactic gamma-ray flux from radio galaxies and rich clusters are estimated.

The flux may be dominated by emission from these objects.

With the estimate of the discrete Galactic source flux and the $CO \rightarrow H_2$ ratio, the radial gamma-ray emissivity is compared to the HI, inferred H_2 and possible cosmic ray radial densities in the inner Galaxy. It is shown that a moderate cosmic ray gradient overestimates the gamma-ray flux, unless the metal abundance gradient reduces the inferred H_2 mass.

PREFACE

The work presented in this thesis was carried out between 1981 and 1984 while the author was a research student under the supervision of Professor A.W. Wolfendale, F.R.S., in the Physics Department of the University of Durham.

Part of the work was carried out in collaboration with Professor A.W. Wolfendale and Dr. E.C.M. Young, but the calculations reported represent the work of the author.

Some of the results in this thesis have been published, as follows:

Houston, B.P., and Wolfendale, A.W., 1982, Irish Astron. J., 15, 181.

Houston, B.P., and Wolfendale, A.W., 1983, Astron. Astrophys., 126, 22.

Houston, B.P., Wolfendale, A.W., and Young, E.C.M., 1984, J. Phys. G., 10, L147.

Houston, B.P., and Wolfendale, A.W., 1984, J. Phys. G., 10, 1587.

Bhat, C.L., Issa, M.R., Houston, B.P., Mayer, C.J., and Wolfendale, A.W., 1984, Nature (submitted).

Houston, B.P., and Wolfendale, A.W., 1984, J. Phys. G. (in the press).

CONTENTS

°

CHAPTER ONE

INTRODUCTION

1.1 Historical development

Since their discovery by Hess (1912), cosmic rays have

continued to stimulate the interests of both experimental

and theoretical physicists. There has been substantial

progress in measuring cosmic ray energy spectra and important

advances have been made in the field of elementary particle

physics. Particle accelerators have now superceded cosmic

ray studies as the primary source of data on high energy

particle interactions. However, analyses of the highest

energy cosmic ray initiated air showers are still the

only means of constraining phenomenological theories above

about 10^{14}eV. The low energy cosmic rays ($\lesssim$ 10 MeV)

produced by the Sun do not concern us in this work. Answers

to the fundamental questions concerning the origin and

acceleration of the extra-solar cosmic rays still elude

us. It is the purpose of this thesis to assess the relevance

and limitations of current gamma-ray astronomical data

to the cosmic ray origin problem.

Hess' experiments and those of subsequent workers

demonstrated conclusively the existence of increasing

residual ionization with height above the Earth's surface,

thus excluding natural radioactive elements as the source.

Millikan and Cameron (1926) concluded that the ionizing radiation must

originate outside the Earth and he speculated on the

existence of a universal flux of ultra-energetic gamma-

rays. Bothe and Kolhorster (1929) demonstrated this to be false with the conclusive evidence that the cosmic rays are charged particles.

Even at the highest energies we are unable at sea-level to detect the primary component of the cosmic ray flux. We must either place the detectors above the atmosphere or measure the secondary products of the electromagnetic cascade initiated by cosmic rays incident on the top of the atmosphere. High energy photons constitute one of the important products of these air showers.

The development of gamma-ray astronomy and its relationship to cosmic ray astrophysics is comparatively recent. Hayakawa (1952) and Hutchinson (1952) considered gamma-ray production by cosmic rays in the wider context of the interstellar medium. Their work stimulated further developments on the gamma-ray fluxes to be expected from cosmic ray interactions in the Galaxy; notably Morrison (1958), Felten and Morrison (1963). Gamma-ray astronomy was perceived as a means of shedding fresh light on the unresolved questions pertaining to cosmic rays.

Gamma-ray astronomy, still in its infancy, has so far been an inconclusive arbitrator. The poor quality of present gamma-ray data is an important factor in this respect. However, it is also important to recognise the constraints arising from the interrelation of cosmic ray and gamma-ray astrophysics with many other areas of astrophysical research.

1.2 Gamma-ray astronomy and the origin of cosmic rays

Before we consider gamma-ray astronomy as a probe
of the cosmic ray origin question, it is useful to briefly
outline the latter. The primary cosmic radiation has
two distinct components, the nucleonic (protons, antiprotons
and heavier nucleii) and the electronic (electrons and
positrons). Measurements of the cosmic ray energy spectra
show that protons constitute about 92% of the nucleonic
flux above 1GeV/nucleon. In collisions with nucleons
in the interstellar medium they produce π°'s which
decay into gamma-ray photons. At the same energy the
electron flux is a few percent of the nucleonic component.
The electrons produce gamma-rays by bremsstrahlung, inverse
Compton scattering off low energy starlight and microwave
background photon fields and synchrotron radiation. Gamma-
ray absorption in the interstellar medium is essentially
negligible in the MeV to GeV energy range. However, pair
production processes ($\gamma + \gamma \rightarrow e^{+} + e^{-}$) become more important
at higher energies. This mechanism must be considered
whenever high energy gamma-rays traverse low energy photon
fields. We do not consider here the mathematical formulation
of gamma-ray production and propagation in an astrophysical
context. This is treated extensively by many workers
(e.g. Ginzburg and Syrovatsky, 1964; Stecker, 1975; Longair,
1981; and references therein).

There are in essence two views on the origin of the
cosmic ray flux. The first contends that it is universal
in origin, that is the cosmic rays pervade the entire

Universe with a uniform energy density. Cosmological
processes must then be invoked to explain the production
of the particles at a much earlier epoch. There are variants
on this theme in which the cosmic rays are confined to
lesser volumes; superclusters or perhaps clusters. These
refinements have been postulated in the light of the
enormous energy requirements for a truly universal origin
($\sim 4 \times 10^{73}$ erg, corresponding to a few percent of the
observed baryonic rest mass energy within one Hubble radius)
However, energy requirements alone cannot rule out the
possibility of a meta-Galactic origin for the particles.

The alternative explanation favours a Galactic origin
for the particles, up to about 10^{18} eV above which origin
in the local Virgo cluster seems likely. This model can
be viewed as a further reduction in scale from the meta-
Galactic theories. Its most important features are the
relatively low energy requirements ($\sim 5 \times 10^{54}$ erg for
our Galaxy) and the prediction of a cosmic ray gradient
within the Galaxy.

The inverse Compton reactions on the universal micro-
wave background radiation effectively screen the Galaxy
from electrons which diffuse out from other Galaxies.
In this respect the observed cosmic ray electrons must
be localized to our own Galaxy, that is they are Galactic
in origin.

Gamma-ray astronomy holds out the best opportunity
to investigate the large scale distribution of cosmic

rays within our own Galaxy and thereby discriminate between the Galactic and meta-Galactic origin theories. In Chapter 2 we review the gamma-ray spectrum from about 1 MeV to 10^{15}eV, excluding the medium energy range covering 50 - 1000 MeV. The latter is reviewed in Chapter 3 with the emphasis on previous analyses and their limitations. Two major areas of uncertainty are identified, the discrete gamma-ray source contribution and the mass of gas; particularly in the inner Galaxy. In Chapter 4 we re-analyse the SAS II data-base searching specifically for confirmation of the discrete sources claimed by COS B. A Monte-Carlo analysis is developed in Chapter 5 which allows us to place limits on the unresolved source flux from the Galactic plane. The important question of cosmic ray interactions with giant molecular clouds is addressed in Chapter 6 through an analysis of the gamma-ray flux from the Orion complex. In addition we derive a new calibration of the CO/H_2 ratio appropriate for typical molecular clouds. In Chapter 7 we briefly consider the extragalactic gamma-ray flux and the possible contributions from radio galaxies and rich clusters. Finally in Chapter 8 we re-analyse the large scale Galactic gamma-ray emissivity, taking account of the expected discrete source contribution and the new estimates of the molecular hydrogen distribution. Conclusions are drawn on the origin of the cosmic ray flux at these energies and an outline is given for future developments.

CHAPTER TWO

THE GAMMA-RAY SPECTRUM

2.1 Introduction

Gamma-ray emission has been detected from a variety

of sources and regions primarily in our Galaxy, in the

energy range 10^5 - 10^{16}eV. This is a wide energy range

and it is not surprising that there is much diversity

in the nature of the emission. Whereas the work described

in this thesis is primarily concerned with gamma-rays

in the medium energy ($E_\gamma \sim$ MeV to GeV), it is worthwhile

to start with a summary of the gamma-ray emission at

other energies.

It is evident that in the broad area of gamma-ray

astronomy we are always observing the results of high

energy processes, either diffuse (in the interstellar

medium) or discrete in origin. These processes must

involve high energy cosmic rays (as discussed in Chapter

1) and as such through gamma-ray astronomy we are obtaining

information relevant to the origin and propagation of

cosmic rays. Aside from the energy band often described

as 'medium energy gamma-ray astronomy' (which will be

reviewed in detail in the following chapter), there

are three distinct phenomena, or areas of study: gamma-

ray line astronomy, gamma-ray bursts and ultra high

energy gamma-ray sources. Each branch is characterised

by its own observational techniques and limitations.

While it is beyond the scope of the present work to

discuss the details of the detection systems employed

for gamma-ray astronomy we wish to consider briefly

the present observational status of each of these branches,

indicating the great potential each holds for unravelling

some of the problems associated with the origin of cosmic

rays.

2.2 Gamma-ray line astronomy

Gamma-ray line emission is expected when nuclei

are excited above the ground state, for example, as a

result of nuclear collisions. Emission also occurs

during the radio-active decay of certain species. Cyclotron

lines (both emission and absorption) are generated from

electron transitions between Landau levels of atoms

in strong magnetic fields. For magnetic field strengths

believed typical for neutron stars ($\sim 10^{12}$G), the chara-

cteristic cyclotron transition energy is $\sim$ 50 keV.

Also of considerable importance is the positron annihilation

line at 511 keV, the positrons coming from nuclear inter-

actions , or the β-decay of nucleosynthesis products.

Collisions between cosmic rays and the gas in the

interstellar medium are also expected to generate a

series of gamma-ray lines. Most of the lines are expected

to arise from cosmic ray nucleons with energies in the

range $\sim$ 1 - 100 MeV, which is a region where the energy

spectrum of cosmic rays in interstellar space is not

well defined, being subject to strong solar modulation

effects. However, useful predictions have been made

from models based on an extrapolation of the nucleon
spectrum from measurements above the modulation cut-
off, and the likely density increase of both low energy
cosmic rays and heavy elements towards the inner Galaxy.
Ramaty and Lingenfelter (1981) consider the most important
lines to be: 0.847 MeV (^{56}Fe), 4.438 MeV (^{12}C) and
6.129 MeV (^{16}O), none of which have been detected to
date. This is a field where future improved observations
will help constrain the MeV region of the cosmic ray
spectrum, allow for a better understanding of the effects
of solar modulation and enable the distribution of the
low energy cosmic ray flux with position in the Galaxy
to be studied.

The hot big bang model of the universe is generally
accepted as a sufficient framework for the primordial
synthesis of all the elements up to helium. The absence
of zero metal stars in our Galaxy and the overall scarcity
of low metal abundance stars is attributed to further
element synthesis in pregalactic or supermassive stars.
Additional element formation (especially Lithium, Beryllium
and Boron) results from cosmic ray spallation of Carbon,
Nitrogen and Oxygen in the interstellar medium. However,
explosive nucleosynthesis, both in the late stages of
massive star evolution and in supernovae, is essential
for the production of all the heavy elements above carbon.
It will be seen later (Section 5.4) that the continued
recycling and enrichment of the interstellar medium

with heavy elements may have important consequences
for the interpretation of medium energy gamma-ray emission
from the inner Galaxy, through the effects of heavy
elements on estimates of the mass of gas (primarily
H_2). It is believed that many gamma-ray lines should
be detectable as a consequence of the nucleosynthesis
process, thereby providing firm evidence for the continuing
evolution of the elemental composition of the Galaxy.
The strongest lines are expected to be: 1.809 MeV
($^{26}Al \rightarrow {}^{26}Mg$), 1.332, 1.173, 0.059 MeV ($^{56}Fe \rightarrow {}^{60}Co \rightarrow$
^{60}Ni) and 1.156, 0.078, 0.068 MeV ($^{44}Ti \rightarrow {}^{44}Sc \rightarrow {}^{44}Ca$).
Additionally, the positron annihilation line (511 keV)
should accompany these decays both in supernovae explosions
and, later on, in the surrounding supernova remnants
due to the diffusive escape of e^+.

Recently Matteson (1982) has claimed a detection
of the 1.809 MeV $^{26}Al \rightarrow {}^{26}Mg$ line from the direction
of the Galactic centre. If confirmed, this would be
the first detection of a gamma-ray line from a product
of explosive nucleosynthesis. Several workers have
detected lines from the Crab nebula including one at
around 400 - 410 keV (Leventhal et al., 1977; Yoshimori
et al., 1979, Ayre et al., 1981) which could be inter-
preted as the 511 keV positron annihilation line redshifted
in the strong gravitational field expected near the
surface of a neutron star. Another line at about 73 keV
has been detected from this object (Ling et al., 1979;

Ayre et al., 1981) with possible evidence for both time variability and pulsation (Strickman et al., 1982); and has been interpreted as due to cyclotron emission near the polar cap of the neutron star.

The positron annihilation line has definitely been detected from the direction of the Galactic centre (Leventhal et al., 1978, Riegler et al., 1981. The first detection was probably by Johnson and Haymes 1973). Taken together, the data imply significant time variability in the line flux and a positron annihilation rate $\sim$ 10^{43} s^{-1} for a typical average flux of 2 x 10^{-3} ph $cm^{-2}s^{-1}$. Several mechanisms have been suggested as plausible explanations of this line emission. Cosmic ray interactions in the interstellar medium at the Galactic Centre region could give rise to e^+e^- annihilation radiation. However, the observed flux would require a large enhancement in the cosmic ray density in that region which would conflict with the gamma-ray flux levels for $E_\gamma \geqslant 100$ MeV. Additionally if diffuse cosmic ray interactions were the source, the 511 keV would also be accompanied by observable emission lines at other energies, notably the 4.4 MeV line from ^{12}C and other MeV lines from Mg, Si and Fe. None of these has been detected. Additionally it is difficult to account for the time variability of the flux (at least a factor of 5 between 1974 and 1979, Riegler et al., 1981) in this model. Indeed, the variability implies a maximum source size $\lesssim$ 1 light

year. Since the annihilation rate of $\sim 10^{43}$ s^{-1} is

two orders larger than that expected from a pulsar $\sim$

10^{41} s^{-1} (Sturrock and Baker, 1979), a massive rotating

black hole, $\sim 10^6 M_\odot$, has recently also been postulated

as the source of the 511 keV line. In this model infalling

matter would form an accretion disk. Ultraviolet radiation

from the disk coupled with strong dynamo action of the

rotating hole would initiate an electromagnetic cascade

thereby providing the required $e^+ e^-$ annihilation rate.

Ramaty and Lingenfelter (1981) note that this model

can provide the necessary $e^+ e^-$ G.C. line flux while

not being inconsistent with observations at infrared

and hard X-ray wavelengths.

With increased sensitivity it will become possible

to map out the distribution of positrons in the Galaxy

from large scale surveys of the 511 keV line.

2.3 Gamma-ray bursts

Colgate (1968) first considered the possibility

that detectable bursts of gamma-ray emission should

accompany supernovae events. However, between 1967

and 1979, 111 burst events were detected and catalogued

(Klebesadel et al., 1982), but none simultaneously with

a known supernova event. Indeed only one burst (1979

March 5) has been sufficiently localized to allow a

probable identification with the supernova remnant N49,

situated in the Large Magellanic Cloud. It should be

noted, however, that this identification would imply

a peak luminosity $\sim 10^{45}$ erg s^{-1} and it has been argued
that this was either an atypical event or because of
energy requirements for certain burst source models
that the identification is a line of sight effect.
The poor spatial determinations of many gamma-ray bursts
are a consequence of the indirect methods of photon
detection.   Arrival directions are determined by triangulation,
a technique dependent on accurate timing and long baselines
between the detectors to achieve good resolution.   The
positional accuracies are being improved to arc minute
accuracy, with the use of distant interplanetary satellites.

The observed energy range of bursts extends from
several keV to a few MeV and the bursts generally last
between 0.1s and 10s, with fluxes in the range 10^{-7}
to 10^{-3} ergs cm^{-2}.   From the analysis of the accumulated
data three distinct features are apparent in burst spectra.
(i)   Short, single peak bursts generally obey an exponential
type spectral form:

$$ ^{dN}/_{dE} \; = \; N_o \; \exp(^{-E}/_{kT}) $$

with $kT \simeq 150$ keV (Cline et al., 1976).   High resolution
spectra of several of these bursts show evidence for
both emission and absorption line features.   The emission
features are widely believed to be from free-free electron
bremsstrahlung in an optically thin medium; however,
synchrotron processes could also be considered if the
absorption features are interpreted as cyclotron absorption.

(ii) There are only two cases of recurrent emission from burst sources, the 1979 March 5 event repeated three times while the 1979 March 24 event recurred twice. The recurrent bursts exhibited variations in luminosity by up to two orders of magnitude, which along with their recurrent nature has been taken as evidence to suggest that these two events may form a separate class of gamma-ray bursts.

(iii) High resolution temporal analysis has identified periodicity in two events : 1977 October 29 (4.2s) and 1979 March 5 (8s) which strongly favours pulse-related phenomena as the burst sources.

Hurley (1983) has reviewed the observational data on gamma-ray bursts and concluded that 'no self-consistent explanation of the observations has yet been found'. Lack of precise identification with other known objects coupled with lack of simultaneous detection in other regions of the electromagnetic spectrum has confounded attempts to understand these enigmatic events. If the bursts were extragalactic in origin their energy requirements (like the 1979 March 24 event) would be enormous. It is generally believed that they must represent a local Galactic phenomenon. Jennings (1982) has modelled the observed log N - log S distribution for the bursts and finds the best fit to the data to be a disk source geometry with a scale height greater than 300 pc. Many models

have been considered for gamma-ray bursts including
flare stars, accreting objects such as white dwarfs,
neutron stars and black holes, star quakes and evaporating
black holes. Verter (1981) has extensively reviewed
each of these candidate models and considers that the
two models most widely favoured are neutron star accretion
and neutron starquakes. The non unique identification
of any gamma-ray burst with other unusual astrophysical
objects is good evidence in itself that at least one
class of objects must exhibit violent sporadic outbursts
of activity over and above their normally quiescent
states.

2.4 Ultra high energy gamma-ray sources

Extensive air showers have for many years been
utilized to study the energy spectrum and to a lesser
extent the composition of cosmic rays in the range 10^{14}eV
to 10^{20}eV. It is only indirectly through the cascade
of secondary particles and radiation initiated in the
upper atmosphere that these highest energy cosmic rays
can be detected. As a part of these cascade processes,
Cherenkov radiation is also produced which propagates
to ground level as a collimated pool of light of radius
$\sim 100 - 200$m. Its intensity and distribution can be
used to estimate the initial energy of the primary event
as well as provide directional information accurate
to a few degrees ($\lesssim 2° - 3°$). The application of this

technique to primary photons as opposed to cosmic ray
particles is very difficult because of the low ratio
of primary photons to particles ($\sim 10^{-6}$ at $\sim 10^9$eV).
Nevertheless experiments have successfully detected gamma-
ray showers above few 10^{11}eV. There are two distinguishing
features of a gamma-ray initiated shower which help distinguish
it from the more frequent cosmic ray showers, though
it has not always been possible to utilize these features
due to limited instrumental sensitivity. The higher
energy gamma-ray showers are expected to be increasingly
muon poor and to exhibit a smoother radial density of
particles (mainly electrons at ground level) than those
showers originating from cosmic ray particles. These
effects are due to the gamma-ray shower being essentially
an electromagnetic process, whereas the cosmic ray shower
will also lose energy through nuclear interactions.
However cosmic rays are charged particles and their inter-
actions with the Galactic magnetic field acts to tangle
their trajectories. This renders cosmic rays almost
isotropic except at the highest energies, the anisotropy
being $\sim 0.1\%$ from 10^{12}eV to 10^{14}eV and rising to only
$\sim 1\%$ by 10^{17}eV. Any spatial anisotropy in arrival directions
of showers is therefore clear evidence of uncharged particles
or photons coming from a discrete source. Allowing for
relativistic effects the nearest identified sources at
these energies are too distant for the showers to have
been generated by neutrons (scale length ~ 0.6 $(^E/_{10^{14}})$pc),
notwithstanding the problems associated with accelerating

uncharged particles. Similarly periodicity of the shower
arrival time implies pulsation and a discrete source
origin.

To date the results have been in many cases in-
conclusive or inconsistent due to low statistics, which
may in part have been due to time variability of the
emitting objects. Both the Crab and Vela pulsars have
been considered as possible sources of ultra high energy
gamma-ray emission. In the case of the Crab this is
reinforced by its well defined periodicity at other wave-
lengths, its relatively young age and its comparative
closeness. Measurements have been made covering the
energy range $\sim 10^{11}$eV to few 10^{13}eV with many experiments
only being able to give upper limits to the flux (e.g.
Helmken et al., 1973; Grindlay et al., 1976; Erikson
et al., 1976; Bhat et al., 1980a). Nevertheless several
positive detections have been made and the most recent
observations point to short ($\sim$ 15 min) periods of pulsed
emission (Dowthwaite et al., 1983). The situation with
the Vela pulsar is similar with the evidence suggesting
strong time variability of the signal (Grindlay et al.,
1975; Bhat et al., 1980a).

The gamma-ray spectra for both these pulsars have
been measured by the SAS II and COS B experiments (Section
3.7). The exponents of the COS B power law differential
spectra are -1.9 and -2.2 for the Crab and Vela respectively.
These spectra can be extrapolated from the medium energy
satellite measurements to those at 10^{11} - 10^{13}eV. In

the case of the Crab pulsar the data suggests that the extrapolated spectrum must steepen slightly above ~ 10 GeV. However, for Vela the situation is markedly different. Based on the extrapolated spectrum, the predicted fluxes above 10^{11} eV are about three orders of magnitude larger than the observed upper limits. Clearly the Vela energy spectrum must steepen significantly above the present medium energy observations. It is interesting to speculate whether the required steepening of the Vela spectrum is related to its greater age in comparison to the Crab (Vela $\sim 10^4 - 10^5$ years, Crab 930 years).

The most consistent source of ultra high energy gamma-rays yet detected is the binary object Cygnus X-3 which has been monitored continuously by various groups since the radio outburst in 1972 (e.g. Vladimirsky et al., 1973; Galper et al., 1977; Dowthwaite et al., 1983). Phase analysis of the air shower arrival times have confirmed the 4.8hr. periodicity of this source which has been well established at other wavelengths. Through comparison of these accumulated data sets two interesting conclusions have been obtained. The gamma-ray flux ($\gtrsim 10^{12}$ eV) varies with time, showing an overall decreasing trend since the first observations, a feature which is also apparent for radio and X-ray observations over the same period. This in itself is most interesting but it may also be related to the apparently conflicting observations of this object above 100 MeV (Section 3.6). Secondly the

absolute phase of the peak emission changes with epoch
and although the statistics are limited in some cases
there is also evidence favouring a double peak structure.

Recently Cyg X-3 pulsed emission has also been detected
at higher energies (10^{14} - 10^{16}eV) by groups using the
extensive air shower and Cherenkov techniques (

Samorski and Stamm 1983a; Lloyd-Evans et
al., 1983). These measurements are highly significant
when it is remembered that space is essentially transparent
to gamma-ray photons except above $\sim 10^{14}$eV, the threshold
for e^+e^- pair production from photon-photon collisions
involving the microwave background radiation field (Section
1.2). The most recent distance determination of Cyg X-3
is based on measurements made during the 1982 radio
outburst and place the object at a minimum distance of
11.6 kpc from the sun (Dickey 1983). The gamma-ray flux
above 10^{14}eV must therefore suffer quite severe attenuation
over the intervening path due to the presence of the
isotropic microwave background photon field. Taking
the attenuation into account the corrected fluxes are
plotted in Figure 2.1, a general summary of the gamma-
ray measurements of Cyg X-3. It should be noted that
the corrections have been derived assuming the distance
to be 11.6 kpc. and the microwave background temperature
to be 2.7K both of which are matters of some contention,
especially as the absorption coefficient for this process
varies as T_{ph}^3. Assuming all these observations to be
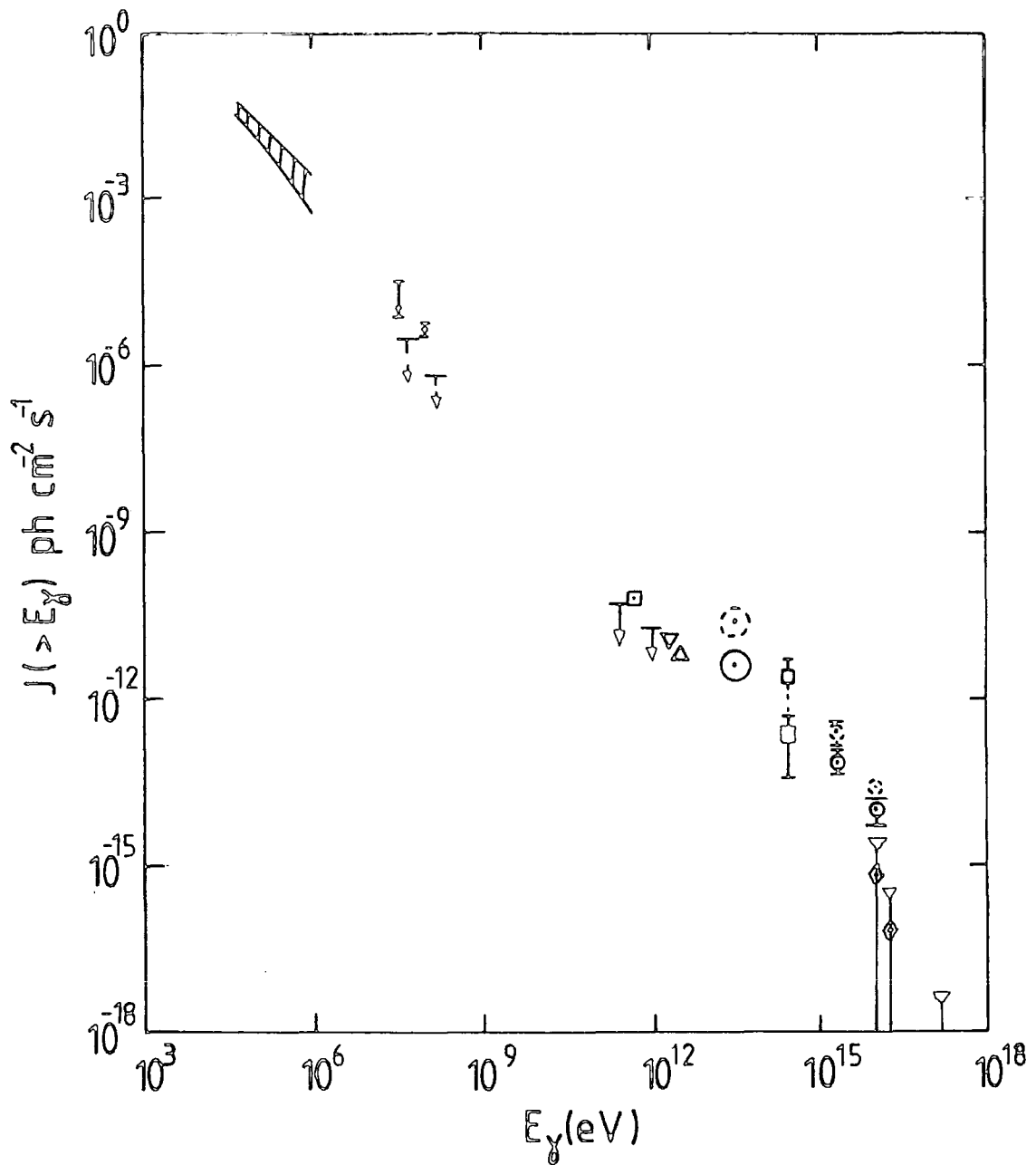
Figure 2.1   The integral spectrum for Cygnus X-3.

▨ Meegan et al. (1979), Ī Lamb et al. (1977), SAS II,

⊤ Hermsen (1983), COS B, ⊤. Weekes et al. (1977),

▽ Danaher et al. (1981),   △ Mukanov et al. (1979),

⊡ Lamb et al. (1982),   ⌽ Samorski and Stamm (1983a),

⊙ Morello et al. (1983),   ⌶ Bhat et al. (1984d), ⌀ Lloyd-Evans et al.
(1983)

The broken points are the observations corrected for

attenuation as described in the text.   It should be noted

that these observations span a period of almost 10 years.

Many of the features in the spectral shape may be due to

time variability, a well established phenomenon at other

energies.

correct it is apparent from Figure 2.1 that the spectral
shape in the region above $\sim 10^{14}$eV exhibits unusual structure
and that the emission cannot be described by a single
power law extending over all energy ranges. Further
observations are needed here to confirm the nature of
the spectral features and to bridge the gap between a
few GeV and 100 GeV.

Samorski and Stamm (1983b) have also found tentative
evidence for up to five more ultra high energy gamma-ray
sources, while the Adelaide group (Protheroe et al., 1984a)
have reported the detection of a pulsed signal ($\gtrsim 10^{15}$eV)
from Vela X-1. It is increasingly apparent that the evidence
for the existence of ultra high energy gamma-ray sources
is very strong indeed. There are several important implications
arising from the production of gamma-rays up to $\sim 10^{16}$eV
in Galactic sources which will be briefly discussed.

Anisotropies in the arrival direction of cosmic ray
showers have long been studied for clues as to the possible
origin of these energetic particles. Although many early
results in this field were inconsistent there is now a
generally accepted view that between 10^{12} and 10^{14}eV the
cosmic rays appear remarkably isotropic (anisotropy $\sim 0.1\%$
and the phase of the first harmonic of the arrival directions
remaining constant). However, Wdowczyk and Wolfendale
(1983, 1984) have studied the accumulated data on air
shower arrival directions at these energies. They have
found evidence for an excess of air showers ($10^{14} - 10^{16}$eV)

from the Galactic plane and preferentially from the inner
Galaxy. In the light of the Cyg X-3 and other observations
at these energies they consider it likely that ultra high
energy gamma-ray sources contribute significantly (perhaps
as much as 0.1%) to the primary cosmic radiation. They
find the observations consistent with the rapid variations
in phase and anisotropy. Furthermore, they conclude that
the gamma-ray flux from such objects must fall rapidly
above about 3×10^{16} eV (as air shower measurements suggest)
to be consistent with the observed anisotropy of the highest
energy air showers. Finally, they note the possible con-
sequences for cosmic ray energy requirements on the basis
of Cyg X-3 observations. Assuming isotropic emission
the minimum gamma-ray luminosity for this object is $\sim$
10^{37} - 10^{38} erg s^{-1} above 10^{15} eV. It seems plausible to
expect 10^{15} eV protons to be emitted with at least the
same efficiency. The total estimated energy in cosmic
rays in the Galaxy is $\sim 3 \times 10^{40}$ erg s^{-1} above $\sim 10^{9}$ eV
and the implication is clear that a small population of
Cyg X-3 type objects could provide most if not all, of
the observed cosmic ray flux at least up to $\sim 10^{16}$ eV.

Ultra high energy gamma-ray ($\sim 10^{15}$ eV) interactions
with photons of the microwave background will produce
$e^{+}e^{-}$ pairs each with energy $\sim 10^{14}$ eV which can then synchrotron
radiate to give X-rays of energy few keV up to few MeV.
In applying these considerations to a possible Galactic
population of Cyg X-3 type sources there are many

uncertainties, not least in the time variability of the
gamma-ray output but also in the spatial variations of
the Galactic magnetic field and uncertainty in the total
number of such sources. Nevertheless, Rana et al. (1984)
have addressed this problem and have found that there
should be a significant contribution to the hard X-ray
flux above $\sim$ 100 keV at high Galactic latitudes, even
if there is just one Cyg X-3 type source in the Galaxy.

Finally, mention should also be made of the gamma-
ray flux (0.4×10^{-10}ph cm^{-2}s^{-1} above 3×10^{11}eV) detected
by Grindlay et al. (1975) from the nearby radio galaxy
Centaurus A (distance $\sim$ 6.3 Mpc), but unconfirmed by other
groups. Interestingly Protheroe et al. (1984b) claim to
have detected emission from this object above $\sim 10^{15}$eV.
If these observations are confirmed it will be difficult
to reconcile them with the severe attenuation expected
from photon-photon collisions on the intervening microwave
background radiation. Nevertheless it would appear that
even for this first extragalactic ultra high energy gamma-
ray source, time variability is an important characteristic
of the emission.

It is clear from the brief review presented in this
chapter that the various branches of gamma-ray astronomy
all show good evidence for time variability of the source
emission and especially in the case of ultra high energy
emission strongly imply that a Galactic origin for most
cosmic rays (at least up to $\sim 10^{16}$eV) is not unreasonable.

CHAPTER THREE

MEDIUM ENERGY GAMMA-RAY ASTRONOMY

3.1 Introduction

In the region of the gamma-ray spectrum from a few tens of MeV to several hundred MeV the signal from the Galaxy and beyond is masked from ground based observations by the presence of secondary photons, generated by cosmic ray particles in the earth's atmosphere. Thus satellite borne spark chamber detectors are generally used for observations in this energy range. However, at the lower end of the range high altitude balloons have also made useful contributions to our knowledge of the spectrum. Spark chambers have poor angular resolution, often characterised by a cone of half-angle σ_θ containing 68% of the reconstituted arrival directions of incident photons. Typically $\sigma_\theta \simeq$ 8° - 10° at 30 MeV and improving to about 1° - 2° above several hundred MeV. Coupled with this lack of definition is the intrinsically low flux, adding uncertainty to the data interpretation.

The first detection of non-atmospheric gamma-rays above 100 MeV was made by scintillators aboard Explorer XI (Kraushaar et al., 1965). Using a spark chamber, OSO III in 1967 was able to detect a finite flux from the Galactic plane above 50 MeV. The angular resolution was very poor (Gaussian, full width half maximum = 24°), however analysis of the data showed an enhancement from the region of the Galactic centre and some evidence from high latitude observations for an isotropic component

of possible extragalactic origin (Kraushaar et al., 1972).

Since then our knowledge of the gamma-ray sky has been significantly improved through analysis of the data collected by NASA's SAS II satellite and ESA's COS B. SAS II, launched five years after OSO III, was able to survey more than half the sky before an instrumentation failure terminated the mission after only six months. This database produced the first detailed picture of the Galaxy in gamma-rays. In addition, it provided the first observations of gamma-ray pulsars and confirmed the existence of an apparently isotropic component of the emission at high Galactic latitudes.

In terms of instrumental performance, COS B was in many ways similar to SAS II. Whereas SAS II covered the energy ranges 35-100 MeV, 100-1000 MeV, COS B energy resolution extended over 50-150 MeV, 150-300 MeV and 300-5000 MeV. Angular resolution was similar in both cases (about 3.6° - 3.8° degrees above 100 MeV). However, COS B suffered from a large and uncertain instrumental background which was essentially negligible in SAS II. This tended to restrict COS B usefulness to regions close to the Galactic plane. The background problem is further discussed in Section 4.3 in relation to the detection of discrete sources. The longer lifetime of COS B (1975 - 1982) enabled it to significantly improve the counting statistics along the Galactic

plane, with an estimated 100,000 useful events obtained
in comparison to 13,500 for SAS II and only 621 for
OSO III. Analysis of the COS B data is still continuing,
although many results have already been obtained.

COS B was able to confirm many of the SAS II results
but the major scientific importance of COS B rests
with the claim to have detected 25 discrete gamma-ray
sources, 22 of which lie within 10° of the Galactic
plane. The existence of these sources, their consequences
for gamma-ray astronomy and its role in interpreting
Galactic cosmic ray dynamics has proved to be the most
enduring and as yet unresolved issue within the subject.

While the questions relating to gamma-ray sources
are central to the work of this thesis, it is appropriate
here to review the preceeding work on medium energy
gamma-ray astronomy, giving perspective to the arguments
we shall develop in subsequent chapters.

3.2 General features of the Galactic gamma-ray emission

The data from SAS II and COS B have been used in
conjunction with measuremnts of HI, H_2 (via CO), galaxy
counts and radio synchrotron emission to elucidate
the relationship between cosmic rays and the constituents
of the interstellar medium. These studies have been
carried out on a variety of scales ranging from small
scale structures and the local interstellar medium
(such as nearby molecular clouds) through to comparison
with large scale Galactic structure as traced by the

spiral arm features.

Interpretation of the data over such a wide range of scale lengths is necessarily dependent on our knowledge of additional inter-related factors. Our understanding of the composition of the interstellar medium decreases as we move further away from the local stellar environment. Specifically, the mass of molecular hydrogen plays a major role in limiting the precision of large scale Galactic studies. Analyses and conclusions drawn must consider the problems of deriving the column density of H_2, N_{H_2}, from CO measurements and the possible effects of the Galactic metallicity gradient upon the conversion. Similarly the contribution to the gamma-ray emission from inverse Compton processes depends on our inferred knowledge of the photon distributions in the Galaxy. While these problems can, to some extent, be tackled independently of the gamma-ray measurements, the role of discrete gamma-ray sources poses severe uncertainties for any large scale analysis of the gamma-ray data, particularly in the inner Galaxy.

Generally we find the uncertainties in the conclusions drawn from the data increase with the scale over which we perform the analysis. However, progress has been made and while many uncertainties still remain, it is clear that gamma-ray astronomy can benefit from observations in other regions of the electromagnetic spectrum. Indeed, in some cases the knowledge gained

from gamma-ray observations can be used to constrain
the interpretation of related astronomical phenomena.

3.3 Gamma-ray correlations with Galactic tracers

The data collected by the SAS II experiment have
been extensively analysed by the NASA group (e.g. Fichtel
et al., 1975; 1978a; Kniffen et al., 1977; Hartman
et al., 1979). These workers presented the variation
of the gamma-ray flux with Galactic longitude and lat-
itude. The improved resolution and statistical accuracy
over that achieved by OSO III enabled several features
to be identified. Figure 3.1 is an intensity contour
map of the Galactic plane derived from the tabulated
SAS II data, published by Fichtel et al. (1978b).
An enhanced region along the Galactic plane is visible
extending from $l \simeq 335°$ to $l \simeq 40°$ without showing
a narrow peak at the Galactic centre. The longitudinal
and latitudinal distributions have been shown to correlate
well with Galactic structure, in particular the spiral
arm patterns. Good correlations also exist between
the gamma-ray observations and measurements of gas
column density N_{HI} and with radio synchrotron data.
These studies permitted the identification of gamma-
ray emission from the local concentration of clouds
known as Gould's belt.

The COS B data enabled a more detailed analysis
of the Galactic gamma-ray flux to be made. Mayer-
Hasselwander et al. (1980, 1982) have presented these
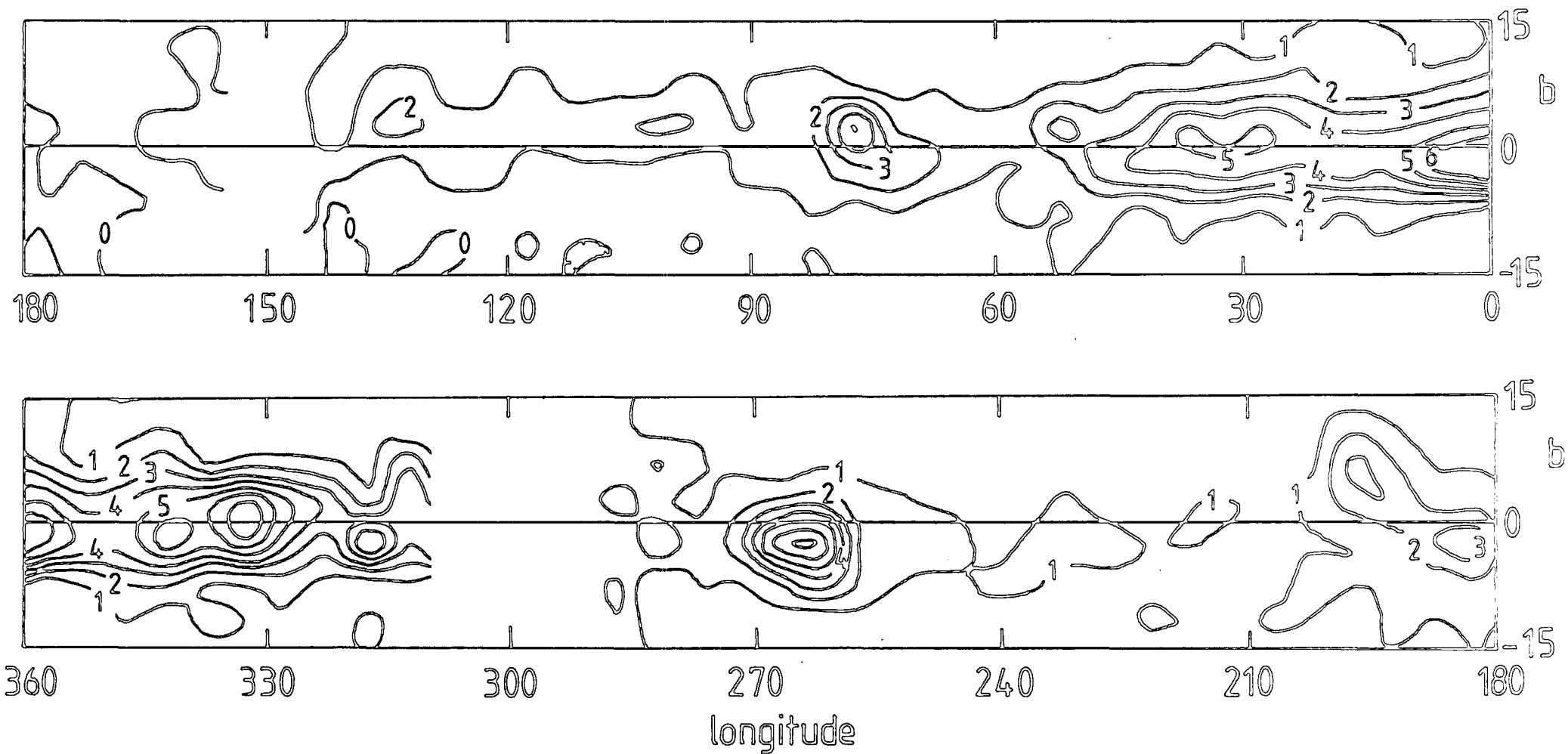
Figure 3.1 Gamma-ray intensity contours ($E_\gamma > 100$ MeV) derived from the SAS II data. The contour levels are $i \times 10^{-4}$ ph cm^{-2}sr^{-1}s^{-1}. Two longitude ranges totalling $\triangle l = 30°$ are excluded as the data are inadequate.

data and confirmed both the large and small scale relation-
ships between features of Galactic structure and the
gamma-ray observations.

Haslam et al. (1981) made a detailed spatial com-
parison between the COS B data and radio continuum
emission at 408 MHz. These workers were able to show
that both data sets exhibited a strong similarity.
They considered it good evidence that cosmic rays,
gas and magnetic fields in the Galaxy are dynamically
coupled, at least along the Galactic plane, and strongly
suggestive of a diffuse origin for the bulk of the
observed gamma-rays.

Many workers have used the gamma-ray data to investi-
gate the Galactic distribution of cosmic rays, by comparing
the observed fluxes with those expected from cosmic
ray interactions with the gas and photons of the inter-
stellar medium (e.g. Bignami et al., 1975; Fichtel
et al., 1976, Kniffen et al., 1977; Lebrun et al.,
1983, Fichtel and Kniffen 1984). Other workers (e.g.
Puget and Stecker, 1974; Strong and Worrall, 1976;
Caraveo and Paul, 1979, Issa et al., 1981 ; Li et al.,
1982) unfolded the gamma-ray data to a radial emissivity
distribution. Comparison with radial gas distributions
then in principle allowed the cosmic ray radial density
to be determined. The unfolding procedure is limited
in that it requires assumptions on radial symmetry
and scale heights, thus losing much of the small scale

variations.

Initially there was modest evidence from both
the unfolding and direct approaches for the existence
of a cosmic ray enhancement (by a factor $\simeq$ 4-10) towards
the Galactic centre. However, these arguments were
subject to the limitations imposed by uncertainties
in the mass of gas in the inner Galaxy. Additionally,
it was possible that an unresolved population of discrete
gamma-ray sources could mimic the longitudinal variation
of the gamma-ray flux while being consistent with a
uniform cosmic ray intensity throughout the Galaxy.

In an attempt to overcome both these difficulties
Dodds et al. (1975) considered only the outer Galaxy
where the contribution from discrete sources could
reasonably be expected to be small.

Similarly the uncertainties in the gas distribution
were believed to be negligible, the gas being primarily
atomic hydrogen. These workers concluded that a reduced
cosmic ray density relative to the local value could
explain the observed gamma-ray fluxes. Such a reduction
in the cosmic ray density outside the solar circle
could only reasonably be accommodated within a Galactic
origin model for these particles.

Interestingly, Bloemen et al. (1984a,b) have repeated
this analysis with COS B data and improved measurements
of HI and CO in the outer Galaxy. Using results from
three energy bands they concluded that the data are

consistent with a gradient (and hence Galactic origin)
for cosmic ray electrons and a uniform distribution
of cosmic ray protons. There remain uncertainties in
the gas distribution in the outer Galaxy and in the
relative contributions from electron and proton gamma-
ray processes to the observed COS B signal. Further
work is required before the latter conclusion can be
confirmed.

Instead of analysing the data in the Galactic
plane many workers have recently considered intermediate
latitudes ($|b| \simeq 10° - 20°$) as a restrictive probe
of the local interstellar medium. Thus the probable
contributions of H_2 and discrete sources are restricted,
adding weight to the conclusions.

Issa et al. (1981) analysed the SAS II and HI
data and found evidence for a local cosmic ray gradient,
extending over Galacto-centric radii $\sim$ 8-12 kpc.
A similar analysis using both COS B and SAS II data
and galaxy counts as a total gas tracer made by Bhat
et al. (1984a) has supported the existence of a local
cosmic ray gradient.

Galaxy counts can be used as an indirect tracer
of gas (Section 6.3) and the extensive available
sky coverage has prompted several workers to combine
them with gamma-ray data. This technique is generally
limited to regions away from the Galactic plane, saturation
effects making it less reliable at small Galactic latitudes.

Lebrun and Paul (1983) analysed the SAS II data
in this manner, comparing the observed fluxes with
those predicted from cosmic ray interactions with gas
as derived from galaxy counts. The correlations between
gamma-rays and galaxy counts were shown to be better
than between gamma-rays and HI, thus inferring the
presence of additional non-atomic gas, presumably H_2.
Strong et al. (1982) and Lebrun et al. (1982) analysed
the COS B data ($|b|$: 11° - 19°) with similar conclusions
to those obtained by Lebrun and Paul. They were also
able to use the gamma-rays, galaxy counts and HI to
map out on a scale of a few degrees the local distribution
of molecular gas at these latitudes. Recent CO observations
by Lebrun and Huang (1984) have confirmed the general
nature of this H_2 distribution in the Sagitarius
region. Although their measurements of N_{H_2} are less
than inferred by Strong et al. (1982) ($\sim$ a factor
of 2) part of the difference is likely due to uncertainties
in the gas-to-dust and CO-to-H_2 ratios. Nevertheless
the essential technique is correct, illustrating how
gamma-rays can provide a useful indicator for other
astronomical measurements.

3.4 Spectral shape of the diffuse Galactic emission

Both COS B and SAS II provided limited energy
resolution of the observed gamma-ray spectrum. After
allowing for the energy response of the detectors it
was possible to derive the spectral shape of the incident

flux. These data are plotted in Figure 3.2 along with
the theoretical predictions made by Fichtel and Kniffen
(1984) based on current best estimates of the gas and
photon distributions within the Galaxy. Additional
low energy data come from balloon experiments. From
their detailed analysis of the longitude and latitude
distributions of the observed intensities they concluded
that there was reasonable agreement with their models
based on contributions to the intensity from cosmic
ray nucleon-nucleon collisions, bremsstrahlung and
inverse Compton emission. They also noted the areas
of potential uncertainty : point source contributions
(especially below 100 MeV), the shape of the interstellar
electron spectrum below about 1 GeV and the absolute
mass of H_2 determined from CO. Bertsch and Kniffen(1983)
concluded from their balloon measurements (10 - 80 MeV)
that the spectral shape observed by SAS II and COS B
appears to continue down to at least 10 MeV. Studies
of the spectral shape can be used to constrain the
interstellar electron spectrum below 1 GeV where direct
measurements are not obtainable (e.g. Strong and Wolfendale,
1981, Lebrun et al. 1982, 1983).

Mayer-Hasselwander et al. (1982) noted that the
spectral shape of the COS B data ($|b|$ < 10°) did not
vary significantly with longitude and was in close
agreement with that determined by Lebrun et al. (1982)
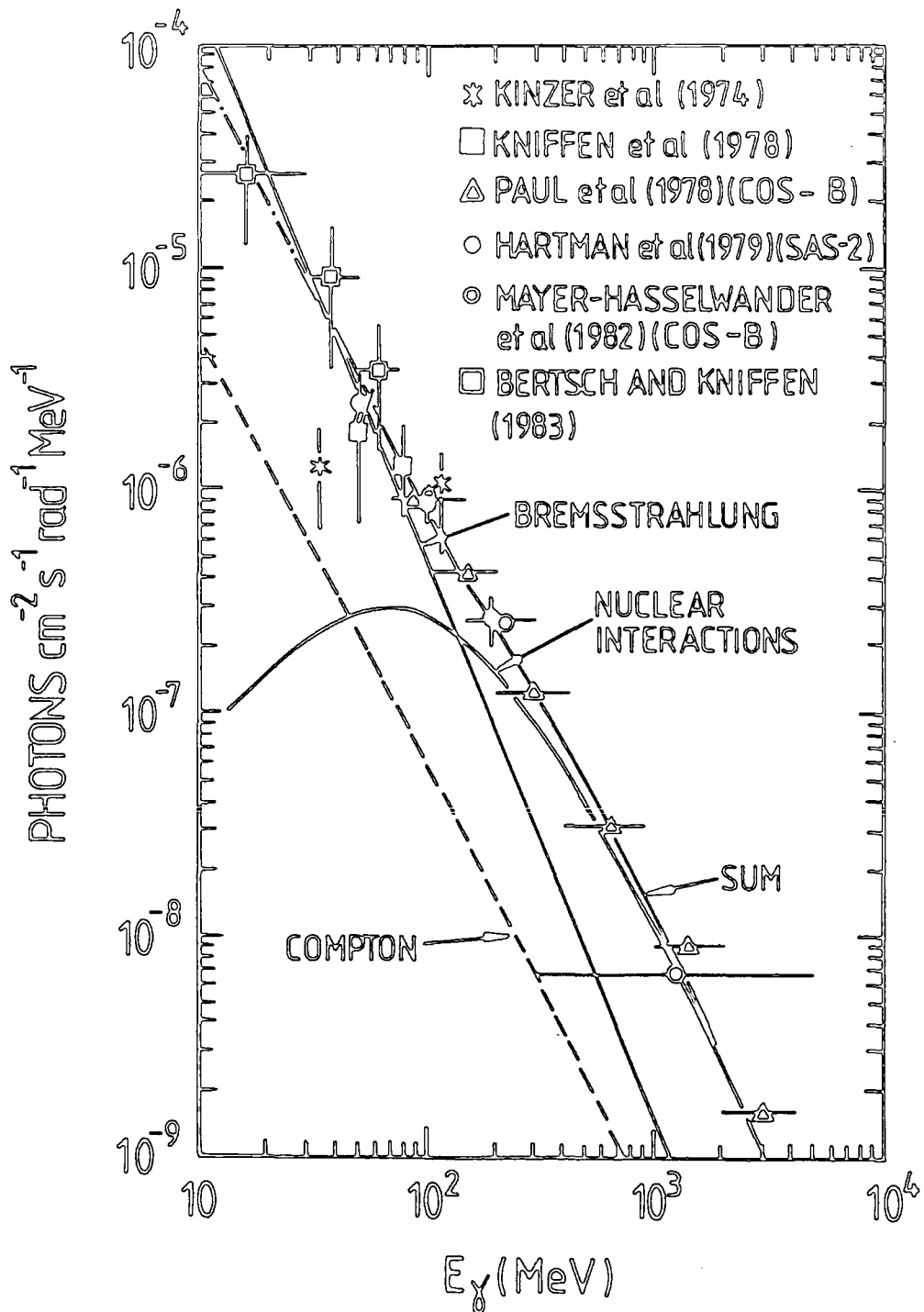
Figure 3.2 Observations of the Galactic gamma-ray spectrum compared with the calculated model of Kniffen and Fichtel (1984) for a region near the Galactic centre.

from the local interstellar medium. As an approximation

the gamma-ray data (> 100 MeV) can be described by

a single power law $(N(E) \sim E^{-\gamma})$ of index $\gamma \sim 2.0$.

3.5 Gamma-ray emission from molecular clouds

Several workers have analysed the expected gamma-

ray fluxes from local molecular clouds ($\lesssim$ 2 kpc).

The Orion molecular clouds have been detected in both

the SAS II data base (Wolfendale, 1981) and that of

COS B (Caraveo et al., 1980). Issa and Wolfendale

(1981a) have analysed the gamma-ray fluxes from the

directions of 13 nearby molecular clouds. They were

able to show that the flux from most clouds required

cosmic ray intensities within a factor of 2 of the

local value. The remainder, requiring cosmic ray intensities

in excess of the ambient local value, were considered

as possible cases of cosmic ray enhancement within

the clouds. The Orion complex is the best resolved

both in gamma-rays and in CO measurements. Recent

work has focused on these clouds to calibrate the local

$CO \rightarrow H_2$ conversion (Bloemen et al., 1984c, Houston and

Wolfendale, 1984b). These clouds are treated in more

depth in the present work (Chapter 6) where an investigation

is made of the degree of penetration of the dense mole-

cular gas by the ambient cosmic ray flux.

Black and Fazio (1973) first considered molecular

clouds as possible gamma-ray 'sources' because of their

high column density relative to the general interstellar

medium and the poor angular resolution of gamma-ray
detectors. These objects would not be genuine discrete
gamma-ray sources, but rather unresolved regions of
enhanced emission. Interestingly one of the sources
originally claimed by COS B (2CG 353 + 16) is now
acknowledged to be consistent with cosmic ray irradiation
of the extensive molecular complex ρ Ophiuci. The
earlier claims for its discrete nature were based on
a subset of the complete COS B data base.

Li and Wolfendale (1981, 1982) and Arnaud et al.
(1982) used Monte- Carlo techniques to analyse the extent
to which molecular complexes irradiated by cosmic rays
could be mistaken for discrete sources when observed
by a typical gamma-ray detector. From their analyses
they concluded that many of the weaker sources claimed
by COS B could be explained as unresolved giant molecular
clouds. The implications of these studies for the
COS B sources are most important, particularly in relation
to the discrete source contribution to the observed
emission. This is pivotal to the present work and
the role of these pseudo sources is developed in Chapters
4 and 5.

3.6 Discrete gamma-ray sources

The angular resolution and statistics collected by
OSO III were insufficient to permit the identification
of any discrete gamma-ray sources. The data collected

by SAS II and COS B enabled spatial and temporal (pulsed
emission) identification of discrete sources to be
made. Two distinct classes of gamma-ray sources exist
at present. Those identified with known objects observed
at other wavelengths, and hence genuinely discrete,
and the majority detected by COS B which remain unidentified.

The SAS II group was able to detect pulsed emission
from the Crab (Kniffen et al., 1974) and Vela pulsars
(Thompson et al., 1975) and from Cygnus X-3 (Lamb et
al., 1977). They also observed pulsed emission from
an unknown source situated towards the Galactic anti-
centre. COS B confirmed the detections of the Crab
and Vela pulsars. Initially the source in the anti-
centre (now known as Geminga or 2CG 195 + 5) was confirmed
by both spatial and temporal analyses. Detection by
COS B of the pulsed emission was later retracted, though
it now appears that the initial COS B and SAS II results
were essentially correct (Bignami et al., 1984).

COS B was unable to detect the characteristic
4.8 hr. period pulsed emission from Cygnus X-3 (Swannenburg
et al., 1981). This non-detection by COS B does not
invalidate the observations made by SAS II. As pointed
out previously (Section 2.4) repeated observations
of this object have shown strong long term temporal
variability in radio, X-ray and ultra-high energy gamm-
ray fluxes, with the flux $\gtrsim 10^{12}$eV passing through

a minimum during the period of the COS B observations.
It is not inconsistent to expect the flux $>$ 100 MeV
to also exhibit variability. The COS B data can be
regarded as strongly suggesting that Cygnus X-3 is
in fact a time variable medium energy gamma-ray source.
One further source (2CG 356 + 00) detected by COS B
in 1 out of 5 observation periods is also considered
to be time variable.

From comparison of the SAS II and COS B data there
is no evidence for long term temporal variation of
the fluxes from Crab, Vela and Geminga, within the
statistical limits of the observations.

Further analysis of the SAS II data for gamma-
ray pulsars was unable to produce any positive results
(Thompson et al., 1983). Similar results have been
found by COS B (Buccheri et al., 1983) though further
work is continuing.

Through a statistical analysis of the spatial
distribution of the COS B data a complete catalogue
of gamma-ray sources has been derived (Hermsen, 1980;
Swannenburg et al., 1981). The 2CG catalogue comprises
25 sources (including the now resolved ρ Ophicui
molecular cloud). One source is identified with the
quasar 3C273 (Bignami et al., 1981) and our own analysis
of the SAS II data produced similar fluxes, Table 3.1.
Another high latitude source (2CG 010 - 31) has only

been observed once and remains unidentified.

Of the remaining 22 sources ($|b| < 10°$) only the
Crab and Vela have been positively identified. Geminga
is most probably identified with the periodic X-ray
source detected by Bignami et al. (1983, 1984) using
data from the EINSTEIN and EXOSAT satellites. The
X-ray source has been detected as a faint optical source
($m_v \sim 21$) (Caraveo et al., 1984). Searches for pulsed
radio emission have as yet proved unsuccessful.

The relatively large error circles (typical radii
being $1° - 1.5°$ for the weaker sources) on the remaining
low latitude 2CG sources preclude identifications on
purely positional coincidences. X-ray and radio pulsar
searches of the error circles are continuing for objects
with unusual characteristics. No conclusive identifications
have yet been made and are unlikely to be made until
refined gamma-ray data become available.

3.7 The nature of the gamma-ray sources

The 20 unidentified 2CG sources are termed Galactic
because of their narrow latitude distribution ($<b> \simeq 1.5°$).
Several models have been proposed for these objects.
Lamb (1978) suggested they may be young supernova remnants
while Montmerle (1979) considered the combination of
a supernova remnant with a nearby OB association (SNOB).
These are extended source models relying on cosmic
ray interactions with components of the interstellar

medium. In this respect unresolved molecular clouds (Section 3.5) have also been suggested for several of the 2CG sources.

Free radio pulsars and accreting neutron stars in binary systems are the favoured models for genuine discrete sources, in light of the identifications of the Crab and Vela pulsars and the observations of Geminga. Bignami and Hermsen (1983) have summarized the present data on the 2CG sources, observations at other wavelengths and the details of the various theoretical models under consideration.

The spectral characteristics of the Crab, Vela and Geminga sources are similar. The COS B data can be well described by power law spectra with indices $(N(E) \sim E^{-\gamma})$ γ = 2.2, 1.9, 1.8 respectively. For the quasar 3C273 (2CG 289 + 64) γ = 2.6 and the remaining unidentified sources are consistent with $<\gamma>$ = 2.0.

Both the Crab and Vela exhibit double pulsed structure at gamma-ray energies > 50 MeV with reduced interpulse emission. The Crab gamma-ray light curve exhibits strong similarities with the light curves at radio, optical and X-ray energies. For Vela the light curves differ at radio, optical and gamma-ray energies, though interestingly the phase separation of the double gamma-ray peaks in Vela is similar to that for Crab.

Early speculation on the nature of the gamma-ray sources considered them as a new class of astrophysical

objects. While this possibility cannot as yet be completely
rejected it does appear most unlikely. The present
2CG source catalogue is not considered complete in
the sense of only containing genuine discrete sources.
Rather the present work favours a mixture of discrete
sources (probably pulsars or neutron stars) and unresolved
regions of enhanced emission (the cosmic ray irradiated
giant molecular clouds).

3.8 Extragalactic gamma-ray emission

Analysis of the SAS II data (Fichtel et al., 1978b)
confirmed the tentative results from OSO III on the
existence of a diffuse extragalactic component to the
gamma-ray flux. Correlation of the gamma-ray data
with HI and radio synchrotron emission indicated a
residual component to the gamma-ray flux towards the
North Galactic pole. This has since been confirmed
in studies using galaxy counts as total gas tracers
(Thompson and Fichtel, 1982; also Section 7.2). The
residual flux has a relatively steep differential spectral
index ($\simeq$ 2.8) compared with the low latitude Galactic
component ($\simeq$ 2.0). COS B has been unable to confirm
these measurements because of its large instrumental
background which made it unsuitable for observations
at high Galactic latitudes (i.e. low flux regions).

The sparse nature of the data on the extragalactic
gamma-ray component has given rise to extensive theoretical
speculation on its origin. Indeed there is the possibility
that it is not truly extragalactic but results from

inverse Compton interactions of cosmic rays diffusing
out of our Galaxy (Worrall and Strong, 1977; Worrall,
1977). Although the statistics are poor the high
latitude ($|b| \gtrsim 30°$) SAS II data are relatively
isotropic on scales greater than the angular resolution.
In terms of a simple halo model for the additional
high latitude flux the isotropy requires a halo radius
$\gtrsim$ 50 kpc. This in turn necessitates much greater
diffusion of the cosmic ray particles (primarily electrons)
than is conventionally assumed in the Galactic plane.
Recent analysis of the SAS II and 408 MHz synchrotron
data (Riley and Wolfendale, 1984) has suggested a modest
contribution to the Galactic flux from an extended
inverse Compton component. Thus it is likely that
a small fraction of the extragalactic flux should be
associated with our own Galaxy. However, there are
compelling reasons to believe that a truly extragalactic
component must also be present.

Our Galaxy can itself be thought of as a single
gamma-ray source and it is to be expected therefore
that other normal galaxies should contribute to an
extragalactic flux. Analysis of the SAS II data from
the region of the Large Magellanic Cloud (LMC) supports
this contention. For this object we estimate F_γ (> 100
MeV) (1.5 $\pm$ 1.4) x 10^{-6} ph $cm^{-2}s^{-1}$, not inconsistent
with a simple model assuming gamma-ray luminosity scales
as the galactic mass. The Small Magellanic Cloud (SMC)

and M31 have not been detected at these energies, but
their fluxes are expected to lie just below the current
threshold.

From the SAS II data we can derive the upper limit
to the flux above 100 MeV from M31. We find F_γ
(>100 MeV) $\lesssim$ 0.3 x 10^{-6} ph $cm^{-2}s^{-1}$ (Table 3.1) and
assuming the spectral shape is similar to our own Galaxy
(N(E) $\sim$ E^{-2}) then F_γ (> 10^{12}eV) $\lesssim$ 0.3 x 10^{-10} ph $cm^{-2}s^{-1}$.
Dowthwaite et al. (1984) have detected a flux above
10^{12}eV from M31 using the atmospheric Cherenkov technique.
They find F_γ (> 10^{12}eV) = 2.2 $\pm$ 0.7 x 10^{-10}ph $cm^{-2}s^{-1}$,
an order of magnitude above the upper limit expected
from the SAS II data. These measurements strongly
suggest the spectrum is flatter than E^{-2} or has an
additional component at ultra-high gamma-ray energies.

Turning to active galaxies, Cen A has been detected
both at X-ray energies (10 keV - MeV; Dean and Ramsden
1981 and references therein) and also at ultra-high
gamma-ray energies (Section 2.4). Similarly the flux
from the Seyfert galaxy NGC 4151 has been measured
from keV up to MeV energies (see Dean and Ramsden,
1981). There is some evidence from the SAS II data
and we have estimated the fluxes from these objects,
Table 3.1. In Chapter 7 we explore further the role
of discrete sources (specifically radio galaxies and
galaxy clusters) as a component of the extragalactic
flux.

| | SAS II | | COS B |
Object	F_γ(35–100 MeV)	F_γ(> 100 MeV)	F_γ(> 100 MeV)
LMC	3.4	1.5 $\pm$ 1.4	
M31	0.5	0.3	0.8
Cen A	2.3 $\pm$ 1.6	1.5	1.2
NGC4151	0.4 $\pm$ 0.3	0.6 $\pm$ 0.4	0.9
3C273	0.4 $\pm$ 0.3	0.6 $\pm$ 0.4	0.6 $\pm$ 0.4

Table 3.1   All fluxes are in units of 10^{-6}ph cm^{-2}s^{-1}. The SAS II values are derived by us from the tabulated data of Fichtel et al. (1978b). The COS B values are from Pollock et al. (1981) assuming $N(E) \sim E^{-2}$. The SAS II upper limits are 1 σ , those from COS B are maximum likelihood estimates.

The low angular resolution of present gamma-ray detectors renders it impossible to resolve potential extragalactic sources such as galaxies or clusters. However, the possibility remains that the extragalactic flux may be predominantly diffuse in nature. It is useful to compare present measurements with those extending down to several hundred keV, as shown in Figure 3.3.

Two models have been proposed to explain a genuinely diffuse extragalactic gamma-ray flux. Ginzburg (1968) and Stecker (1969) have considered the interactions of cosmic rays in the early universe. In this model gamma-rays are produced at high redshifts and the characteristic π° peak at $E_\gamma \simeq 67$ MeV (Section 1.2) is displaced to lower energies during the cosmic expansion. These workers noted that the gamma-ray spectrum and the bump evident at a few MeV (Figure 3.3) would be consistent with the redshifted production spectrum after allowing for distortions by cosmological effects.

A similar cosmological explanation has been suggested by Stecker (1983), Stecker and Wolfendale (1984) and draws its inspiration from the baryon symmetric cosmology developed by Omnes (1969). Here the universe is partitioned into matter-antimatter regions, at least on the scale of galaxy clusters. The formation of these cells in the early universe would have given rise to matter-antimatter annihilations ($p\bar{p}$) producing gamma-
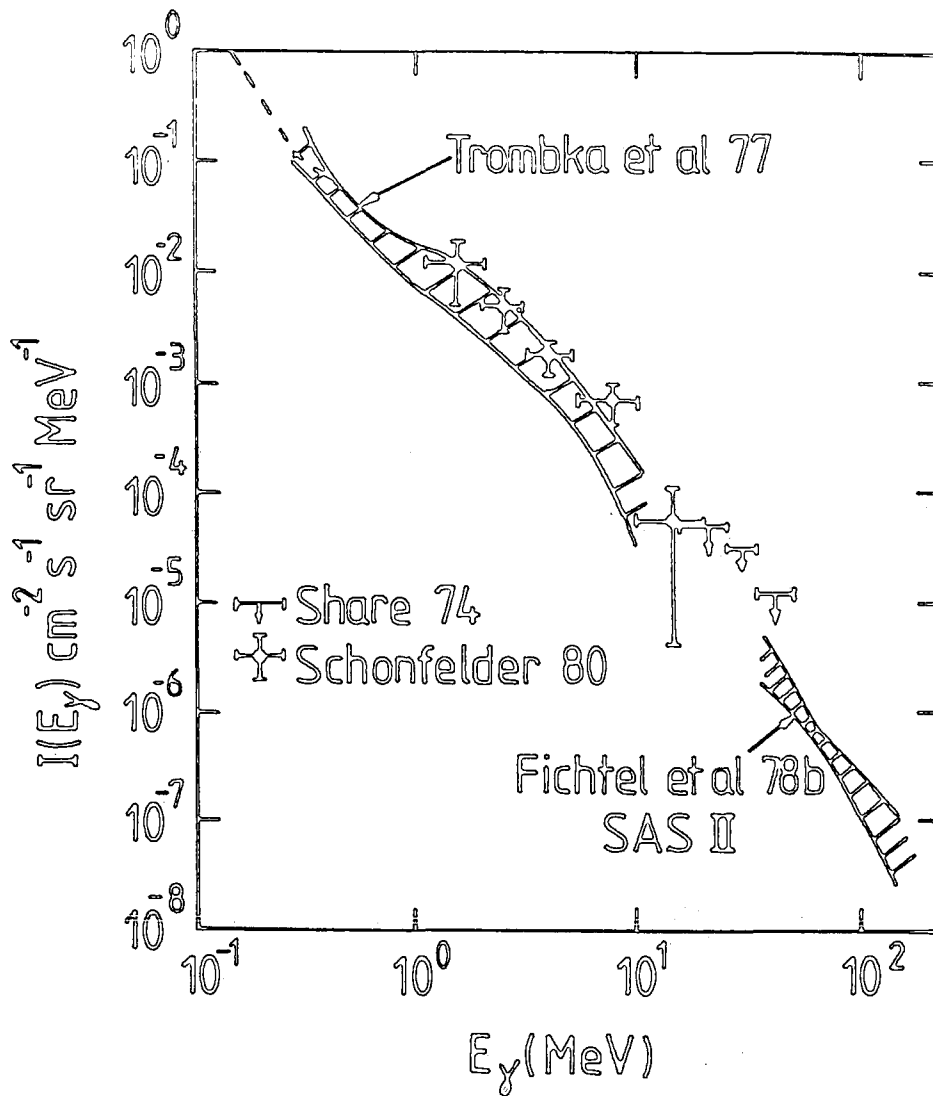
Figure 3.3 The observed diffuse gamma-ray spectrum, presumed to be extragalactic in origin. The bump around a few MeV is apparent when compared with the extrapolation from lower energies.

rays from π^0 decays. The spectrum from these early
epochs would then be redshifted to produce that observed
today.

An additional prediction of the latter model is
the existence of antimatter in the cosmic ray flux.
Buffington et al. (1981) have detected an antiproton
flux, $F_{\bar{p}} = (1.7 \pm 0.5) \times 10^{-4} \bar{p} \, m^{-2} sr^{-1} s^{-1} \, MeV^{-1}$ between
130-320 MeV. This is in excess ($\sim$ a factor of few
10^2) of that expected from Galactic production in spallation
products of protons and heavier nucleii with the inter-
stellar medium. Galactic black holes have been suggested
as sources of the additional antiprotons (Kiraly et
al., 1981; Protheroe, 1983). However Stecker and Wolfendale
also consider that the excess might be consistent with
the extragalactic gamma-ray flux and matter-antimatter
cosmology. A conclusive test of these ideas must await
the positive detection of antinuclei (Z > 1) in the
cosmic radiation and the resolution of the gamma-ray
flux into filaments delineating the matter-antimatter
boundaries.

Said et al. (1982) have compared the SAS II extra-
galactic flux above 100 MeV with that expected for
several Universal cosmic ray origin models involving
combinations of cosmic ray density and estimates of
gas in galaxy clusters and the intergalactic medium
at the present epoch. They conclude that the measured
extragalactic gamma-ray flux indicates that at least

90% of cosmic ray protons in the energy range 1–10 GeV
are Galactic in origin.

CHAPTER FOUR

SAS II - THE EVIDENCE FOR DISCRETE SOURCES

4.1 Angular resolution of the gamma-ray data

Both SAS II and COS B employed spark chambers for
detection of incident gamma-rays. The incoming photons
produced electron positron pairs which were deflected
through the spark chamber stack and an energy calorimeter.
The latter provided an estimate of the gamma-ray energy
while reconstruction of the spark chamber tracks allowed
the incident direction to be derived. The angular resolution
of these detectors was limited by the uncertainty in re-
constructing the characteristic forked·track of the electron
positron pair.

Preflight calibration using tagged gamma-ray beams
has shown that the angular response of both SAS II and
COS B is well described by a point spread function of
the form

$$f(\theta) \quad = \quad N \exp - (\theta / \theta_o)^{2c} \qquad\qquad 4.1$$

where N is an appropriate normalization factor. The para-
meters θ_o, c are energy dependent and were determined
experimentally. Hermsen described in detail the calibration
of the COS B instrument while Fichtel et al. (1975) gave
similar information for SAS II. We adopt $\theta_o = 5.0°$,
c = 0.8 and $\theta_o = 1.52°$, c = 0.5 for SAS II E_γ : 35-100 MeV
and $E_\gamma > 100$ MeV respectively. For COS B the relevant
parameters are $\theta_o = 1.4°$, c = 0.5 ($E_\gamma > 100$ MeV).
Above 100 MeV the SAS II width is larger because of the
relative data bin sizes ($\Delta l \times \Delta b = 2.5° \times 0.8°$ for SAS II

0.5° x 0.5° for COS B). The two width parameters are related by assuming an equivalent circular area of radius θ_{eq} = 0.58° for the SAS II bins and adding this in quadrature to the COS B parameter.

The angular resolution can be defined by a cone of half angle σ_θ , containing 68% of the arrival directions of photons from a point source. In terms of the point spread function f(θ) this can be expressed as

$$0.68 \; = \; \int_{o}^{\sigma_\theta} 2\pi\theta f(\theta)d\theta \Big/ \int_{o}^{\infty} 2\pi\theta f(\theta)d\theta \qquad\qquad 4.2$$

Substitution of the appropriate values for θ_o, c yield σ_θ (SAS II, E_γ : 35-100 MeV) $\simeq$ 6.1°, σ_θ (SAS II , E_γ > 100 MeV) $\simeq$ 3.8° and σ_θ (COS B, E_γ > 100 MeV) $\simeq$ 3.6°. Angular resolutions of a few degrees clearly restrict the ability to identify point sources, their fluxes being smeared out over the underlying background structure.

4.2 The cross-correlation technique

To improve the detectability of point sources the COS B group employed a cross-correlation technique, described in detail by Hermsen (1980). The method involved cross-correlating the raw gamma-ray data with a matrix representing the appropriate point spread function. Structure in the raw data consistent with the point spread function produces a maximum signal whereas wider and narrower structures are suppressed. Assuming the observed counts in any bin are sufficiently large ($\gtrsim$ 10) they can be regarded as following a Gaussian distribution. Figure 4.1 illustrates the idealized case of a point source superimposed on a
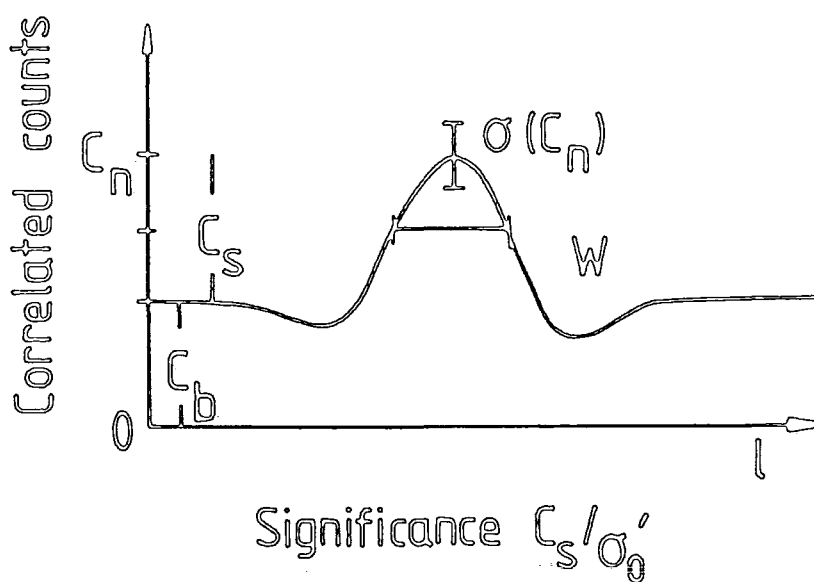
Figure 4.1 Idealized profile of the correlated
count versus longitude for a peak of height C_s super-
imposed on a background of height C_b. W is the
width parameter described in the text (Section 4.2).

$$C_s/\sigma_o' = C_s / \sqrt{(\sigma^2(Cn) - \gamma C_s)\,(1 + C_s/[\Sigma N - C_s]\,)}$$

γ is a parameter dependent on the point spread
function (Hermsen, 1980). ΣN measures the number
of photons in a $10^o \times 10^o$ area centred on the
particular bin.

smooth background. The significance of the excess correlated
count can be calculated and is related to the Gaussian
probability that the excess in a given bin is due to an
upward statistical fluctuation. The expression derived
by Hermsen for the significance

$$C_s / \sigma'_o = C_s / \sqrt{(\sigma^2(C_n) - \gamma C_s)(1 + C_s / \Sigma N - C_s)} \quad 4.3$$

allows for the contribution to the excess count which
could be due to a local enhancement of the underlying
background at that point.

The 2CG catalogue (Hermsen 1980, Swannenburg et al. 1981)
was compiled using the cross-correlation technique with
two criteria applied for the identification of a peak
as a discrete source.

(i) A minimum significance level $C_s / \sigma'_o \geqslant 4.75$ was required.
This corresponds to a Gaussian probability $\mathbb{P} \leqslant 10^{-6}$
per bin of the excess being statistical. For the Galactic
plane data (1 : 0° - 360°, $|b| < 10°$) there are 28,800
COS B data bins. Thus the probability of one spurious
source being included in the 2CG catalogue is about 2.9%.

(ii) The measured width W (Figure 4.1) of the correlation
function should be consistent with the point spread function.
From our own analysis of the published correlation profiles
(Hermsen, 1980) we estimate $3.5° < W < 6.0°$ as appropriate
for the 2CG sources. The spread in allowed width reflects
both the statistical nature of the data and the effect
of underlying background structure in contributing to
the excess signal.

In principle a source catalogue derived from these criteria should be genuine, that is contain no spurious sources. However, the cross-correlation analysis makes the assumption that the background is smoothly varying and thus produces a zero correlation signal. In the gamma-ray data this is not the case, the background being highly structured over scales comparable with the point spread function. As described earlier (Section 3.5) other workers have shown that this effectively reduces the significance of excesses because upward fluctuations of the background structure can satisfy the above criteria (i.e. appear source like). We shall return to this in Section 4.3.

Given the importance of gamma-ray sources to inter-pretation of the data it is clear that there is a need to re-examine the significance of those sources already detected, that is the 2CG catalogue. We endeavour to address this problem from two distinct standpoints. In this chapter we use the earlier SAS II data and employ the cross-correlation technique to assess the evidence for or against the 2CG sources. In the second approach (following chapter) statistical methods are used to estimate the number of spurious sources attributable to confusion effects. By combining with the number of genuine sources we determine the best estimate of the Galactic gamma-ray flux coming from genuine discrete sources.

4.3 Cross-correlation analysis of SAS II

The complete SAS II data were published by Fichtel

et al. (1978b). The data consist of binned counts
($\Delta l \times \Delta b = 2.5° \times 0.8°$) and sensitivity factors for
two energy ranges E_γ : 35-100 MeV, $E_\gamma > 100$ MeV. The
total numbers of photons recorded in these respective
energy bands were 6415 and 6085, collected over a period
of 7 months. The satellite failed prematurely having
only surveyed about two-thirds of the sky.

The 2CG catalogue was based on data accumulated by
COS B over about 5 years, ammounting to about 50,000
photons $|b| < 10°$, $E_\gamma > 100$ MeV. The corresponding number
for SAS II was 4172. The ratio $\simeq$ 12 : 1 indicates
the overall statistical precision of the two data sets.
However in any search for point sources the important
parameter is the effective number of counts above the
background. For SAS II the instrumental background was
effectively zero ($I_\gamma \lesssim 10^{-6}$ ph cm^{-2}sr^{-1}s^{-1}) whereas for
COS B the background was large and uncertain. It has
been estimated (Mayer-Hasselwander et al. 1980) that up
to 25% of the COS B photons detected from the Galactic
plane were due to instrumental effects. Thus the actual
effective count ratio was about 7 : 1. This is confirmed
by considering the mean count per source flux unit (1
flux unit = 10^{-6} ph cm^{-2}s^{-1}, henceforth used throughout
this chapter). For COS B the number is about 80 (Hermsen,
private communication). Our analysis of the SAS II data
indicates the corresponding value to be about 13, a ratio
$\simeq$ 6 : 1. It is therefore considered worthwhile to

analyse the SAS II data for point sources.

Using the appropriate point spread function a cross-correlated count map of the SAS II data is produced. The analysis is restricted to $E_\gamma > 100$ MeV, $|b| < 9.6°$. The lower energy data E_γ : 35-100 MeV were initially subjected to the analysis procedure but because of the low angular resolution ($\sigma_\theta \simeq 6.1°$) no useful information was obtained. Two regions totalling $\Delta l = 30°$ are not analysed due to insufficient statistics (less than 10 photons per $\Delta l = 10°$).

Following the criteria employed for the 2CG catalogue (Section 4.2) a similar selection procedure is used to identify SAS II candidate sources. We adopt a significance level $C_s/\sigma_o' \geqslant 4.28$ corresponding to 3×10^{-2} expected spurious sources in the range analysed (3168 bins). This is comparable to the COS B significance and expected spurious source number. A reduced significance level $C_s/\sigma_o' \geqslant 3.4$ is also employed, corresponding to 1 spurious source over the region analysed. The latter significance cut produces a useful candidate source list for SAS II although it is not directly comparable with the 2CG catalogue. Following the 2CG analysis the width parameter W is required to satisfy $3.5° < W < 6.0°$. This range is compatible with the values measured for the three most significant source peaks (Vela, Crab, 2CG 078) in the SAS II data.

The binning of the SAS II data, coupled with the low statistics make estimation of the correlated background

C_b (Figure 4.1) uncertain. For the present analysis the mean background is derived using a 5-point weighted mean applied to each longitude profile. This background level is further smoothed in several regions, on a subjective basis, to remove statistical spikes. The difference introduced by this additional smoothing is always small and negligible in comparison to the errors on the total count.

Each correlated count longitude profile is analysed for candidate sources. The positions of peaks are measured at the maximum of the significance, after interpolating between the discrete longitude points. The widths W at half maximum source count are also measured from these profiles. By combining the gamma-ray count and sensitivity data binned fluxes are calculated for $E_\gamma > 100$ MeV. A cross-correlated flux map is produced following the procedure for the correlated count. At the positions of the correlated count maxima the corresponding source fluxes are measured.

4.4   Results of SAS II analysis

A total of 30 peaks are identified with $C_s/\sigma_0' \geqslant$ 2.0 and the correct width, regardless of the measured flux. This is the minimum significance level for which a candidate source peak could be identified. At the lower significance levels ($C_s/\sigma_0' \lesssim 2.5$) the confusion between potential sources is increasingly serious. It is clearly not possible to identify two peaks in adjacent bins and there is an area surrounding each observed peak in which another genuine peak could remain unobserved. By checking the positional distribution of all the detected excesses

we estimated the number of dead bins n_D to cover an area
$l \times b = 4° \times 8°$. The significance $^Cs/\sigma_o$' is directly
related to the Gaussian probability P of the excess being
a statistical fluctuation. A good estimate of the number
of undetected peaks surrounding each observed excess is
$n_D \cdot P$. The total number of expected peaks above that
significance level can be expressed as

$$n_T (< P) = N_O (< P) \left[1 + n_D \cdot P \right] \qquad 4.4$$

where $N_O(< P)$ is the number of observed peaks above that
significance level.

The Log N - Log S distribution of the 30 observed
peaks is derived after scaling linearly to allow for the
loss due to incomplete sky coverage (Δl = 30° not analysed).
This corrected distribution is compared with that of the
2CG catalogue ($|b| < 10°$) in Figure 4.2. The expected
Gaussian distribution for 3456 independent SAS II bins
is also shown. The observed SAS II distribution can be
further corrected using 4.4, the broken line in Figure
4.2. It is seen that this improves the fit of the observed
distribution to that expected from statistical fluctuations.
This is encouraging as at the low significances considered
statistical fluctuations should dominate over any inherent
structure within the data. In addition the corrected
distribution falls below expectation at the lowest significances
because the data bins are not truly independent due to
angular resolution effects. The expectation line can
therefore only be considered as an upper limit.
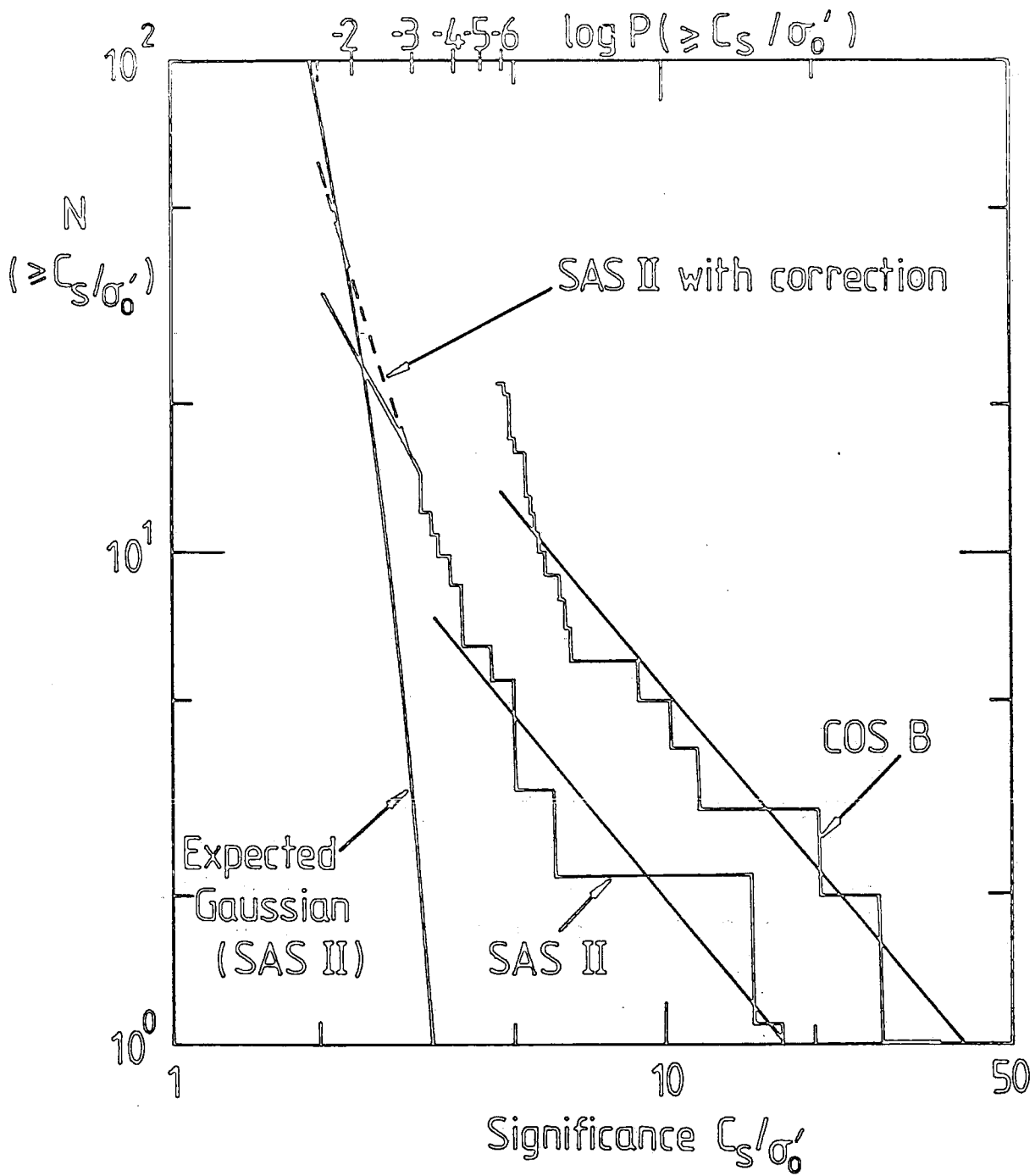
Figure 4.2   Integral distribution of significance
for the COS B and SAS II candidate sources.

It is useful to consider the relative displacement of the SAS II and COS B lines as measured from their high significance tails. From Figure 4.2 this shift is estimated to be about 2.3. For a given flux the significance is approximately a measure of the square root of the number of detected source counts. Therefore $2.3^2 = 5.3$ is to a first approximation the effective count ratio. This parameter is lower than the total count ratio (10 : 1) and is closer to the previous estimates (7 : 1, 6 : 1, Section 4.2).

4.5 Derivation of SAS II discrete source catalogue

We now proceed to restrict our attention to those peaks which satisfy the criteria of Section 4.2 for identification as candidate sources. Selecting only those peaks with $C_s/\sigma_0' \geqslant 4.28$ gives the top candidate sources listed in Table 4.1. Identification is made with a 2CG source if the SAS II peak is within $3.8°$ of this position (1σ width of the point spread function). Reducing the significance level to $C_s/\sigma_0' \geqslant 3.4$ gives a further 5 candidate sources. We expect this list (Table 4.1) to be complete in that it should contain only one spurious source. For those 2CG sources not listed in Table 4.1 a further search of the data is carried out to identify the maximum SAS II peaks within $3.8°$ of the COS B positions. These results are listed in Table 4.2. By combining the data in Tables 4.1 and 4.2 we obtain information on 22 2CG sources. This information from the SAS II experiment is used to group the 2CG sources according to their degree of

TABLE 4.1

SAS II candidate source catalogue for $E_\gamma > 100$ MeV with significance, measured as C_s/σ_0', greater than 3.4. Flux F_γ,m measured in flux units at the position of maximum significance. F_γ,s: flux measured at 2CG position. F_γ, COS B denotes the actual flux measured by the COS B workers and given in the 2CG catalogue.

2CG	1°	b^o	Significance	F_γ,m	F_γ,s	F_γ COS B
359–00	0.0	–1.2	4.5	2.3±0.5	2.2	1.8
078+01	78.2	1.2	6.0	3.2±1.2	2.9	2.5
	125.3	–0.4	5.0	3.8±1.3		
184–05	185.3	–3.6	15.1	3.6±0.8	2.0	3.7
195+04	196.0	5.2	5.0	4.9±1.3	3.8	4.8
263–02	264.1	–2.8	17.1	10.7±1.5	9.0	13.2
	25.0	8.4	3.5	1.4±0.6		
	105.0	1.2	3.7	2.1±0.9		
	114.9	–4.4	3.4	1.7±0.7		
	312.0	7.6	3.7	2.9±1.4		
311–01	314.8	–0.4	3.9	5.6±2.0	0.0	2.1

TABLE 4.2

Data on SAS II peaks ($E_\gamma > 100$ MeV) within 3.8° of those 2CG sources not identified in Table 1. Significance measured as $^C s/\sigma_0$'. W indicates that the profile had the correct width. Flux F_γ,m measured in flux units at the point of maximum significance. $F_{\gamma,COS\ B}$ is the flux measured by the COS B workers. Blank line indicates no peak found. None of the significances is above our lower limit for acceptance (3.4) but it will be seen that the actual values found are not too far away (> 2.0). There is thus some support for nine more 2CG sources and rather more support for the seven which have correct W-values. *(Note 2CG 356±00 'may be variable' and 2CG 284-00 and 288-00 'may be extended').

2CG	l^o	b^o	Significance	Width	F_γ,m	F_γ,COS B
006-00	8.0	-0.4	2.5		1.9±0.9	2.4
013+00					($\lesssim$ 0.7)	1.0
036+01	35.3	0.4	3.9	W	2.0±1.0	1.9
054+01	54.4	1.2	2.3	W	1.9±1.1	1.3
065+00					($\lesssim$ 1.3)	1.2
075+00	74.5	-1.2	2.5	W	2.4±1.3	1.3
095+04					($\lesssim$ 1.5)	1.1
121+04	118.1	6.0	3.1	W	1.8±0.9	1.0
135+01	135.0	2.0	3.2	W	2.7±1.7	1.0
218-00	216.7	-2.0	2.4		1.5±0.8	1.0
235-01	235.0	-0.4	1.7		1.1±0.5	1.0
284-00	283.0	-2.0	2.1	W	2.2±1.2	2.7
288-00					($\lesssim$ 2)	1.6*
333+01	334.0	0.4	2.3	W	3.9±1.7	3.8
342-02	343.0	-1.2	1.5	W	1.9±1.3	2.0
356+00					($\lesssim$ 2)	2.6*

confirmation.

Five 2CG sources are strongly confirmed, in that
the corresponding SAS II peaks satisfied the strict significance
and width criteria. A comparison of the fluxes from Table
4.1 is made in Figure 4.3. Allowing for the possibility
of temporal variability between the SAS II and COS B
observations the best SAS II estimate is presumably between
the two SAS II flux estimates; that at maximum significance
and that at the 2CG position. The ratio of the average
COS B fluxes to the average for SAS II is 1.31 and 0.91
for the upper and lower SAS II estimates respectively.
The mean = 1.1 and is very close to unity. We consider
these 5 excesses as significant, that is genuine gamma-
ray sources. The consistency of the flux estimate also
suggests that long term variability is much less than
the statistical precision of these measurements.

SAS II gives a reduced level of support for 12 further
2CG sources, the latter set in Table 4.1 and those in
Table 4.2. These peaks are detected in SAS II. However
their significances lay below the strict level and in
3 cases the widths are inconsistent with that expected
for a point source. In that these peaks are detectable
in the SAS II data does offer some confirmation to the
COS B observations. It is interesting to compare the
fluxes for these sources as measured by both experiments,
shown in Figure 4.4. The agreement is reasonable when
it is remembered that the SAS II values are the peak values
and the best estimate (as in Figure 4.3) is likely to
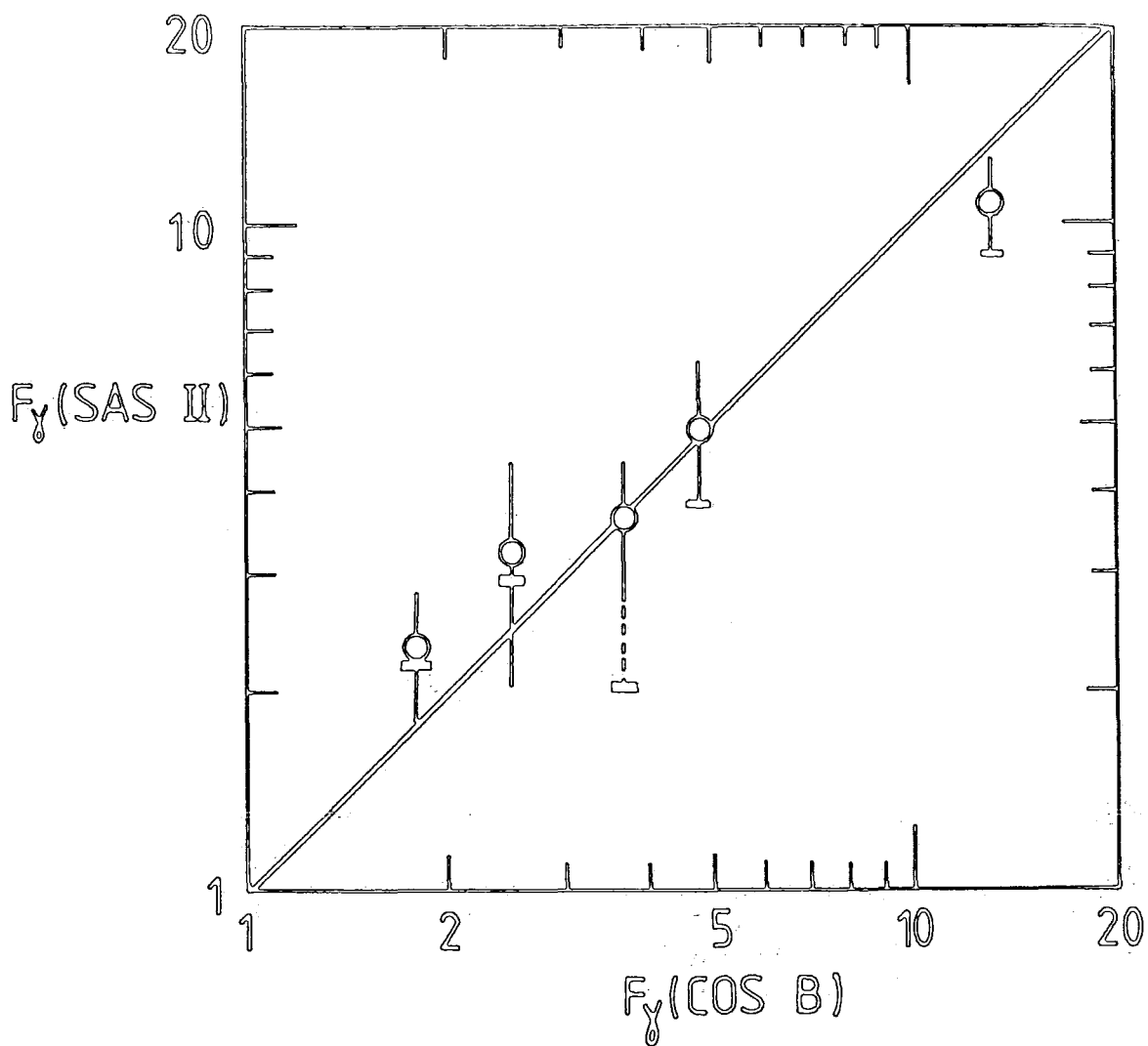
Figure 4.3 Comparison of the fluxes recorded for
the 5 strongest 2CG candidate sources in Table 4.1.
Two estimates are made for SAS II : open circles
corresponding to the peak value for the source (which
is often not coincident with the COS B position)
and horizontal bars corresponding to the SAS II
flux at the COS B peak position.
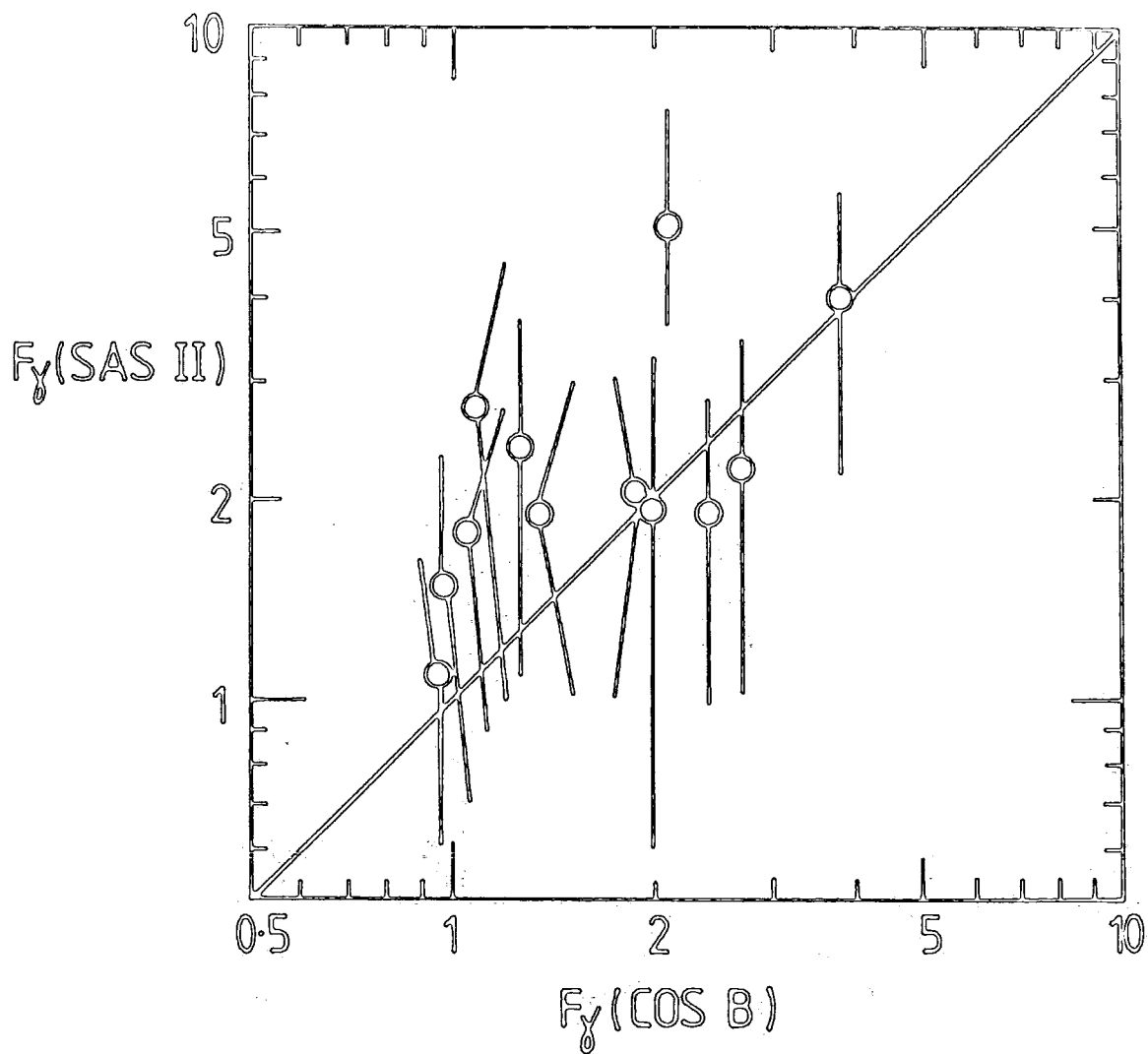
Figure 4.4 Comparison of the fluxes recorded for
the same sources by SAS II and COS B, where the
significance limit of the SAS II source is poorer
than that for COS B.

be about 10% below this level.

There remains 5 2CG sources for which the SAS II
data are unable to offer confirmation in the sense of
peaks being observable above the background. Nevertheless
at these positions we estimate the upper limit to the
SAS II fluxes (Table 4.2). Most of these sources have
low fluxes as measured by COS B (F_γ < 2.6 flux units)
suggesting that some will be undetectable by SAS II.
Two of the strongest of these sources are atypical. The
data collected by COS B suggested that 2CG 284/288 probably
constitute an extended region of enhanced emission associated
with the Carina spiral arm. The region around 2CG 356
was observed 5 times yet this source was only detected
in 1 observing period. Clearly if this object exhibits
strong temporal variability it is likely that its non-
detection by SAS II may be attributed to a quiescent state
at that epoch. It is worth recalling that this source
is close to the Galactic centre a region which is known
to exhibit temporal variability at lower energies, the
511 keV electron positron annihilation line (Section 2.2).
Further observations of this region are needed before
firm conclusions can be drawn on the possible gamma-ray
sources present and the nature of their emission processes
at different energies. Solely on the basis of the SAS II
analysis it is not possible to rule out the existence
of the 3 remaining sources 2CG 013, 065 and 095 which
have F_γ , COS B = 1.0, 1.2 and 1.1 flux units respectively.

Inspection of Table 4.1 shows that 5 sources are visible in the SAS II analysis with significance $^C s/\sigma_0' \geqslant$ 3.4. As this significance level corresponds to 1 spurious source being detected there is seen to be an observed overabundance. Adoption of the stricter significance (corresponding to 10^{-2} spurious sources) still results in 1 candidate source (l,b : 125.3°, -0.4°) being visible in the SAS II data set yet remaining undetected by COS B. A check of the published COS B contour maps (Mayer-Hasselwander et al., 1982) reveals no evidence for point-like excesses at the positions of the 5 unidentified SAS II candidate sources. While this search cannot be considered conclusive it is most unlikely that these 5 excesses are genuine in the sense of being point objects with $F_\gamma > 1$ flux unit. It is more probable that they are upward statistical fluctuations of the underlying background, reflecting a true overabundance on the expected spurious source rate.

We consider the sources common to both the 2CG analysis and the present work, regardless of their significance but satisfying the width criterion. There are 22 2CG sources and 14 counterparts visible in SAS II. The Log N - Log S distribution for these two sets is given in Figure 4.5 along with that for the SAS II sources satisfying the strict significance requirement ($^C s/\sigma_0' \geqslant 4.28$). Both SAS II distributions are scaled to allow for incomplete sky coverage. Above about 2.5 flux units the agreement among the distributions is good. It is seen that the
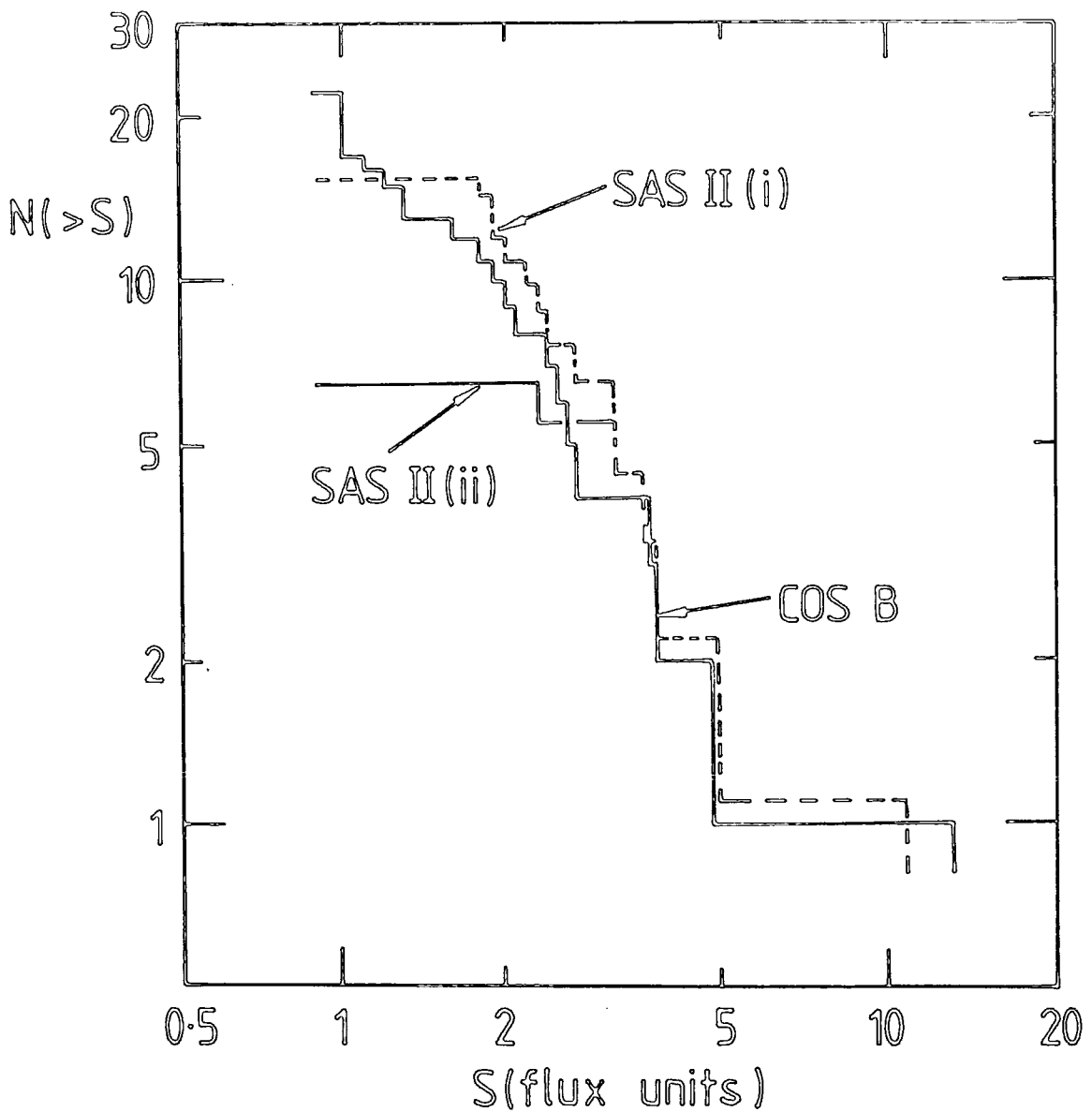
Figure 4.5 Log N – Log S distributions for the
COS B and SAS II catalogues. SAS II (i) : sources
seen in both experiments, down to $C_s/\sigma_o' \simeq 1.5$ for
SAS II. SAS II (ii) : sources seen in SAS II with
$C_s/\sigma_o' > 4.28$.

high significance limit results in the loss of the weaker
2CG sources. Adopting the lower flux limit for SAS II
sources at 2.5 flux units we can compare with that for
COS B, 1.0 flux units. Again the effective count ratio
is seen to be about $2.5^2 \simeq 6.3:1$ in confirmation of previous
estimates. The fluxes measured by SAS II are slightly
larger than the corresponding COS B values. This may
be due to differences in absolute zero level between the
two experiments (primarily the large and uncertain COS B
instrumental background). However, part of the effect
can be attributed to the method of analysis in which the
SAS II fluxes are always measured at the maximum peak
nearest the 2CG positions and thereby biasing our measure-
ments to an overestimate of the COS B value by about 10%
(Figure 4.3).

4.6   The nature of sources detected by the cross-correlation
      technique.

It is pertinent at this stage to briefly discuss
the nature of the sources detected by COS B and of those
candidate sources from our own analysis. There is good
evidence suggesting an overabundance of spurious sources,
assuming of course, the 2CG catalogue forms a complete
sample down to 1 flux unit. The SAS II spurious sources
have a wide flux range (1.4 - 3.8 flux units) and given
the better exposure of COS B it is unlikely that poor
statistics can explain their non-detection by COS B.
The good consistency in measured fluxes for the 5 strongly
confirmed 2CG sources suggest that time variability is

not a property of genuine sources and this explanation

of the SAS II unidentified candidate sources must also

be considered most unlikely. Li and Wolfendale (1982)

found evidence from their Monte-Carlo analysis of COS B

(E_γ > 100 MeV) for the overabundance of spurious sources.

This effect does appear to be real and both analyses strongly

suggest the gamma-ray data more structured than expected

statistically. That is they contain fluctuations of the

structured background which mimic the appearance of genuine

point sources.

We conclude that cross-correlation is a powerful

technique for source analysis. However the complexity of

the gamma-ray data suggest that three distinct features

are likely to be involved:

(i) Genuine discrete sources such as Crab, Vela and Geminga.

(ii) Giant molecular cloud complexes irradiated either

by the ambient cosmic ray flux or by internal cosmic ray

sources and appearing point like because of the limited

angular resolution. These are regions of diffuse emission

which contribute to the structured nature of the observed

background emission. Their role as pseudo gamma-ray sources

is considered by other workers and is more fully discussed

in Section 3.5.

(iii) Spurious peaks which due to the comparatively low

statistics and uneven background appear as random upward

fluctuations.

With improved resolution and statistics the objects in

categories (ii) and (iii) would be more tightly defined.
The case of 2CG 353/ ρ Oph (Section 3.5) is of relevance
in this context.

CHAPTER FIVE

A MONTE-CARLO ANALYSIS OF THE GALACTIC
GAMMA-RAY SOURCE CONTRIBUTION

5.1 General comments

The early work on radio source counts has parallels
with the present situation regarding gamma-ray sources.
Radio source observations were originally expected to
help reveal the geometrical nature of the universe through
measurement of the Log N - Log S distribution at very
low flux levels. However, interpretation of the data
was inconclusive because of source confusion at low flux
levels and the likelihood that evolutionary effects in
the sources would distort the counts at high redshifts.
Murdoch et al. (1973) discussed the effects of noise and
confusion on the radio source identifications, which they
showed had a significant effect on the observations even
at the 5 sigma level. They concluded that at weaker flux
levels the source count was progressively enhanced because
of upward statistical fluctuations in the number of sources
at even fainter flux levels. The statistical noise
effectively degraded the source count in a particular
flux bin, led to an overestimate of the true flux of weaker
sources, and the effect on the integral count was cumulative
below that flux level. For the case of purely Gaussian
noise the effect of the error distribution on the true
flux and differential count can be calculated analytically.
However, for confusion limited surveys this problem is
best treated by a Monte-Carlo method.

The present observational status of gamma-ray sources

is similar, in that confusion is also important at the
weakest flux levels, as borne out by the previous chapter
and the results of other workers (Section 3.5). Whereas
for radio sources the confusiuon is due to the cumulative
effect of weaker sources, it is generally believed that
gamma-ray sources are observed against a background pre-
dominantly diffuse in origin. For gamma-ray sources, confusion
is due both to proximity with other weak sources and to
the difficulty of detection when viewed against a highly
structured background. It is clear that the low angular
resolution of present detectors plays a significant role
in these processes. We can adopt the methods used to
correct the radio source counts. Given an adequate model
of the gamma-ray background, Monte-Carlo methods can be
employed to study confusion in relation to gamma-ray sources.

5.2   The Monte-Carlo background model

Previous analyses and interpretation of the gamma-
ray data have been extensively discussed in chapter 3.
The observed emission is predominately Galactic in origin
and it is clear that, in principle at least, most of the
emission can be explained in terms of cosmic ray interactions
with the gas of the interstellar medium. As a model of
the diffuse gamma-ray emission we therefore adopt the
distribution of total gas and cosmic rays throughout the
Galaxy. The expected gamma-ray intensity along a given
line of sight (l ,b) can be expressed as

$$I_\gamma(l,b) = \left(\frac{q}{4\pi}\right)\int n(l,b,r)\left[I_{cr}(l,b,r)/I_o\right]\,dr \qquad 5.1$$

where $q/_{4\pi}$ is the local gamma-ray emissivity, n the gas density ($HI + 2H_2$), and I_{cr}/I_o the ratio of the cosmic ray intensity to the local value. Atomic hydrogen is sufficiently well mapped to enable an accurate distribution to be obtained, within the limitations imposed by the choice of rotation curve and the effects of random cloud motions. The situation with CO is similar. However the inferred molecular hydrogen distribution is conditional on the conversion parameter ($CO \rightarrow H_2$) and its variation throughout the Galaxy. There is only modest information available on the large-scale Galactic distribution of cosmic rays. Indeed most of the evidence favouring a local gradient ($\lesssim$ 2-3 kpc) is dependent on knowing the gas distribution (Section 3.3). Further towards the inner Galaxy our knowledge of the cosmic ray intensity is proportionately reduced due to both the greater un-certainty in the mass of gas (primarily H_2) and to the unknown contribution of discrete gamma-ray sources to the observed gamma-ray emission. Although the arguments concerning Galactic cosmic ray gradients, gamma-ray sources and the total mass of gas are to a large extent inter-related, the current best estimates (Section 3.3) indicate that the cosmic ray intensity in the inner Galaxy is unlikely to be greater than that locally by a factor of more than about 3-5. As a simplifying approximation we assume the cosmic ray intensity ($\geqslant$ 1 GeV) to be uniform throughout the entire Galaxy and equal to the local value, 5.1 then reduces to

$$I_\gamma (l,b) = (q/4\pi)N(HI + 2H_2) \qquad\qquad 5.2$$

We use this as the basis for our model of the diffuse gamma-ray emission, implicitly assuming that discrete sources (pulsars, unusual objects) make only a small contribution to the gamma-ray background. This latter assumption is of crucial importance when we come to interpret the present data on discrete gamma-ray sources and we shall return to this later (Section 5.13).

5.3   The HI and CO data

The Weaver and Williams (1973) survey of 21 cm atomic hydrogen emission covers the region l : $10°$ - $249°$, $|b| < 10°$. These data give velocity profiles sampled every $0.25°$ in latitude, $0.5°$ in longitude and were obtained with the Hat Creek Observatory 85-foot telescope (half power beam width = $35'.5$). Column densities are obtained by assuming that the gas has a spin temperature T = 125K, to correct for optical depth effects. Close to the Galactic plane, especially in the inner Galaxy, the observed temperature profiles are often optically thick. This is partly due to the large mass of gas towards the Galactic centre but is also affected by velocity crowding of the Doppler shifted profiles in this region. By assuming an infinite spin temperature (i.e. optically thin) the reduction in the column density for the optically thick case is found to be generally $\lesssim 20\%$. The column density N_{HI} is related to the observed temperature profile by:

$$N_{HI} = 1.823 \times 10^{18} \int T\, dv \qquad atoms\ cm^{-2} \qquad 5.3$$

Turning to the large scale distribution of molecular
hydrogen, its magnitude is not well known. Its presence
can be observed directly as emission from transitions
between vibrational states. However, this technique is
limited to local regions ($\lesssim$ 2 kpc) because of saturation
effects at greater distances. The large scale distribution
must be inferred indirectly from observations of other
molecular species, principally CO. It is conventional
to believe that H_2 is substantially confined to dense
regions - the so-called molecular clouds. Inside these
regions the H_2 is shielded from photo-dissociation by
an external shell of HI and HII. The internal chemistry
of molecular clouds has only recently become the subject
of intense study, partly because of the complexity and
profusion of the possible chemical reactions. Nevertheless
millimetre and submillimetre observations of these regions
have confirmed the existence of many complex molecular
species. CO is the most abundant of these species and
as such is an ideal tracer of the large scale distribution
of molecular clouds because it is rotationally excited
through collisions with other molecules (principally H_2).
The most abundant isotope, ^{12}CO, decays (J = 1$\rightarrow$0) emitting
a characteristic wavelength; λ = 2.6 mm ν_o = 115.3 GHz.

^{13}CO ($\lambda = 2.7mm$ $\nu_0 = 110.2GHz$) has been detected from
the more intense sources. Other isotopes (e.g. $^{12}C^{18}O$)
and higher transitions (J = 2 $\rightarrow$ 1) have also been detected
but are less useful in that these observations are limited
to a few sources of intense molecular emission.

The Columbia group have carried out a survey of
^{12}CO (J = 1 $\rightarrow$ 0) covering l : 10° - 100°, b: -5° to
+ 10° and l : 100° - 180°, b: -3° to + 5° (Cohen et
al. 1980; Dame, 1984). These data were obtained using
their 4m telescope, with a resolution (half power beam
width) = 0.125°.

It is commonly assumed that the ^{12}CO line is optically
thick, the rotational levels being thermalized within
the cloud. In this case the observed antenna temperature
uniquely measures the gas kinetic temperature of the
source. This has been confirmed for those clouds in
which higher order CO transitions have been observed.
For these lines similar gas kinetic temperatures are
inferred, supporting the reliability of CO as a thermo-
meter. For sources not in local thermodynamic equilibrium
(non-LTE) calculations of gas kinetic temperature and
column density rely on a radiative transfer model.

It has been shown (e.g. Solomon et al. 1979, Cohen
et al. 1980) that for the LTE approximation the molecular
hydrogen column density N_{H_2} can be expressed as

$$N_{H_2} = X \int T(^{12}CO)dv \qquad\qquad 5.4$$

We follow Arnaud et al. (1982) in adopting X = 2.3 x
10^{20} mol. cm^{-2} (K $kms^{-1})^{-1}$, a value which is by no means

unique. Sanders et al. (1984a) have extensively discussed the arguments surrounding the calibration of X . They note that a wide range of X: $(1.0 - 7.2) \times 10^{20}$ has been adopted by various workers in the past and this in part has led to inconsistency among the different estimates of the total mass of H_2 in the Galactic plane.

5.4 The CO→H_2 calibration, the metallicity gradient

The preferred method of calibrating X has relied on measurements of visual extinction towards local dark clouds (e.g. Dickman, 1978) to give column densities. These are compared with column densities inferred from CO observations. While this method in principle, gives an accurate calibration for an individual cloud, the evidence suggests that X varies from cloud to cloud (Bhat et al. 1984c). These workers find X = (1.25 - 1.5) x 10^{20} mol. cm^{-2} $(K\ kms^{-1})^{-1}$. Many of the local clouds used to calibrate X have relatively low mass ($\sim 10^{2-3} M_\odot$). Giant molecular clouds are believed to be more massive ($\sim 10^{5-6} M_\odot$), probably have higher temperatures and different chemical composition; reflecting the increased activity (turbulence, star formation, supernovae ...) in the inner Galaxy. While it is by no means certain that a locally determined X is applicable to the giant molecular clouds we follow previous workers in implicitly assuming this to be the case. That is, the nearby clouds constitute a reliable sample of those deeper into the inner Galaxy.

Alternative calibration methods have also been employed. The SAS II and COS B data have been compared to the large-scale distribution of H I and CO in the first and second quadrants to estimate X , assuming a uniform cosmic ray distribution throughout the Galaxy. Issa and Wolfendale (1981a) and Lebrun et al. (1983) found X = 1.2 x 10^{20} mol. cm^{-2} (K $kms^{-1})^{-1}$ and (1.0 - 3.0) x 10^{20} mol. cm^{-2} (K $kms^{-1})^{-1}$ respectively, though these analyses are limited by the asusmptions made about the cosmic ray distribution and the role of discrete gamma-ray sources. Nevertheless they are in reasonable agreement with the preferred values obtained locally. In the following chapter we examine the Orion molecular clouds in a further attempt to estimate X appropriate for local massive clouds. From this analysis we find X = 1.85 x 10^{20} mol. cm^{-2} (K $kms^{-1})^{-1}$.

Apart from the uncertainty surrounding the mean value of X, an important additional factor must be considered; the metallicity gradient. This gradient can be characterised by the ratio of Carbon to Hydrogen ([C] /[H]) and is observed to decrease with increasing Galactocentric radius (Pagel and Edmunds, 1981). The variation is due to the increased rate of processing of the interstellar medium towards the inner Galaxy (gas →stars →supernovae →gas). The ratio [CO] /[H] in molecular clouds is in consequence likely to increase with decreasing Galactocentric radius and several workers (e.g. Blitz and Shu 1980, Li et al., 1982, Bhat et al.

1984b) have pointed out the implications for the mass

of H_2 inferred from CO. If the metallicity gradient

is expressed as the abundance ratio $M = [C]/[H]$ then

N_{H_2} could be reduced by a factor $M^{-1} \int T(CO)dv$ or perhaps

as much as $M^{-2} \int T(CO)dv$. The latter reflects the gradient

of $[O]/[H]$ as similar to $[C]/[H]$ and both affect

$[CO]/[H]$. While the existence of the metallicity

gradient is not in dispute there is no agreement as

to whether it affects the estimates of H_2, and if it does,

to what extent.

5.5 Simulation of the diffuse gamma-ray background

For the present analysis we assume the metallicity

to have no effect on N_{H_2} and calculate column densities

direct from the observed ^{12}CO line intensities using

5.4. Predictions of the expected gamma-ray intensity

follows from 5.2 where we assume the local emissivity

$q/4\pi(>100$ MeV$) = 2.2 \times 10^{-26}$ ph at^{-1}sr^{-1}s^{-1} as derived

by Issa et al. (1981). This value is not unique (see

the summary in Tables A1,A2), nevertheless it is chosen

to enable direct comparison with previous work on Monte-

Carlo analysis of pseudo-sources (Li and Wolfendale,

1982). The evidence discussed previously (Section 3.3)

suggests a modest Galactic cosmic ray gradient. The

resulting overproduction of gamma-rays in the inner

Galaxy would be countered (in an approximate manner)

if we were to adopt the metallicity correction to reduce

H_2 in our model. It is interesting that these effects

act to reduce the probable error in the present model.

After binning (Δ l x Δ b = 0.5° x 0.5°), and converting to flux, an expected count map is derived. By considering the 2CG source fluxes and observed counts (Hermsen 1980) we estimate the count rate for a typical source as N_s = 80 counts/flux unit (1 flux unit = 10^{-6}ph cm^{-2}s $^{-1}$, henceforth used throughout). This is confirmed by Hermsen (private communication). We also adopt N_s = 40 counts/ flux unit as a suitable lower bound on this parameter. The count map data are then convolved to the COS B resolution (E_γ > 100 MeV) using the appropriate point spread function (Section 4.1).

Figure 5.1 is a contour map of the expected gamma-ray count map. These data form the basis for the Monte-Carlo background. The structure is confined to within a few degrees of the Galactic plane and is dominant in the inner Galaxy. This is a reflection of the highly structured nature of the H_2(CO) distribution which is predominantly clumped into giant clouds, whereas the HI is rather smoothly distributed throughout the inter-stellar medium. After allowing for Poisson fluctuations (before convolution to the COS B resolution), representing the statistics of counting, a typical count map is shown in Figure 5.2. The small scale structure is now more apparent, and it is this noise which limits the detection of genuine discrete sources.

As an interim check 10 Poisson samples of the back-ground are generated and searched for spurious sources using the cross-correlation method. That is, we look
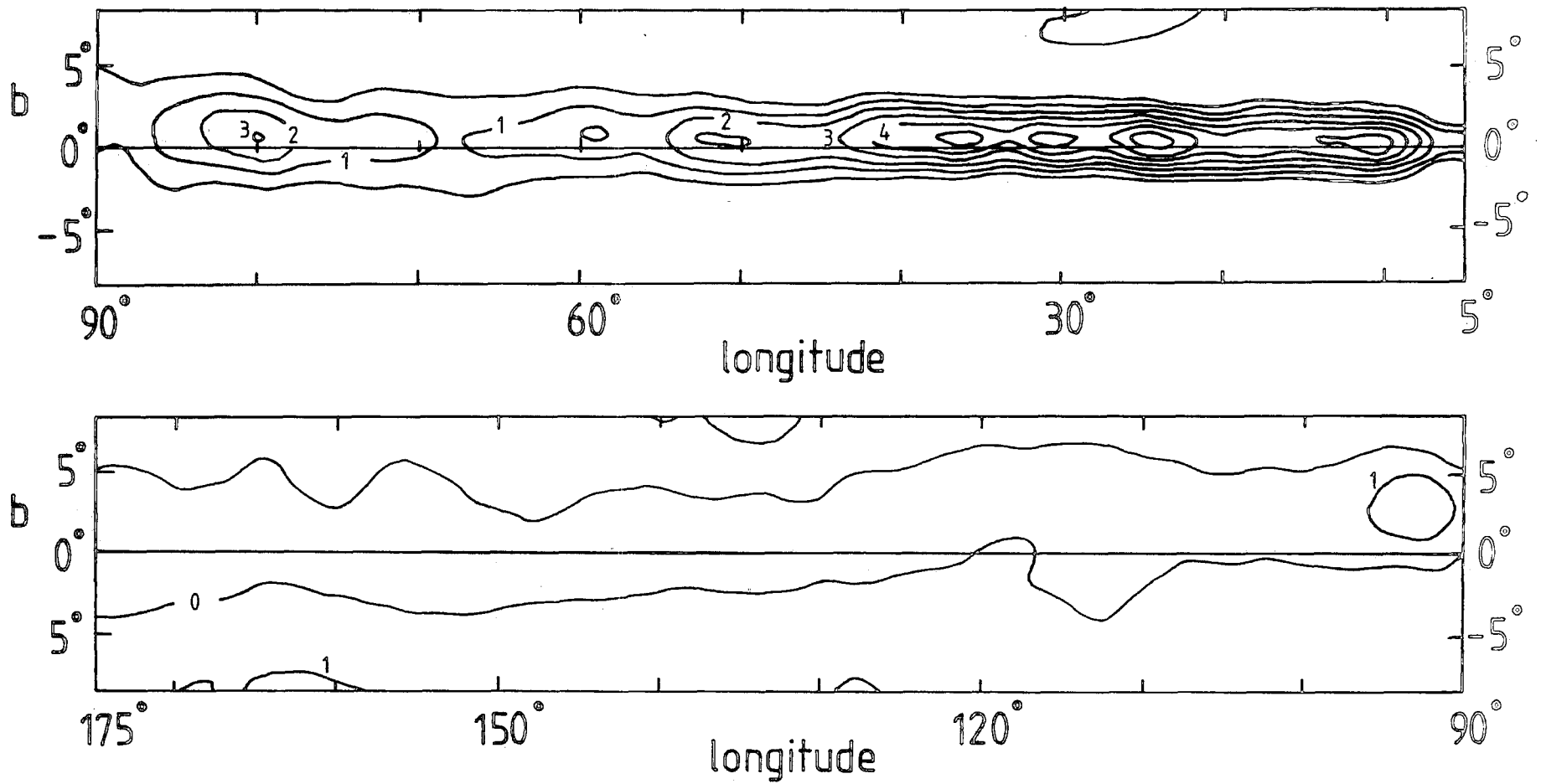
FIGURE 5.1   Cross-correlated flux expected from the background. Contours are F_γ ($>$ 100 MeV) = n x 0.5 x 10^{-6}ph cm^{-2} s^{-1} with a bin size $\Delta 1$ x Δ b = 0.5° x 0.5°
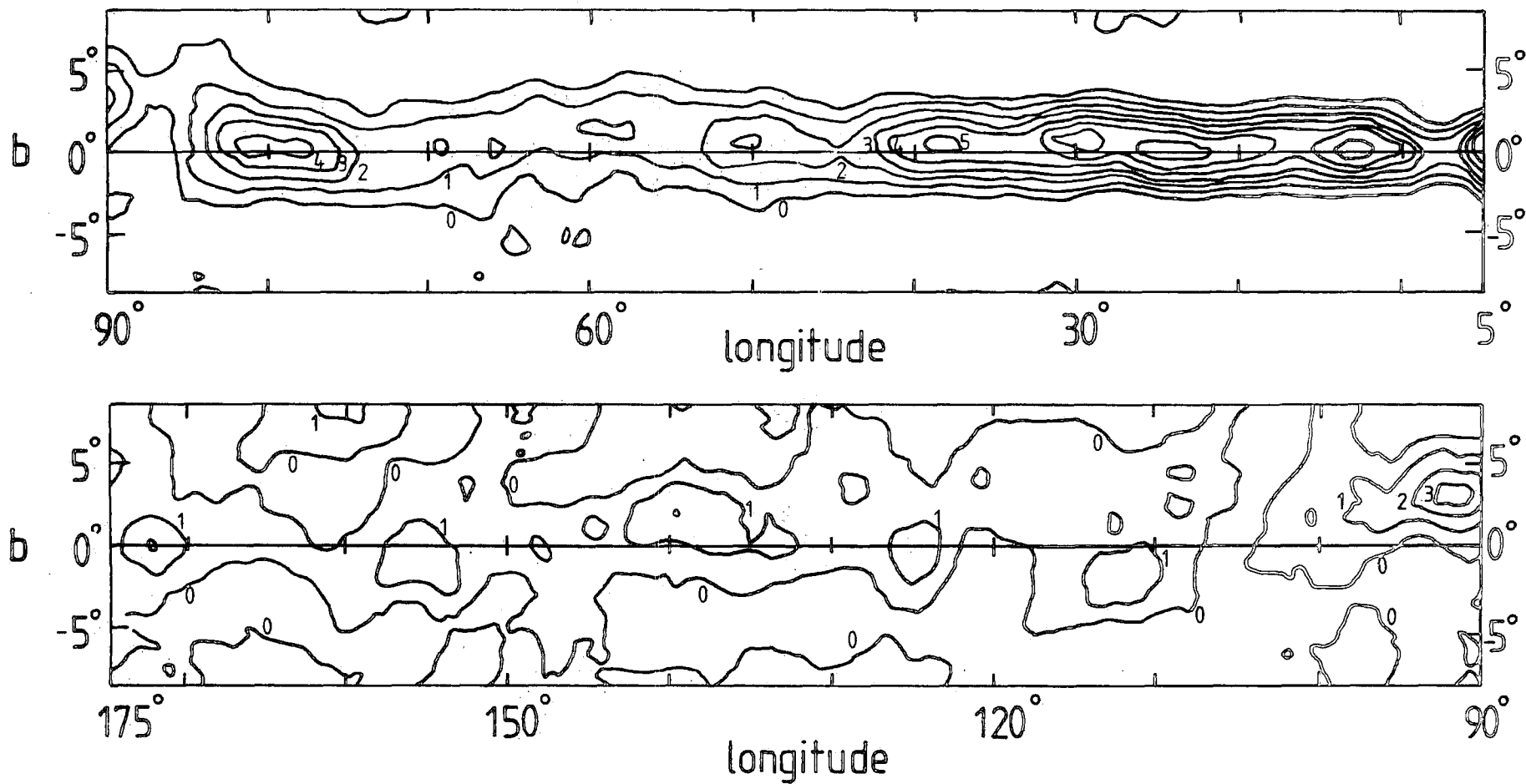
FIGURE 5.2   Cross-correlated flux of a typical Monte-Carlo background sample.
Contours are $F_\gamma (> 100\ \text{MeV}) = n \times 0.5 \times 10^{-6} \text{ph cm}^{-2}\text{s}^{-1}$ (negative fluxes
omitted) with a bin size $\Delta 1 \times \Delta b = 0.5° \times 0.5°$.

for peaks satisfying the COS B significance and width
criteria (Section 4.2). The frequency of occurrence
of these upward statistical fluctuations are found to
be in close agreement with the more extensive earlier
work by Li and Wolfendale (1982), lending weight to the
correctness of the present analysis.

5.6 Monte-Carlo simulation of discrete sources

   We proceed to simulate the count distribution for
a genuine point source. For a given source flux the
point spread function distribution of the count is super-
imposed on the expected background count map. The combined
data are then subjected to Poisson fluctuations. Each
sample is analysed for the expected sources using the
cross-correlation method. In addition to the COS B
criteria, already discussed for source identification
(Section 4.2), a further selection criterion is also
imposed. For positive identification of the simulated
source we require the observed peak to lie within 3.6°
(the angular resolution of the data, $E_\gamma > 100$ MeV)
of the original position.

   Four sources are randomly superimposed on a background
data set, widely separated ($1 > 20°$, $|b| < 2°$) to avoid
possible confusion between two or more sources. Different
combinations of position and source strength are used
to give a wide coverage in longitude for the detection
efficiency of each simulated source flux. We simulate
flux levels F_γ = 0.5, 0.8, 1.0, 1.3, 2.0 and 4.0 flux
units, each configuration being treated for both $N_s = 80$

and N_s = 40 counts/flux unit. While the lowest observed

2CG source flux was 1.0 flux units ($|b|$ < 10°), this

was not due to any selection procedure on source flux.

Therefore it is considered appropriate to simulate sources

weaker than this observational limit in addition to

those comparable to the stronger 2CG sources (c.f.

F_γ , Crab = 3.7 flux units). It is expected that confusion

should be negligible for the strongest sources, while

at the weakest flux levels ($F_\gamma \lesssim$ 1.0 flux units) confusion

is expected to dominate the detection efficiencies.

At the intermediate flux levels ($F_\gamma \gtrsim$ 1.0 flux units),

typical of the weakest 2CG sources, confusion with upward

fluctuations of the background structure will also be

important. It is these 2CG sources which have previously

been considered as consistent with fluctuations of the

underlying background structure (Li and Wolfendale,

1982, Arnaud et al., 1982).

5.7 Discrete source detection efficiencies

By using the Monte-Carlo samples we determine the

detection probabilities for each true source strength

as a function of Galactic longitude. The data from

each source sample are combined, and the detection probabilities

are plotted in Figures 5.3 and 5.4 for N_s = 80, 40 res-

pectively. The overall trend as indicated by the solid

line is apparent, indicating detection efficiency

increasing with both Galactic longitude and true

(i.e. expected) source flux. This is as expected in

view of the reduced background structure evident

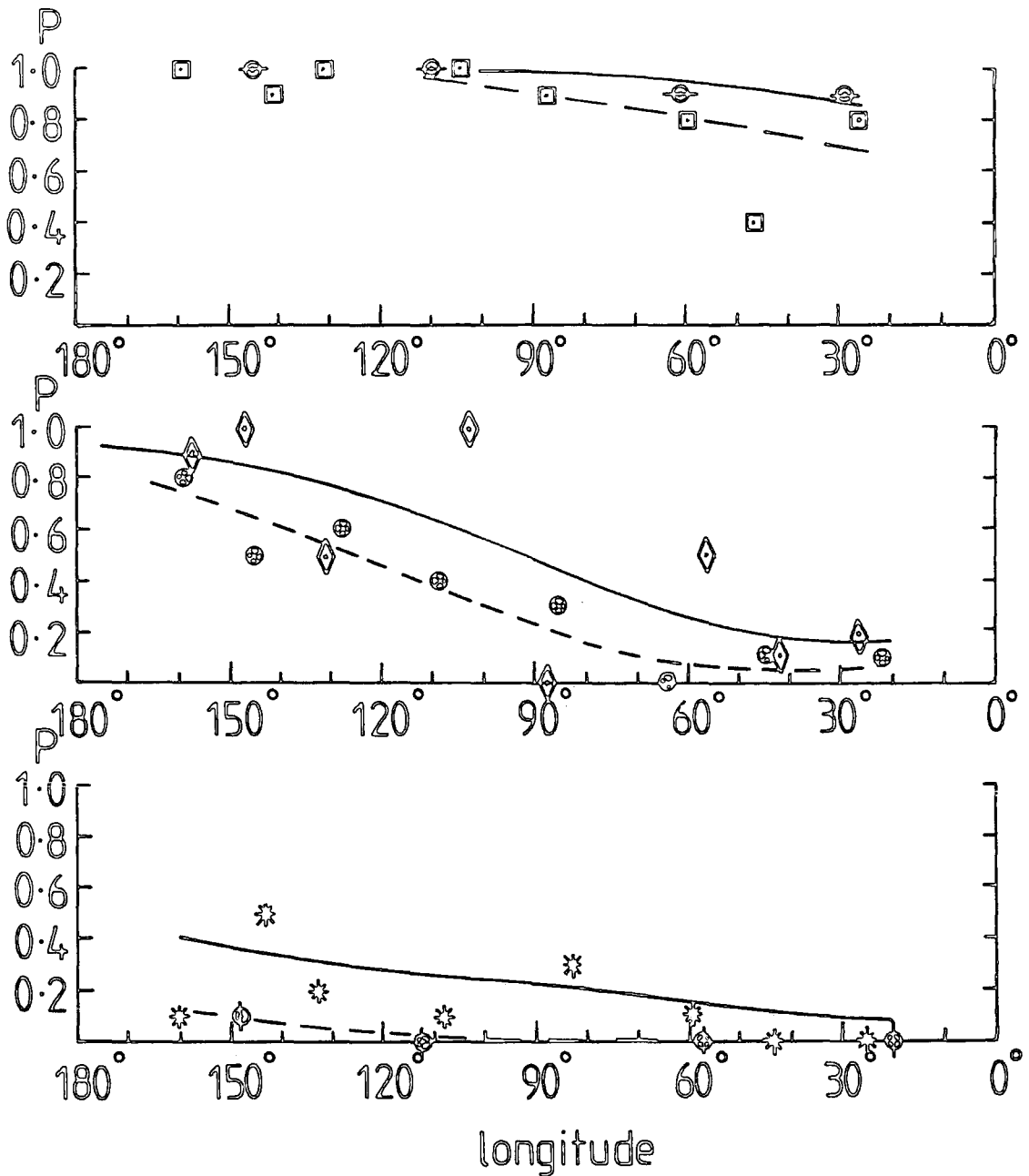Figure 5.3 The longitude variation of the source detection probability as a function of expected flux, each point being based on 10 Monte-Carlo samples. The calculations are for N_s = 80 counts/flux unit. Curves are drawn as a visual aid, illustrating the overall trend.
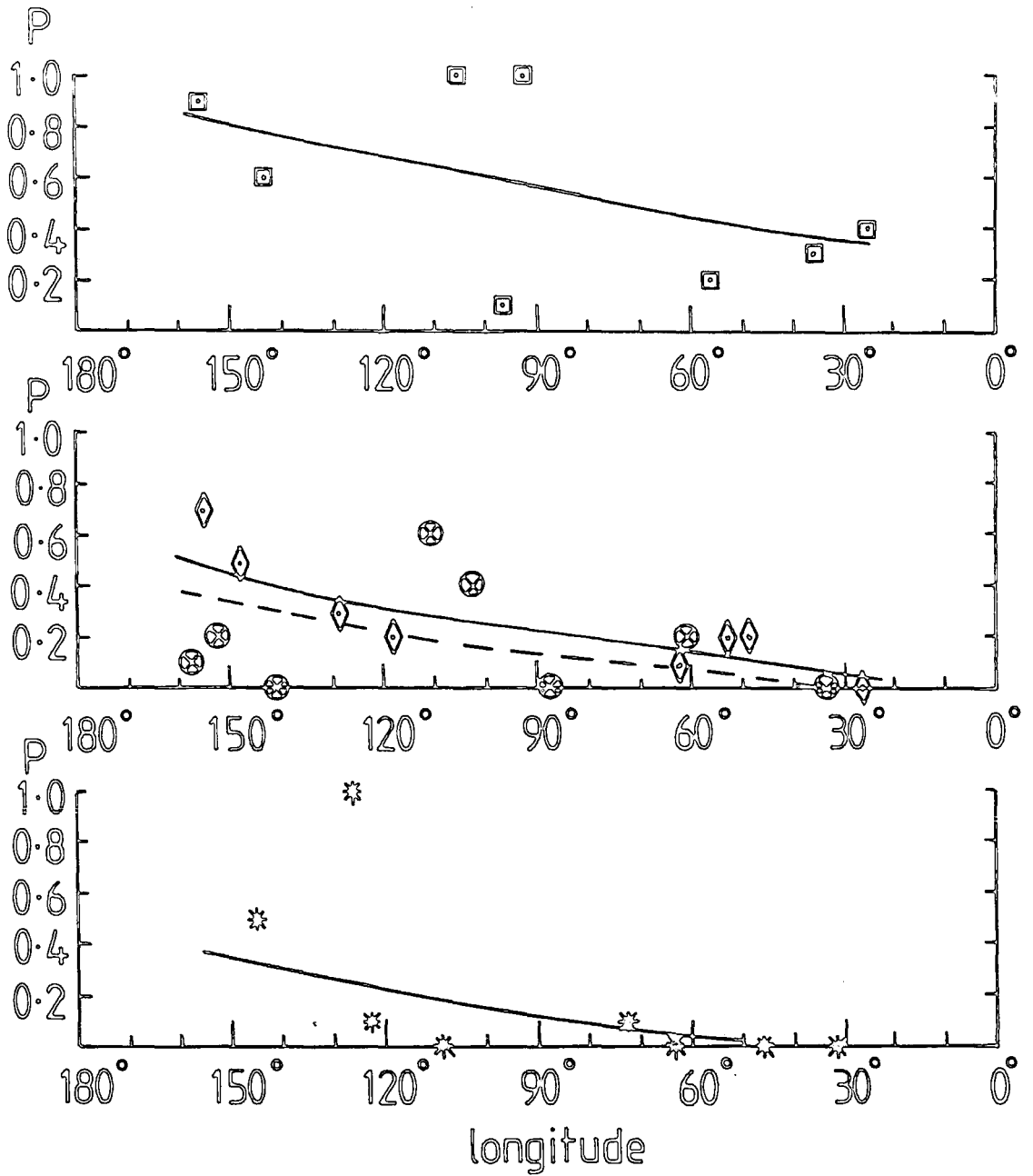
Figure 5.4 The longitude variaiton of the source detection probability as for Figure 5.3 but with N_s = 40 counts/flux unit.

in the outer Galaxy (Figure 5.2), leading to less confusion.

However, several anomalous points are apparent, exhibiting reduced probability at some positions, while for others the reverse is true. Part of this is probably due to statistical fluctuations. However, the data at these positions are further analysed. Close to these positions ($\lesssim 2°$) small scale structure is apparent in the initial background count. In those cases where the background peak is close to the superimposed source the combined counts after fluctuation effectively enhance the true source flux, thereby increasing the detection probability. An initial peak offset from the superimposed source broadens the observed source profile reducing the probability of the source satisfying the width selection criterion. An analysis of the observed source fluxes as a function of the expected flux and Galactic longitude (Figures 5.5 and 5.6) confirms this behaviour. Detected sources (i.e. those satisfying the selection criteria) are found on average to have their true flux enhanced. Interestingly those sources for which F_γ , expected = 0.5, 0.8 flux units are only detectable whenever F_γ , observed $\geqslant$ 1.0 flux units and no sources are detected with F_γ , observed < 1.0 flux units. This seems to account for the lower flux limit of 1.0 flux units evident in the 2CG catalogue ($|b|$ < 10°).
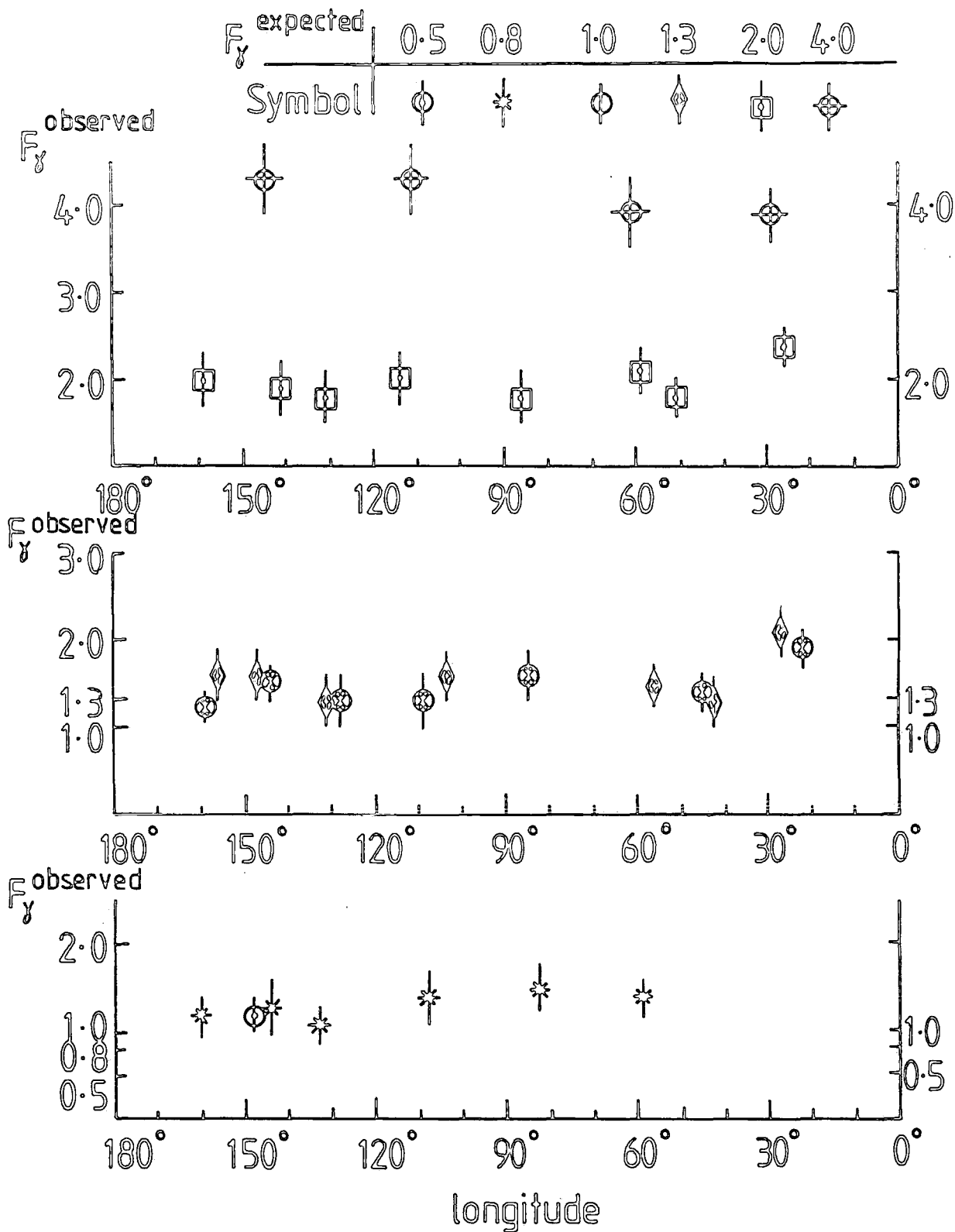
Figure 5.5   The longitude variation of the observed source flux as a function of expected flux for N_s = 80 counts/flux unit.   Error bars are $\pm$ 1σ.

expected

F_γ

	0.8	1.0	1.3	2.0
Symbol	✳	◍	◈	▨

observed

F_γ

3.0

2.0

3.0

2.0

180° 150° 120° 90° 60° 30° 0°

observed

F_γ

3.0

2.0

1.3

1.0

180° 150° 120° 90° 60° 30° 0°

observed

F_γ

2.0

1.0
0.8
0.5

180° 150° 120° 90° 60° 30° 0°

longitude
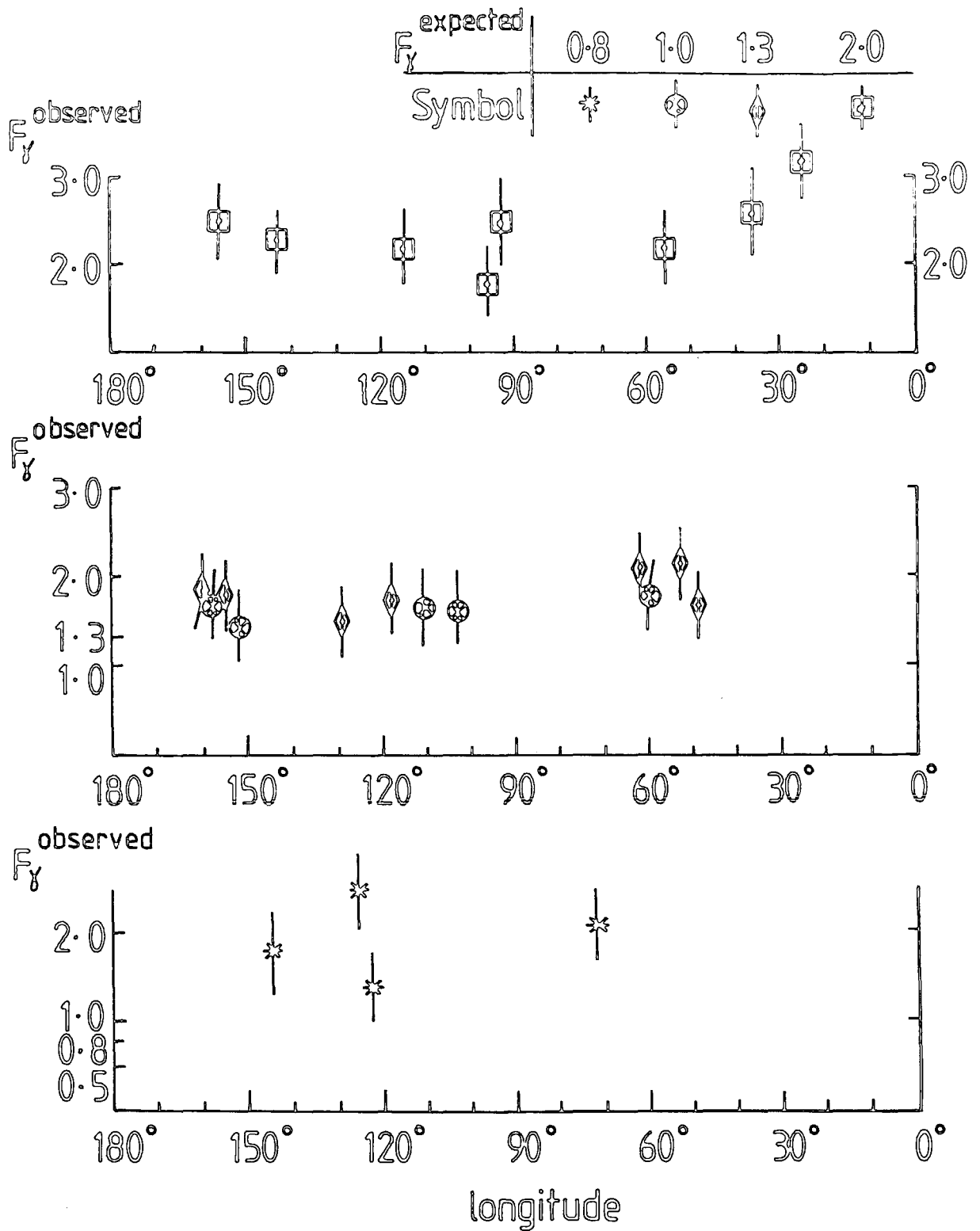
Figure 5.6   The longitude variation of the expected

source flux as for Figure 5.5 but with N_s = 40 counts/

flux unit.

5.8 Application of detection efficiencies to the Log N -

Log S distribution

The results of the Monte-Carlo simulations complement the conclusions of the SAS II analysis (Chapter 4). Specifically we find that the probability of source detection is altered by confusion and that the observed flux is likely to be higher than the true value. The combined effect on the true log N - log S distribution is important at low flux levels where confusion is shown to be significant. The Monte-Carlo analysis gives us information on the relative numbers of sources which will remain undetected in a typical observation of the parent population. We seek to combine these data with the observed 2CG source distribution to correct for losses, and thereby obtain the true distribution.

We begin by assuming that the 2CG catalogue is genuine and complete down to 1.0 flux units, giving 22 sources with $|b| < 10°$. The source detection efficiencies (Figures 5.3 and 5.4) are observed to vary continuously with longitude, and ideally these correction factors should be applied similarly. However, the limited statistics of the observed sample necessitate the use of mean corrections applied over large regions of the sky. The sources are considered in two specific regions, the inner Galaxy $(270° < l < 90°)$ and the outer Galaxy $(90° < l < 270°)$.

The average detection efficiencies for these longitudes are derived directly from Figures 5.3 and 5.4 and are plotted in Figure 5.7 as a function of true source flux
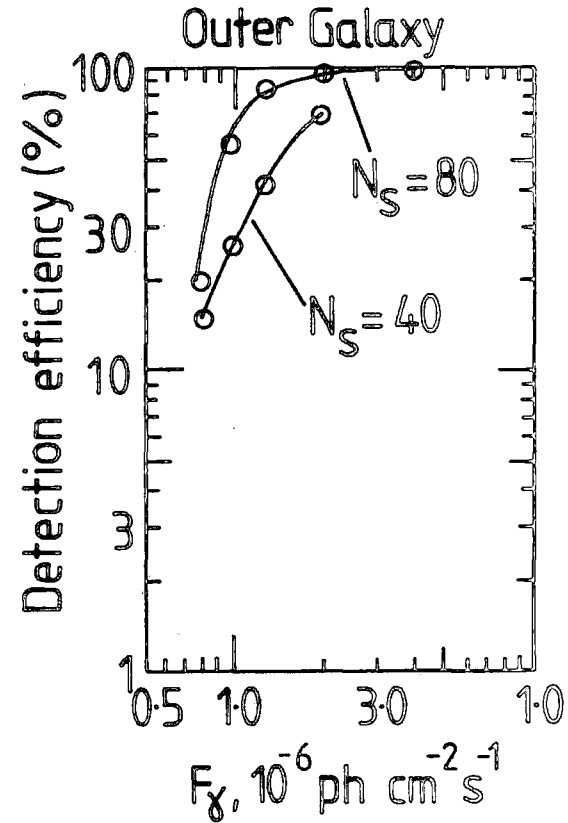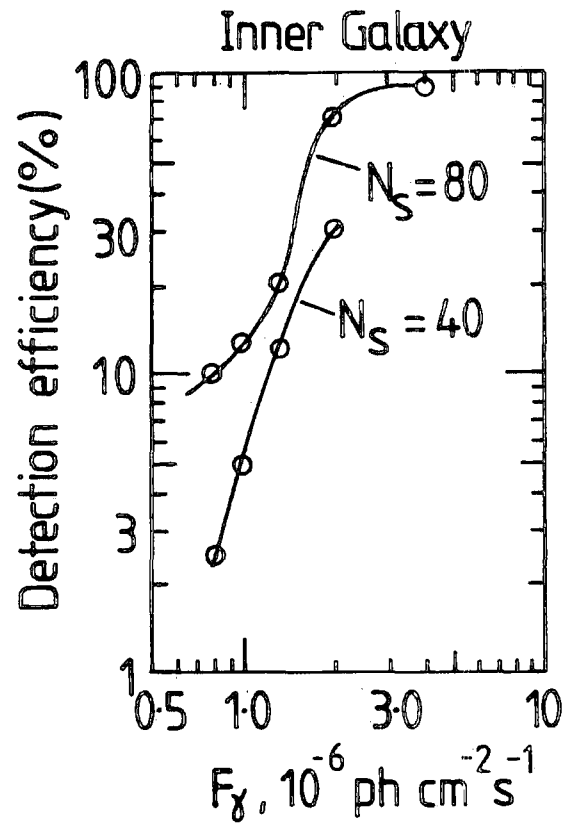
Figure 5.7   Source detection efficiencies derived from Figures 5.3, 5.4 by averaging over the respective longitude ranges for the Inner Galaxy ($270^O < 1 < 90^O$) and the Outer Galaxy ($90^O < 1 < 270^O$).

for the two cases N = 80, 40 counts/flux unit. The 2CG

sources in the inner Galaxy are binned in $\triangle S = 0.2$

flux units to obtain the differential count $(\triangle N/\triangle S)$

after interpolating between the discrete flux levels

of the integral count. The binned counts are then corrected

using the efficiencies of Figure 5.7, making allowance

for the small effect of flux enhancement apparent in

Figures 5.5 and 5.6. We only correct for the case N_s = 80

counts/flux unit and note that relative to the N_s =

40 counts/flux unit corrections this is a lower limit.

However, the former is considered more appropriate for

the 2CG sources, the latter serving only as an upper

bound to illustrate the trend of the corrections. That

is, detection efficiency decreases with reduced exposure.

The resultant distributions are rebinned and a power

law least squares regression fitted. The corrected

distributions, with statistical errors and best fit power

laws, are plotted in Figure 5.8. The procedure is repeated

for the sources in the outer Galaxy.

Comparison of these distributions shows that the

two are intrinsically different in terms of both absolute

slope and magnitude at 1.0 flux units. We interpret

this as evidence for a population density which varies

strongly with Galactocentric distance. It is worth

remembering that the corrected source distributions

(Figure 5.8) correspond to the true distribution of
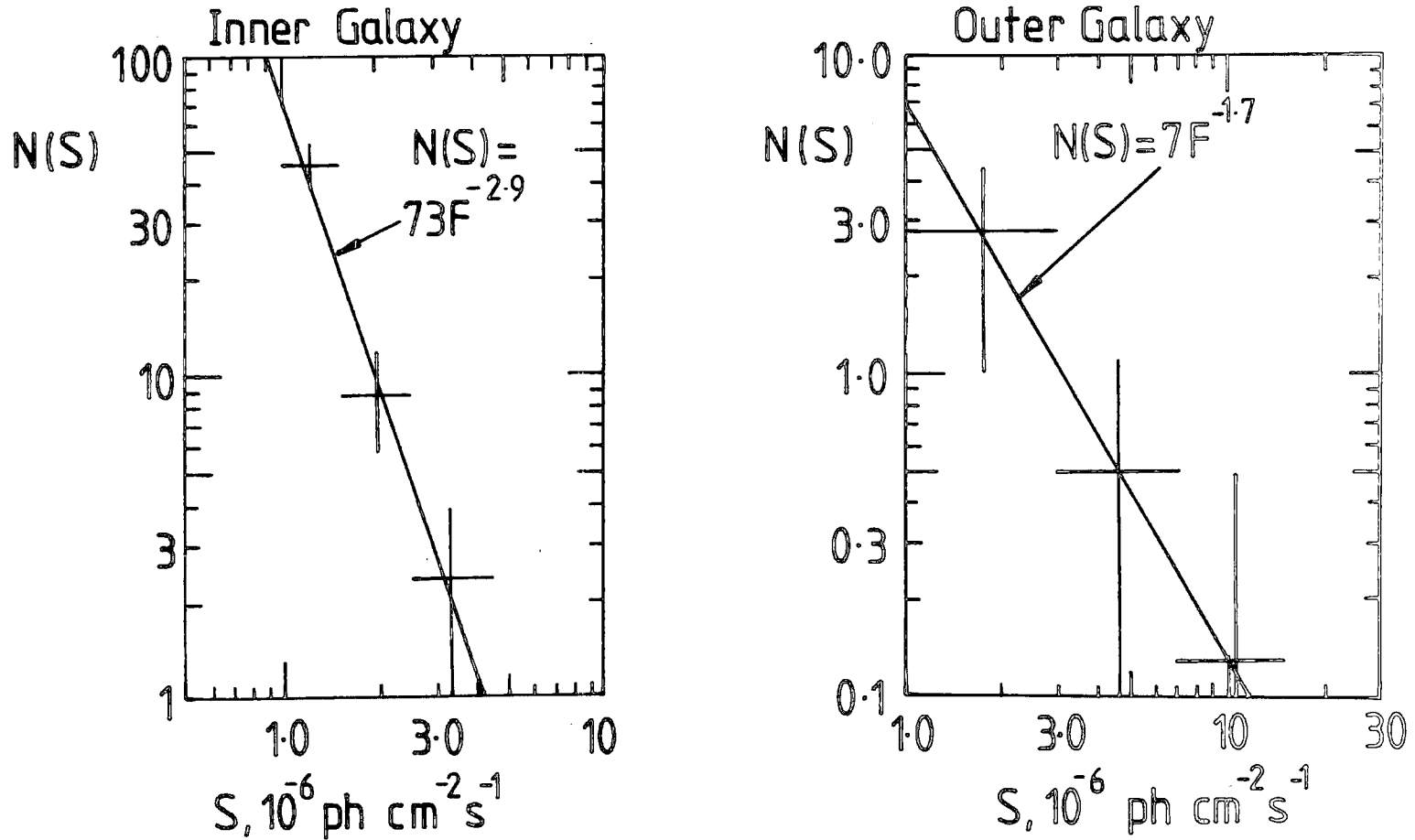
sources down to 1.0 flux units and the overall Galactic

Figure 5.8   Log N – Log S distributions derived from the total 2CG source list (|b| < 10°) after applying the appropriate correction factors from Figures 5.5, 5.6, 5.7.   Error bars are ± 1σ and the least-squares power law regressions are given in each case.

distribution necessarily extends much fainter. Knowing
the minimum source flux level we can therefore estimate
the total source contribution.

The minimum source flux is not known but we can
make the assumption that the Crab pulsar (2CG 184) is
a mono-luminosity source typical of the Galactic population.
Its distance ($\simeq$ 2 kpc) and flux (= 3.7 flux units)
correspond to a lower flux limit $\simeq$ 0.03 flux units
when placed on the far edge of the Galaxy (radius 15 kpc).
In the inner Galaxy we assume the power law distribution
derived above 1.0 flux units can be extrapolated down
to this lower limit. Integrating and including separately
the contribution above 1.0 flux units, as derived in
Figure 5.8 ($\simeq$ 60 flux units), gives 1973 flux units.

The observed COS B flux for this region is not
directly available. However, the gross similarity of
COS B and SAS II are sufficient to allow a useful comparison
with SAS II. From these data (Fichtel et al., 1978b)
we obtain F_γ (> 100 MeV) = 230 $\pm$ 5 flux units (270°<
1 < 90°, $|b| < 4.8°$). The discrepancy between the
observed Galactic flux and that expected from sources
is serious. However, the assumption of uniform power
law dependence is unlikely to be valid. A genuine Galactic
source population would have a geometry dependent distri-
bution which would be reflected in the differential
count at lower flux levels. In the following section
we therefore consider possible source populations, and
use the observed distributions above 1.0 flux units

to constrain the total number of Galactic sources.

5.9 Model source populations

Two different source populations are considered. The first assumes an exponential dependence of source concentration with Galactocentric radius. In this model the gamma-ray sources have a distribution similar to that of young active stars, which Montmerle (1979) previously considered as possible candidates for the 2CG sources. The second model assumes a radial dependence following that of supernovae remnants (Kodaira, 1974). Supernovae, and their associated shock fronts, are widely considered to be efficient sources of cosmic rays (up to about 10^{14} eV, e.g. Cesarsky and Lagage 1983). Only two Galactic plane gamma-ray sources (the Crab and Vela pulsars) have been identified with astronomical objects and it is not unreasonable to expect supernovae and their remnants to form a Galactic source population.

For both models we make the assumption of azimuthal symmetry, and a Z dependence $\propto \exp -(Z/Z_o)^2$, where Z is the height above the Galactic plane, and Z_o a variable parameter. The expected integral count can be expressed as

$$N(>S) = \int_l \int_b \int_o^{r_s} n_o \rho(R) \exp-(Z/Z_o)^2 r^2 \, dr \cos b \, db \, dl$$

$$5.5$$

The source densities $\rho(R) = \exp-(R/R_o)$ or $F(R)^P$ respectively for the exponential or supernova remnant density relative to the local value. The supernovae

remant density F(R) relative to the local is taken
from Kodaira (1974), and p is a dimensionless scaling
factor. n_o is an appropriate normalization factor,
R the Galactocentric radius and $r_s = (^L\gamma/4\pi S)^{\frac{1}{2}}$ is the
line of slight distance from us, with L_γ the intrinsic
source luminosity.

We implicitly assume the Galactic gamma-ray sources
to have mono-luminosity, as with only two positive
identifications, the form of the luminosity function
remains open to speculation. From the distances to
the Crab and Vela pulsars (2.0 and 0.4 kpc respectively)
we estimate L_γ (> 100 MeV) to lie within (0.2 - 1.7)
x 10^{39} ph s^{-1} assuming both emit isotropically and have
differential gamma-ray spectra of index -2. (The spectral
indices measured by COS B are -2.2 and -1.9 for Crab
and Vela respectively over the energy range E_γ : 70
- 5000 MeV). We make no allowance for the relative
ages of the two pulsars, but adopt a mean luminosity
L_γ (> 100 MeV) = 10^{39} ph s^{-1}, and note that variations
in the luminosity may make this uncertain by perhaps
as much as 50%.

5.10 Model source calculations

The parameters (R_o, Z_o) and (p, Z_o) determine
the slope of the Log N - Log S distributions. For each
model 5.5 is evaluated numerically over 0° < l < 90°,
90° < l < 180°, |b| < 5° and $R_{Gal.}$ = 15 kpc, the results
being doubled and converted to give the differential
count for the inner and outer Galaxy regions. The parameters

of each model are varied and the differential slope α ($N(S) = k\,S^{-\alpha}$) in each case evaluated above 1.0 flux units. The results for $\alpha(R_0, Z_0)$ and $\alpha(p, Z_0)$ are given in Figure 5.9. From these data we seek a unique set of parameters which reproduce the slopes derived from the corrected 2CG distributions : $\alpha = 2.9 \pm 0.32$, 1.72 ± 0.20 for the inner and outer Galaxy regions respectively.

The best fits are found to be:

exponential model: $R_0 = 0.80 {}^{+\,0.90}_{-\,0.25}$ kpc

$Z_0 = 0.14 {}^{+\,2.10}_{-\,0.10}$ kpc

supernova remnant model: $p = 4.6 {}^{+\,2.9}_{-\,2.3}$

$Z_0 = 0.13 {}^{+\,6.17}_{-\,0.12}$ kpc

The $1\,\sigma$ errors come from the previously determined errors on the source counts. It is seen that both models are only weakly dependent on Z_0, as expected for a thin slab type distribution. For each model, n_0 is then chosen to normalize onto the corrected count distribution at 1.0 flux units. It is not possible to find a unique normalization compatible with both inner and outer Galaxy distributions. This may, in part, be due to the low statistics in the outer Galaxy, though it could also suggest a smaller radial variation than implied by the present
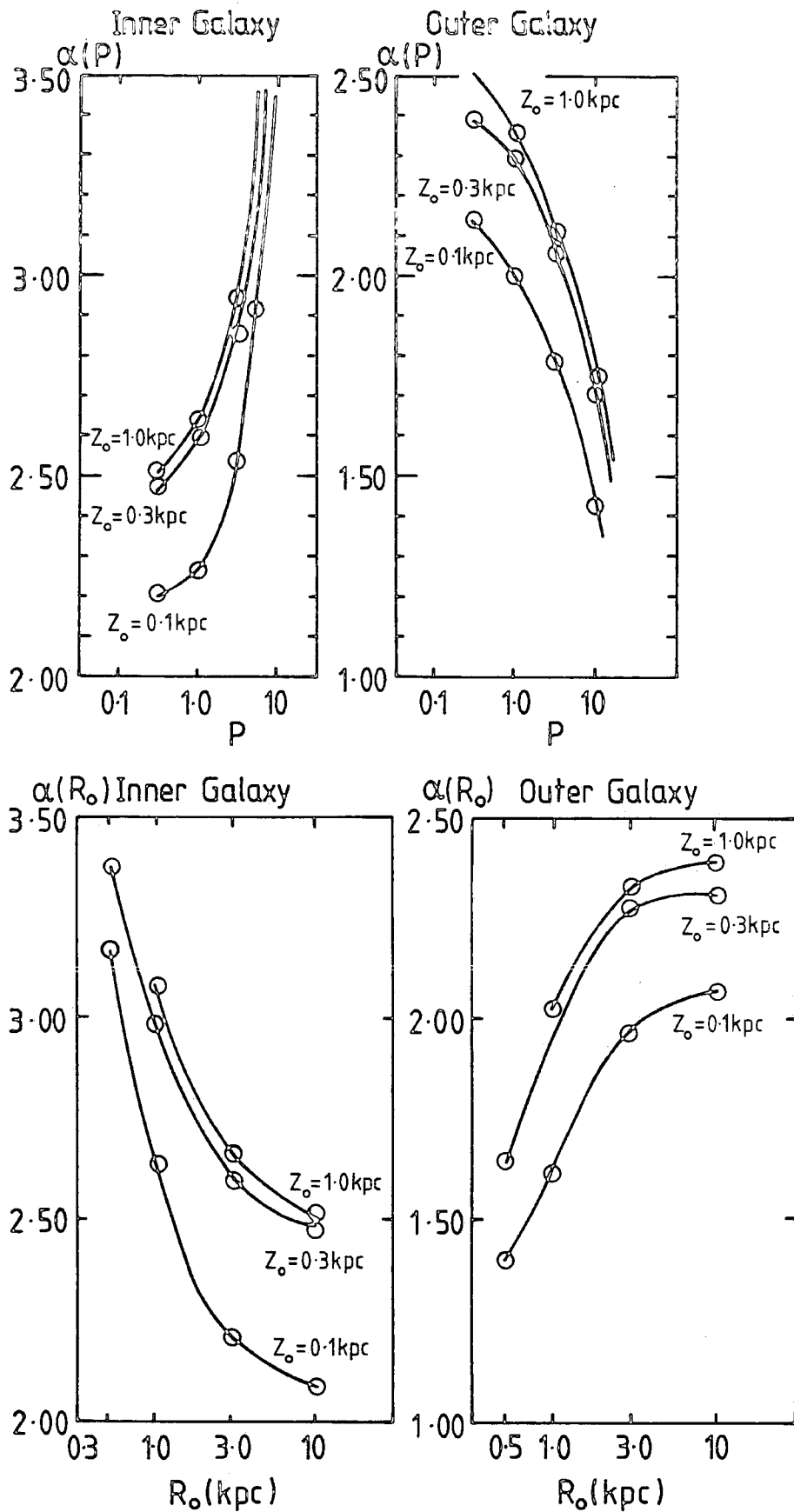
Figure 5.9 Variation of the slope parameter α for model source distributions. Top : $\alpha(p, Z_o)$, supernovae remnant distribution. Bottom : $\alpha(R_o, Z_o)$, exponential distribution.

models. We therefore normalize the models to the data

for the inner Galaxy. Both source populations are then

integrated over the Galaxy from the minimum flux up

to 1.0 flux units. These are combined with the corrected

distributions (Figure 5.8) to give the total source

count and flux in each case (Table 5.1).

The large upper limits to the expected number and

flux, especially for the exponential case, can be understood

in terms of the corresponding parameters R_o and p.

Small R_o implies rapidly varying Galactocentric density,

exponentially increasing continuously towards R = 0.

This is an unsatisfactory feature of the model which

would be improved by considering a flatter distribution

near the Galactic centre. In this respect the supernovae

remant model is probably more appropriate in assuming

the density decreases smoothly for R < 5 kpc.

Nevertheless both models clearly predict an over-

abundance in the flux from the Galactic plane, when

comparison is made with the SAS II observations. This

is unacceptable and we conclude that at least one of

the initial assumptions is invalid. It is possible

(though unlikely) that discrete sources dominate the

Galactic emission in which case the Monte-Carlo model

of the diffuse emission is not appropriate. However,

the limited angular resolution would require pure source

confusion (as with the radio sources) to be considered.

In that the total observed flux would then be due to

TABLE   5.1

		Inner Galaxy (l : 270°–0°–90°)	Outer Galaxy (l : 90°–180°–270°)
Exponential model	Total flux	$4.1 \,^{+\,430}_{-\,4.0} \times 10^{-2}$	$5.2 \,^{+\,120}_{-\,4.7} \times 10^{-7}$
	Total source count	$4.7 \,^{+\,150}_{-\,4.6} \times 10^{5}$	$1.0 \,^{+\,36}_{-\,0.9}$
SNR model	Total flux	$4.7 \,^{+\,16}_{-\,1.5} \times 10^{-4}$	$9.1 \,^{+\,140}_{-\,8.6} \times 10^{-7}$
	Total source count	$4.0 \,^{+\,21}_{-\,1.2} \times 10^{3}$	$1.9 \,^{+\,40}_{-\,1.8}$
SAS II	Total Flux ($|b| < 4.8°$)	$(230 \pm 5) \times 10^{-6}$	$(110 \pm 4) \times 10^{-6}$

Table 5.1

Flux (ph $cm^{-2}s^{-1}$) and source count for the two models fitted to the corrected 2CG source list. The SAS II flux is derived from the data of Fichtel et al. (1978b).

an unresolved clumped source distribution, the detection efficiences are likely to be similar to the present case, and the flux overabundance would remain. The alternative, and more likely possibility, is that not all the observed sources are genuine, particularly those at the weakest flux limit. In this case, the corrected numbers would be greatly reduced, decreasing both the slope and absolute number of the differential count. The model predictions are consequently reduced.

We conclude, therefore, that the 2CG catalogue most likely contains several spurious low flux sources. These, like the unidentified sources extracted from the SAS II analysis (Section 4.5), can be explained as upward statistical fluctuations of the structured background. While the present analysis cannot distinguish between genuine and spurious sources, it does suggest that a reduced genuine source population is likely to be more compatible with the total observed Galactic plane flux.

5.11 Derivation of the best genuine source list

As the results of the previous section suggest that the 2CG catalogue is unlikely to be competely genuine, we now endeavour to assess all the evidence on each source to determine a best catalogue of genuine sources. Using these we can then rework the previous analysis to derive an improved estimate of the total Galactic contribution from genuine sources. This can be compared with the total emission.

The 22 2CG sources ($|b| < 10°$) are considered
in Table 5.2. We draw on the SAS II cross-correlation
analysis (Chapter 4) which is able to offer varying
degrees of confirmation for each of these sources.
In addition we use the results of Li and Wolfendale
(1982) and Arnaud et al. (1982). These workers employ
a Monte-Carlo analysis of the expected gamma-ray sky
from cosmic ray interactions with HI and H_2 over the
range   l : 65° - 180°. In essence this is similar
to the Monte-Carlo model of the sky background in the
present analysis (Section 5.2). They find sufficient
consistency between peaks in the HI and H_2 distributions
(principally H_2) and several of the 2CG sources. These
are identified in Table 5.2 as giant molecular clouds.

These objects can be further categorized into two
types by comparing the observed flux with that expected
assuming a uniform distribution of cosmic rays throughout
the Galaxy. Those requiring cosmic ray enhancements
close to unity (i.e. irradiated by the ambient cosmic
ray flux) are most likely considered to be giant molecular
clouds not resolved by the gamma-ray detectors. For
several, however, enhancement factors $\geq$ 2 are required,
and the giant molecular cloud explanation must be considered
less certain. Though we also note that cosmic ray enhance-
ments of the order of 10 may be possible in giant clouds
(Dogiel et al. 1983, Houston and Wolfendale, 1984) and
that the exclusion of cosmic rays above few 10^8eV is
considered unlikely (Skilling and Strong, 1976). Indeed

TABLE   5.2

F_γ,COS B	2CG	SAS II	G.M.C.	Genuine (max)	Genuine (min)
2.4	006			*	*
1.0	013		b	*	
1.9	036	a	b		
1.3	054	a		*	*
1.2	065		b		
1.3	075	a	b		
2.5	078		b		
1.1	095				
1.0	121	a	c	*	
1.0	135	a	c	*	
3.7	184			*	*
4.8	195			*	*
1.0	218			*	*
1.0	235			*	*
13.2	263			*	*
2.7	284	a		*	*
1.6	288	*			
2.1	311	a	d	*	
3.8	333	a	d	*	
2.0	342	a	d	*	
2.6	356			*	
1.8	359			*	*

Table 5.2 The 2CG source list ($|b|{<}10°$), F_γ, COS B being the source flux ($\times 10^{-6}$phcm^{-2}s^{-1}) measured by COS B. SAS II indicates those peaks confirmed from an analysis of the SASII data (Table 4.1, Table 4.2)   (a) being those peaks detected at reduced significance. (Note non-detection by SAS II does not exclude the possible reality of a source) G.M.C. those sources which as explained in the text can be explained in terms of cosmic ray irradiation of giant molecular clouds. (b) Li & Wolfendale (1982), (c) Arnaud et al. (1982), but both require cosmic ray enhancement > 2 relative to the local value. (d) Riley et al. (1984) based on incomplete data. Genuine (max), (min) are the best estimates of the maximum and minimum number of genuine sources.

the work of Issa and Wolfendale (1981b) suggests that enhancements may be required for nearby clouds. These topics are dealt with more fully in the following chapter in relation to the Orion molecular cloud.

We also utilize the analysis by Riley et al. (1984), who attempt to apply the same criteria to the HI + H_2 and gamma-ray data in the fourth Galactic quadrant. To date CO surveys in this region have been limited in extent (either $|b| < 1°$ or a series of thin latitude slices). This makes any analysis less than complete, as a wide coverage is required for convolution with the gamma-ray point spread function to enable an accurate comparison to be made. Nevertheless, progress can be made and we include these data in Table 5.2.

We derive two discrete source sets; the maximum and minimum samples. The major difference between the two lies in the uncertainty over the fourth quadrant data. Presumably the best estimate is somewhere between these two sets. From our knowledge of the previous analyses of the data in the first and second quadrants, we expect the best estimate to be closer to the minimum.

5.12 Best estimate of the genuine source flux

We follow the methods previously described in correcting both genuine source lists for losses due to confusion, using only the corrections for $N_s = 80$ counts/flux unit (Figure 5.7). The results and best fit power laws to the differential counts are given

in Figure 5.10. In all but one case the regression
fits have a differential slope α < 2.0, and the
best estimates for both inner and outer Galaxy regions
have α < 2.0.

For a uniform, two dimensional mono-luminosity
source distribution the differential slope α = 2.0,
which can be considered the limiting case of a uniform
thin slab Galactic disk population. If the source density
decreases with Galactocentric radius then α > 2.0,
α < 2.0 for the inner and outer Galaxy respectively.
The case of α < 2.0 in the inner Galaxy requires the
source density to decrease with distance from us, at
least over the distance corresponding to F_γ > 1.0
flux units (about 3 kpc for the assumed L_γ = 10^{39}ph s^{-1}).
This requires a physically unacceptable source geometry,
and the corrected inner Galaxy distribution with α < 2.0
must be rejected as due to small sample behaviour.

Remembering that the minimum sample set of Table
5.2 is considered more plausible we adopt N(S) = 10 S^{-2}
as best describing the genuine source distribution for
the inner Galaxy. By necessity we must also have
α = 2.0 in the outer Galaxy and the flatter distribution
derived in Figure 5.10 is rejected as also due to small
sample behaviour.

This approach is not without difficulty in that
the need to restrict the corrected count distributions
effectively limits our estimate of the true source geometry
to a uniform, or at most a very slowly varying, Galactocentric

Inner Galaxy

$N(S) = 26.2 S^{-2.12}$

Outer Galaxy

$N(S) = 5.8 S^{-1.39}$

$N(S) = 4.8 S^{-1.48}$

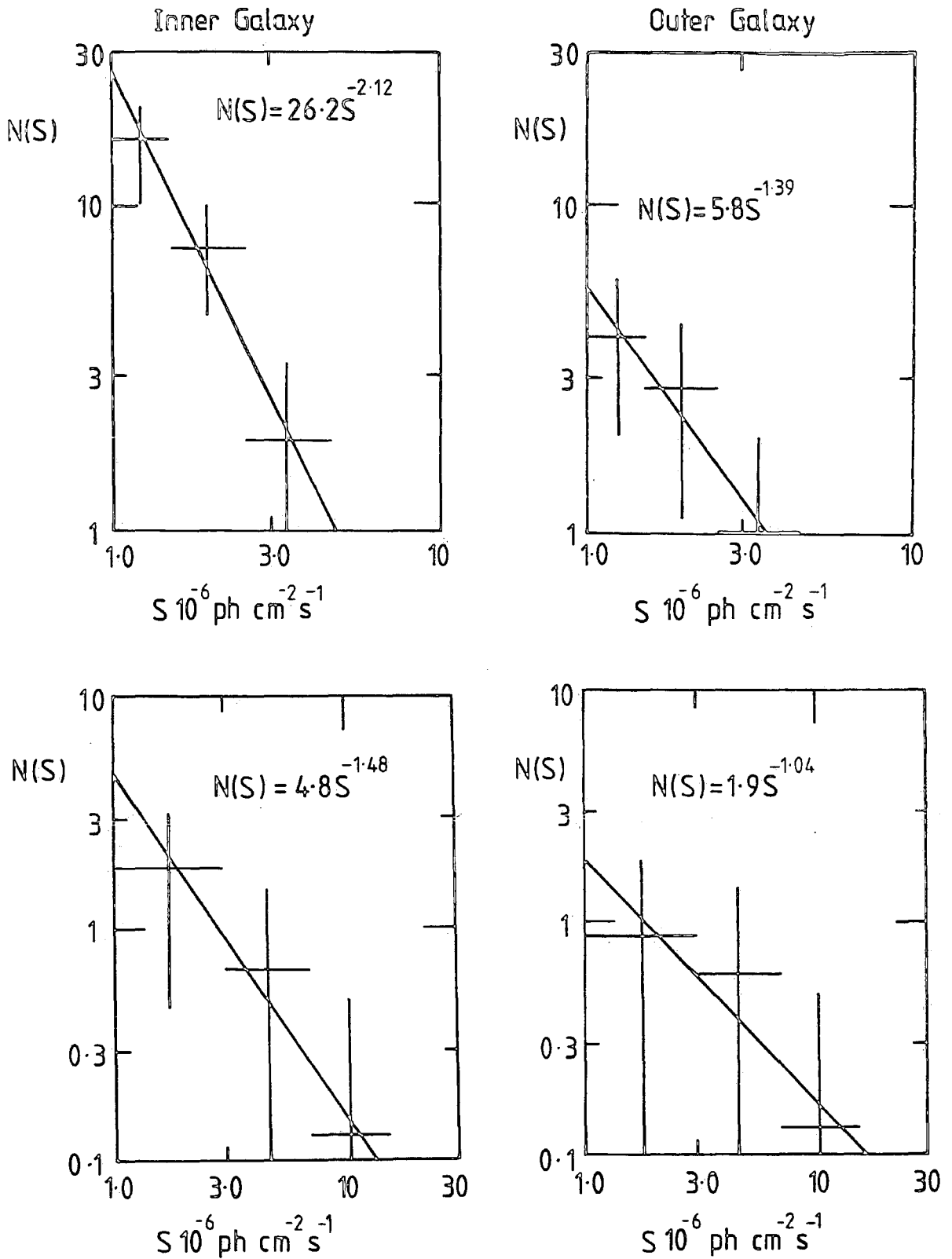$N(S) = 1.9 S^{-1.04}$

$S \ 10^{-6} \ ph \ cm^{-2} s^{-1}$

Figure 5.10 Log N - Log S distributions derived from
the maximum (top) and minimum (bottom) genuine source
lists of Table 5.2, after applying the appropriate
correction factors. Error bars are $\pm 1\sigma$ and least
squares regression lines are given.

radial density. The true source density may indeed
vary, but due to very small numbers locally the nature
of the variaiton may not be apparent in the observed
count distribution. Nevertheless we proceed.

Rather than make a detailed analysis of the type
already performed for the entire 2CG source list, we
assume that Z_O = 0.13 kpc and vary p, R_O to obtain $\alpha \simeq$ 2.0
for the inner Galaxy. We find p = 0.1 and R = 20 kpc
for the supernova remnant and exponential models respectively
fit this criterion, giving similar fluxes in both cases.
The results in Table 5.3 include the contributions from
our minimum estimate of the genuine sources above 1.0
flux units.

5.13 Discussion of the discrete source contribution

It is seen that the expected total source flux
is less than the SAS II observations of the Galactic
plane. This is encouraging, but the large percentage
contributed by sources (23%, 27% for the inner and outer
Galaxy respectively) are not consistent with our initial
assumption that the total observed flux is dominated
by diffuse processes. An improved model should take
account of these results iteratively by repeating the
Monte-Carlo analysis using a reduced background intensity.
We can not consider a reduction of the emissivity in
the inner Galaxy, that is the cosmic ray intensity must
be at least equal to the local value. However, the
situation regarding the absolute density of H_2 is still

TABLE   5.3

		Inner Galaxy (l:270°–0°–90°)	Outer Galaxy (l:90°–180°–270°)	Inner/ Outer
	Total	230	111	2.1
Flux	Sources	52(26)	30(25)	1.7(1.0)
	Diffuse	178(204)	81(86)	2.2(2.4)
Source/ Total		23(11)%	27(23)%	0.9(0.5)
Diffuse/Total		77(89)%	73(77)%	1.1(1.2)

Table 5.3

Best estimates of the gamma-ray flux x 10^{-6}ph cm^{-2}s^{-1}
($>$ 100 MeV) for $|b| < 5°$. Two values are given for the
genuine source flux the former corresponds to the calculations
based on the original Monte-Carlo background whereas the
latter bracketed values are estimated for the case of
a reduced diffuse background.

uncertin (Section 5.4). Indeed, we can view the Monte-
Carlo results as indirectly confirming the need for
a decreased distribution of target material in the inner
Galaxy. Such a situation is consistent with the arguments
for including the metallicity gradient in deducing H_2
from CO.

Use of the metallicity gradient clearly lowers
the gas column density in the inner Galaxy, and thus
the intensity of the structured background. We make
an approximate estimate of these effects without re-
calculating the detection efficiencies for the reduced
background model. This background is likely to be rather
similar to that for the outer Galaxy in the present
model. Therefore the latter correction factors (Figure
5.7) can be applied to the revised genuine source distri-
bution. As indicated in Table 5.3 we estimate the genuine
source fluxes to be further reduced by a factor of 2.

We are now able to percieve a reasonably self-
consistent picture of the Galactic gamma-ray emission
from the results of Table 5.3. Most of the Galactic
emission can be explained as diffuse in origin with
sources (observed and unresolved) contributing about
11-23% of the total flux. This is in good agreement
with the independent estimate by Harding (1981), who
considers the Galactic pulsar population and calculates
their total integrated flux to be about 15-20%.

Finally, we note the low source to diffuse flux ratio
in Table 5.3. We assume the cosmic rays at these energies
(above about 1 GeV) are predominantly Galactic in origin,
and both cosmic and gamma-ray sources have similar
distributions; for example that of supernovae remnants.
The low ratio is then interpreted as evidence for significant
diffusion of the cosmic ray particles from their sources.
That is, the diffuse emission traces the cosmic rays
in the interstellar medium, while discrete gamma-ray
sources indicate the initial distribution of cosmic
ray sources.

CHAPTER   6

THE ORION MOLECULAR CLOUD COMPLEX

6.1 Giant molecular clouds in the Galaxy

Molecular cloud complexes have become a widely studied phase of the interstellar medium. Observations of cloud dynamics, internal chemistry and their relationship to star formation are important areas of investigation. Scoville and Solomon (1975) made the first Galactic plane survey of Giant Molecular Clouds (GMC) by way of observations of CO. Further observations (e.g. Gordon and Burton 1976; Cohen and Thaddeus 1977; Solomon, Sanders and Scoville 1979; Cohen, Tomasevich and Thaddeus 1979; Kutner and Mead 1981; List, Xiang and Burton 1981, Sanders 1981; Robinson, McCutcheon and Whiteoak 1982; and Solomon, Stark and Sanders 1983) have extended the coverage to include the first, second and fourth Galactic quadrants.

These surveys generally provide undersampled observations in l and b, nevertheless much information has been obtained. There is a wide consensus of opinion on the origin of the CO emission. Specifically it is localized to the regions which typically have H_2 densities $\simeq 10^{2-3}$ cm^{-3}, linear dimensions $\simeq$ 10-50 pc   and masses $\simeq 10^{4-6} M_\odot$. The question of cloud masses is dependent on the assumed $CO \rightarrow H_2$ conversion factor and the effect if any, of the Galactic metallicity gradient (Section 5.4). There are important consequences for the inferred mass of H_2 in the inner Galaxy and therefore also for the interpretation

of the Galactic gamma-ray emission. Furthermore, following the discussion in Chapters 4 and 5 it is likely that many molecular clouds may be confused for genuine discrete gamma-ray sources.

To further understand the relevance of giant molecular clouds to gamma-ray astronomy, it is worthwhile to study in detail the gamma-ray emission from specific clouds, which we hope are typical of those observed throughout the Galaxy.

6.2 Cosmic rays and molecular clouds

Previous analyses of the gamma-ray flux from molecular clouds have assumed that the clouds are irradiated by the ambient cosmic ray flux and are inert in the sense of containing no cosmic ray sources (Issa and Wolfendale 1981a,b; Bloemen et al., 1984b). Under these assumptions the analysis of the SAS II data by Issa and Wolfendale concludes that for most local clouds the observed flux is approximately consistent with that expected from knowledge of the local cosmic ray spectrum and cloud masses derived from molecular studies. However, in a few cases (Cas OB6, Carina Nebula) the observed flux is greater than expected by factors of up to 20. It is unlikely that the mass estimates could be consistently and significantly low, thus holding out the possibility of enhancement of the ambient cosmic ray flux in at least some clouds. Houston and Wolfendale (1984b) consider the energy density within a cloud and show that a simple equipartition argument also suggests a cosmic ray enhancement.

Theoretical consideration has been given to the interaction of cosmic rays and molecular clouds by several workers. Skilling and Strong (1976) have studied the energy losses of cosmic rays in a dense cloud and the subsequent exclusion of cosmic rays from the cloud due to scattering by self-generated Alfven waves. They conclude that for typical clouds ($M \simeq 10^5 M_\odot$) cosmic rays above about 10 MeV/nucleon can freely penetrate the cloud, though lower energy particles are increasingly excluded. Similar conclusions are obtained by Cesarsky and Volk (1978). Morfill (1982a,b) further considers the effect on cosmic ray electrons, which because of their higher energy than protons of the same rigidity can be convected and accelerated into the cloud by the proton-generated Alfven waves. Gamma-ray production above 100 MeV can occur from cosmic ray nucleons of a few GeV or electrons of several hundred MeV. While the former are un-affected by this mechanism the latter can be enhanced within a typical cloud thereby enhancing electron bremsstrahlung gamma-ray emission.

Dogiel et al. (1983) consider the possibility of accelerating cosmic rays within collapsing clouds, though this is believed unlikely as the energy losses in typical clouds are considered too great.

Montmerle (1979) suggests that spatially linked supernovae remnants and OB associations may enhance cosmic ray and hence gamma-ray fluxes within molecular clouds.

In this model low energy cosmic rays produced in the
stellar wind of OB stars are accelerated by the shock
wave of the supernova remnant interacting with the molecular
cloud.

Present models are necessarily simplified though
they do at least allow the possibility of cosmic ray
enhancement within molecular clouds, whether from the
ambient cosmic ray flux or from sources therein. Any
attempt therefore to use gamma-rays as a probe of the
gas in a molecular cloud should allow for this possibility.

6.3 Dust in the interstellar medium

The origin of dust grains and their role in the
field of interstellar chemistry is still poorly understood,
though their effects on observational astronomy have
been extensively studied. The formation and reprocessing
of dust grains is intimately linked to processes of molecule
formation in the high density regions known as molecular
clouds. Dust's most significant function in these regions,
the likey sites of star formation, is to re-radiate optical
and UV photons as black-body radiation heating the surrounding
material (~ 30 - 300 K) and making them intense submillimetre
sources.

Interstellar extinction, scattering and polarization
of starlight are widely used by astronomers to investigate
the nature of observed sources and the intervening material
of the interstellar medium. It is the cumulative effect
of dust grains along the line of sight which is responsible

and extensive work is devoted to comparing the optical
data with those expected from models of grain size and
composition. Optical astronomy (including infra-red,
visible and UV) is effectively restricted from regions
of high extinction where recourse to other wavelengths
is necessary to probe the physical processes there and
beyond.

Extinction varies approximately as $^1/\lambda$, at least
over the range of wavelengths corresponding to the B,V
passbands (B(4400, 980A$^{\mathrm{o}}$); V(5500, 890A$^{\mathrm{o}}$)). The ab-
sorption of light is most efficient when the grain size
is of the same order as the wavelength of the incident
radiation. The characteristics of typical extinction
curves (including the "graphite peak" near 2200A$^{\mathrm{o}}$) strongly
suggests the presence of several different types and
sizes of dust grains in the interstellar medium.

The increasing absorption of blue light results in
the reddening of stellar images obscured by dust.
The colour excess or reddening is defined as the
difference in colour index between two stars of the
same spectral class, one reddened the other observed
in normal light. The reduction in apparent magnitude,
that is the extinction A_V, is proportional to the
colour excess E(B-V) or E(U-B). From a combination
of this ratio A_V/E(B-V) and that of gas column density
to colour excess N_H/E(B-V) it is possible to derive

N_H directly from A_v towards specific stars.

In the same way that stellar images suffer extinction, extragalactic objects such as galaxies will also be affected by intervening dust in our Galaxy. Assuming that galaxies are uniformly distributed on the sky, variations in the galaxy count from position to position can be used to map out the extinction and hence total gas throughout the Galaxy.

Lilley (1955) used Hubble's (1933) galaxy counts to derive optical extinction values, and hence the optical depth of dust, for a region below the Galactic plane (b $\sim$ -10° to -20°) incorporating the dark clouds in Perseus, Orion and Taurus. He compares these values with the optical depths obtained from a survey of HI 21 cm emission, assuming the HI to be optically thin. Although the data are of low quality there is a good correlation between τ_{gas} and τ_{dust} and evidence for residual gas in the absence of dust, i.e. τ_{gas} = a τ_{dust} + b. Lilley considers this as most likely due to a variation in the gas to dust ratio in the regions observed. At that time HI was considered to be the dominant constituent of the interstellar medium, though van de Hulst (1954) had discussed the possibility of H_2 existing in significant quantities. As H_2 is not detected by 21 cm emission it was believed that this additional component of gas would also contribute to the extinction.

With the advent, in the late 1960's, of widespread
detections of increasingly complex molecular species
by radio-astronomical techniques, the understanding of
the interstellar medium has changed substantially.
H_2 must be a major constituent of the gas in the inter-
stellar medium and as such must also contribute to
extinction through any dust associated with it. Addi-
tionally, a small fraction ($\sim$ 4%) of the hydrogen in
the interstellar medium is ionized and exists in high
density regions, usually associated with areas of recent
star formation. It is assumed that HII will also be
associated with dust thereby contributing to interstellar
extinction. Dust can therefore be used, in theory at
least, to estimate the column density of all gas along
the line of sight to the observed source.

The relevance to gamma-ray astronomy is apparent
when it is remembered that the diffuse component of
Galactic gamma-rays are produced by cosmic ray interactions
with the gas and radiation of the interstellar medium.
For E_γ > 100 MeV, it is widely believed that p-p collisions
are the dominant production mechanism (Section 1.2)
and therefore knowledge of the total gas in the Galaxy
is essential. In an early analysis of the SAS II data,
Puget et al. (1976) use the extinction as measured to
nearby stars ($\lesssim$ 2 kpc) to estimate the contribution
to the observed flux from cosmic ray interactions in
the local interstellar medium. By subtracting off this

expected local irregular longitudinal flux distribution
they are better able to analyse the large scale variation
in Galactic gamma-ray emission, comparing the unfolded
radial distribution with that of other Galactic tracers.
They also note one of the limitations of using extinction
to estimate gas column density. For regions of high
extinction (E(B-V) $\gtrsim$ 1.5, Av $\gtrsim$ 4.5) the method only
gives a lower limit to the total column density. This
tends to be a serious problem for the central regions
of dense molecular clouds and close to the Galactic
plane in the direction of the inner Galaxy.

6.4 The gas-to-dust ratio

Calibration of the ratio $N_H/E(B-V)$ (gas column
density to colour excess) for the local interstellar
medium requires direct measurements of both gas column
densities and extinction. Savage et al. (1977) use
UV data from the Copernicus satellite to measure the
column density of H_2 towards local stars ($\lesssim$ 500 pc).
The technique utilizes the absorption of UV photons
by H_2 (transition between J = 0 and J = 1 rotational
level of the ν'' = 0 vibrational state), the depth
of the absorption features being proportional to the
column density of molecular gas. The direct measurement
of H_2 by this technique is only possible for the very
local region around the Sun because the absorption
features rapidly saturate at larger distances, thereby

only being able to give lower limits to N_{H_2}.

Similar results are obtained for N_{HI} (Bohlin et al. 1978) by measuring the spectral region for L_α absorption to obtain N_{HI}. Again this technique can only be applied locally; but it has many advantages over measurements of N_{HI} from 21 cm emission which is dependent on instrumental calibration, the need for optical depth corrections and the effects of Galactic rotation on observed emission velocities.

The combined data for 96 star positions gives a calibration value of

$$N(HI + 2H_2)/E(B-V) = 5.8 \times 10^{21} \text{ at } cm^{-2}mag^{-1}.$$

This value does not allow for the presence of HII as it is believed that $\simeq 4\%$ of the total gas in the local interstellar medium is ionized. This is believed to be less than the systematic error in measuring E(B-V) and is consistent with the accepted electron density $<n_e> \simeq 0.03 \text{ cm}^{-3}$ derived from pulsar measurements.

From extensive measurements of extinction curves towards local stars the extinction to colour excess ratio $A_v/E(B-V)$ is estimated to be about 3.1 $\pm$ 0.1 (Savage and Mathis, 1979). This is essentially limited to regions within about 2-3 kpc of the Sun and is thus a local value. Its large scale uniformity strongly suggests the size distribution of grains in the interstellar medium is constant, at least over the region observed.

The gas to dust ratio is a combination of both measurements. There are small anomalous regions, notably in the directions of dense molecular clouds, where this ratio varies significantly from the mean value considered appropriate for the general interstellar medium. Measurements of E(B-V) are limited towards specific stars. Extinction, through the use of galaxy counts, can sample much larger areas of the sky thereby leading to estimates of total gas column density along a line of sight.

6.5   The Orion molecular clouds

The Orion complex is an extensive association of
gas, dust, HII regions, reflection nebulae, infra-red
sources and OB associations, approximately 500 pc from
the Sun in the direction (l ,b) $\sim$ (210°, -20°). It
is generally believed that this is a region of ongoing
star formation. HI observations (e.g. Lilley, 1955;
Menon . 1958; Gordon 1970) reveal emission with a velocity
pattern suggestive of an expanding shell. Tucker et
al. (1973) made initial observations of the molecular
gas (via CO) around Orion B (NGC 2024). These workers
discovered intense CO emission which extended over more
than 1^O.

Since then the Columbia group have pursued a detailed
observational program of ^{12}CO and ^{13}CO emission line
studies from the Orion-Monoceros region (Kutner et al.,
1977; Thaddeus, 1982). From these data it is clear
that CO is a good large-scale tracer of the likely star
formation sites. The most intense areas of CO emission
lie along the leading edges of cone-shaped structure
formed by the junction of the two molecular clouds Orion
A and Orion B. Interestingly the bulk of the active
sources (i.e. HII regions, infra-red sources, OB association)
also follow a similar alignment.

Blaauw (1964) studied the four main OB association
subgroups in the Orion complex. Their estimated ages
decrease from Ia ($\sim$ 12 x 10^6yr) to Id ($\sim$2 x 10^6yr).
These subgroups also exhibit a marked spatial alignment

with the oldest Ia lying outside and to the south of
the molecular clouds. The others are distributed along
the leading edges of the intense CO emission observed
in Orion A and B. Kutner et al. (1977) observed a systematic
CO velocity gradient in Orion B. This may be suggestive
of an overall rotation of the cloud, though Kutner et
al. note that the sense of rotation does not correspond
with that expected from the Galactic differential rotation
in that region. Furthermore the OB associations do
not exhibit a similar velocity gradient which might
be expected if these were formed in the clouds about
10^{6-7} years ago.

An alternative explanation is that the mechanism
responsible for the star formation might have produced
the velocity gradient. Kutner et al. (1977) and Thaddeus
(1982) believe this model is more likely as the conical
shape of the clouds and the distribution of OB associations
is indicative of a shock or wind sweeping into the cloud
from the direction of the oldest OB association. This
picture is further supported by detailed studies of
H_2 emission (vibrational transitions) and high resolution
kinematic features of ^{12}CO and ^{13}CO emission in the
Orion nebula (NGC 1976) (Beckwith et al., 1979; Loren
1979; Beckwith et al. 1983).

The Orion nebula has been widely studied at many
wavelengths and in the central region (diameter $\simeq 0.1$ pc)
H_2 densities $\gtrsim 10^6$ cm^{-3} are inferred from observations

of NH_3 emission (Batrla et al., 1983). This is direct
evidence of high density clumping within the overall
cloud structure, for which mean H_2 densities of 10^{2-3} cm^{-3}
are estimated from ^{12}CO and ^{13}CO observations.

Berger (1981) made polarimetry and photometry studies
of the Orion nebula and concluded that the reddening
$A_v/E(B-V)$ is abnormally large $\simeq$ 5-6. Polarimetry
measurements show the mean grain size is larger around
the nebula. It is believed that the smaller grains
are destroyed by radiation from hot stars in the region,
and the extinction $E(B-V)$ is therefore less at shorter
wavelengths. This has interesting consequences for
the estimates of gas column density based on the galaxy
count technique. We return to this topic later (Section
6.11).

Talent and Dufor (1979) studied the Galactic metallicity
gradient as determined from observations of local HII
regions. They find that the radial gradient (8-14 kpc)
in the spiral arms (Orion, Perseus and Sagittarius)
is 2-3 times greater than that determined for the overall
interstellar medium. The observations in the Orion
arm are limited to the Orion nebula and NGC 2467, though
Hawley (1978) finds a similar result for the Orion arm
based on 6 HII regions. It is not clear whether this
metal deficiency is characteristic of all the gas in
the Orion arm, and specifically that in the molecular
cloud complex, or is relative only to the HII regions.

Clearly, in the former case, making allowance for the effect
of the metallicity correction on the conversion factor
α (Section 5.4) reduces the mass estimates for the
clouds.

The metal abundances in the Orion nebula have been
studied in detail by Peimbert (1982). After correcting
the Orion measurements for electron temperature variations
Peimbert finds the differences between Orion and the
Sun are of the same order as the absolute accuracy of
the abundance determinations ($\simeq 0.2 - 0.5$ dex, i.e.
a factor of 1.6-3). However the abundances in Orion
are consistently lower than measured for the Sun strongly
suggesting the difference is genuine. Peimbert estimates
the Orion nebula is about 0.2 dex deficient in heavy
elements (C,N,O,S,Ne) relative to the Sun. This compares
with the metal deficiencies $\simeq 0.08$ dex and 0.13 dex
for the Orion arm determined by Hawley (1978) and Talent
and Dufor (1979) respectively.

6.6 The method of analysis

The Orion molecular complex is sufficiently close
($\simeq$ 500 pc) to be fully observed in radio emission
(CO and HI) and resolved in the gamma-ray data ($E_\gamma > 100$ MeV).
Thus as a local giant molecular cloud it is ideally suited
as a test of several basic questions regarding cosmic
ray interactions with molecular clouds. Specifically
two problems must be addressed. The first concerns
the total mass as derived from CO observations by an

appropriate conversion factor $\alpha = 2N_{H_2} / \int T(^{12}CO)dv$.
Secondly we must consider the extent to which the cosmic
ray flux is enhanced or reduced within the cloud.

We can express the observed gamma-ray intensity
I_γ in the following manner:

$$I_\gamma = q/_{4\pi} (N_{HI} + 2N_{H_2}) + I_b \qquad\qquad 6.1$$

or

$$(I_\gamma - I_b) - q/_{4\pi} N_{HI} = q/_{4\pi} [\alpha W_{CO}]^N \qquad\qquad 6.2$$

where $q/_{4\pi}$ is the gamma-ray emissivity N_{HI} the atomic
hydrogen column density and I_b the isotropic gamma-ray
background intensity. W_{CO} is the integrated CO emission,
α the $CO \rightarrow H_2$ conversion factor and we introduce
a scale factor N to approximate the effect of cosmic
ray enhancement or exclusion in the molecular gas.

As it is not feasible to model the precise geometry
of regions within the cloud which are likely to affect
the ambient cosmic ray flux, we make the reasonable assumption
that the denser regions (high W_{CO}) are more likely to
be the regions of cosmic ray exclusion, enhancement or
production (a simple consequence of the fact that star
formation is greater there). Thus 6.2 should in essence
contain the necessary parameters to represent the gross
relationship between cosmic rays, gas and gamma-rays.

While the potential cosmic ray sources may have
a distribution similar to that of the CO in the cloud,
the contrast in cosmic ray intensity is likely to be
much smaller unless the cosmic rays diffuse away remarkably

slowly. For a cosmic ray of few GeV, the mean free path in the ISM in general is $\lambda \sim 0.1$ pc and the lifetime $\tau \sim 10^7$ yr. Thus the typical linear dimensions of the cosmic ray distribution from a single source is given by $< \chi^2 > = 2\lambda c \tau$. On substitution, we find $X_{rms} \simeq 800$ pc, which is much larger than the dimensions of the Orion cloud. λ will be smaller than 0.1 pc in the cloud but X_{rms} will still be at least the linear dimension of the cloud; thus, it seems appropriate to apply the scale factor N to the CO distribution smoothed to the gamma-ray resolution rather than at its original resolution.

By analysing the appropriate data for the Orion complex we endeavour to derive the best fit values for α, N in 6.2, thereby estimating the total mass and the degree to which cosmic rays interact with the cloud.

It is realized that this method of determining the local value of α is susceptible to many uncertainties, not least the statistical accuracy of the gamma-ray data. Clearly another method, circumventing the cosmic ray, gamma-ray link, would be advantageous. Instead of using gamma-rays as a total gas tracer we can use galaxy counts as a measure of total gas and compare this with direct measurements of HI and H_2 (via CO). Thus we write:

$$N_{H_t}(N_G) = N_{HI} + 2N_{H_2} \qquad\qquad 6.3$$

or

$$N_{H_t}(N_G) - N_{HI} = \left[\propto W_{CO}\right]^N \qquad\qquad 6.4$$

Again we introduce a scaling parameter N. In this
case we are allowing for the gas to dust ratio to vary
within the cloud as the left-hand side of 6.4 is really
a measure of the extinction (i.e. dust) associated with
the molecular cloud.

6.7 Description of the data

Gamma-ray data for the Orion region are available
both from the SAS II and COS B satellites. We use those
collected by COS B because of their superior statistical
accuracy. A restricted subset of the COS B database
is available (Caravane collaboration, private communication).
These data, observed count, estimated background count
and exposure factors for E_γ > 100 MeV, are binned
(Δl x $\Delta b = 1^O$ x 1^O) over the region   l   : 198°
to 222° and b : -5° to -25°. Observed intensities are
calculated, from which an isotropic background level
$I_b = 5.8$ x 10^{-5} ph $cm^{-2}sr^{-1}s^{-1}$ is already subtracted.
This background is an average determined from extensive
analysis of the complete COS B data (Strong, 1984;
Bloemen, private communication). From these data we
derive $I_\gamma - I_b$ (see 6.2). Figure 6.1 is a contour map
of the gamma-ray intensity ($I_\gamma - I_b$) for the Orion
region. As noted previously (Section 4.3), determination
of the COS B isotropic background presents many problems
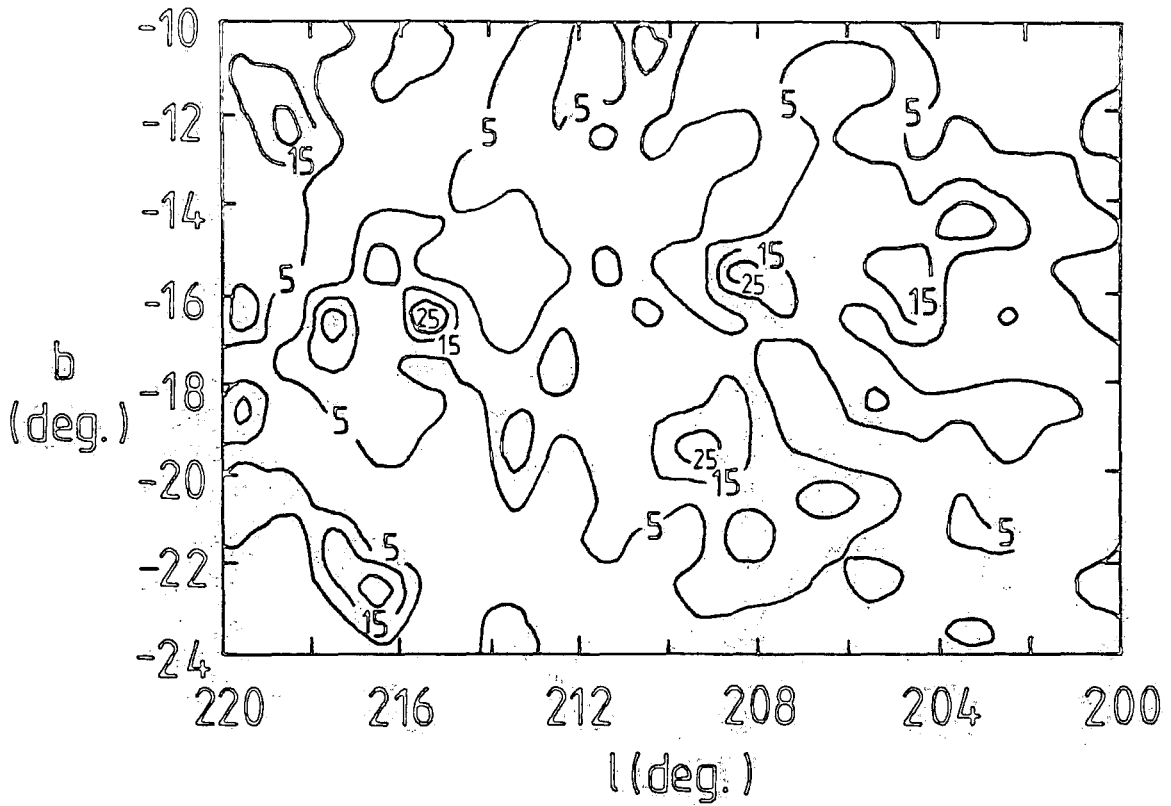
FIGURE 6.1 COS B gamma-ray intensity map for the Orion region. Contours are I_γ (> 100 MeV) x 10^{-5}ph $cm^{-2}sr^{-1}s^{-1}$, with an isotropic background I_b = 5.8 x 10^{-5} ph $cm^{-2}sr^{-1}s^{-1}$ subtracted.
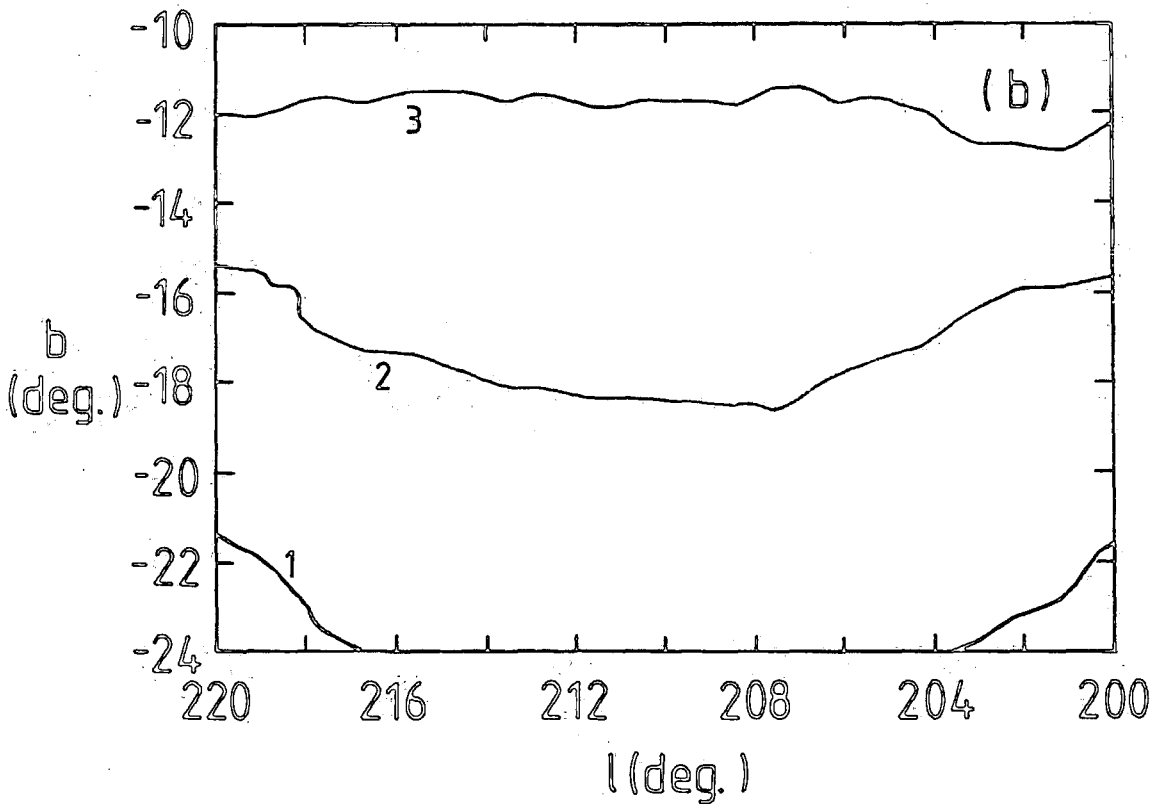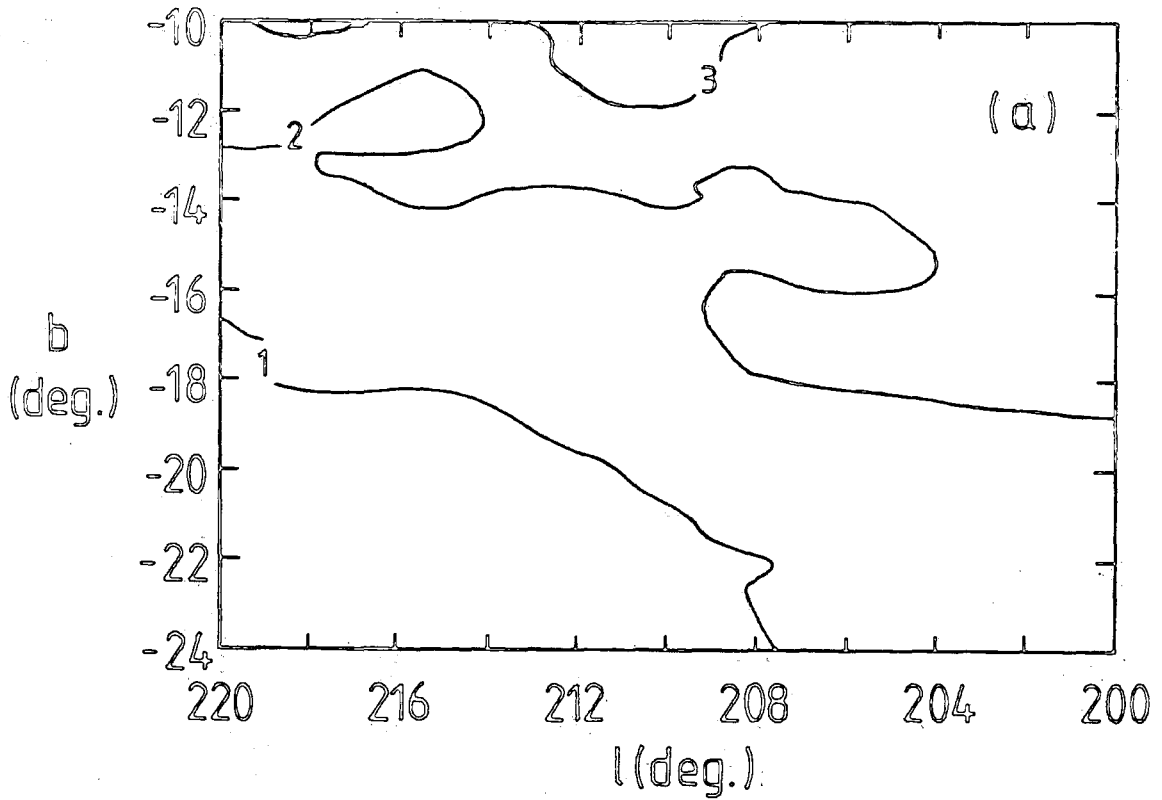
FIGURE 6.2   HI column densities x 10^{21} at cm^{-2},
(a) at original resolution,
(b) smoothed to gamma-ray resolution.

and there is likely to be further uncertainty associated with the present level. We return to this possibility and its effects on the analysis in Section 6.10.

The HI data are taken from the surveys of Weaver and Williams (1973) and Heiles and Habing (1974). We adopt a spin temperature $T_s = 125$ K to calculate the column densities N_{HI} following the procedure described in Section 5.3. For proper comparison with the gamma-ray data the column densities are smoothed to the COS B resolution ($E_\gamma > 100$ MeV). The column densities before and after smoothing are presented in Figure 6.2. The smoothing procedure has a small effect on N_{HI} as the column density is initially smoothly distributed, rising gradually with increasing latitude. Using these data (Figure 6.2b) it is difficult to distinguish spatially the HI gamma-ray component from the background, that is, treat them both as independent variables (see 6.1). It is preferable to consider the gamma-ray intensity from HI as an additional slowly varying background (see 6.2).

Extensive ^{12}CO coverage of Orion is available from the Columbia group (Kutner et al., 1977, Thaddeus, 1982). Figure 6.3a is a contour map of the high resolution (HPBW = $\frac{1}{8}$") integrated ^{12}CO emission. For direct comparison with the gamma-ray and HI data, this map is smoothed to the COS B resolution ($E_\gamma > 100$ MeV), Figure 6.3b). The effect of smoothing on the ^{12}CO distribution is
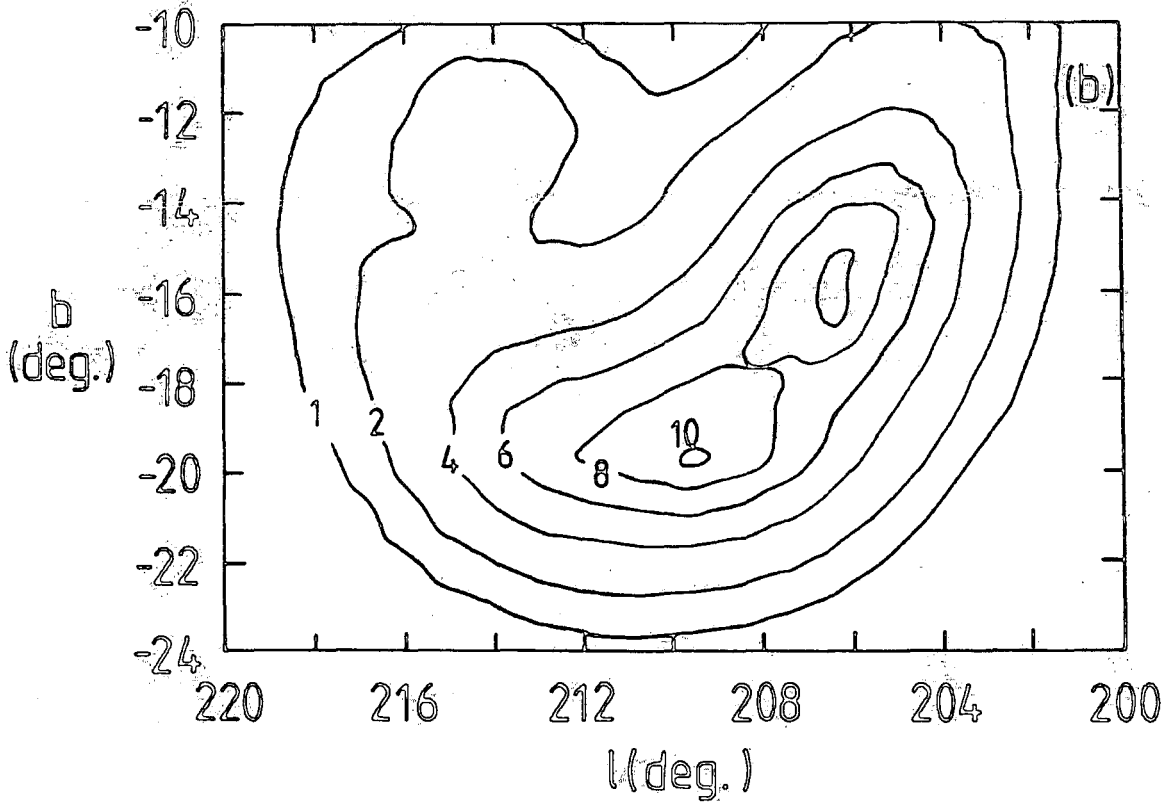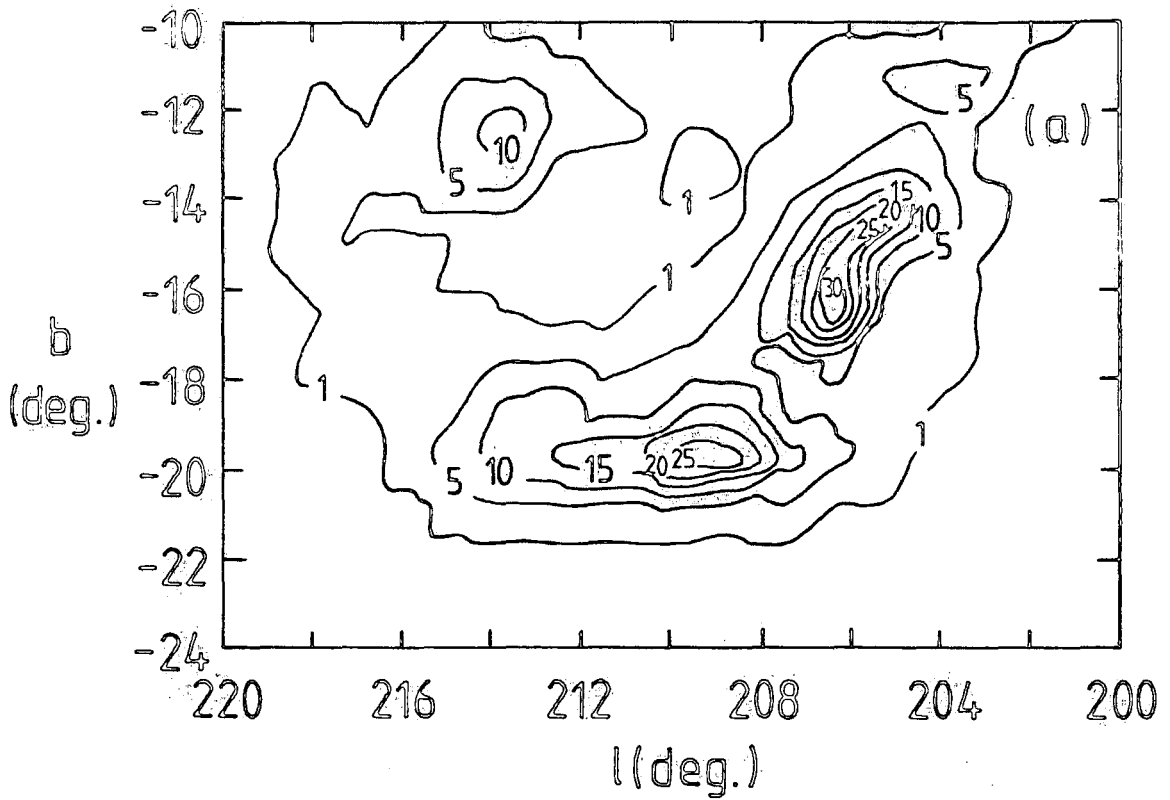
FIGURE 6.3 $\int T(^{12}CO)dv$ in units of K kms^{-1}
(a) at original resolution,
(b) smoothed to gamma-ray resolution.
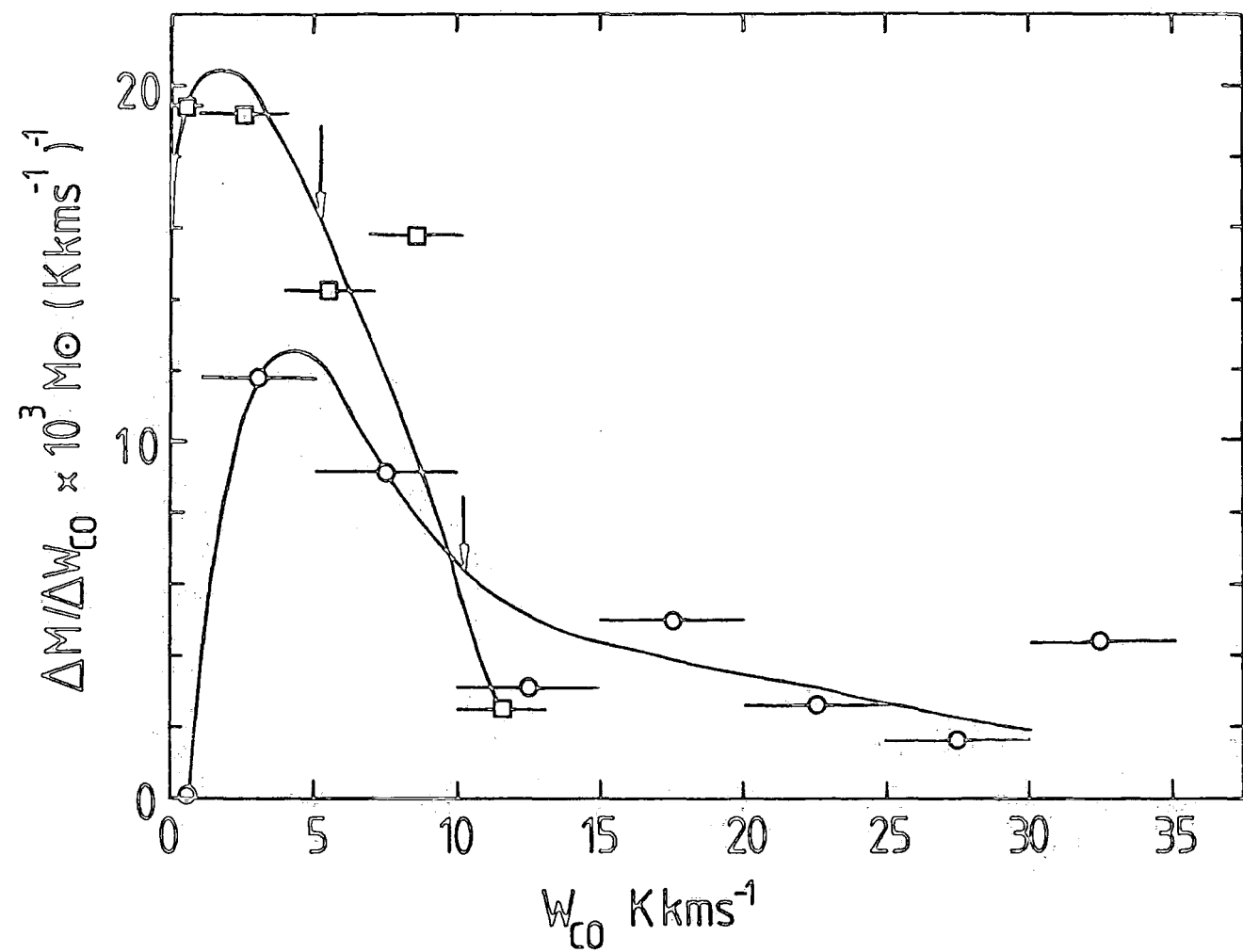
Figure 6.4   Differential mass distributions derived from
the high resolution (circles) and smoothed (squares)
contour maps of Figure 6.3, assuming $\alpha = 4.0 \times 10^{20}$ at $cm^{-2} (Kkms^{-1})^{-1}$
The arrows indicate the median mass contour ($W_{co} > 1.0$ K kms^{-1}).
Curves are drawn as a visual aid to illustrate the
general trend.

apparent in Figure 6.4 where we plot the differential

mass distributions for both the high resolution and

smoothed contour maps of Figure 6.3. Smoothing concentrates

a greater fraction of the observed mass below W_{CO} =

5 K kms^{-1}. Additionally, because of the restricted

area covered in Figure 6.3, degrading the angular resolution

necessarily smooths part of the emission out of the

particular region of interest. By considering the total

emission within W_{CO} = 1 K kms^{-1} in both contour maps

(Figure 6.3) we estimate the reduction to be $\simeq$ 12%.

This loss is considered later (Section 6.11) in relation

to the determination of α from the gamma-ray and

HI data.

The galaxy count data are those of the Lick survey

(Shane and Wirtanen, 1967) reduced to 1° x 1° bins and

corrected for the effect of atmospheric absorption (Strong

and Lebrun, 1982). These counts give the mean number

of galaxies brighter than m_V $\simeq$ 18.0 covering the region

dec. $>$ -20°. The conversion from mean galaxy count

N_G to total gas column density N_{H_t} used in the present

analysis is

$$N_{H_t}(N_G) = 2 \times 10^{21} \log_{10}(N_G^o/N_G) \text{ at } cm^{-2} \qquad 6.5$$

following Strong and Wolfendale (1981), where N_G^o = 75 is

the mean galaxy count per square degree in the absence

of extinction. This value is not unique, with other

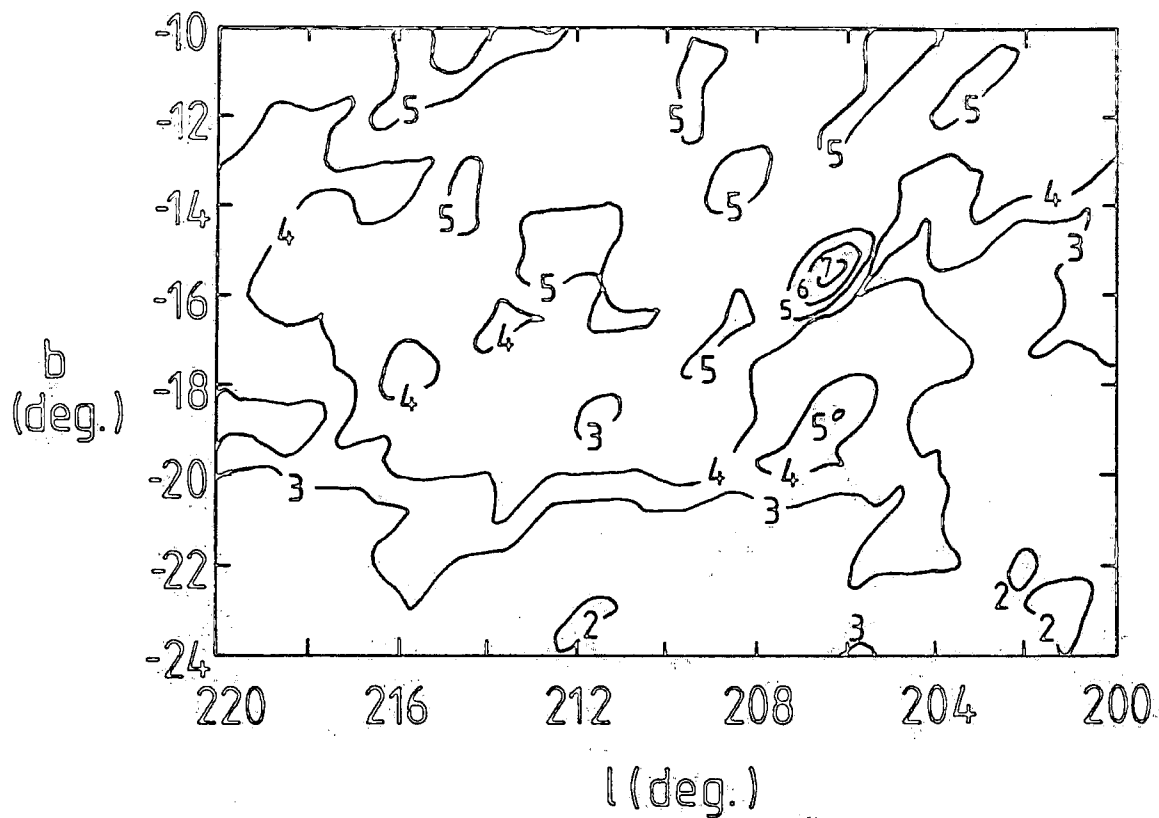workers adopting N_G^o in the range 50-100 giving a systematic

FIGURE 6.5 Total gas column density in units of 10^{21} at cm^{-2} derived from galaxy counts.

shift ($\lesssim$ 10%) in N_{H_t} relative to the present levels.

Over the Orion region many data bins have zero galaxy counts, indicating the presence of saturation where the extinction can only give a lower limit to the total gas column density. It is realized that any method of estimating the total column density in these bins will have a crucial effect on the analysis as it is those bins with $N_G = 0$ which tend to have the most intense CO emission. Figure 6.5 is a map of the total column density derived using 6.5. As described in Section 6.11 minimum values $N_G(min)$ (Table 6.3) are substituted into those bins for which $N_G = 0$.

6.8 The local gamma-ray emissivity

We seek to use 6.2, fitting the gamma-ray HI and CO data to obtain $\propto$ and N. However it is first necessary to know $q/4\pi$, the local emissivity above 100 MeV, appropriate for the Orion cloud region. Many workers have used both the SAS II and COS B data to derive local emissivities in each energy range. Tables A1 and A2 are summary of these results, outlining the relevant analyses used.

Each technique involves fitting the observed gamma-ray intensities to the total gas column densities under the assumption of a uniform cosmic ray density throughout the region analysed. Gas column densities are derived either from HI and CO emission or from the galaxy count technique. Clearly both are subject to the limitations

of the calibrations $CO \rightarrow H_2$ and $N_G \rightarrow N_{H_t}$. Different calibrations are the major source of variation in the derived emissivities. The analyses are generally restricted to intermediate latitudes ($|b| \geqslant 10^o$) where many of the problems are reduced; CO emission being small away from the Galactic plane and galaxy counts are less affected by saturation, though gas-to-dust variations may still be present. In addition the data give a better representation of the local interstellar medium ($\lesssim$ 1-2 kpc) over which the variation in cosmic ray density is likely to be small.

Nevertheless, cosmic ray density variations are likely to limit the analyses and indeed several workers have approached the problem from the perspective of using the data to trace the local cosmic ray gradient (Section 3.3). Theoretical calculations of the local emissivity are themselves limited by the uncertainty in the local interstellar electron spectrum below a few GeV.

Values for $q/4\pi$ are seen to span a wide range: (1.7 - 3.0) x 10^{-26} ph at^{-1}sr^{-1}s^{-1}. We adopt $q/4\pi$ = 2.0 x 10^{-26} ph at^{-1}sr^{-1}s^{-1} for the analysis but are mindful that the results are likely to be sensitive to the chosen emissivity; $q/4\pi$ appearing on both sides of 6.2. The dependence of α on $q/4\pi$ is considered in the following section.

6.9 Analysis of the gamma-ray data

In deriving the best fit for α, it is important to restrict analysis to the region of the clouds as measured by W_{CO}. As a lower boundary we select only those bins (I_γ, W_{CO}, N_{HI}) for which $W_{CO} \geqslant 1.0$ K kms^{-1}. With these data and $q/4\pi = 2.0 \times 10^{-26}$ ph at^{-1}sr^{-1}s^{-1}, we substitute into 6.2 for each test value of N($= 0.5$, 0.8, 1.0, 1.5, 2.0, 3.0) and perform a linear least squares regression.

The combined data are transformed to a linear scale in W_{CO} and binned. In Figure 6.6 we plot the excess intensity, $I_\gamma - I_b - q/4\pi\, N_{HI}$, against $q/4\pi\, W_{CO}$. The smooth curves are the least squares lines for each N when transformed to the linear scale. These curves give the expected gamma-ray intensity from gas in the Orion clouds for each value of α and N. Figure 6.7a shows the results obtained for the regression values of α_{20} ($\alpha_{20} = \alpha/10^{20}$ at cm^{-2} (K kms^{-1})$^{-1}$) for each case of N. The χ^2 parameter is used to test the goodness of fit for each N with the results given in Figure 6.7b.

The trend indicated by χ^2 suggests that N > 1.0 with a best fit N $= 1.7$ ($\alpha_{20} = 2.5 \pm 0.9$) at the 64% significance level. Given the uncertainties involved, N $= 1.0$ ($\alpha_{20} = 3.7 \pm 0.6$) must also be considered at the 17% significance level. For N $= 1.0$ we repeat the analysis for a range of emissivities spanning the values given in Table A1 . The least squares values of
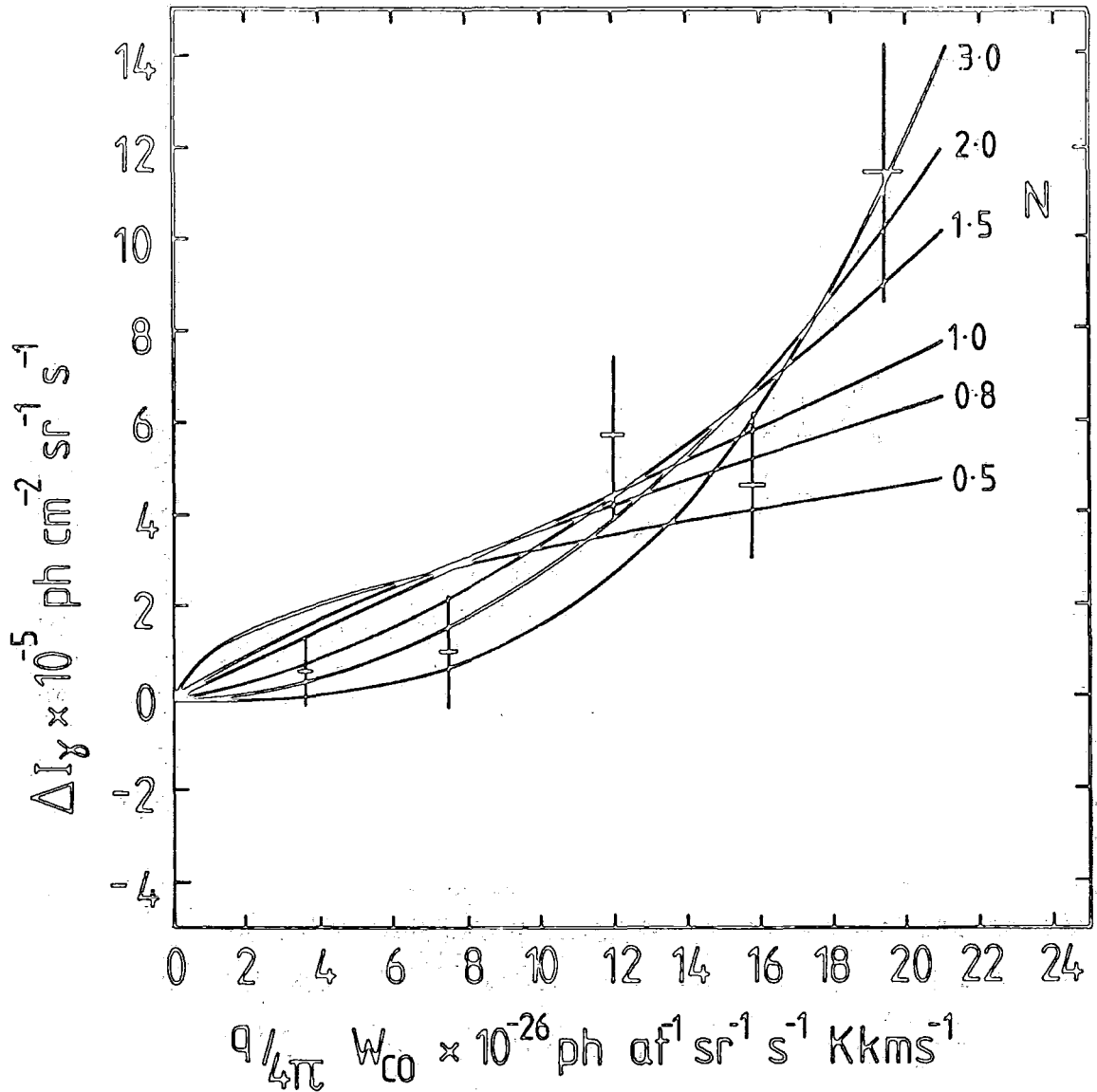
Figure 6.6 Variation of the excess intensity ΔI_γ
(> 100 MeV) as a function of $^q/4\pi\left[W_{co}\right]^N$, for the Orion
clouds. The binned observations are plotted with
standard errors. Smooth curves give the expected gamma-
ray intensity for each case of N.
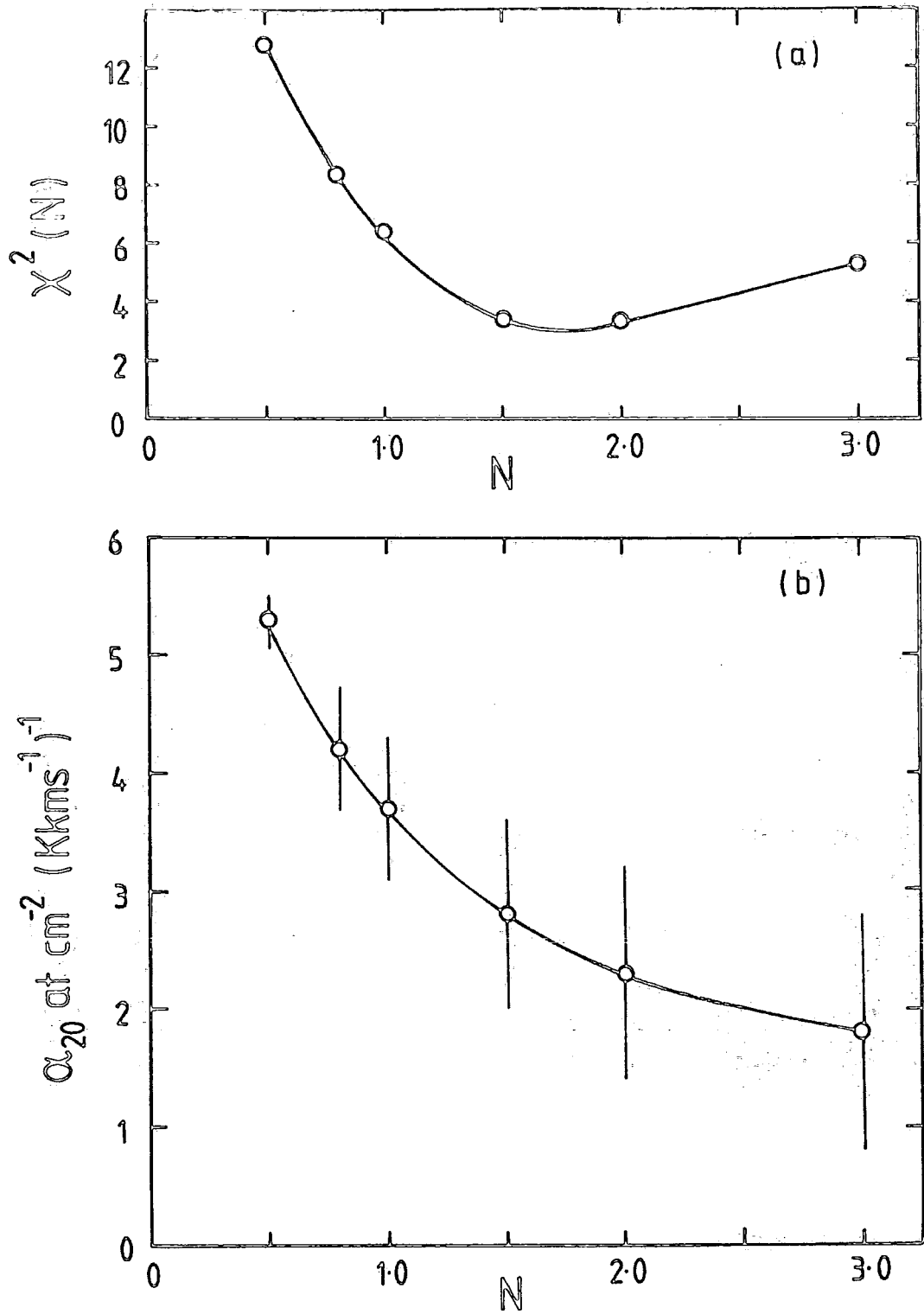
Figure 6.7 (a) Variation of χ^2 as a function of N,
(b) α_{20} ($\pm 1\sigma$) as a function of N; from the data of
Figure 6.6. $\alpha_{20} = 2N_{H_2}/W_{co}$ in units of 10^{20} at cm^{-2}
$(K\ kms^{-1})^{-1}$.
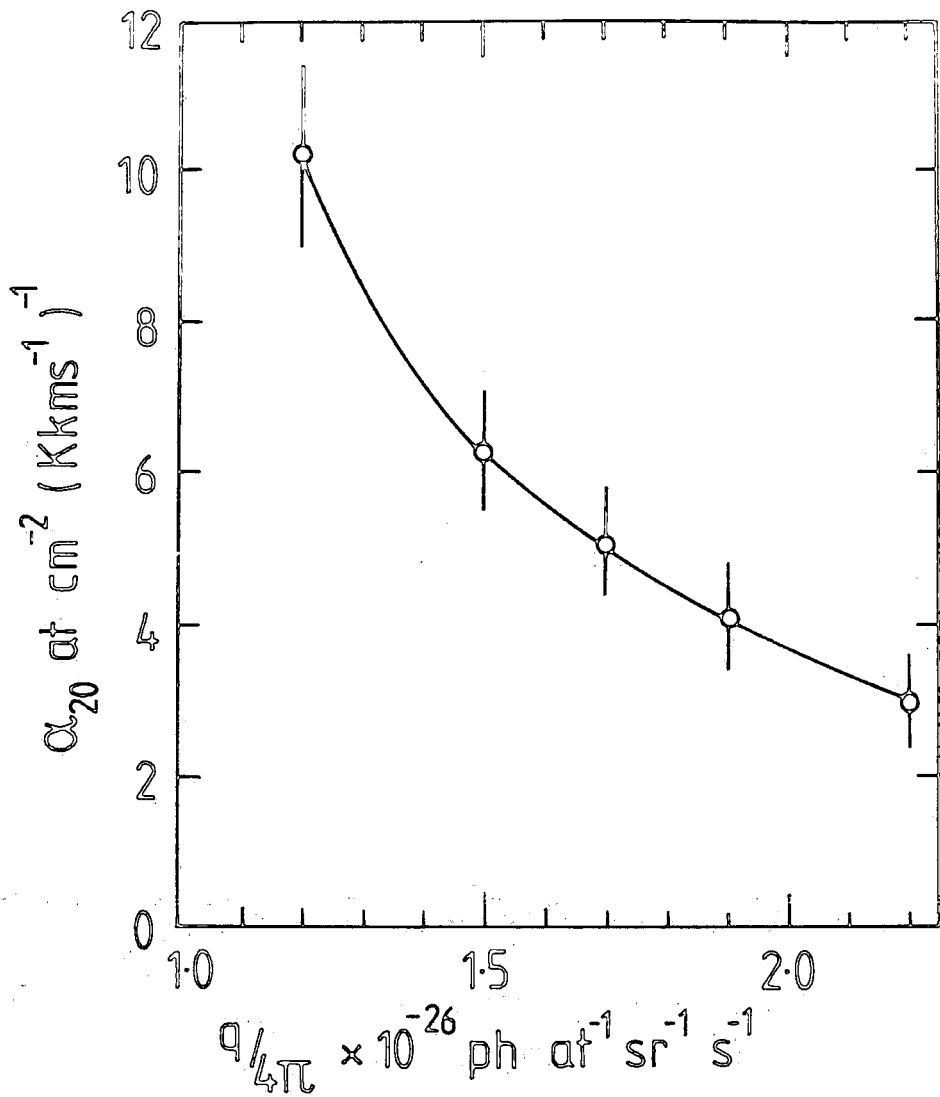
Figure 6.8 α_{20} ($\pm$ 1σ) as a function of $q/4\pi$ for the case N = 1.0.

α_{20} as a function of $q/4\pi$ are plotted in Figure 6.8. We estimate that a $\pm$ 20% uncertainty on $q/4\pi$ = 2.0 x 10^{-26} ph at^{-1}sr^{-1}s^{-1} introduces factors of -35%, $+50\%$ variation in α_{20}, ignoring the statistical uncertainty in α_{20}.

Bloemen et al. (1984b) make a similar analysis of the Orion region and derive α_{20} = 5.2 $\pm$ 2.4, corresponding to the N = 1.0 case. This value is higher than derived above; however the discrepancy can be attributed to specific differences between the two analyses. Bloemen et al. use an emissivity, $q/4\pi$ = 1.7 x 10^{-26} ph at^{-1}sr^{-1}s^{-1} derived from a previous analysis of the COS B data (Table A.2). More recent analyses (Table A.2) suggest this is likely to be an underestimate and we note from Figure 6.8 that reducing $q/4\pi$ significantly increases α_{20}. Furthermore Bloemen et al. treat the gamma-ray background term I_b(6.2) as a variable and perform the analysis over the entire Orion region indicated in Figure 6.1 (480 sq. deg.); whereas the present method is restricted to the clouds ($W_{CO} \geqslant 1$ K kms^{-1}).

As a consistency check we perform the regression analysis over all the data bins (480 sq. deg.), taking N = 1.0, $q/4\pi$ = 1.7 x 10^{-26} ph at^{-1}sr^{-1}s^{-1}. We obtain α_{20} = 5.0 $\pm$ 0.7, in close agreement with α_{20} = 5.2 derived by Bloemen et al. We also reduce the isotropic background to I_b = 5.1 x 10^{-5} ph cm^{-2}sr^{-1}s^{-1} (as obtained by Bloemen et al.) and a similar analysis gives
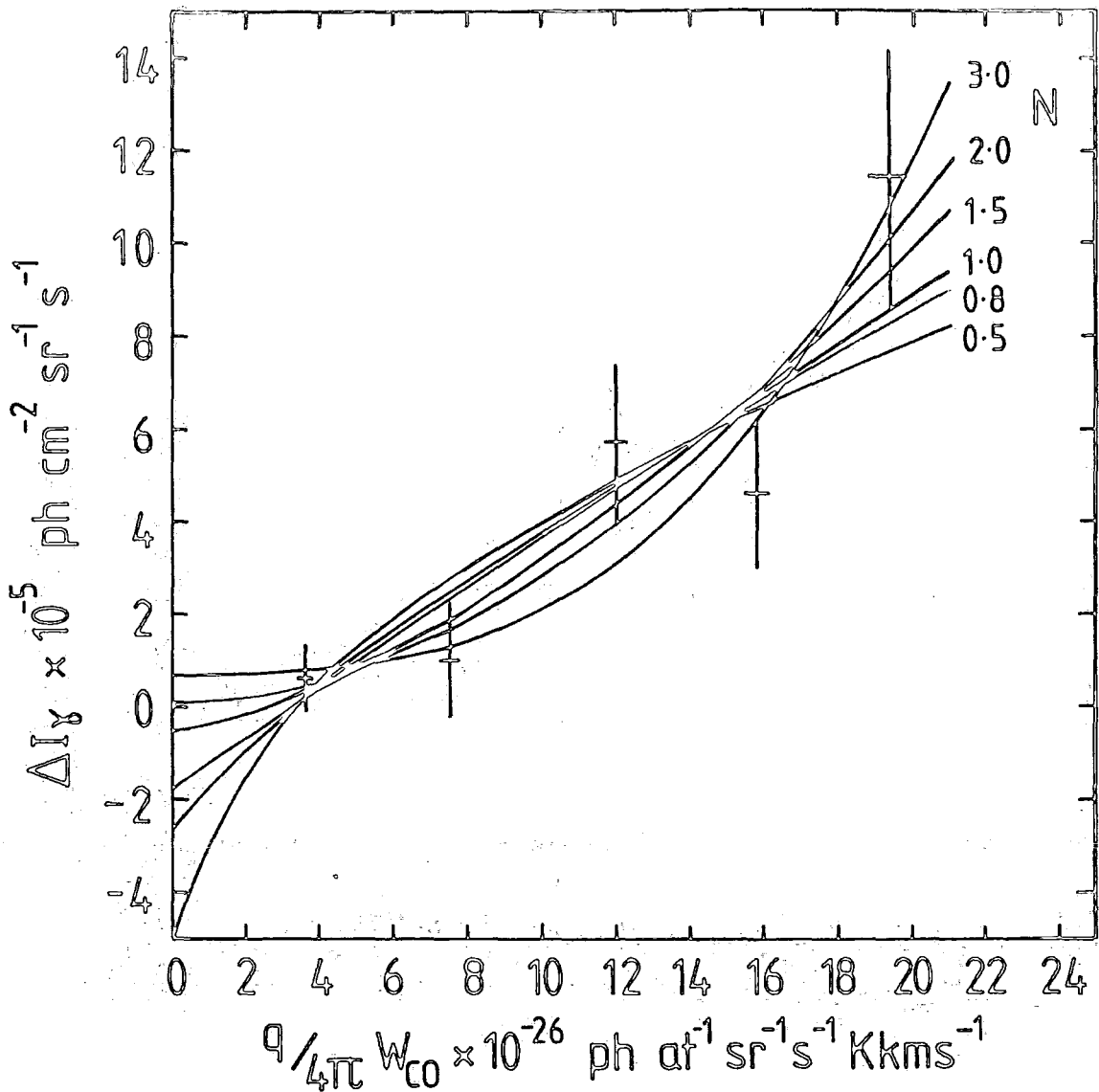
Figure 6.9. Variation of the excess intensity ΔI_γ (>100 MeV) as a function of $\frac{q}{4\pi}\left[W_{co}\right]^{N}$, for the Orion clouds. The isotropic background intensity I_b is treated as a variable. The binned observations are plotted with standard errors. Smooth curves give the expected gamma-ray intensity for each case of N.
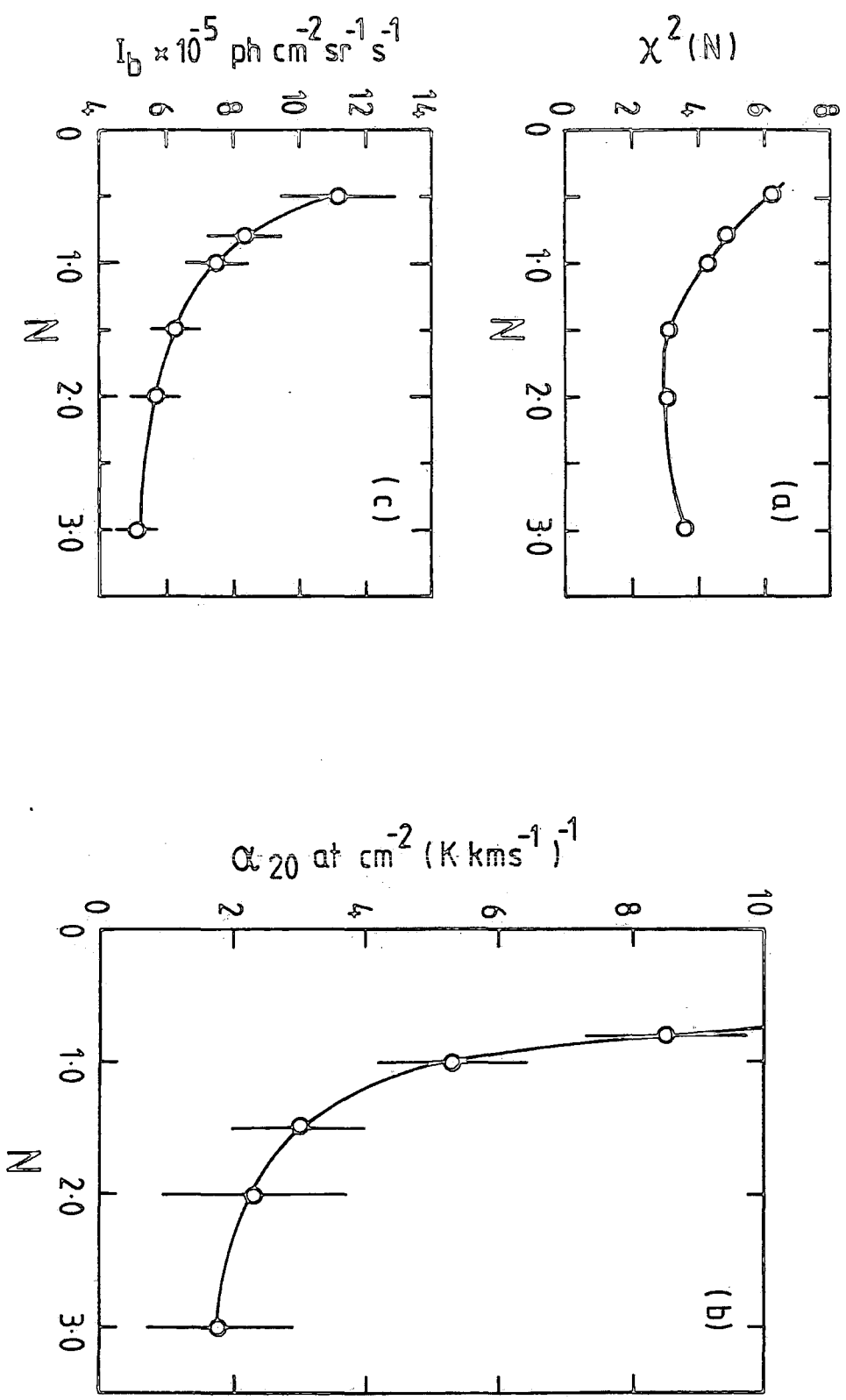
Figure 6.10. The dependence of the parameters χ^2 (a), α_{20} (b) and I_b (c) on N for the data of Figure 6.9. Errors bars are $\pm 1\sigma$, $\alpha_{20} = 2N_{H_2}/W_{co}$ in units of 10^{20} at cm^{-2} $(K\ kms^{-1})^{-1}$.

$\alpha_{20} = 5.9 \pm 0.7$. We conclude there is no significant discrepancy between the present analysis and that of Bloemen et al. Nevertheless it is apparent that the determination of α_{20} is sensitive to the emissivity adopted in the analysis.

It is possible that the gamma-ray background used by us ($I_b = 5.8 \times 10^{-5}$ ph cm^{-2}sr^{-1}s^{-1}) is not absolutely determined. We now consider the effect of treating the background as an additional variable. We proceed as before performing linear regressions on the data with $q/4\pi = 2.0 \times 10^{-26}$ ph at^{-1}sr^{-1}s^{-1} and N = (0.5, 0.8, 1.0, 1.5, 2.0, 3.0). The results for each N are presented on a linear W_{CO} scale in Figure 6.9 as smooth curves. χ^2 values are derived and these are plotted in Figure 6.10a along with the best fit values of α_{20}, Figure 6.10b, and the corresponding fitted backgrounds, Figure 6.10c.

The best fit is obtained for N = 2.3 ($\alpha_{20} = 2.0 \pm 1.3$, $I_b = 5.4 \times 10^{-5}$ ph cm^{-2}sr^{-1}s^{-1}). N = 1.0 ($\alpha_{20} = 5.3 \pm 1.1$, $I_b = 7.8 \times 10^{-5}$ ph cm^{-2}sr^{-1}s^{-1}) also produces a reasonable fit; though the magnitude of the background is large in comparison to the COS B determined level, $I_b = 5.8 \times 10^{-5}$ ph cm^{-2}sr^{-1}s^{-1}. However, it is unlikely that the background could be underestimated by $\simeq$ 25% in the COS B analysis.

Thus we consider a further case where the background is reduced to $I_b = 5.1 \times 10^{-5}$ ph cm^{-2}sr^{-1}s^{-1} in accordance
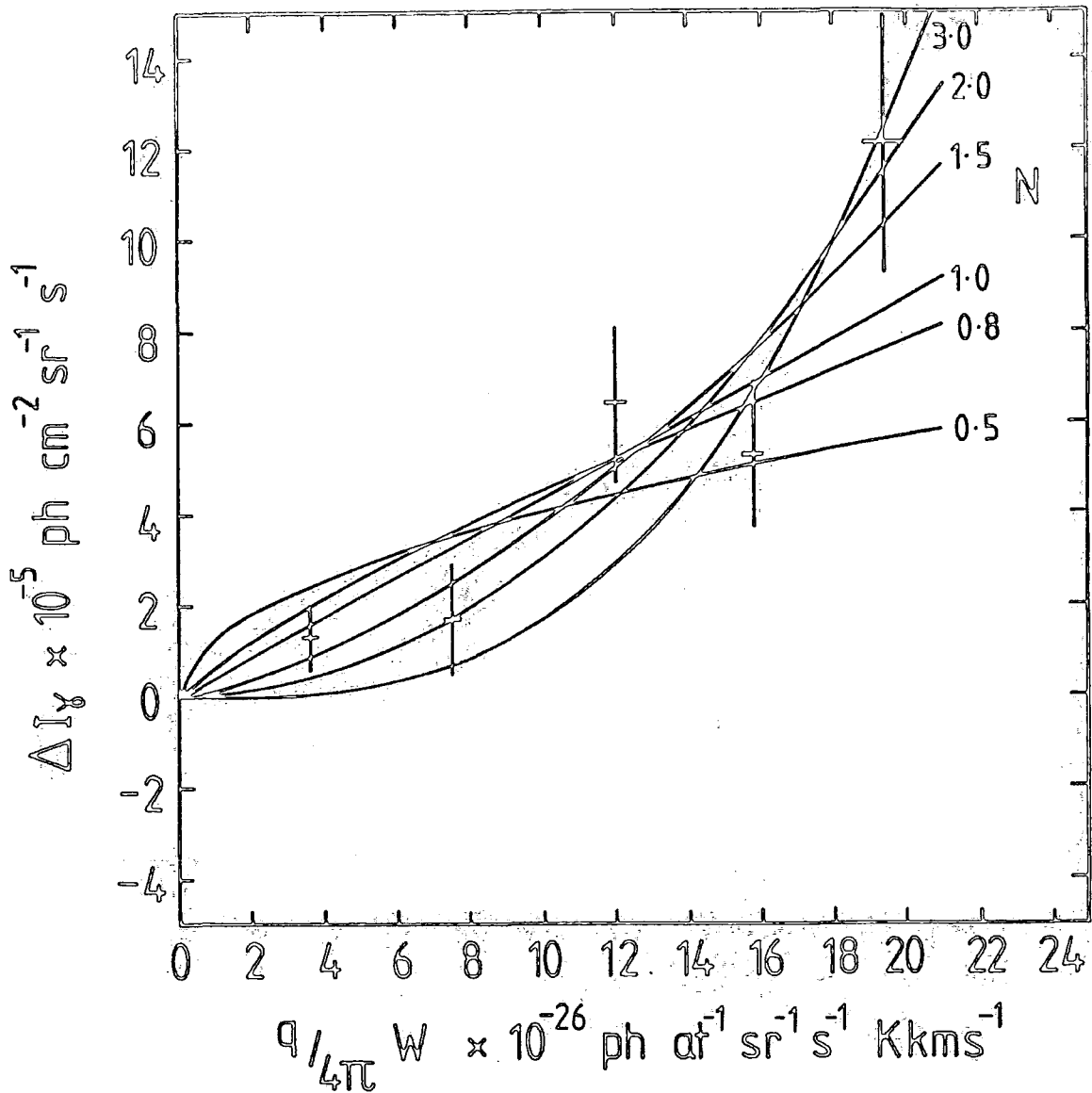
Figure 6.11 Variation of the excess intensity ΔI_γ (> 100 MeV) as a function of $q/4\pi\left[W_{co}\right]^N$, for the Orion clouds. A reduced fixed isotropic background intensity is assumed. The binned observations are plotted with standard errors. Smooth curves give the expected gamma-ray intensity for each case of N.
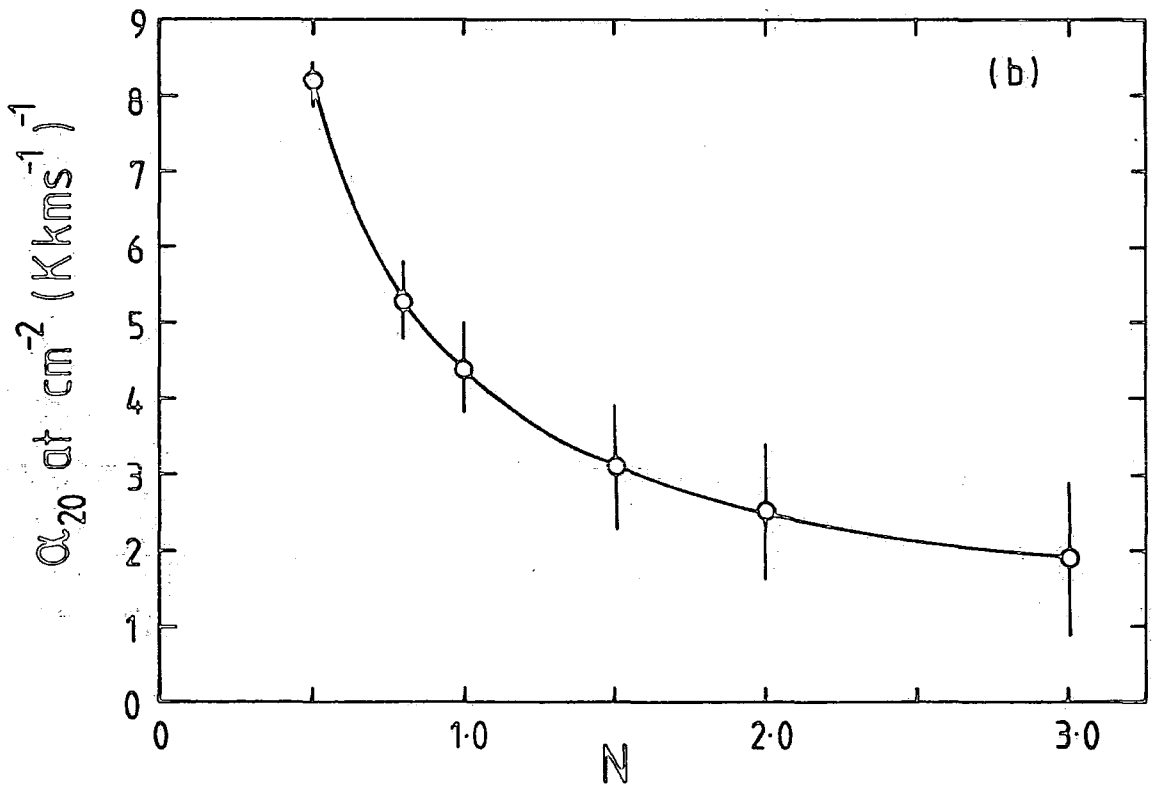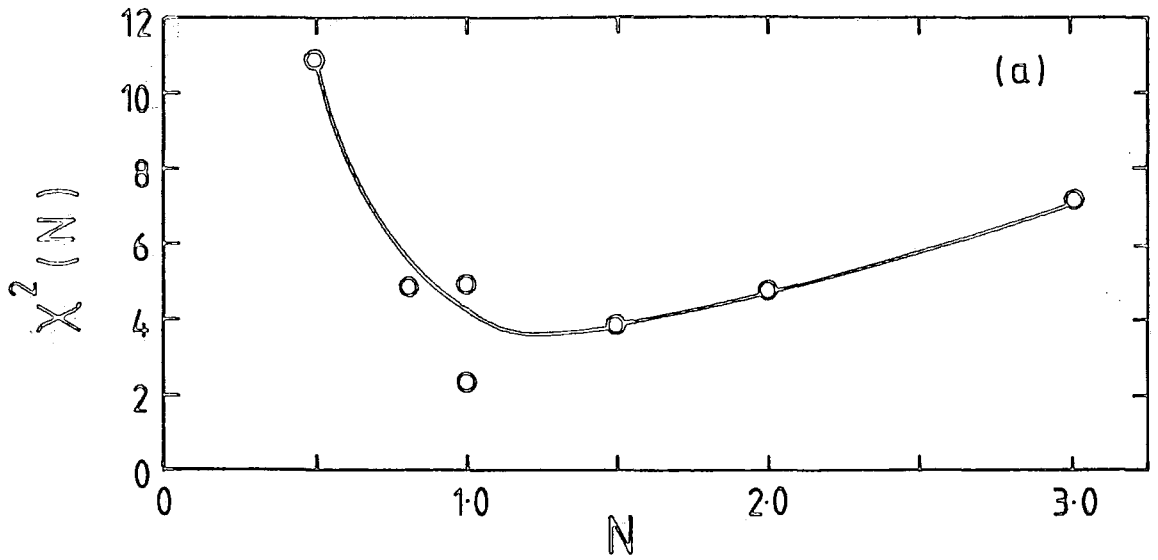
Figure 6.12. The dependence of χ^2 (a) and α_{20} (b) on N for the data of Figure 6.11. Error bars are $\pm\ 1\sigma$, $\alpha_{20} = 2N_{H_2}/W_{co}$ in units of 10^{20} at cm^{-2} $(K\ kms^{-1})^{-1}$.

with the fitted value of Bloemen et al. (1984b) and the analysis repreated for $q/4\pi = 2.0 \times 10^{-26}$ ph at^{-1}sr^{-1}s^{-1}, N = (0.5, 0.8, 1.0, 1.5, 2.0, 3.0). The regression plots are given in Figure 6.11 χ^2 and α_{20} are plotted in Figure 6.12. For N = 1.0 α_{20} = 4.4 $\pm$ 0.6 and the best fit gives N = 1.2, α_{20} = 3.7 $\pm$ 0.7.

6.10 Interpretation of the results

The results of the three separate regression sets are summarized in Table 6.1. Taken together they indicate the best case to be N > 1.0. Certainly it seems unlikely that N $\ll$ 1.0 is consistent with the data. Under the initial assumption of cosmic ray intensity inside the cloud scaling with W_{CO}, N < 1.0 is interpreted as increasing cosmic ray exclusion from the denser regions of the cloud. Uniform cosmic ray irradiation of the cloud corresponds to N = 1.0 and N > 1.0 indicates cosmic ray production (or enhancement) within the cloud; the enhancement rising towards the denser regions. We conclude that although N = 1.0 (α_{20} = 3.7 $\pm$ 0.6) is consistent with the data there is modest evidence favouring 1.0 < N < 2.0, α_{20} being correspondingly reduced.

Table A3 is a summary of α_{20} values derived by several workers from different methods. Most methods are based on comparison of optical extinction measurements to molecular line observations towards different clouds, though comparisons with gamma-ray data are also now being made. The present value (α_{20} = 3.7 $\pm$ 0.6) is generally lower than conventional estimates based on

		Best fit	Fit for N=1.0
Gamma-ray analysis	N	α_{20}	α_{20}
$I_b = 5.8 \times 10^{-5}$ ph cm^{-2}sr^{-1}s^{-1} fixed background	1.7	2.5 ± 0.9 (64%)	3.7 ± 0.6 (17%)
floating background	1.8	2.5 ± 1.2 (57%)	5.3 ± 1.1 (38%)
$I_b = 5 \times 10^{-5}$ ph cm^{-2}sr^{-1}s^{-1}	1.2	3.7 ± 0.7 (46%)	4.4 ± 0.6 (35%)
Galaxy count analysis	0.7	2.2 ± 0.1 (15%) (4.0)	1.5 ± 0.1 (1%) (2.7)

Table 6.1   Summary of the results from the gamma-ray
analysis (Section 6.10) and the galaxy count analysis
(Section 6.12). The best fit (minimum χ^2) values
for N and α_{20} ($\pm$ 1σ) are given and also α_{20}($\pm$ 1σ)
for the case N = 1.0. $\alpha_{20} = \alpha / 10^{20}$ at cm^{-2} (K kms^{-1})$^{-1}$.
Significance levels for each fit are also given. Two
values for α_{20} are given for the galaxy count analysis.
The bracketed values are corrected for the abnormal
reddening in the Orion nebula as described in Section
6.11.

extinction measurements. However, these analyses rely
on indirect arguments concerning local thermodynamic
equilibrium and virial theorem estimates applied to
the clouds. The present analysis concerns a single
giant molecular cloud, measuring the mass directly from
the gamma-rays produced therein. Taking account of
possible cosmic ray density variations limits this
technique. Nevertheless in gamma-ray astronomy it is
the giant molecular clouds which are believed to be
important cosmic ray targets in the Galaxy. Thus the
present analysis is considered more appropriate in relation
to typical giant molecular clouds.

We recall from Section 6.8 that allowing for the
low angular resolution of the gamma-ray data results
in the loss of about 12% of the CO emission. This is
not a uniform reduction on all the data bins but is
more dominant towards the edge of the clouds, that is
at low W_{CO} and negligible at high W_{CO}. It is therefore
not appropriate to simply increase α_{20} by 12%. We
estimate the net reduction in α_{20} to be much less than
this and certainly less than the statistical error on
α_{20}.

For the present data we directly estimate the H_2
mass in Orion for the case of uniform cosmic ray irradiation
($N = 1.0$, $\alpha_{20} = 3.7$). For the best fit ($N > 1$) the
situation is more complicated. We can interpret
α_{20} as directly measuring N_{H_2} and these reduced mass

	$N = 1.0$ $\alpha_{20} = 3.7$	$N = 1.7$ $\alpha_{20} = 2.5$	HI	HII
Orion A (51 sq.deg.)	0.74	0.50	0.08	0.12
Orion B (52 sq.deg.)	0.60	0.41	0.05	0.07

Table 6.2   Constituent masses of the gas components in the Orion clouds. The units are $10^5 M_\odot$. The H_2 mass estimates are derived from the high resolution ($1^\circ \times 1^\circ$ binning) data of Figure 6.3b. Allowing for metallicity effects may reduce the H_2 masses by a factor 1.3 − 1.6, Section 6.10. As explained in Section 6.10, the true H_2 mass estimate may lie between the limits given here.

estimates are also given in Table 6.2. In this case the additional gamma-rays must be produced by the increasing enhancement of the cosmic ray flux towards the denser regions of the cloud (i.e. high W_{CO}). Alternatively the cosmic ray flux may be constant throughout the cloud. The cloud masses are then identical to the $N = 1.0$ case and $N > 1.0$ then implies that W_{CO} increasingly underestimates N_{H_2} at large W_{CO}. Intermediate cases of cosmic ray enhancement and W_{CO}/H_2 variation within the clouds will have corresponding H_2 masses between the two limits given in Table 6.2. We also give the estimates of HI and HII mass derived by Houston and Wolfendale (1984b) for the Orion complex.

We can also make allowance for the effect of the metallicity correction on α_{20} (Section 5.4) writing $\alpha_{20} \rightarrow \alpha_{20}/[M]$ where $[M]$ is the metal abundance relative to the solar value. For the Orion nebula $[M] \simeq -0.1$ to -0.2 dex (Section 6.8). If these abundances are typical of the entire cloud then the local estimate of α_{20} is reduced by $\simeq 1.3 - 1.6$.

6.11 Analysis of the galaxy count data

We turn now to the second technique described in Section 6.7. The limitation with this method lies in the galaxy count saturation effect ($N_G = 0$) over the more intense W_{CO} regions of Orion. In an attempt to overcome this problem we use the results of the previous section to estimate the column density N_{H_2} in those

bins for which $N_G = 0$. As a first approximation, we assume that $N = 1.0$, $\alpha_{20} = 3.7$ correctly predicts the H_2 distribution within Orion. Using the CO data at its original resolution (Figure 6.3a) and the N_{HI} data smoothed to the same resolution, we derive the total gas column density $N_{H_t} = \alpha_{20}W_{CO} + N_{HI}$. For those bins with $N_G = 0$ we can then invert 6.5 to derive the equivalent $N_G(min)$.

We restrict the analysis to those bins with $W_{CO} \geqslant$ 1 K kms^{-1} and $N_G = 0$. Mean values for $N_G(min)$ are derived for several ranges of W_{CO}. These are given in Table 6.3. It is interesting to note that only two of the bins with $W_{CO} \geqslant 20$ K kms^{-1} also have $N_G = 0$. This is surprising in that we might expect greater extinction in the regions of high W_{CO}. However, these results are consistent with the bulk of the CO emission in these bins being restricted to small regions or knots within the main cloud. Therefore while the extinction towards the CO cores is very high ($N_G = 0$) it is much lower in the surrounding regions ($N_G > 0$) giving a mean non-zero galaxy count. The relative numbers of zero to non-zero galaxy count bins is low for $W_{CO} \geqslant 20$ K kms^{-1} suggesting that the most intense regions of CO emission tend to be more tightly clumped.

We proceed by taking one value of $N_G(min)$ and applying it to estimate N_{H_t} from 6.5 for each bin in the cloud ($W_{CO} \geqslant 1.0$ K kms^{-1}) with $N_G = 0$. We substitute the galaxy

W_{CO} K kms^{-1}	Total no. of bins	No. of bins with $N_G = 0$	N_G(min)
1.0 - 10.0	137	47	1.48
10.0 - 20.0	13	8	0.023
20.0 - 36.0	7	2	0.008

Table 6.3   The distribution of bins in the Orion region as a function of W_{CO} (original resolution). The values of N_G(min) are derived for those bins with zero galaxy counts ($N_G = 0$) as described in Section 6.10.

count, HI and CO data into 6.4 and, for each test value of N(= 0.3, 0.5, 0.8, 1.0, 1.5, 2.0), we perform a linear regression analysis to obtain α_{20}. For each fit we calculate a reduced χ^2 and the procedure is repeated for each of the three values of N_G(min). In all cases the fits are poor, χ^2 increasing with N. For N = 0.3 the best fit is significant at the 3% level. For N < 0.3, the W_{CO} data are increasingly compressed and the scatter converges to thin vertical strips. Determining a best fit for N is thus less than meaningful, nevertheless χ^2 does not show any rising trend down to at least N = 0.1.

Given the wide range in N_G(min) derived in Table 6.3 it is perhaps not surprising that a single value fails to produce a best fit to the data as described by 6.4. Therefore we estimate N_{H_t} using the value of N_G(min) appropriate for the intensity of CO emission in that bin. The data are again substituted into 6.4 and a linear regression performed for each value of N. The data are binned and transformed onto a linear W_{CO} scale. The results of these regressions are plotted as curves in Figure 6.13. χ^2 is plotted in Figure 6.14 a and corresponding values of α_{20} in Figure 6.14 b. From Figure 6.14 a we find the best fit to be N = 0.7 (α_{20} = 2.2 $\pm$ 0.1).
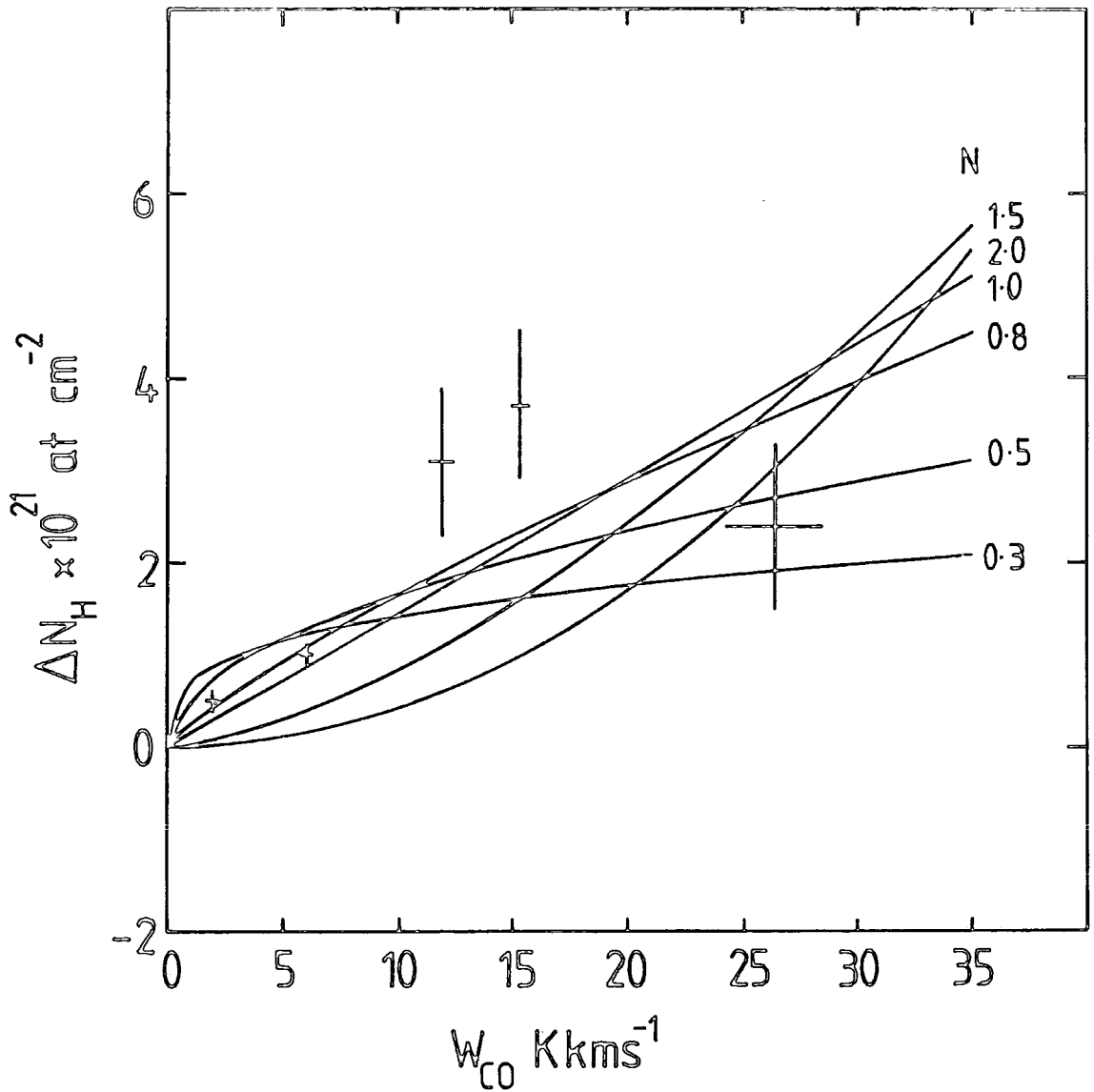
Figure 6.13. Variation of the excess gas column density $\Delta N_H = N_{H_t}(N_G) - N_{HI}$ as a function of W_{CO} for the Orion clouds. The binned observations are plotted with standard errors. Smooth curves give the expected excess column density for each case of N.
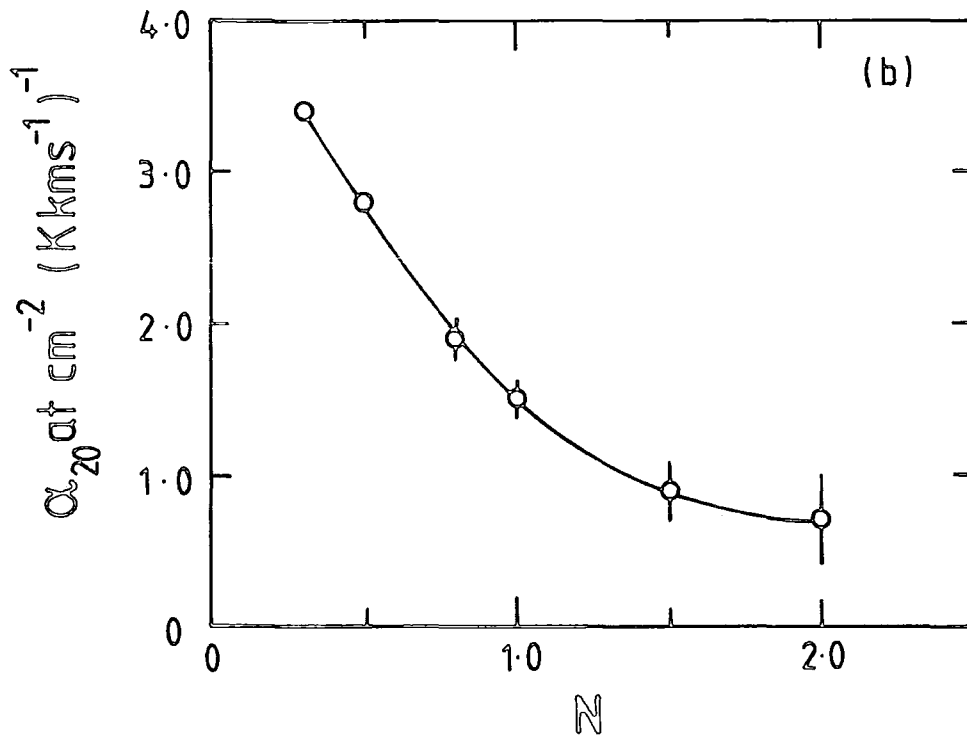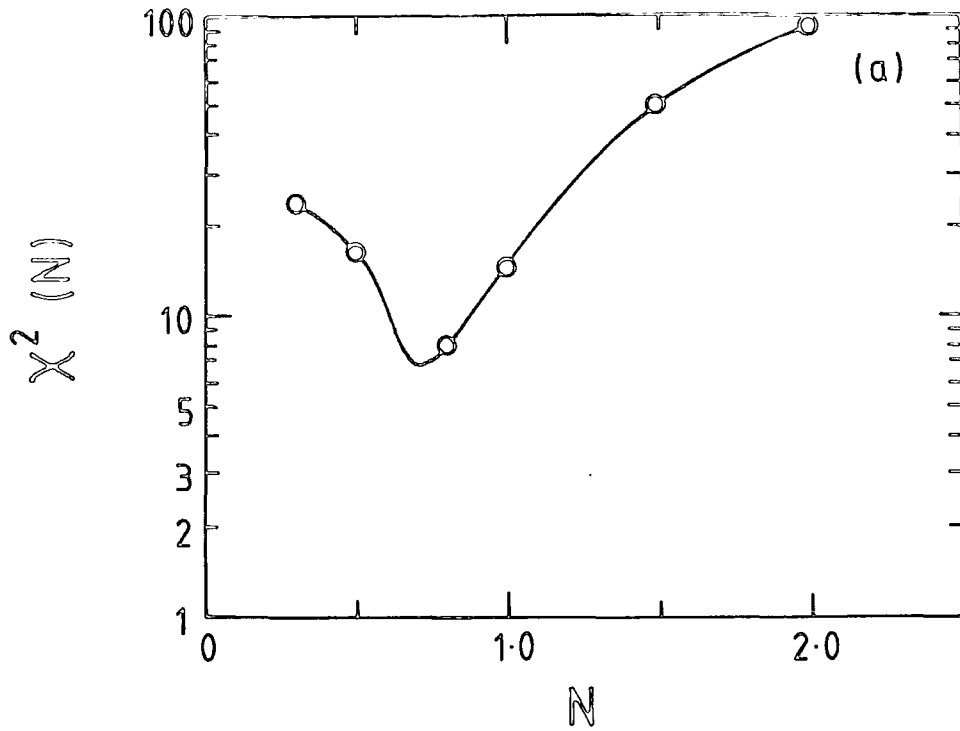
Figure 6.14. Dependence of the parameters χ^2 (a) and α_{20} (b) on N for the data of Figure 6.13. Error bars are $\pm 1\sigma$ (if larger than symbols), $\alpha_{20} = 2N_{H_2}/W_{co}$ in units of 10^{20} at cm^{-2} $(K\ kms^{-1})^{-1}$.

This result is necessarily heavily dependent on the initial assumptions used to estimate N_{H_t} whenever $N_G \doteq 0$. Although $N = 1.0$ cannot be excluded it does seem unlikely that N is greater than 1.0. In the galaxy count analysis (Figure 6.13), we are essentially comparing the excess extinction ΔE, not associated with HI, with the total gas (H_2) in Orion as estimated from W_{CO}. The slope of the regression line $\partial \Delta E / \partial W_{CO}$ is therefore the dust to gas ratio, the extinction being due to the dust. For a best fit case of $N < 1.0$, $\partial \Delta E / \partial W_{CO}$ decreases with W_{CO}, that is, the gas to dust ratio increases with W_{CO}. This is consistent with the observations of abnormally large reddening in the Orion nebula region (Section 6.5) and suggests the abnormal reddening may be more widespread within the cloud complex and may vary with position.

We recall from Section 6.5 that the large reddening is interpreted as arising from larger than average dust grains. Thus the low value of α_{20} obtained from the galaxy count analysis can be understood in relation to the reduced colour excess ($E(B-V)$) towards this region. Therefore to estimate the total gas column density from α_{20} (galaxy counts), we must first correct this value to the mean reddening appropriate for the general inter-stellar medium. The situation is complicated by the uncertainties of the size spectrum of dust grains throughout Orion and the likelihood that the gas to dust ratio

may vary within this complex. Nevertheless we assume $A_v/E(B-V) \simeq 5.5$. We also assume that α_{20}, determined from extinction measurements (galaxy counts), scales inversly with the reddening. The scaling factor for Orion is then $5.5/3.1 \simeq 1.8$. The best fit α_{20} is increased from 2.2 to ~ 4.0, similarly the fit for N = 1.0 is increased from 1.5 to ~ 2.7.

It is apparent that these corrected values are in better agreement with those obtained from the gamma-ray analysis (Table 6.1). The closeness may in part be fortuitous, but the results are at least consistent with our limited knowledge of the dust particles in the Orion complex.

CHAPTER SEVEN

THE GAMMA-RAY FLUX FROM EXTERNAL GALAXIES

7.1 Introduction

The nature of the isotropic gamma-ray background
was discussed in relation to previous analyses of the
data in Chapter 3. In this chapter we consider the pos-
sibility that unresolved extragalactic sources, specifically
radio galaxies and galaxy clusters, might contribute
to the extragalactic gamma-ray background. In the present
work we endeavour to use radio and X-ray observations
to help constrain the possible gamma-ray flux from extra-
galactic objects. In the context of a simple model we
compare the expected gamma-ray fluxes with those derived
from an analysis of the SAS II data and estimate the
total flux contribution from these extragalactic sources.

The primary difficulty in searching for extragalactic
sources relates to the problem of estimating the background
signal, which in this case results from cosmic ray inter-
actions throughout the Galaxy. Clearly, the best region
to search for extragalactic emission is at high Galactic
latitudes where the net flux is significantly reduced.
At high latitudes there is only information on the distribution
of atomic hydrogen but it is widely believed that there
is relatively little molecular hydrogen at these latitudes,
a belief confirmed by the CO survey results for the Galactic

plane which indicate that the scale height of CO (and therefore H_2) varies between 60 pc and 80 pc (Cohen et al. 1980; Sanders et al. 1984a). Recent high latitude observations of ^{12}CO (Dewey et al. 1983) cover six small regions with high HI column densities and low galaxy count (i.e. high extinction); and these regions would be expected to have significant column densities of H_2 ($\simeq$ 6 x 10^{20} at cm^{-2}). However, the results place upper limits on the column density $N_{CO} \lesssim 10^{15}$ mol. cm^{-2} implying $N_{H_2} \lesssim$ 2 x 10^{20} at cm^{-2}. Without an all-sky CO survey, estimates of the total gas in the Galaxy based only on HI emission are necessarily incomplete and another approach is needed.

The standard procedure adopted to overcome the limitation of lack of CO data relies on the use of galaxy counts to estimate the total gas column density along the line of sight. The expected diffuse Galactic gamma-ray flux can therefore be estimated as the product of the gas column density and the mean cosmic ray emissivity; a method similar in approach to that adopted in Chapter 5 to model the expected gamma-ray flux from the Galactic plane. We implicitly assume that discrete Galactic sources make a negligible contribution to the high latitude emission. The use of galaxy counts and their limitations as a tracer of total gas are discussed in detail in Chapter 6.

7.2 Extragalactic background radiation

The question of the relative contribution from each class of extragalactic object to an extragalactic gamma-

ray background is at present not well understood. Indeed
the absolute level of this background is still a matter
of uncertainty. We can consider the situation at other
wavelengths.

In the radio and optical bands the sky brightness
is the summed contribution from individual sources, that
is, discrete in origin. The microwave background is
conventionally interpreted as truly diffuse emission,
a relic from the era of recombination, within the framework
of a hot big bang cosmology. Ultraviolet measurements
have yet to place firm limits on the extragalactic background
at these wavelengths; while the recent IRAS satellite
observations confirms the existence of an infra-red back-
ground along with many extragalactic sources.

The situation at keV X-ray energies is still a matter
of controversy. Satellite measurements have established
the X-ray background to be $\simeq$ 2.4 x 10^{-8} erg $cm^{-2}sr^{-1}s^{-1}$
(2-6 keV) with resolved fluxes from normal galaxies, radio
galaxies, Seyferts, quasars and galaxy clusters. Table 7.1
is a summary of the relative contributions from extragalactic
objects to the diffuse X-ray background at these energies.
Not all the diffuse flux can currently be attributed
to discrete sources. Murray (1981) suggests that an
unresolved high redshift population of strongly evolving
quasars may be present. Alternatively, Silk (1973) points
out that a truly diffuse component of the X-ray background

TABLE 7.1

Type	L_x(ergs^{-1})	(Mpc^{-3})	df(erg cm^{-2}sr^{-1}s^{-1})
Normal galaxies	2×10^{39}	0.03	0.24×10^{-8}
Radio galaxies	6×10^{41}	3×10^{-5}	0.07×10^{-8}
Seyferts	10^{42}	3×10^{-4}	1.2×10^{-8}
QSO's	3×10^{45}	10^{-8}	0.08×10^{-8}
Clusters	2×10^{44}	10^{-6}	0.8×10^{-8}

Uhuru results on diffuse X-ray background 2-6 keV from review by Kellog (1973).

could originate from thermal bremmstrahlung in a hot
inter-cluster gas. Further measurements are required
with increased sensitivity and resolution to search for
additional sources and small scale anisotropies in the
background before this important question can be resolved.

In the gamma-ray region the interpretation of the
observations is hampered by low statistics and the poor
angular resolution of present detectors. Nevertheless
we endeavour to place limits on the flux from likely
extragalactic gamma-ray sources and any analysis of the
data must necessarily rely on gross statistical properties
of individual classes of sources, rather than a complete
sample of observed discrete sources.

7.3 Gamma-ray luminosity

We begin by considering normal galaxies and assume
our Galaxy to be typical with $L_\gamma(> 100 \text{ MeV}) \simeq 1.3 \times 10^{42}$ ph s^{-1}
(Strong and Worrall, 1976). Adopting a mean space density
for normal galaxies of $\rho = 10^{-2}$ Mpc^{-3} ($H_o = 50$ kms^{-1}
Mpc^{-1}, $q_o = \frac{1}{2}$; henceforth used throughout this chapter)
and neglecting evolutionary effects, the universal flux
F_u is given by

$$F_u = \int_o^{R_H} \frac{L_\gamma}{4\pi r^2} \rho(r) \, dV \qquad\qquad 7.1$$

$$F_u = L_\gamma \, \rho \, R_H \qquad\qquad 7.2$$

where R_H is the Hubble radius. Substitution yields F_u (>100 MeV) $\simeq 0.9 \times 10^{-6}$ ph cm^{-2}s^{-1} which is negligible when compared with the observed extragalactic flux F_γ (> 100 MeV) $\simeq (1.4 \pm 0.3) \times 10^{-4}$ ph cm^{-2}s^{-1} from the SAS II experiment (Section 7.11). Of course this is dependent on the use of our Galaxy as a typical normal galaxy. We recall from Section 3.8 that the upper limits to the gamma-ray flux from M31 and the LMC are consistent with the luminosity of our Galaxy if we assume that gamma-luminosity scales as the mass of the parent galaxy. Clearly, if discrete sources are to make a significant contribution to the extragalactic gamma-ray background we must consider (in analogy with the X-ray background) active galaxies, clusters of galaxies and quasars.

Above 100 MeV the dominant production mechanism of the diffuse Galactic gamma-ray emission is proton induced π° decay, with electron processes contributing about 20-30%. A useful estimate of the gamma-ray luminosity, L_γ, from p-p collisions can be derived from the gross properties of the Galactic matter and cosmic ray distribution. L_γ can be expressed as

$$L_\gamma \simeq \tfrac{1}{3} \sigma_{pp} \, n \, c \, \varepsilon_{cr} \, V \qquad\qquad 7.3$$

where σ_{pp} is the inelastic cross-section for p-p collisions, n is the mean density of target nucleii, c the velocity of light, ε_{cr} the cosmic ray energy density and V the volume over which the gamma-rays are produced. The factor

of $\frac{1}{3}$ allows for the probability that the collision product is a π^0 as opposed to $\pi^\pm$.

For our Galaxy cosmic rays can be considered to fill a disk of radius 15 kpc with a scale height $\simeq$ 1 kpc. The gas, however, has a maximum scale height $\simeq$ 100 pc with a similar radial extent. The latter disk thickness is more appropriate when considering gamma-ray production; the former for particle trapping. Taking typical values for $n \sim 1$ at cm^{-3} and $\varepsilon_{cr} \sim 1$ eV cm^{-3} (appropriate for cosmic rays above 1 GeV), then substitution in 7.3 yields L_γ (> 100 MeV) $\simeq$ 9.5 x 10^{50} eV s^{-1}. The Galactic gamma-ray spectrum above 100 MeV can well be described by an E_γ^{-2} power law, which over the SAS II energy range 100 MeV to 1000 MeV corresponds to a mean photon energy $\bar{} $ 2.6 x 10^8 eV. Thus we find L_γ (> 100 MeV) $\simeq$ 3.7 x 10^{42} phs^{-1}. Making an allowance for a 20% electron contribution we estimate L_γ(> 100 MeV) $\simeq$ 4.6 x 10^{42} phs^{-1} for the diffuse Galactic emission. Strong and Worrall's estimate, derived from the SAS II data, includes a discrete source component. The results of Chapter 5 suggest that at these energies discrete sources contribute about 20% of the Galactic flux. After allowing for this correction we estimate the observed diffuse luminosity to be about (1.0 - 1.1) x 10^{42} phs^{-1}. Thus our simple model over-estimates the diffuse flux by about a factor of 4. To achieve improved agreement would require more detailed

modelling of the cosmic ray and gas distributions throughout the Galaxy. However, the present model is considered sufficient as an order of magnitude estimate.

We could, in principle, use 7.3 to estimate the proton contribution to the gamma-ray flux, though first we require knowledge of the parameters n, $\mathcal{E}_{cr}$ and V. Radio synchrotron data yields information on the interactions of relativistic electrons and magnetic fields within a source region. In radio astronomy such measurements are often used to obtain estimates of the total energy in relativistic electrons. By assuming an appropriate ^{e}/p ratio for the observed region the total cosmic ray proton energy can thus be estimated.

7.4 The radio synchrotron minimum energy condition

Many workers have dealt with the minimum energy requirement for a synchrotron source (e.g. Ginzburg and Syrovatskii, 1964; Longair 1981). In this approach the total energy in the source region is expressed as the sum of magnetic field energy and relativistic particle energy as a function of magnetic field. For a power law electron spectrum $N(E) \sim E^{-\gamma}$ and synchrotron spectrum $S_\nu \sim \nu^{-\alpha}$ ($\gamma = 2\alpha + 1$) the minimum energy condition can be expressed as

$$W_{min}(erg) = 13.34 \ V(m^3)^{3/7} \left[G_\eta \ L_\nu \ (WHz^{-1}) \right]^{4/7}$$

7.4

where

$$G = \frac{2.34 \times 10^{23}}{(\gamma - 2)} \frac{\nu_{min}^{\frac{2-\gamma}{2}} - \nu_{max}^{\frac{2-\gamma}{2}}}{a(\gamma) \nu^{\frac{1-\gamma}{2}}} (1.0022)^{\gamma}$$

7.5

and $a(\gamma)$ is a constant dependent on γ such that

γ	1	1.5	2	2.5	3	4	5
$a(\gamma)$	0.283	0.147	0.103	0.0852	0.0742	0.0725	0.0922

It is assumed that cosmic ray protons have an energy spectrum similar to that of electrons and $\mathcal{E}_{total} = \eta \, \mathcal{E}_{electrons}$. The synchrotron power $L_{\nu}(WHz^{-1})$ is measured at an observed frequency ν (MHz) with a spectral index $\alpha = \frac{\gamma - 1}{2}$. Normally ν_{min} and ν_{max}, the limits of the synchrotron spectrum, are taken to be 10 MHz and 100 GHz respectively. For the minimum energy condition it can be shown that W(magnetic field) = $\frac{3}{4}$ W(particles) which is closely associated with the idea of equipartition of energy between magnetic fields and relativistic particles. In our Galaxy the large scale distribution of energy between protons and electrons is such that $\eta \sim 33$, though for the Crab pulsar $\eta \sim 1$, and it is often assumed that η can vary from 1 - 100 in radio galaxies.

Thus by using synchrotron data from known sources we can derive from 7.3, 7.4, 7.5 an estimate of the expected proton induced gamma-ray flux above 100 MeV.

7.5 Estimates of gamma-ray luminosity for nearby galaxies

Before applying this method to known extragalactic radio sources it is first necessary to test its usefulness by applying it to several objects for which firm gamma-ray measurements are available. It is not possible to use our Galaxy in this context because of the large uncertainties involved in deriving the total radio flux from local measurements.

First we consider the nearby galaxy M31, similar in size and structure to our own. Beck and Grave (1981) have made a detailed study of the synchrotron emission from this object and estimate S_ν (408 MHz) $\simeq$ 11.85 Jy, $\alpha \sim 0.75$. Their integrated flux is smaller than previous measurements which were unable to distinguish the additional background contribution from distant radio galaxies. Adopting a distance of 670 kpc and η = 33 (as for our Galaxy) we find from 7.4 W_{min} (erg) $\sim$ 2.0 x 10^{54} $R^{9/7}$ (kpc). In that M31 is not a spherical source it is inappropriate to adopt a single radius R. However, the equivalent effective radius must be between 10 kpc and 20 kpc yielding $W_{min} \sim$ 0.4 - 0.9 x 10^{56} erg. Adopting W = 0.6 x 10^{56} erg and n = 1 at cm^{-3} we expect F_γ (> 100 MeV) $\simeq$ 0.7 x 10^{-6} ph $cm^{-2} s^{-1}$. For M31 we estimate the observed flux at this energy to be $\simeq$ 0.3 x 10^{-6} ph $cm^{-2} s^{-1}$ from the SAS II data (Section 3.8). Given the many sources of uncertainty the two values are not inconsistent, though by no means conclusive. We proceed by considering an active radio-

galaxy.

The giant elliptical galaxy M87 lies at a distance of
of 25 Mpc close to the centre of the local Virgo cluster.
Allen (1973) summarized the synchrotron data on this object:
S_ν (100 MHz) $\simeq$ 1800 Jy, $\alpha \sim 0.8$. For a spherical region,
radius R = 20 kpc and η = 100, 7.4 gives $W_{min} \simeq$ 1.1 x
10^{59} erg. Taking n = 1 at cm^{-3} over the source region
yields on substitution in 7.3 F_γ (> 100 MeV) $\simeq 10^{-6}$ ph $cm^{-2}s^{-1}$.
No absolute flux has been measured and an analysis of
the SAS II data gives an upper limit F_γ (> 100 MeV)
$\lesssim$ 0.3 x 10^{-6} ph $cm^{-2}s^{-1}$.

The detection by COS B of a finite flux from NGC
1275 (Strong and Bignami, 1983) suggests we should also
consider this object. Allen (1973) gives S_ν (100 MHz)
$\simeq$ 130 Jy, $\alpha \sim 0.8$ for NGC 1275, at a distance of 116 Mpc.
As for η and R we again adopt the canonical values 100
and 20 kpc respectively, yielding from 7.4 $W_{min} \simeq$ 1.5
x 10^{59} erg. For n = 1 at cm^{-3} we expect L_γ (> 100 MeV)
$\simeq$ 9.4 x 10^{46} ph s^{-1}. This time, the COS B observations
have given a detection and they imply L_γ (> 100 MeV)
$\simeq$ 8.6 x 10^{47} ph s^{-1} for this source.

It is also important to remember that these estimates
are only for the proton component of gamma-ray emission
and it is probable that in many cases electron processes
will make a more significant contribution than in our
Galaxy. We now consider the extreme case of pure electron
source, η = 1. The minimum energy varies as $\eta^{4/7}$ and

is thus reduced by a factor $(0.01)^{4/7} \simeq 0.07$. For an unionized gas the total energy loss rate due to electron bremmstrahlung is given by

$$L_\gamma = 7.26 \times 10^{-16} \ n \ E \ eV \ s^{-1} \qquad\qquad 7.6$$

where n is the gas density (at cm^{-3}) and E the total electron energy in eV. For NGC 1275 we find $W_{min} \simeq$ 1.5×10^{59}erg for $\eta = 100$ and $W_{min} \simeq 1.1 \times 10^{58}$erg for $\eta = 1$. Substitution into 7.6 with $n = 1$ at cm^{-3} yields $L_\gamma(> 100 \ MeV) \simeq 1.9 \times 10^{46}$ ph s^{-1}.

For intermediate cases of $1 < \eta < 100$ the total estimated gamma-ray luminosity correspondingly lies between the limits $(1.9 - 9.4) \times 10^{46}$ ph s^{-1}. However the uncertainty attached to the parameters η, n and V, and indeed the possibility of non-equipartition for individual sources, increases the uncertainty on the expected gamma-ray luminosity. Nevertheless,from the limited sample considered, observation and model estimates agree to within an order of magnitude and the technique is applicable to derive a subset of gamma bright extragalactic radio objects.

As an estimate of the uncertainty in the expected fluxes we can assume $V \propto R^3$. The dependence of n on R is not obvious. For our Galaxy n is virtually independent of Galactocentric radius $(4 < R < 10 \ kpc)$ though in other galaxies (e.g. NGC 6946, NGC 4321) n appears to decrease slowly with R (Bhat et al., 1984(b)). For the present

purposes we take $n \propto R^{-1}$ and in conjunction with 7.3 and 7.4 we find $F_\gamma \sim R^{2/7} \eta^{4/7}$. Substituting probable values of R and η for an extragalactic radio source (R = 5-50 kpc, η = 1-100) the variation of F_γ is seen to be small, less than a factor of ten. It is concluded that the minimum energy technique is a useful indicator of gamma-ray activity, at least to within an order of magnitude.

We aim,therefore, to use data on known radio sources to estimate the expected gamma-ray flux for the canonical values of R, η and n. The radio bright objects are expected to be gamma-ray sources and can form the basis for a search of the gamma-ray data for extragalactic sources.

7.6 Activity in galaxy clusters

X-ray properties of rich clusters of galaxies have been extensively studied (e.g. Gursky and Schwartz, 1977; Soltan and Henry, 1983; Abrampoulos and Ku, 1983; Jones and Forman, 1984), and there is now a broad consensus on the interpretation of the accumulated data.

Observations of clusters indicate that the spectra are most likely thermal in nature, the bulk of the emission being genuinely diffuse in origin, although in some cases (e.g. Perseus) there are additional non-thermal components of emission associated with active members of the clusters. In clusters, the thermal emission is believed to originate in an intra-cluster ionized gas with temperature $T \sim 10^{7-8}K$ and density $n \sim 10^{-3} - 10^{-4}$ at cm^{-3} in the

core region (radius $\sim$ 200 - 300 kpc).

The observations in Perseus, Virgo and Coma of a
spectral feature at about 6.7 keV is interpreted as iron
line emission from the intra-cluster gas (Serlemitsos
et al., 1977). This is very strong evidence supporting
the thermal nature of the diffuse emission and demonstrates
that a significant fraction of the gas has been through
a cycle of stellar evolution. The origin of the gas
is still uncertain. It may be a remnant from the era
of cluster and galaxy formation which is continuously
accreting onto the galaxies and being re-expelled. Alter-
natively it may be due to the expulsion of enriched galactic
gas.

For a rich cluster with about 100 normal members
we see from Table 7.1 that cluster X-ray luminosity is
typically more than three orders of magnitude greater
than that of its constituent galaxies. Many workers
find a strong correlation of luminosity with cluster
morphology (e.g. Gursky et al., 1972; McHardy, 1978;
Kowalski, 1982; Abrampoulos and Ku, 1983; Soltan and
Henry, 1983). Soltan and Henry find the mean cluster
luminosity increases with richness class; L_x(2 - 10 keV)
varying from 4.4 x 10^{44} erg s^{-1} for richness R = 1 to
8.3 x 10^{44} erg s^{-1} for richness R = 4 and 5. Abrampoulos
and Ku find correlations between X-ray luminosity, richness,
central galaxy density and velocity dispersion.

Associations between radio sources and rich clusters are also extensively studied (e.g. van den Bergh, 1961; Fomalont and Rogstad, 1966; Riley, 1975). Radio emission from clusters is generally associated with individual radio galaxies but with occasional extended emission as in the Coma cluster (Sastry and Shevgaonkar, 1983). There does not appear to be any correlation between radio luminosity and cluster richness though the radio emission is often associated with giant CD type galaxies in the cluster cores. About 10% - 15% of clusters have one or more radio galaxies as members. Radio galaxies have luminosities $\sim 10^{4-6}$ times those of normal galaxies and their presence in clusters is further indication of violent activity therein.

The evidence from X-ray and radio emission in clusters suggests the presence of copious energy sources. X-ray emission in particular appears to be a wide-spread characteristic. However, its thermal nature does not by itself indicate the presence of relativistic particles necessary for gamma-ray production. The extensive ionized gas in the intra-cluster medium could provide a target for gamma-ray production by relativistic particles diffusing out of active galaxies or being accelerated in situ.

7.7 Gamma-ray emission from rich clusters

Measurements of the cosmic ray flux ($\gtrsim 1$ GeV) in our Galaxy indicate that the particles traverse about 6 g cm^{-2} of the interstellar medium, that is approximately

[1]/10 of the interaction length. Unless the diffusion
coefficient and grammage are markedly different in other
galaxies then the cosmic rays will only lose about 10%
of their energy in the parent galaxy and the bulk of
the cosmic ray flux will diffuse out into the surrounding
medium.

For isolated galaxies, like our own, the cosmic
rays escape into the intergalactic medium and presumably
finish many tens of Mpc away. However, for radio galaxies
situated in rich clusters the cosmic rays will diffuse
into the cluster cores. These regions are typically
200-300 kpc in radius and X-ray measurements indicate
mean gas densities to be $\sim 10^{-3}$ at cm^{-3}. Dennison (1980)
suggests that the diffusion of primary protons and the
subsequent production of relativistic electrons, through
collisions with the intra-cluster medium, can account
for the energy requirements of the radio halo observed
in the Coma cluster. However, Valtaoja (1984) has shown
that the distribution of halo radio emission in Coma
is best described by the diffusion of primary electrons.

Although only about 10-15% of clusters are believed
to have radio halos this is more likely due to the absence
of extensive intra-cluster magnetic fields, rather than
low cosmic ray fluxes (Valtaoja, 1984). Thus, assuming
relativistic protons are also produced in the radio galaxies,
gamma-ray production will necessarily occur both in the
radio galaxy and the surrounding medium.

Taking NGC 1275 as a typical cluster radio source we have already estimated $L_\gamma (> 100$ MeV$) \simeq 9.4 \times 10^{46}$ ph s^{-1}. If this corresponds to 10% of the cosmic ray energy loss, then the total gamma-ray luminosity is likely to be about 9.4×10^{47} ph s^{-1}. Interestingly this is in close agreement with the luminosity implied by the COS B observations, $\simeq 8.6 \times 10^{47}$ ph s^{-1} above 100 MeV. The gamma-ray emission from the core region will not be uniformly distributed but will depend on the distribution of cosmic rays diffusing from the central source, folded with the gas profile.

We can apply these criteria to the original luminosity estimate for M87 in the Virgo cluster. The net gamma-ray luminosity will then be $L_\gamma = 7.0 \times 10^{47}$ ph s^{-1} above 100 MeV and correspondingly $F_\gamma (> 100$ MeV$) \simeq 10^{-5}$ ph cm^{-2} s^{-1}. This is approximately a factor of 30 above the SAS II upper limit for M87 ($\lesssim 0.3 \times 10^{-6}$ ph cm^{-2} s^{-1}), indicating that the parameters ($\eta = 100$, R = 20 kpc) adopted for the present model are too large for this particular object.

7.8 Description of the data

(i) Radio galaxies

The combined data collected by Pooley and Henbest (1974), Riley and Pooley (1975) and Jenkins et al. (1977) constitute a complete sample of 3CR radio sources; S_ν (178 MHz) $\geqslant 10$ Jy, dec $> 10°$ and $|b| \geqslant 10°$. Of the 182 sources 109 have optical identifications and hence distance estimates. It is these which are considered

in the present analysis.   In many cases the sources have
multiple components corresponding to central hot-spots,
double side-lobes and extended tails.   We always use
the flux measurements from the central region as rep-
resentative of the source for the purposes of estimating
the cosmic ray energy therein.   The spectral indices
are obtained from a comparison of the flux densities
at 5GHz with those at 178 MHz.

McHardy (1979) selects those 4C and 4CT radio sources
(S_ν (178 MHz) $\geqslant$ 2 Jy and dec > 10°) lying within 0.9 Mpc
of an Abell cluster centre and identified with a galaxy
which is almost certainly a member of that cluster.
The angular resolution of the 4C survey ($\sim$ 3 arc min
at 408 MHz) is such that extended sources are excluded
from the catalogue.   To eliminate possible distance biasing
only those sources definitely or most probably identified
with a cluster are accepted.   This restricts the sample
to 49 sources for which McHardy gives data on the radio
power at 408 MHz, the spectral index and the distance.

The range of luminosity of the 158 identified radio
sources extends over several orders of magnitude.   To
analyse the gamma-ray data at all these positions results
in the use of many non-independent bins.   Additionally
the signals from weaker sources are unlikely to be detectable,
contributing only to the local background flux in those
directions.

For all the radio sources standard values of R = 20 kpc.,

η = 100 and n = 1 at cm^{-3} are adopted. Using 7.3,
7.4, 7.5 the expected flux above 100 MeV is evaluated
for each source and only those with F_γ, expected
$\geqslant 10^{-10}$ ph $cm^{-2}s^{-1}$ are selected for analysis. These
data are further divided into two luminosity classes:
those with F_γ, expected $> 10^{-8}$ ph $cm^{-2}s^{-1}$ (15 sources)
and those with 10^{-10} ph $cm^{-2}s^{-1} < F_\gamma$, expected
$< 10^{-8}$ph $cm^{-2}s^{-1}$ (48 sources). The parameters for both
these sets are given in Tables A.4 and A.5.

(ii) Rich clusters

The source of data on galaxy clusters is the Abell
catalogue (Abell, 1958) containing 2172 rich clusters.
A subset of these (1682 members) is defined as a statistically
complete sample for dec > - 27°. Each cluster in the
catalogue is assigned to one of 5 richness classes, dep-
ending on the number of galaxies in the cluster. The
mean distance to each cluster is catalogued in one of
6 intervals, based on the magnitude of the 10th brightest
galaxy in the cluster (m_{10}). For an object of unknown
redshift, $\dot{m}_{10}$ is usually taken as an indicator of distance.
This is a standard technique developed by Hubble which
assumes that on average the 10th brightest members of
clusters always have the same intrinsic luminosity.
The Hubble diagram $(m_{10} - Z)$ is used as the conversion
from brightness m_{10} to redshift, and distances are cal-
culated using the standard relation:

TABLE 7.2

Distance Class D	m_{10}	$\bar{Z}$	$\bar{R}$(Mpc)	n(D)
1	13.3 – 14.0	0.027	155	9
2	14.1 – 14.8	0.038	214	2
3	14.9 – 15.6	0.067	359	33
4	15.7 – 16.4	0.090	464	60
5	16.5 – 17.2	0.140	666	657
6	17.3 – 18.0	0.180	808	921
1–4	(15.54)	0.072		104

Richness Class R	No. of galaxies	n(R)
1	50 – 79	1224
2	80 – 129	383
3	130 – 199	68
4	200 – 299	6
5	300 +	1

The distributions in distance and richness·classes of Abell's complete cluster sample.

$$D = {}^c/H_oq_o^2(1+z)^2 \left\{ q_oZ + (q_o-1) \left[(1+2q_oZ)^{\frac{1}{2}}-1 \right] \right\}$$

7.7

For the purposes of the present chapter, we assume $q_o = \frac{1}{2}$ and $H_o = 50 \text{ K kms}^{-1} \text{ Mpc}^{-1}$. The definitions of Abell's distance and richness classes are given in Table 7.2.

For the present analysis 83 clusters are selected from Abell's complete sample. This restriction is due in part, to the limited coverage of the SAS II data for several sky regions. However, the primary selection is on the distance class criterion with only $D \leqslant 4$ being accepted, effectively limiting the richness to $R \leqslant 2$. The distribution of the clusters finally used is given in Table A.6.

(iii) Galaxy counts

The Lick galaxy counts of Shane and Wirtanen (1967) are used to estimate the total gas column density away from the Galactic plane. These data and their limitations are discussed more fully in Chapter 6. In this chapter we use the same conversion from mean galaxy count N_G to column density N_{H_t}:

$$N_{H_t}(N_G) = 2 \times 10^{21} \log_{10}(N_G^o/N_G) \text{ at cm}^{-2}$$

7.8

taking $N_G^o = 75$ as the mean galaxy count per square degree in the absence of extinction.

In their analysis of the gamma-ray flux from the direction of NGC 1275, Strong and Bignami (1983) draw attention to the effect of galaxy clustering leading to an underestimate of the total gas as measured directly by HI. An inspection of the galaxy count data (1° x 1° binning) shows that in many bins containing clusters there is an excess count relative to the surrounding bins. Thus it is important to consider the likely effects of clustering on estimates of the column density obtained using 7.8.

Austen and Peach (1974) give a general luminosity distribution for field galaxies:

$$\log_{10} N(\leqslant m_v) = -8.99 + 0.60\, m_v \qquad\qquad 7.9$$

expressed in galaxies per square dgreee in the absence of absorption. The Lick survey is complete to a limiting magnitude $m_v \simeq 18.0$, and from 7.9 we therefore expect about 65 galaxies per square degree in the field. Given the uncertainties associated with defining the low-luminosity tail of the field galaxy distribution this value is in reasonable agreement with $N_G^o = 75$ adopted for the present work.

In the present work attention is restricted to distance classes $D \leqslant 4$ and richness classes $R \leqslant 2$. For this subset of the Abell catalogue we find from Table 7.2 the mean number of galaxies per cluster to be about 75. The Abell radial size criterion for clusters is 3 Mpc, which for a mean redshift $Z = 0.072$ corresponds to an area $\simeq 0.5$ deg^2

on the sky. For this sample the mean cluster richness

(75 galaxies over 0.5 deg^2) is therefore significant

in relation to the field count ($\simeq$ 65 galaxies over 1 deg^2).

However, to allow for the angular resolution of the gamma-

ray data, the galaxy counts are averaged over 3 x 3 bins

corresponding to an area $\simeq$ 18 deg^2 (Section 7.9).

The total field count is then = 1170, to be compared

with 75 for the mean cluster. The number of galaxies

due to a cluster is thus comparable to the statistical

noise level on the background. We expect cluster en-

hancement on these scales to be small but nevertheless,

it is likely to consistently lead to an underestimate

of the gas column density towards cluster positions.

Thus gamma-ray excess intensities above the Galactic

background are likely to be overestimated.

7.9 Derivation of extragalactic intensities and local
emissivities

It is not expected that statistically significant

fluxes from individual sources can be detected. But

by summing together the signals from many positions it

is hoped to see a finite excess signal over and above

the background from cosmic ray interactions in the Galaxy.

The technique used is therefore to compare the gamma-

ray intensity at source positions with the total column

density of gas in that direction. The latter is taken

as a direct measure of the expected intensity from the

Galaxy, assuming that the cosmic ray intensity is uniform

along the line of sight. This, of course, is a matter

of debate. However even with the existence of a Galactic

cosmic ray gradient it is generally believed that the

scale height out of the plane is about 1 kpc. The assumption

of uniform intensity is therefore reasonable for latitudes

well away from the plane, which effectively only sample

the local interstellar medium.

For the SAS II data with E_γ > 100 MeV arrays of

3 x 3 bins centred on each cluster position are chosen,

and for E_γ:35 - 100 MeV 5 x 5 bins are adopted; corresponding

respectively to 5.5 x 10^{-3}sr and 1.5 x 10^{-2}sr. Because

of the limited angular resolution of the gamma-ray data,

which smears out the point-like image of a galaxy cluster,

the galaxy count data are smoothed to the same resolution.

This is done for both energy bands using the point spread

functions appropriate for the SAS II detector (Section

4.1). Column densities are then calculated using 7.8.

All the data for |b| >9.6° are then grouped in

3 x 3 and 5 x 5 arrays; except,of course, for regions

with neither gamma-ray exposure or galaxy count coverage.

To reduce the large errors associated with individual

gamma-ray intensities the data are further grouped into

column density bins,and mean values derived by summing

over the respective galaxy counts, number of photons

and sensitivity. These data are plotted in Figure 7.1

where the weighted least squares linear regressions are

indicated by the solid lines. It is interesting to compare
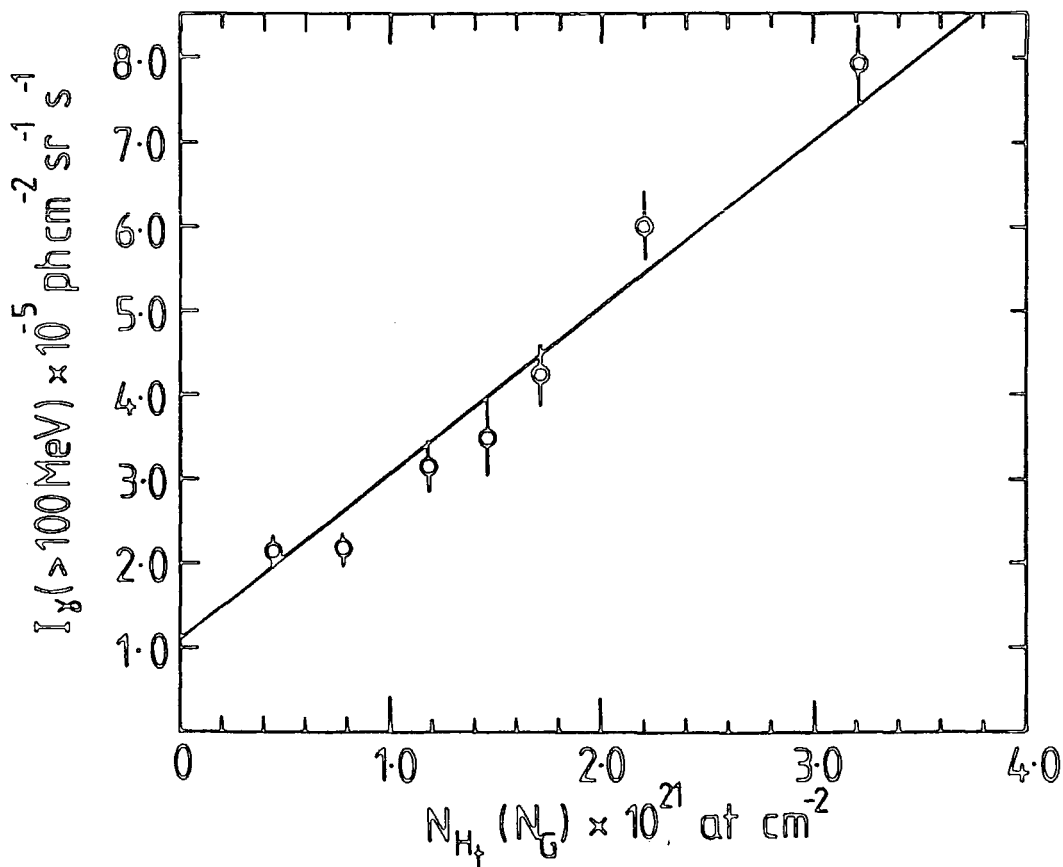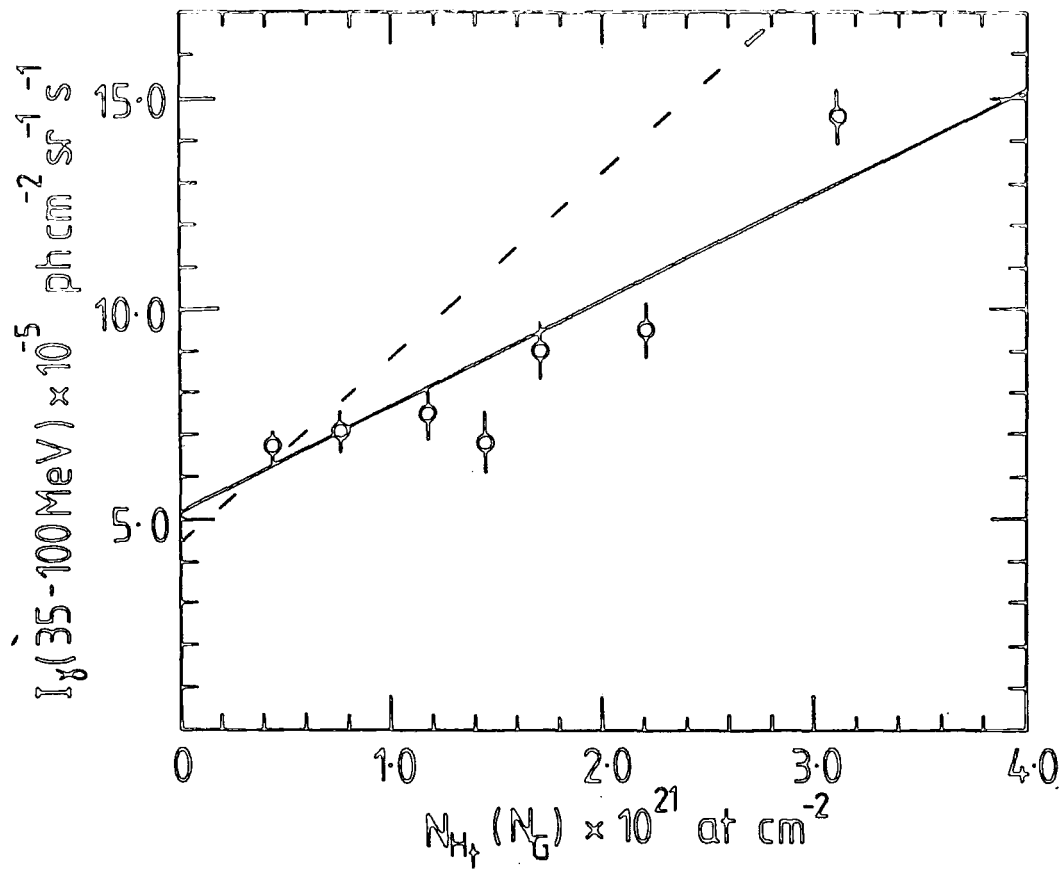
FIGURE 7.1   SAS II intensities $I_\gamma(\pm 1\sigma)$ versus $N_{H_t}(N_G)$ covering those regions $|b| > 9.6°$ with both gamma-ray and galaxy count exposure.   The solid lines are the weighted least squares fits to the data.

these results with those obtained in an earlier analysis
by Thompson and Fichtel (1982), the broken line, after
allowing for the difference in N_G^o in 7.8.

While the data are in excellent agreement for
$E_\gamma > 100$ MeV there is a systematic offset between the
two lines for E_γ : 35–100 MeV. The discrepancy is
due to the use of a single sensitive area ($\simeq 31.4$ cm^2)
by the SAS II group for E_γ : 35–100 MeV., whereas we
adopt the area factors given in the tabulated SAS II
data (40 cm^2 and 30 cm^2 for $|b| < 10°$ and $|b| > 30°$
respectively). The agreement above 100 MeV results from
both analyses employing the corresponding energy area
factors from the tabulated data (59 cm^2 and 66 cm^2 for
$|b| < 10°$ and $|b| > 30°$ respectively). The sensitive
area value 31.4 cm^2 is used in an earlier analysis of
the SAS II data (Fichtel et al., 1977) and is consistent
with a single assumed input gamma-ray spectrum $E_\gamma^{-1.5}$
(Mayer, private communication). However subsequent
analyses of both SAS II and COS B data show the observed
spectrum to be consistent with E_γ^{-2}, at least in the
Galactic plane.

The tabulated data and corresponding area factors
used for the present analysis implicitly assume that
the high latitude spectrum is steeper than that of the
Galactic plane, reflecting the presence of the extragalactic
component. To determine the spectral shape of the extra-
galactic intensity requires an iterative analysis to

derive the appropriate sensitive areas.

For the present analysis it is sufficient to adopt the factors given by Fichtel et al. (1978b) as we are primarily interested in the excess intensity and not its precise spectral shape. The extragalactic intensities are found by extrapolating the regression lines to zero column density giving:

$$I_\gamma(35\text{--}100 \text{ MeV}) = (5.2 \pm 0.7) \times 10^{-5} \text{ ph cm}^{-2}\text{sr}^{-1}\text{s}^{-1}$$

$$I_\gamma(> 100 \text{ MeV}) = (1.1 \pm 0.2) \times 10^{-5} \text{ ph cm}^{-2}\text{sr}^{-1}\text{s}^{-1}$$

The local emissivities are obtained directly from the slopes of the regression lines:

$$q/4\pi (35\text{--}100 \text{ MeV}) = (2.5 \pm 0.5) \times 10^{-26} \text{ ph at}^{-1}\text{sr}^{-1}\text{s}^{-1}$$

$$q/4\pi (> 100 \text{ MeV}) = (2.0 \pm 0.2) \times 10^{-26} \text{ ph at}^{-1}\text{sr}^{-1}\text{s}^{-1}$$

7.10 Analysis of the data

Turning now to the question of excess emission from radio galaxies; the intensities from these positions are calculated by summing over 3 x 3 and 5 x 5 bins, centered on the galaxy, for the energy ranges $E_\gamma > 100$ MeV and $E_\gamma : 35 - 100$ MeV respectively. The column densities at these positions are also calculated over the same regions of the sky from the galaxy count data convolved to the appropriate SAS II resolution.

The data on the strong radio sources (F_γ, expected $> 10^{-8}$ph cm^{-2}s^{-1}) and the weak sources (10^{-10} ph cm^{-2}s^{-1} $< F_\gamma$, expected $< 10^{-8}$ph cm^{-2}s^{-1}) are treated separately

for each energy range.   Each data set is grouped into several
column density bins to reduce the statistical uncertainty
attached to individual points.   The results for both
radio source sets (63 sources, E_γ : 35-100 MeV) are presented
in Figure 7.2 and those for E_γ > 100 MeV (60 sources)
are presented in Figure 7.3.   A slightly reduced coverage
in exposure for the SAS II data E_γ > 100 MeV (due to
improved angular resolution) results in three fewer source
positions being considered in this energy band.

The excess intensity (over the mean extragalactic
background value) from radio galaxies is estimated by
fitting a linear least squares line to the points in
Figures 7.2 and 7.3.   The mean source intensity is given
by the height of this intercept relative to that of the
background line.   Adopting this procedure gives a line
non-parallel with that of the background.   This is undoubtedly
a reflection of the statistical noise associated with
each data point and to some extent, the probable range
of radio galaxy luminosities.   As the present technique
is only attempting to look for a mean source excess
on a statistical basis it is more appropriate to fit
the source points by a weighted least squares line parallel
to the mean background.   These are indicated in Figures
7.2 and 7.3 by the broken lines.   The excess intensities
attributable to the radio sources are given in Table
7.3.

FIGURE 7.2 SAS II intensities I_γ(35–100 MeV)($\pm 1\sigma$) versus $N_{H_t}(N_G)$ for the radio source positions. The solid lines are the fits to the mean backgrounds. The excess intensities are given by the broken lines.
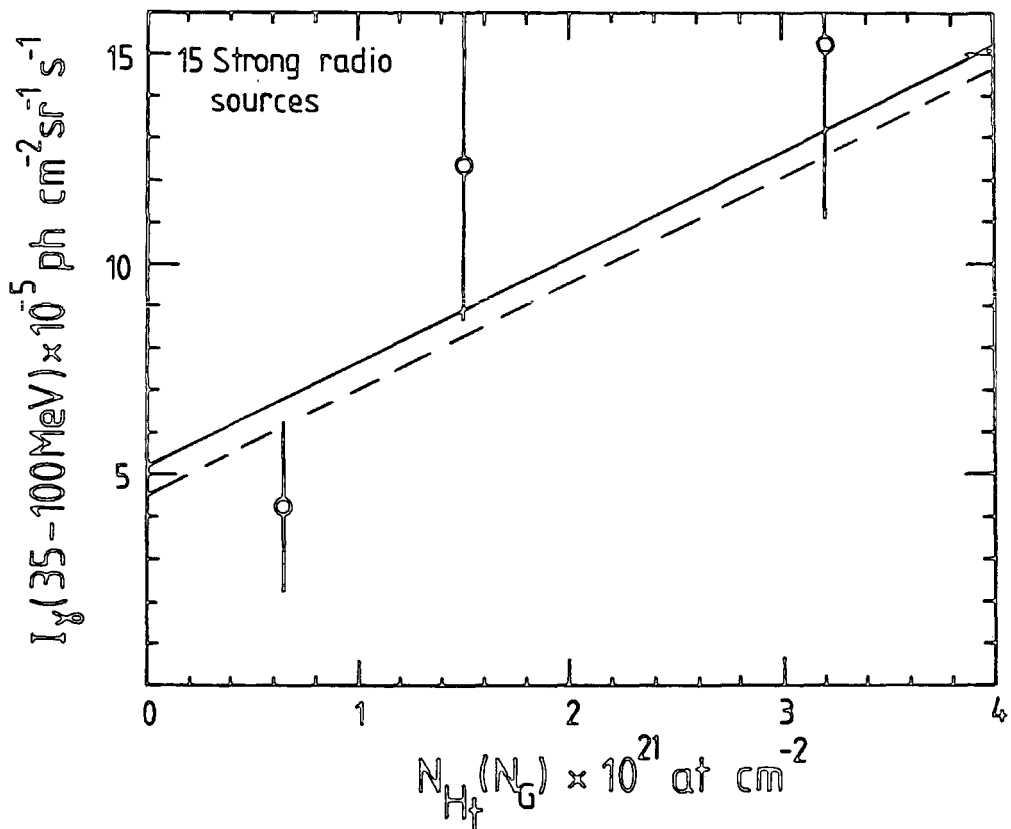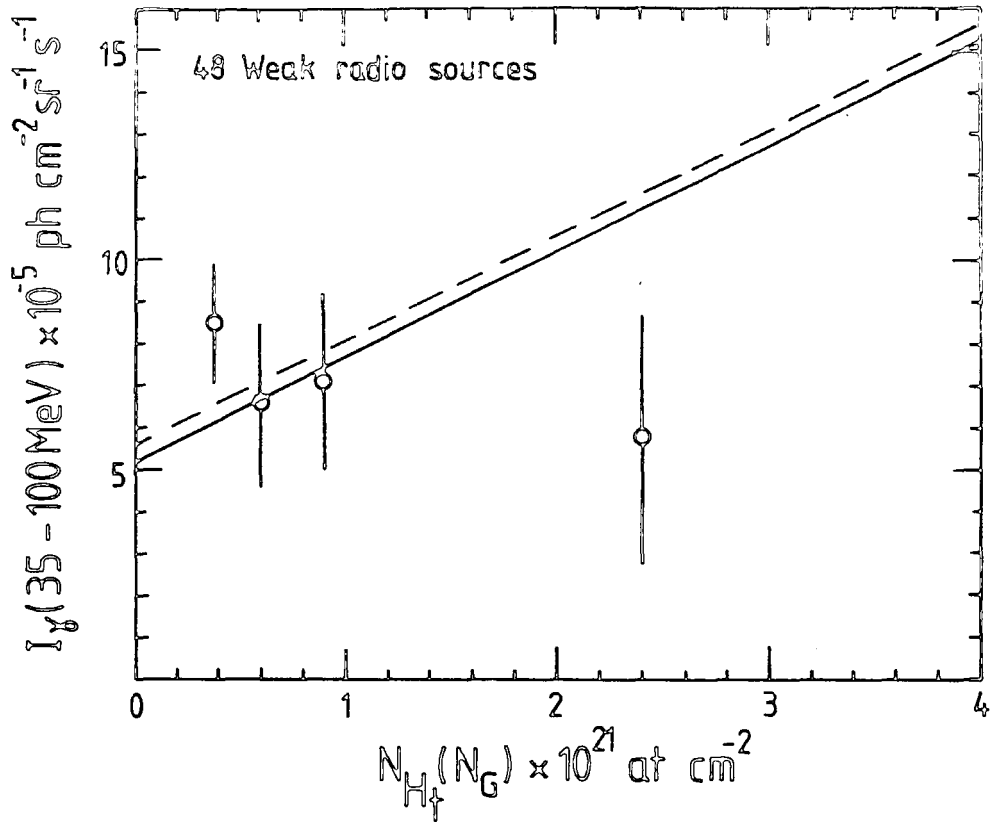
FIGURE 7.3 SAS II Intensities $I_\gamma(>100\ \text{MeV})(\pm 1\sigma)$ versus $N_{H_t}(N_G)$ for the radio source positions. The solid lines are the fits to the mean backgrounds. The excess intensities are given by the broken lines.
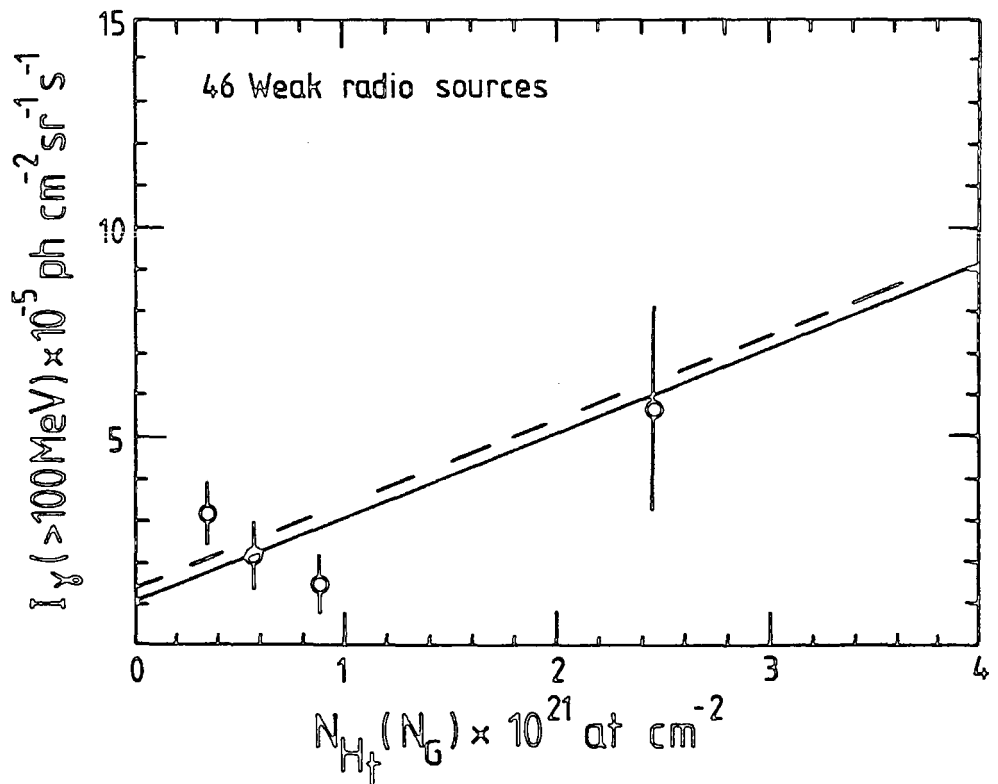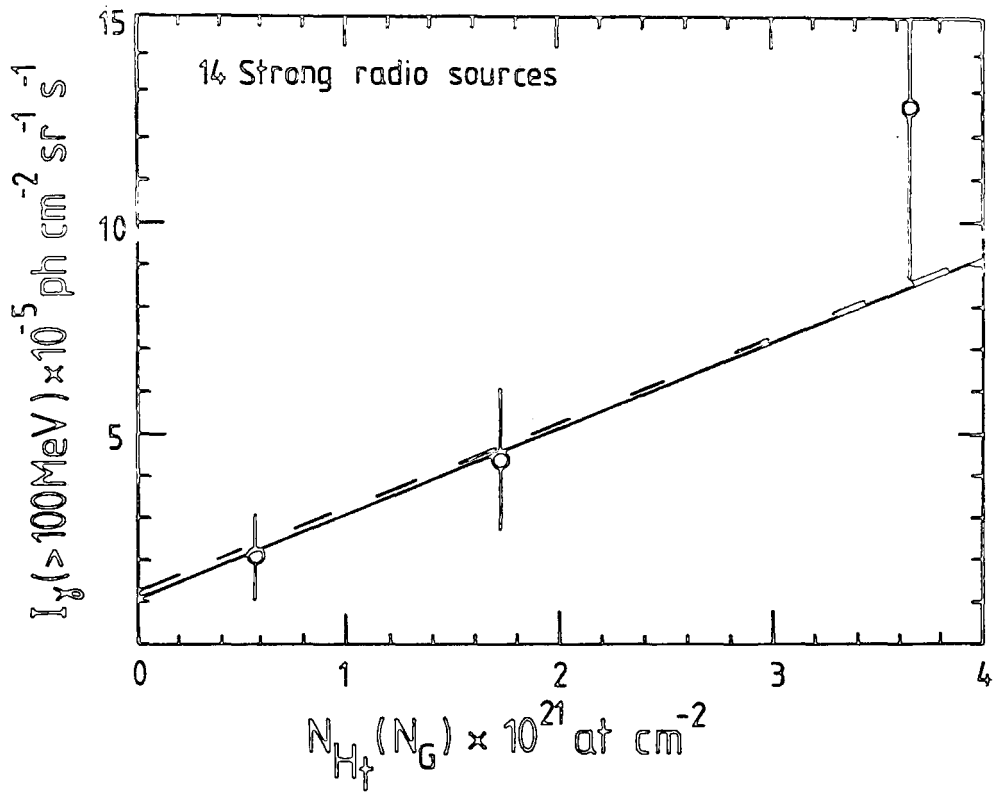
The analysis is repeated using the positions of
81 Abell clusters ($E_\gamma > 100$ MeV) and 83 positions
(E_γ : 35–100 MeV). The additional positions considered
in the lower energy band are due to the increased coverage
at this energy. These data are plotted as circles in
Figure 7.4.

We also check whether galaxy clustering leads to
an underestimate of the column densities and hence a
spurious excess intensity. The column densities at the
cluster positions are rederived using the bins surrounding
those initially used to calculate the intensities and
column densities. We take 16 and 24 bins (9.7×10^{-3} sr
and 1.5×10^{-2} sr) for $E_\gamma > 100$ MeV and E_γ : 35–100 MeV
to calculate the local background column densities.
These data are plotted as indicated in Figure 7.4 by
the squares.

There is a small systematic horizontal shift of
the points to the right. This indicates that over the
scales used galaxy clustering effects are on average
decreasing the inferred column densities. Excess intensities
are derived for the clusters using both the on-source
and off-source estimates of N_{H_t}. For the off-source
data the intensities are reduced by about 10% and 33%
for E_γ : 35 – 100 MeV and $E_\gamma > 100$ MeV respectively.
The relative magnitude of the effect reflects the improved
angular resolution of the data above 100 MeV. The excess
intensities given in Table 7.3 are obtained using the

FIGURE 7.4   SAS II intensities $I_\gamma(\pm 1\sigma)$ versus $N_{H_t}(N_G)$ for the rich cluster positions.   The solid lines are the fits to the mean backgrounds.   The circles are the column densities derived at the cluster positions.   The squares are the column densities derived from the galaxy count surrounding the cluster positions.   The latter are used to derive the excess intensities, given by the broken lines.

FIGURE 7.5 SAS II intensities $I_\gamma (\pm 1\sigma)$ versus N_{H_t} (N_G) for the clusters with radio sources. The solid lines are the fits to the mean backgrounds. The column densities are estimated from the galaxy count surrounding each cluster position. The excess intensities are given by the broken lines.
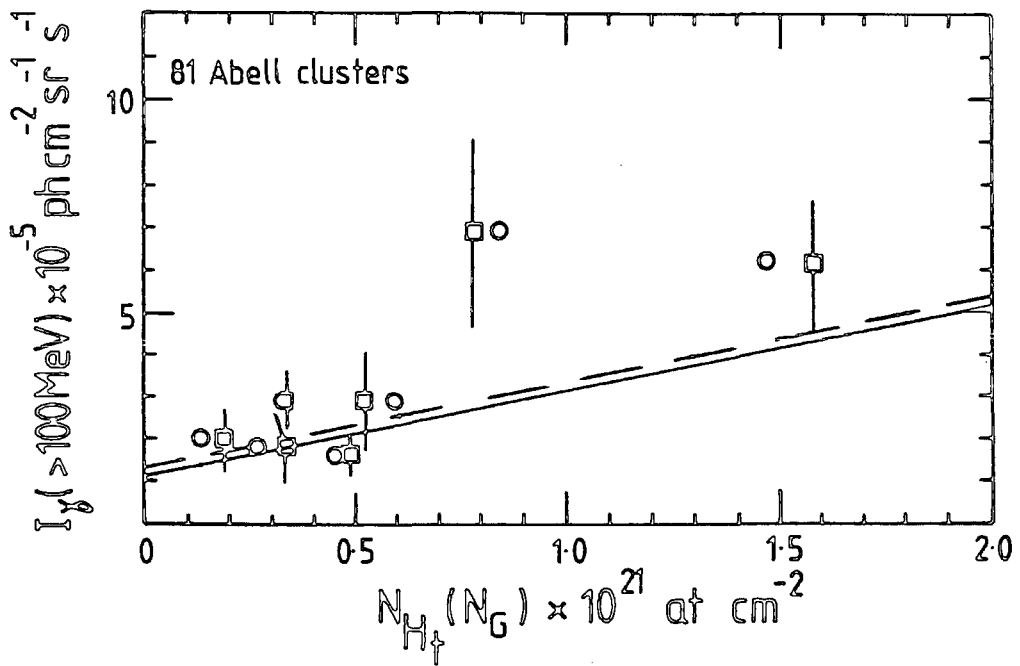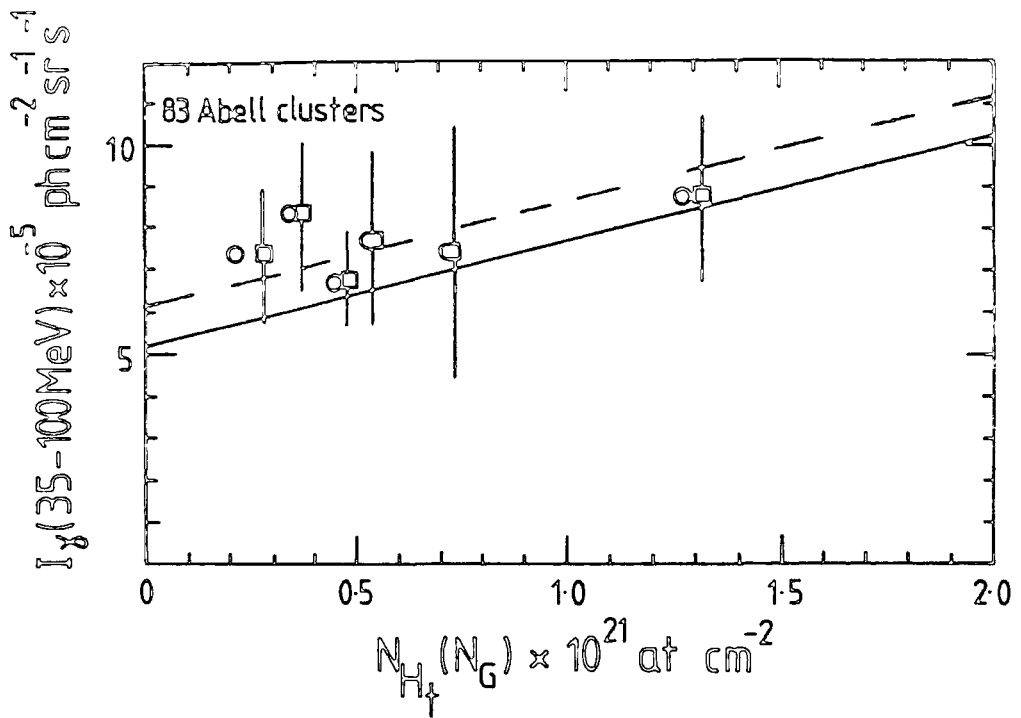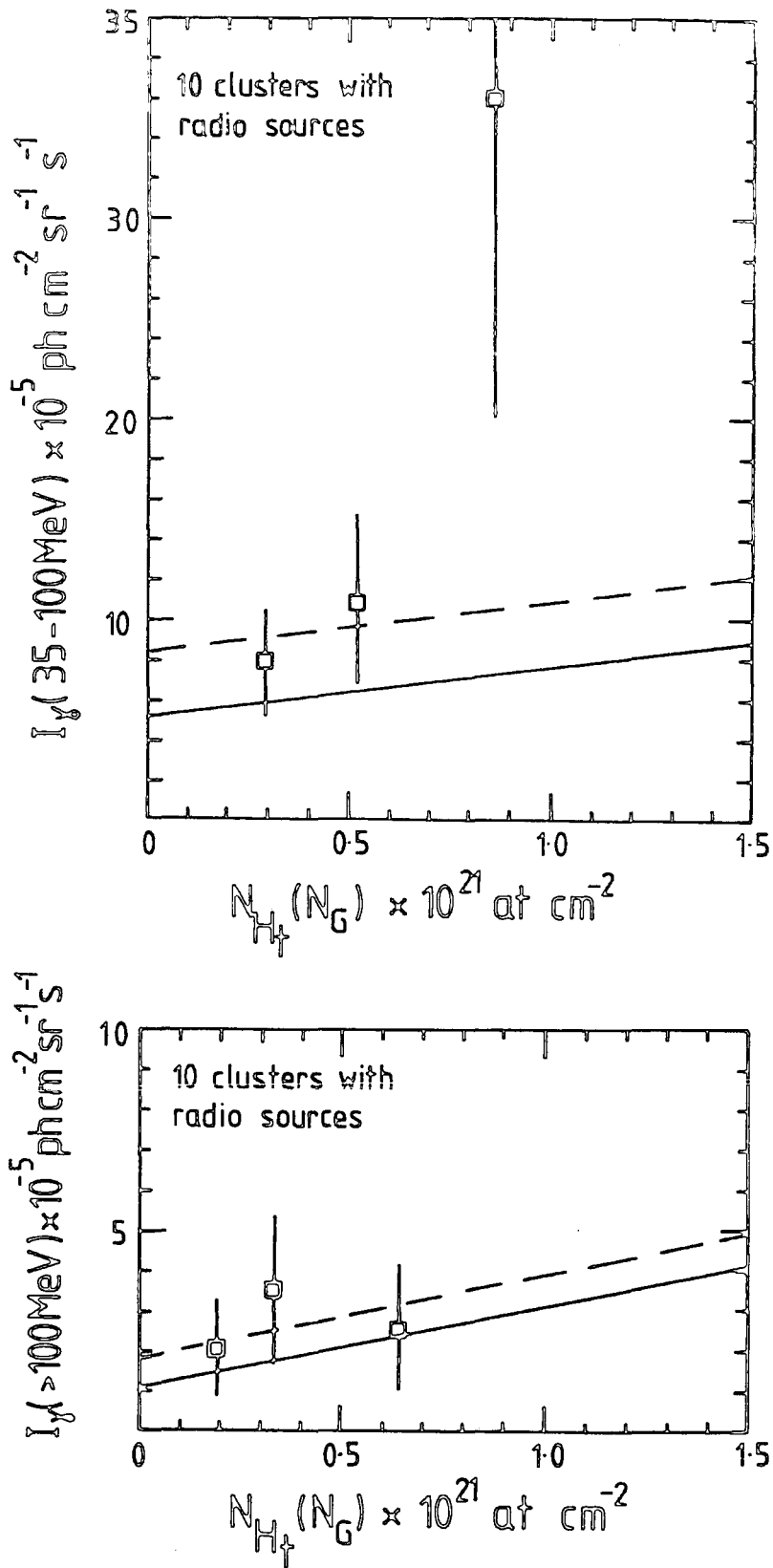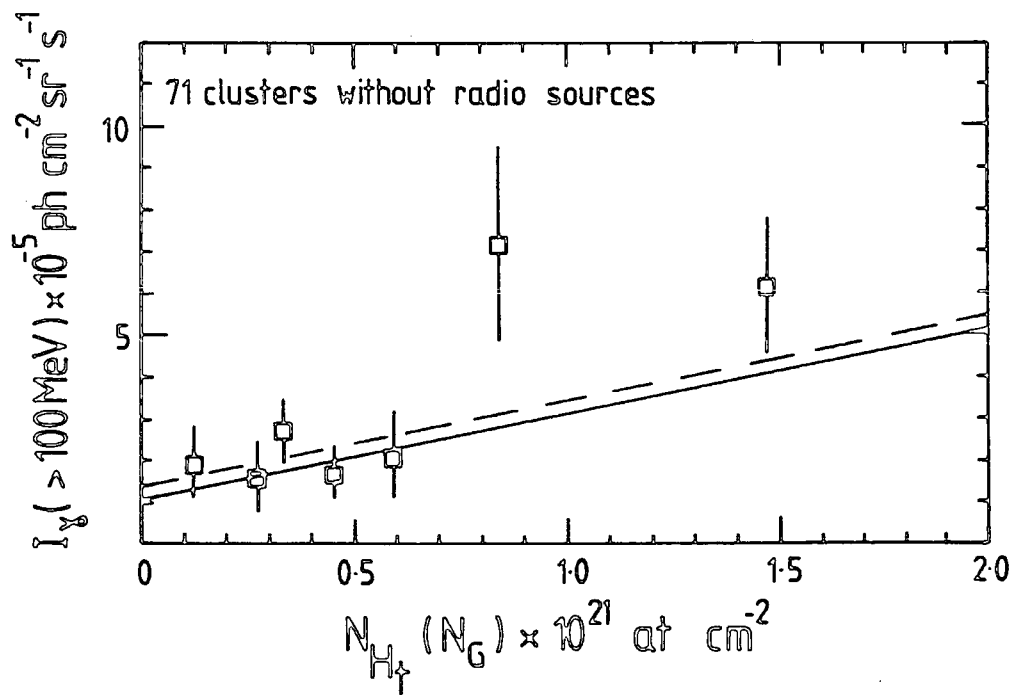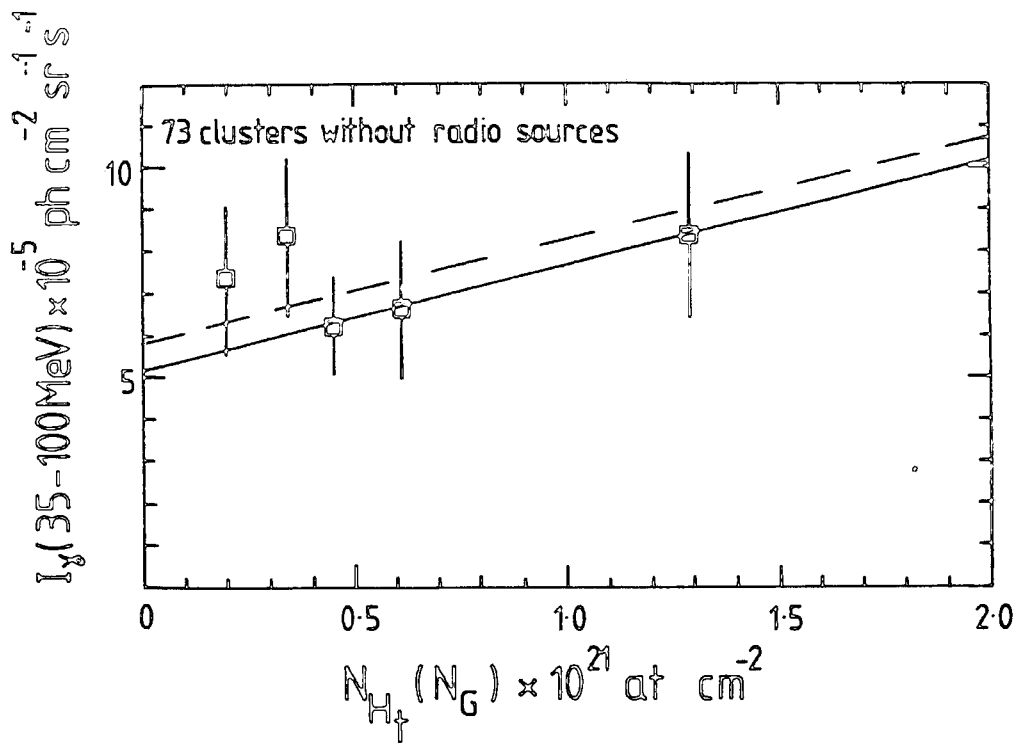
FIGURE 7.6   SAS II intensities $I_\gamma(\pm 1\sigma)$ versus $N_{H_t}(N_G)$
for the clusters without radio sources. The solid lines
are the fits to the mean backgrounds. The column densities
are estimated from the galaxy count surrounding each
cluster position. The excess intensities are given by
the broken lines.

off-source data points, and should therefore be a better
estimate of the mean intensity from galaxy clusters.

Of the 48 weak radio sources (Table A.5) 40 are
associated with rich clusters. Only 10 of these sources
are included in the sample of 83 Abell clusters. This
relative abundance ($\simeq$ 12%) is in good agreement with
that obtained by McHardy (1979) for the occurrence of
4C sources in Abell clusters ($\simeq$ 10-15%), indicating
that the cluster sample used in the present analysis
is unbiased. The remaining 30 clusters with weak radio
sources consist of clusters beyond distance class D_4
and clusters not belonging to Abell's complete sample.
The mean intensity from radio sources in clusters could
be considered as similar to that for the weak radio sources
alone. However, a better estimate can be made by selecting
those 10 clusters which have associated radio sources.
These data are plotted in Figures 7.5 and 7.6 and the
excess intensities given in Table 7.3.

7.11   Interpretation of the results

From an inspection of Table 7.3 it is clear that
the observed excesses have rather poor significances.
The statistical errors arise from a combination of the
low number of photons detected at the source positions
and the errors on the background lines. Nevertheless
it is useful to take the excess intensities and derive
the mean luminosities for each class of object.

The excess fluxes are calcualted over the solid angles used in the analysis (1.5×10^{-2} sr and 5.5×10^{-3} sr for E_γ : 35-100 MeV and $E_\gamma > 100$ MeV respectively) and are increased by 30% to allow for the loss of signal from a point source smeared out by the poor angular resolution of the detector. Adopting the distances for the radio sources as given in Tables A.4 and A.5 the mean value of $^1/d^2$ is calcualted, and assuming isotropic emission from the sources, the luminosity derived. For the Abell clusters we use the mean distances for each distance class $\leqslant D_4$ given in Table 7.2. We calculate the mean of $^1/d^2$ ($= \sum n_i/D_i{}^2/\sum n_i$) where n_i is the number of clusters in a distance class D_i ($i \leqslant 4$). The mean luminosities for each class are given in Table 7.4.

We can in principle, use the mean luminosities to estimate the contributions to the extragalactic flux from each class. McHardy (1979) determined the density of radio sources to be $\simeq 3 \times 10^{-5}$ Mpc^{-3} and that of radio clusters $\simeq 0.7 \times 10^{-7}$ Mpc^{-3} from his analysis of the 4C survey at 408 MHz. The mean cluster density determined by Bachall and Soneira (1983) is $\simeq 0.73 \times 10^{-6}$ Mpc^{-3}, after allowing for the loss of clusters by Galactic obscuration and enhancement due to the local Virgo super-cluster. By substituting the values from Table 7.4 in 7.2 we estimate the universal flux for each class, Table 7.5. For the weak radio sources the universal fluxes

TABLE 7.4

Luminosity L_γ ph s^{-1}

	E_γ:35–100 MeV	E_γ>100 MeV
Strong radio sources	$< 1.7 \times 10^{47}$	$(0.3 \pm 2.6) \times 10^{46}$
Weak radio sources	$(1.7 \pm 7.5) \times 10^{48}$	$(0.5\ 1.4) \times 10^{48}$
Abell clusters	$(2.7 \pm 2.2) \times 10^{48}$	$(2.7 \pm 4.5) \times 10^{47}$
Clusters with radio sources	$(3.1 \pm 3.8) \times 10^{48}$ $(3.1 \pm 3.8) \times 10^{48}$	$(2.7 \pm 2.4) \times 10^{47}$
Clusters without radio sources	$(1.9 \pm 2.9) \times 10^{48}$	$(3.1 \pm 4.5) \times 10^{47}$

The luminosities derived for each source type from the observed mean intensities in Table 7.3. The upper limit for strong radio sources is 1σ.

TABLE 7.5

$$F_{universal} \times 10^{-4} \text{ ph cm}^{-2} \text{ s}^{-1}$$

	E_γ: 35–100 MeV	$E_\gamma > 100$ MeV
Strong radio sources	< 32.1	0.6 ± 4.9
All Abell clusters	12.4 ± 10.1	1.2 ± 2.1
Clusters with radio sources	1.4 ± 1.7	0.12 ± 0.11
SAS II extragalactic flux	6.5 ± 0.9	1.4 ± 0.3

The net universal fluxes estimated for each source type.
The upper limit for strong radio sources is 1σ. The
SAS II extragalactic fluxes are derived from our own
analysis of the SAS II data.

are found to be more than a factor of 100 above the SAS II observed flux levels. Thus, no useful information is obtained. Also given are the extragalactic fluxes derived from our own analysis of the SAS II data (Section 7.9).

Only for the radio clusters can we usefully compare their net flux with the observed extragalactic background. While they may contribute all of the flux E_γ : 35-100 MeV their contribution is unlikely to be more than about 20% above 100 MeV.

We note that the data are not inconsistent with a significant fraction of the observed extragalactic flux coming from 'discrete' sources. However, further observations are clearly needed, both to improve the statistics and the angular resolution, before more detailed conclusions are drawn. In particular several of the radio cluster sources in Table A6 are expected to have fluxes just below the present detectability threshold. These are prime candidates for future study. Detection of gamma-ray emission above 100 MeV from the cores of radio clusters would be strong evidence for the presence of relativistic protons in these objects.

CHAPTER   EIGHT

CONCLUSIONS

8.1   Summary of the present work

In the preceding chapters, several of the problems associated with the interpretation of the current gamma-ray data have been addressed. We began by outlining the links between gamma-ray astronomy and the salient aspects of the origin and propagation of cosmic rays. The information obtained from gamma-ray astronomy is relevant to many facets of the questions posed by cosmic ray physicists. As the clues appear we cautiously begin to perceive the underlying pattern.

The medium energy domain ($E_\gamma \sim$ few 10^7eV – few 10^9eV) deals indirectly with the cosmic ray nucleons and electrons having energies of a few 10^8eV – few 10^{10}eV, constituting the bulk of the local cosmic ray energy density. The best method of discriminating between a Galactic or meta-galactic origin for the nucleonic component (energy loss rates for electrons require them to be Galactic) is to compare their density in the Galaxy, particularly towards the inner Galaxy, with the local value. The role of gamma-ray sources is identified as an important limitation in our ability to interpret the Galactic gamma-ray flux and hence the cosmic ray density.

In Chapter 4 an analysis was made of the SAS II data for supportive evidence on the 2CG sources detected

by COS B. It was important to seek independent evidence
to asses the true nature of these candidate sources,
most of which are unidentified with known astrophysical
objects. The existence of the strongest sources : 2CG
263 (Vela), 2CG 195 (Geminga), 2CG 184 (Crab), 2CG 078
and 2CG 359 is unambiguously confirmed. A further 12
sources are confirmed at a lower level of significance.
On the basis of the inferior statistical precision of
the SAS II data we are unable to positively identify
the remaining 5 sources and we note that the SAS II data
are not inconsistent with those of COS B, time variability
being excluded.

More importantly there is good evidence to suggest
that many of the weaker sources are not genuine in the
sense of being discrete. Rather, it is likely that they
can be explained as unresolved regions of enhanced gamma-
ray emission, identified with cosmic ray irradiation
of local giant molecular clouds. Very recent analysis
of the COS B data supports this conclusion (Bignami,
1984).

Before interpreting the observed Galactic gamma-
ray flux allowance must be made for the unresolved discrete
sources and the statistical fluctuations and pseudo-sources,
which are really elements of the diffuse emission. A
Monte-Carlo model of the diffuse gamma-ray emission was
constructed in Chapter 5 and used to investigate the
detection efficiency of genuine discrete gamma-ray sources.
With these data and reasonable models of the discrete

source population limits are derived on the total flux

from genuine gamma-ray sources in the Galactic plane.

In the content of this model the source flux (>100 MeV)

is estimated to contribute $\simeq$ 11-23% of the observed

emission from the inner Galaxy ($|b|<5°$.) and $\simeq$ 23-27%

in the outer Galaxy. These estimates are small, though

not negligible. They are subject to many systematic

effects, related to the assumptions of the basic model

for the diffuse emission. The most probable area of

uncertainty, the distribution of H_2 in the inner Galaxy,

is also related to the wider problem of deriving the

variation in Galactic cosmic ray density from the gamma-

ray data.

The nearby Orion molecular complex provides an excellent

opportunity to investigate the coupling between cosmic

rays and the giant molecular (H_2) clouds. An analysis

of the COS B gamma-ray data from this region was performed

in Chapter 6. We find no evidence for the exclusion

of cosmic rays from the molecular gas. Rather, there

is weak evidence favouring a modest enhancement of cosmic

rays ($\sim n_H^{0.7}$) throughout the cloud. For the case of

uniform cosmic ray irradiation we derive a new calibration

for the conversion ratio $\alpha = 2N_{H_2} / \int T(^{12}CO)dv = (3.7 \pm 0.6)$

x 10^{20} at cm^{-2} (K $kms^{-1})^{-1}$, lower than conventional

estimates based on molecular line studies.

Progress in understanding the extragalactic component

of the gamma-ray flux is still severely limited by the low exposures obtained for the present data. In Chapter 7 the role of extragalactic sources (radio galaxies and rich clusters) was examined. The results are tentative but suggest that the extragalactic flux may be predominantly discrete in nature.

Future gamma-ray observations with increased resolution and exposure will greatly improve our understanding of the gamma-ray emission, both Galactic and extragalactic. In addition a complete CO survey of the Galactic plane will help shed more light on the 2CG sources, particularly in the fourth Galactic quadrant. Detailed studies of more nearby molecular clouds are required to reduce the possible systematic effects present in the analysis of the Orion complex, and to look for further evidence of cosmic ray enhancement or exclusion therin. An extension of the Monte-Carlo technique both to the third and fourth quadrants and to other energy bands will further constrain the discrete source contribution and its energy spectrum.

8.2 The implications for the origin of cosmic rays

We now combine the results of the preceding work in relation to the central question on the origin of the nucleonic component of the cosmic ray flux. The methods of previous workers (Section 3.3) are followed, viz by comparing the unfolded radial gamma-ray emissivity with that expected from cosmic ray interactions with the interstellar medium.

In view of the superior statistical quality of the
COS B data over those of SAS II we adopt the radial emissivity
unfolded from the COS B data by Mayer-Hasselwander et
al. (1982). Attention is restricted to the first Galactic
quadrant (1 < 90°) where coverage of CO emission close
to the Galactic plane is extensive.

The observed radial emissivity can be separated
into two components, one arising from diffuse processes,
the other from discrete sources. Based on the work of
Chapter 5 we adopt the supernovae remnant (SNR) distri-
bution of Kodaira (1974) as a reasonable approximation
for the gamma-ray source population, with these sources
contributing 20% of the inner Galaxy emission. In Figure
8.1 the relative gamma-ray emissivity as a function of
Galactocentric radius is plotted, along with the expected
source contribution weighted by the SNR distribution.

Also plotted in Figure 8.1 are the radial SNR distri-
bution (Kodaira, 1974), the relative metal abundance
$M = [O]/[H]$ (Li et al. 1983) and a possible cosmic ray
Galactic density distribution ($\propto \exp - R/6$). The latter
is necessarily idealized. Though assuming supernovae
are the main sources of Galactic cosmic rays then after
allowing for diffusion the cosmic ray distribution will
be smoother than that of their sources. For $R > 5$ kpc
the exponential cosmic ray variation is likely to be
reasonable. From analysis of the local gamma-ray emission
several workers find the inferred cosmic ray distribution
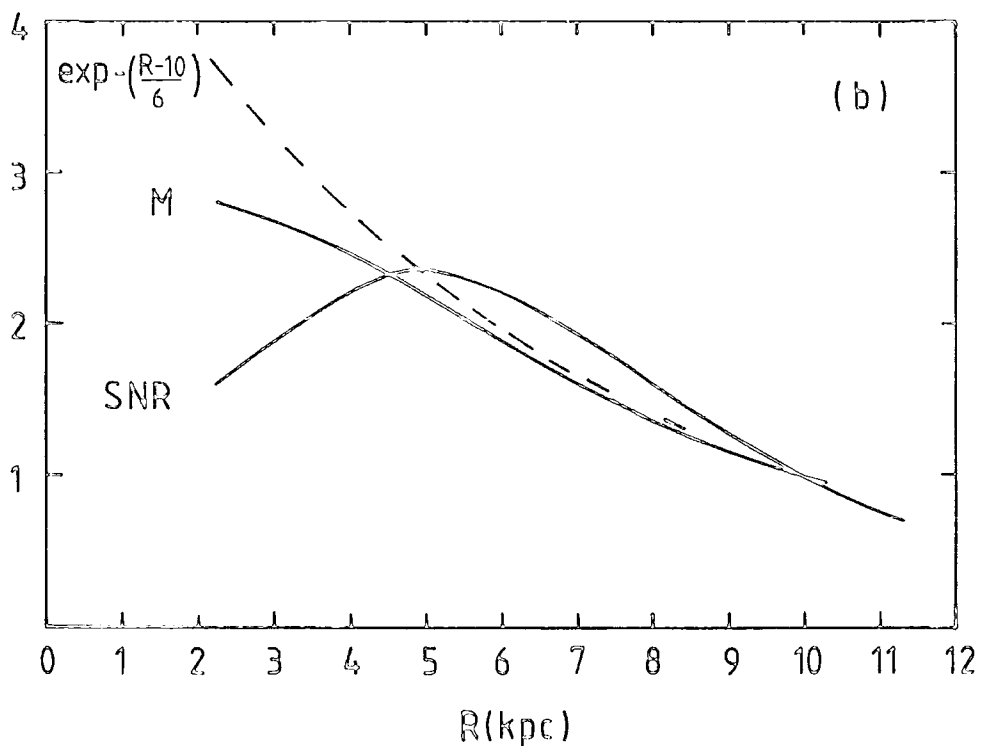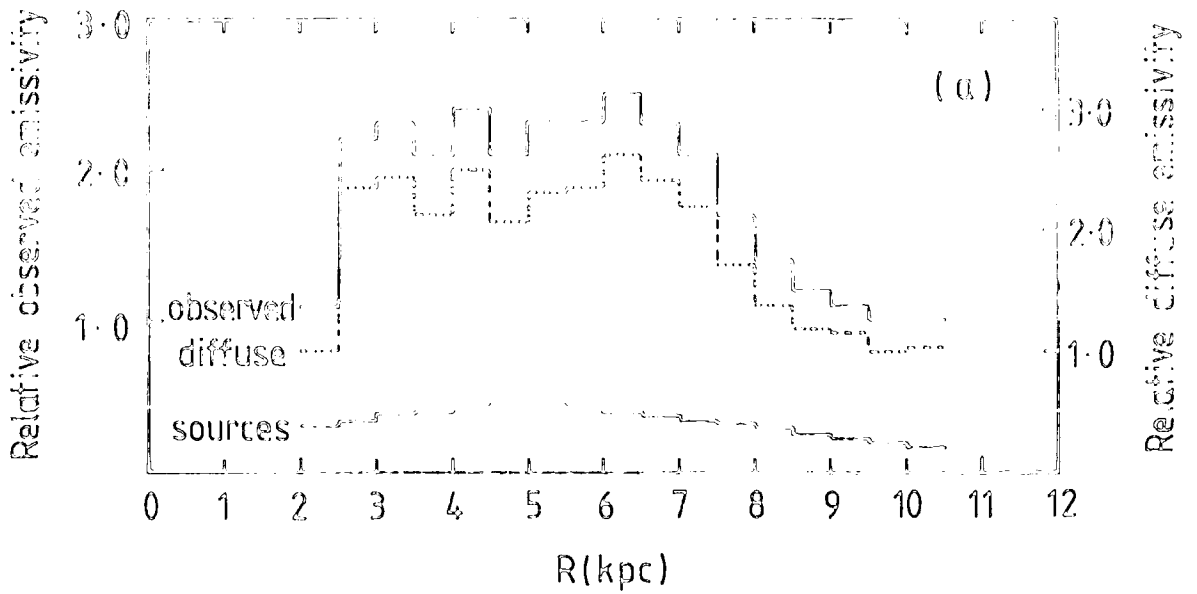
<u>Figure 8.1</u>   (a) The unfolded COS B emissivity $E_\gamma > 100$ MeV.
(Mayer-Hasselwander et al., 1982).   Local normalization = 2.1
x 10^{-25} ph cm^{-3}s^{-1}.   The diffuse emissivity is that expected
after subtracting a 20% source component. (b) The supernova
remnant surface density (Kodaira, 1974) and the metallicity
gradient M = $[O]$ / $[H]$ (Li et al., 1983).   The exponential
represents a possible cosmic ray distribution.   All are
normalized locally at R = 10 kpc.
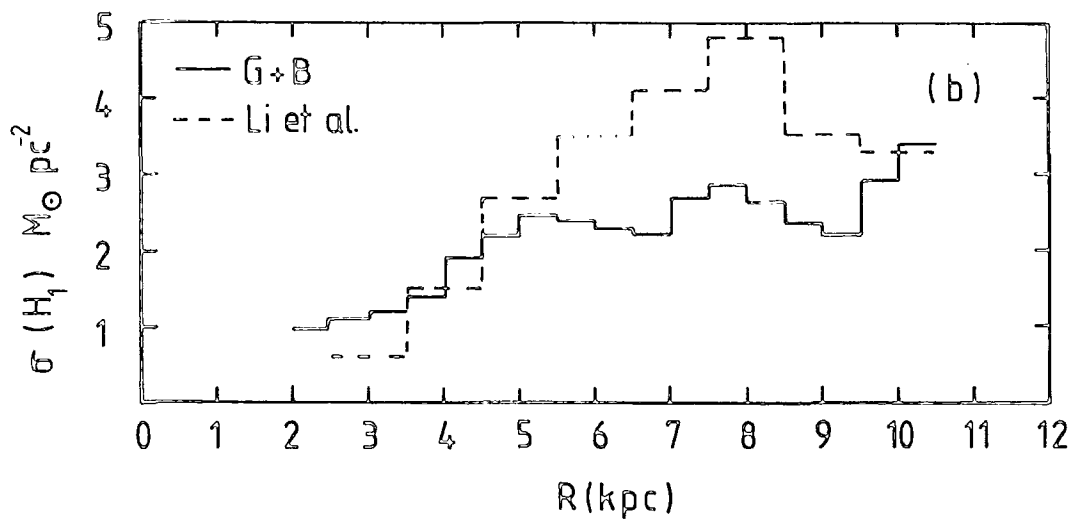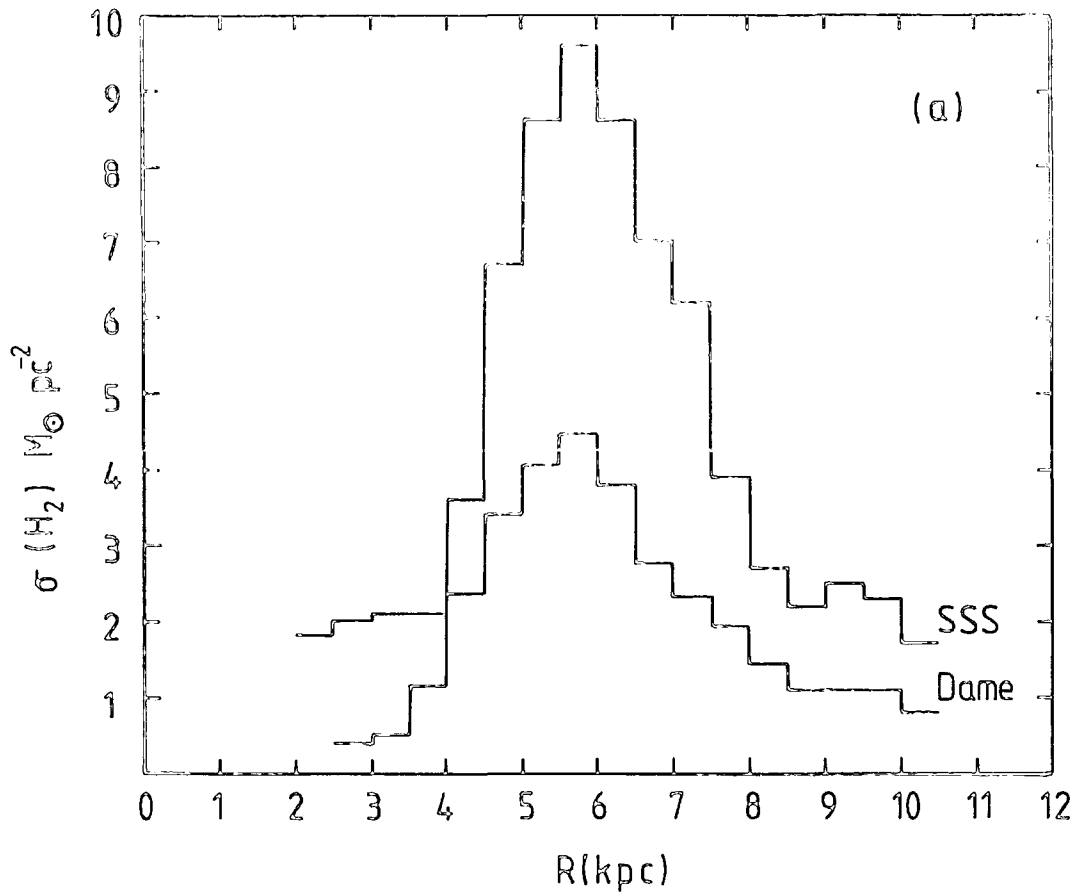
Figure 8.2   (a) The surface densities of H_2 derived from the ^{12}CO surveys by Sanders, Solomon and Scoville (1984a): SSS and Dame (1984). Both are corrected to α = 3.7 x 10^{20} at cm^{-2} (K $kms^{-1})^{-1}$ as described in the text. (b) The surface densities of HI from the data of Gordon and Burton (1976): G + B and Li et al. (1983).

can be approximated by an exponential variation. However
for R < 5 kpc the situation becomes less certain, especially
when we consider the possibility of additional cosmic
ray production and diffusion from the region around the
Galactic centre.

Radial surface densities of atomic hydrogen, $\sigma(HI)$,
have been derived by Gordon and Burton (1976) and Li
et al. (1983) for $l < 90^{\circ}$. These are plotted in Figure
8.2. For 5 kpc < R < 10 kpc the difference between the
two distributions reflects the use of different rotation
curves for the inner Galaxy and different optical depth
corrections. Also plotted in Figure 8.2 are the surface
densities of molecular hydrogen, $\sigma(H_2)$, from Sanders,
Solomon and Scoville (1984a) (henceforth SSS) and Dame
(1984). Both distributions are scaled to our preferred
value of $\alpha = 3.7 \times 10^{20}$ at cm^{-2} $(K\ kms^{-1})^{-1}$. The
differences in $\sigma(H_2)$ are significant, $\sigma(SSS)/\sigma(Dame)$
$\simeq 2.4$ over 3 kpc < R < 9 kpc. The observed CO intensities
of SSS are on average only $\sim 30\%$ higher than those of
Dame. It is believed that the discrepancy in surface
densities arise from differences in the unfolding procedures
applied to the repsective data sets (Sanders and Dame,
private communication), Dame's data being regarded as
unfolded correctly.

We assume Gaussian distributions for the gas normal
to the Galactic plane, with $Z_{\frac{1}{2}}(HI) = 130$ pc and $Z_{\frac{1}{2}}(H_2)$
$= 70$ pc locally. For the local gas density this gives

$n(HI + H_2) \simeq 1.1$ at cm^{-3} and 0.8 at cm^{-3} for $\sigma(H_2, SSS)$
and $\sigma(H_2, Dame)$ respectively. For the local gamma-ray
emissivity we adopt $q/4\pi(>100 \text{ MeV}) = 2.0 \times 10^{-26}$ ph
$at^{-1}sr^{-1}s^{-1}$, as estimated in Chapter 6. Thus the local
volume emissivities $\varepsilon_\gamma(>100 \text{ MeV})$ are

$$\varepsilon_\gamma = 2.0 \times 10^{-25} \text{ ph } cm^{-3}s^{-1} \quad (\text{Dame})$$

$$\varepsilon_\gamma = 2.8 \times 10^{-25} \text{ ph } cm^{-3}s^{-1} \quad (\text{SSS})$$

to be compared with the local normalization derived by
Mayer-Hasselwander et al. (1982) for the unfolded COS B
data:

$$\varepsilon_\gamma = 2.1 \times 10^{-25} \text{ ph } cm^{-3}s^{-1}$$

The gamma-ray emissivity at a distance R from the
Galactic centre can be expressed as

$$\varepsilon_\gamma(R) \propto f(R) \left[\sigma(HI; R) + \sigma(H_2; R)/M(R) \right]$$

where $f(R)$ is the ratio of the cosmic ray density relative
to the local value times the local gamma-ray emissivity,
and the metallicity factor M^{-1} affects the $CO \rightarrow H_2$ conversion
(i.e. $N_{H_2} \sim \int Tdv/M$).

Initially we consider the cosmic ray density $f(R)$
to be uniform throughout the Galaxy (corresponding to
a metagalactic origin) and the $CO \rightarrow H_2$ conversion to
be independent of the metallicity gradient. The diffuse
emissivity (Figure 8.1) is compared with that expected
using $\sigma(H_2, Dame)$ and both estimates of $\sigma(HI)$, Figure
8.3. For both HI distributions the expected relative
emissivities significantly underestimate the observations
for $R < 5$ kpc. This may in part be due to the difficulties
in unfolding the gas distributions because of velocity
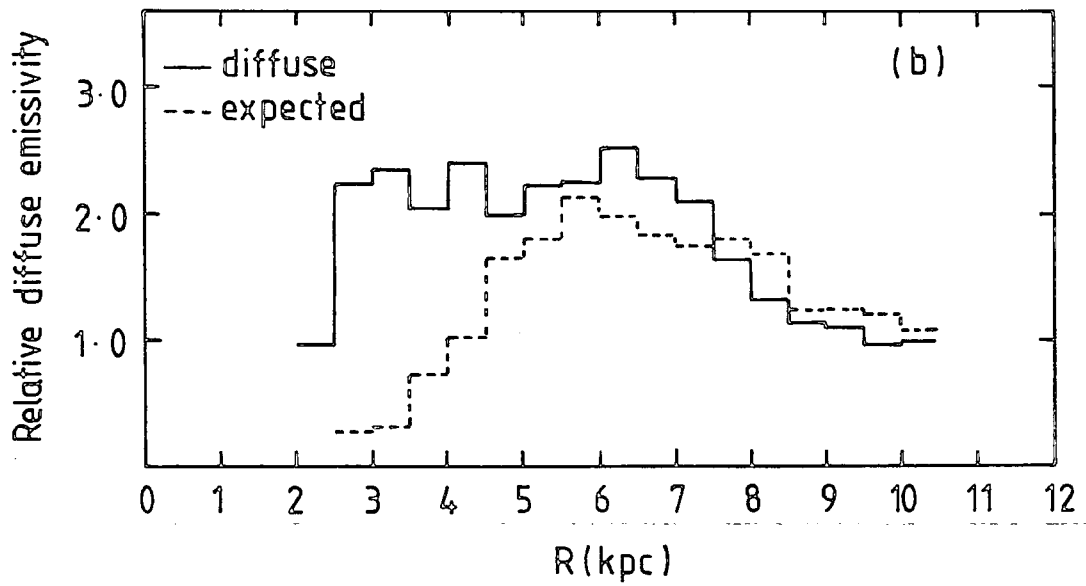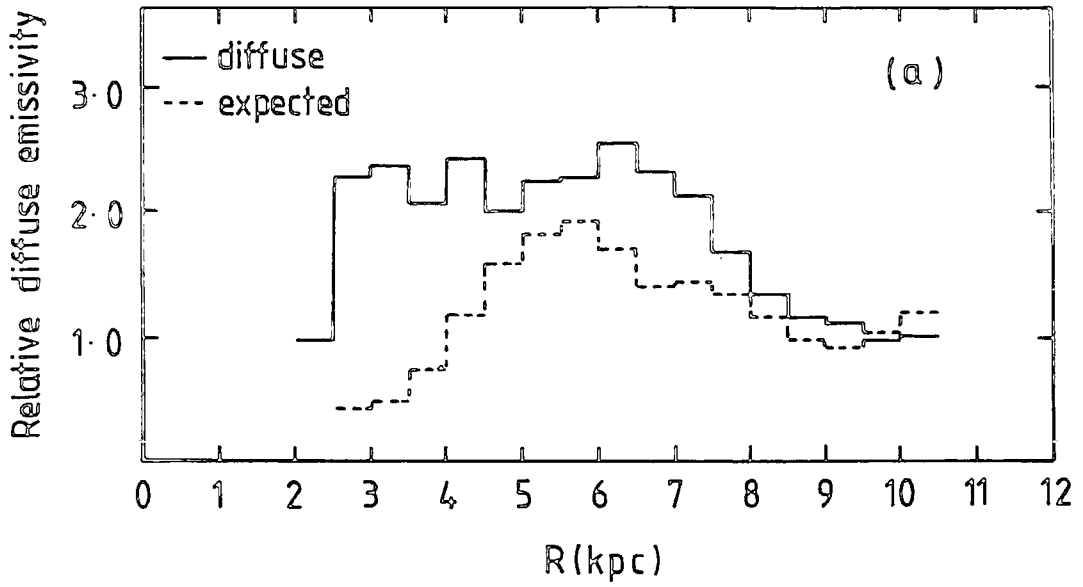
Figure 8.3   The diffuse emissivity of Figure 8.1 compared
with that expected from the gas distributions, assuming
uniform cosmic ray density and no metallicity effect.
(a) σ (HI, Gordon and Burton).   (b) σ (HI, Li et al.),
both use σ (H_2, Dame).

Figure 8.4 The diffuse emissivity of Figure 8.1 compared
with that expected from the gas distributions, assuming
the cosmic ray density $\propto$ exp $(^{-R}/6)$ and $\sigma(H_2)$ is
reduced by the metallicity factor M^{-1}. (a) $\sigma(HI$, Gordon
and Burton). (b) $\sigma(HI$, Li et al.), both use $\sigma(H_2,$
Dame).

crowding of the emission profiles and non-circular rotation.
For R > 5 kpc use of σ(HI, Li et al.) gives the better
fit.

Alternatively a Galactic cosmic ray gradient
($\propto$ exp $-\ ^R/6$) is assumed and the metallicity correction
applied to σ(H$_2$). For this case the expected diffuse
emissivities are compared to the observations in Figure
8.4. Using σ(HI, Gordon & Burton) the agreement is
generally good for R $\gtrsim$ 6 kpc whereas with σ(HI, Li et
al.) the model consistently overestimates the observations
for R $\gtrsim$ 4.5 kpc. However, for both cases it must be
remembered that $f(R) \propto$ exp $-\ ^R/6$ probably overestimates
the cosmic ray density for R < 5 kpc again leading to
reduced emissivities for this region. Use of σ (H$_2$,
SSS) produces an unacceptable fit with $\mathcal{E}_\gamma$ (R = 6 kpc)
overestimated by a factor ~ 1.9. Models with only a
cosmic ray gradient or a metallicity correction also
produce unacceptable fits.

For the region R $\gtrsim$ 5 kpc we can be more certain
of the unfolded distributions. However, there is still
sufficient variation in the estimates of σ(HI) to ensure
both the uniform cosmic ray, no metallicity correction
model (Figure 8.3b) and the cosmic ray gradient, with
metallicity correction model (Figure 8.4a) fit the ob-
servations. Other workers consider a gradient likely
both in the outer Galaxy and in the local interstellar
medium (Section 3.3). The present work indicates that
a large scale Galactic cosmic ray gradient can only be

accommodated by allowing for the effect of the metallicity gradient on the CC $\rightarrow$ H$_2$ conversion. Finally we note the constraints placed on the mass of H$_2$ in the inner Galaxy by the gamma-ray data. For 2.5 kpc < R < 10.5 kpc M(HI) $\simeq$ (1.5   2.1) x 10^9M$_\odot$, depending on the assumed radial distribution (Figure 8.2). Taking Dame's data on σ(H$_2$) (corrected for our value of $\propto$ = 3.7 x 10^{20} at cm^{-2} (K kms^{-1})$^{-1}$) M(H$_2$)   1.2 x 10^9M$_\odot$ over 2.5 kpc < R < 10.5 kpc. For the preferred combination of cosmic ray gradient and metallicity dependent conversion factor then M(H$_2$) is reduced to $\simeq$ 0.8 x 10^9M$_\odot$ over the same region.

APPENDICES A1 - A6

$$q/4\pi \times 10^{-26} \; \text{ph at}^{-1}\text{sr}^{-1}\text{s}^{-1}$$

Source	(35-100 MeV)	(100 MeV)	Comments
Fichtel et al. (1978a)	4.3 ± 1.5	3.0 ± 0.8	$\vert b\vert > 12.8°$, $I_\gamma \propto N_{HI}$
Lebrun and Paul (1980)	3.0 ± 0.2	2.0 ± 0.15	$\vert b\vert > 10°$, $I_\gamma \propto N_{H_t}$ (N_G)
Issa et al. (1981)		2.2 ± 0.3	$\vert b\vert > 10°$, $I_\gamma \propto N_{HI} + 2N_{H_2}$
Thompson and Fichtel (1982)	3.4 ± 0.5	1.8 ± 0.2	$\vert b\vert > 10°$, $I_\gamma \propto N_{H_t}$ (N_G)
Lebrun and Paul (1983)	1.8 ± 0.1 2.4 ± 0.2	2.1 ± 0.1 2.4 ± 0.2	$\vert b\vert > 10°$, $I_\gamma \propto N_{HI}$ $I_\gamma \propto N_{H_t}$ (N_G)
This work (Chapter 7)	2.5 ± 0.5	2.0 ± 0.2	$\vert b\vert > 9.6°$, $I_\gamma \propto N_{H_t}$ (N_G)

TABLE A.1

Local emissivities ($\pm 1\sigma$) derived from the SAS II data. All analyses assume the cosmic ray intensity is constant along the line of sight and compare the gamma-ray intensity I_γ with the total gas column density. Column densities are estimated either directly, N_{HI} ($+2N_{H_2}$), or indirectly from galaxy counts N_{H_t} (N_G).

Source	(70–150 MeV)	(150–300 MeV)	(300–5000 MeV)	(>100 MeV)	
Mayer-Hasselwander et al. (1982)				1.67	$\lvert b\rvert<10°$, $I_\gamma \propto N_{HI}$ *
Lebrun et al. (1982)				2.1 ± 0.3	$10°<\lvert b\rvert<20°$, $I_\gamma \propto N_{H_t}$ (N_G)
Strong et al. (1982)	1.4	0.53	0.59	(1.8)	$11°<\lvert b\rvert<20°$, $I_\gamma \propto N_{H_t}$ (N_G)
Strong (1984)	1.55,1.76	0.93,0.83	0.85,0.55	(2.4)	$10°<\lvert b\rvert<20°$ } $I_\gamma \propto N_{HI} + N_{H_2}$
Strong (1984)	1.27,1.48	0.80,0.70	0.75,0.48	(2.1)	$10°<\lvert b\rvert<20°$ } $N_{H_2} = N_{H_t}(N_G) - N_{HI}$

TABLE A.2

As Table A.1, but for the COS B data. Strong (1984) derives the emissivities for N_{HI}, $2N_{H_2}$ separately. Two calibrations of the $N_{H_t}(N_G)$ relation are employed. The former (Strong and Lebrun, 1982) resulting in higher emissivities than the latter (Strong, 1984).

Source	α_{20}	Derivation
Gordon and Burton (1976)	4.6	Comparison of optical extinction with CO emission in rotating dust globules.
Blitz (1978)	15.0	Dark cloud derivation.
Solomon, Sanders and Scoville (1979)	12.0	Radiative transfer analysis of inner Galaxy clouds.
Solomon, Scoville and Sanders (1979)	7.2	non-LTE analysis of inner Galaxy clouds.
Blitz and Thaddeus (1980)	7.8	Comparison of extinction in Rosette Nebula with ^{13}CO emission.
Blitz and Shu (1980)	3.6	Comparison of dark cloud extinctions with ^{13}CO emission.
Young and Scoville (1982)	8.0	Comparison of Wco with N_{H_2} derived from extinction (dark clouds) and LTE analysis (GMC cores).
List (1982)	10.0	Comparison of Wco with N_{H_2} for Ophiucus and mean cloud parameters.
Lebrun et al. (1983)	2.0-6.0	Gamma-ray analysis of 1st Galactic quadrant $|b| < 5.5°$.
Sanders, Scoville and Solomon (1984)	9.2	Virial theorem analysis of inner Galaxy clouds.
Sanders, Solomon and Scoville (1984a)	7.2	Comparison of dark cloud extinction with ^{13}CO emission.
Bloemen et al. (1984b).	5.2	Gamma-ray analysis of Orion region.
Bhat et al. (1984b)	2.3	Galaxy count analysis towards nearby clouds.
This work	$3.7^{\pm}0.6$	Gamma-ray analysis of Orion clouds.

TABLE A.3

Summary of previously adopted conversion factors $\alpha_{20} = 2N_{H_2} / \int Tdv / 10^{20}$ at $cm^{-2} (K\,kms^{-1})^{-1}$ and their derivation.

TABLES A.4, A.5

The parameters of the two radio source samples. The weak radio sources (Table A.4) are those for which 10^{-10} ph cm^{-2}s$^{-1} \lesssim F_\gamma$, expected (> 100 MeV) $<$ 10^{-8} ph cm^{-2}s^{-1}. The strong radio sources are those for which F_γ, expected (> 100 MeV) $\geq 10^{-8}$ ph cm^{-2}s^{-1} (see Section 7.8). Two measures of the synchrotron flux are used : S_ν the flux at 5GHz (1 Jy = 10^{-26} W Hz^{-1} m^{-2}) or the radiated power P (W Hz^{-1}) at 408 MHz. The spectral index α is obtained from the spectral flux $S_\nu \propto \nu^{-\alpha}$ using additional measurements at 178 MHz (Jenkins et al., 1977). The distances are for the optical counterparts (H_o = 50 kms^{-1} Mpc^{-1}, $q_o = \frac{1}{2}$). The minimum energy W_{min} and the gamma-ray luminosity L_γ (> 100 MeV) are derived from the minimum energy requirements for each source (Section 7.4).

Those clusters marked with an asterisk (*) do not meet the requirements for inclusion in Abell's complete statistical sample.

Source	l^{II}, b^{II}	S_ν(5GHz) Jy	log P(408) W Hz^{-1}	α	r(Mpc)	W_{min} erg	L_γ(>100 MeV) ph s^{-1}	$F_\gamma \times 10^{-8}$ phcm^{-2}s^{-1}	Comments
3C123	170.6, −11.7	6.6		1.0	2000	6.2×10^{60}	3.9×10^{48}	0.81	20^m galaxy
3C236	190.1, 54.0	1.48		0.6	550	2.4×10^{59}	1.5×10^{47}	0.41	DE4 galaxy
3C295	97.5, 60.8	3.6		0.9	2070	3.8×10^{60}	2.4×10^{48}	0.46	21^m galaxy
3C346	35.3, 35.8	1.28		0.6	580	2.5×10^{59}	1.6×10^{47}	0.39	16^m galaxy
3C388	74.7, 20.2	0.79		1.0	520	4.2×10^{59}	2.6×10^{47}	0.81	15^m D3 galaxy
3C293	54.6, 76.1	1.7		0.6	260	1.1×10^{59}	6.9×10^{46}	0.84	14.5^m galaxy
3C273	289.9, 64.4		26.55	0.45	733	2.9×10^{59}	1.8×10^{47}	0.28	quasar
3C218	242.9, 25.1		26.14	0.82	349	2.0×10^{59}	1.3×10^{47}	0.85	CD2 galaxy in cluster A780 (Hydra A)
4C10. 35A	317.8, 72.8		26.07	0.69	690	1.6×10^{59}	1.0×10^{47}	0.18	A1684
4C10. 43.1A	17.1, 48.1		26.02	0.65	774	1.5×10^{59}	9.4×10^{46}	0.13	A2091
4C12.76	70.1, −31.8		26.39	1.1	774	3.8×10^{59}	2.4×10^{47}	0.33	A2396[*]
4C13. 17A	164.2, −38.9		25.17	0.64	340	4.9×10^{58}	3.1×10^{46}	0.22	A401
4C15. 39E	258.6, 73.8		26.06	0.7	690	1.6×10^{59}	1.0×10^{47}	0.18	A1462
4C15.53	28.8, 44.5		24.80	0.44	203	2.9×10^{58}	1.8×10^{46}	0.36	A2147
4C17.66	29.9, 44.0		24.87	0.60	182	3.2×10^{58}	2.0×10^{46}	0.51	A2151
4C17.89	76.1, −34.6		25.64	1.90	512	4.4×10^{59}	2.8×10^{47}	0.87	A2433[*]
4C18. 41F	24.7, 56.6		25.43	0.73	410	7.3×10^{58}	4.6×10^{46}	0.23	A2036[*]
4C21. 13	169.6, −24.6		26.13	0.49	747	1.7×10^{59}	1.1×10^{47}	0.16	A468[*]

Source	l^{II}, b^{II}	S_ν(5GHz) Jy	log P(408) W Hz^{-1}	α	r(Mpc)	W_{min} erg	L_γ(>100 MeV) ph s^{-1}	$F_\gamma \times 10^{-8}$ ph cm^{-2}s^{-1}	Comments
4C21.44A	28.9, 60.2		25.68	1.4	690	2.3×10^{59}	1.4×10^{47}	0.25	A2009
4C25.36	216.2, 75.6		24.11	0.75	512	1.3×10^{58}	8.1×10^{45}	0.03	A1380
4C26.35A	213.5, 78.1		26.37	0.66	690	2.4×10^{59}	1.5×10^{47}	0.26	A1425
4C26.42	33.8, 77.2		25.69	0.7	340	1.0×10^{59}	6.3×10^{46}	0.45	A1795
4C27.50	99.7, −31.3		26.20	0.35	590	1.8×10^{59}	1.1×10^{47}	0.27	A2584*
4C27.53A	102.8, −32.4		24.80	1.1	328	4.7×10^{58}	2.9×19^{46}	0.23	A2622*
4C29.41B	201.5, 69.0		25.55	0.56	266	7.8×10^{58}	4.9×10^{46}	0.52	A1213
4C32.52A	54.8, 36.6		24.98	0.75	340	4.1×10^{58}	2.6×10^{46}	0.18	A2241*
4C34.45	57.6, 35.0		25.36	0.75	420	6.8×10^{58}	4.3×10^{46}	0.20	A2249*
4C35.06A	150.6, −19.9		25.13	0.84	258	5.4×10^{58}	3.4×10^{46}	0.42	A407*
4C35.16A	182.2, 18.3		25.31	1.05	310	8.7×10^{58}	5.4×10^{46}	0.47	A568*
4C37.48	60.8, 41.8		26.43	0.8	804	2.9×10^{59}	1.8×10^{47}	0.23	A2214*
4C38.29B	67.2, 67.5		25.83	2.0	690	6.5×10^{59}	4.1×10^{47}	0.71	A1914
4C39.29	182.6, 55.9		25.15	0.75	690	5.1×10^{58}	3.2×10^{46}	0.06	
4C39.49.1	64.0, 35.6		25.56	0.95	335	1.1×10^{59}	6.9×10^{46}	0.53	A2250
4C41.23	217.7, −40.7		25.80	0.75	387	1.2×10^{59}	7.5×10^{46}	0.42	A490
4C41.24	136.0, 75.5		26.27	0.75	774	2.2×10^{59}	1.4×10^{47}	0.19	A1562
4C41.26	92.6, 73.5		26.68	0.75	1604	3.8×10^{59}	2.4×10^{47}	0.08	A1763
4C46.23	153.3, 66.6		26.33	0.75	750	2.4×10^{47}	1.5×10^{47}	0.22	A1361
4C50.33	147.6, 64.1		25.48	0.75	747	7.9×10^{58}	4.9×10^{46}	0.07	
4C51.29.1	139.8, 63.8		25.47	0.74	340	7.7×10^{58}	4.8×10^{46}	0.35	A1452*
4C57.37B	82.0, 40.8		25.88	0.69	549	1.3×10^{59}	8.1×10^{46}	0.22	A2220*
4C55.29A	96.1, 56.2		25.97	0.76	633	1.5×10^{59}	9.4×10^{46}	0.24	A1940
4C58.23C	135.3, 57.9		26.61	0.82	633	3.7×10^{59}	2.3×10^{47}	0.48	A1446

Source	l^{II}, b^{II}	S_ν(5GHz) Jy	log P(408) W Hz^{-1}	α	r(Mpc)	W_{min} erg	L_γ(>100 MeV) ph s^{-1}	$F_\gamma \times 10^{-8}$ ph cm^{-2}s^{-1}	Comments
4C64.20.1A	94.0, 34.9		25.12	1.1	295	7.2×10^{58}	4.5×10^{46}	0.43	A2255
4C66.07A	149.4, 33.0		25.98	1.1	660	2.2×10^{59}	1.4×10^{47}	0.27	A629
4C67.21D	125.7, 49.9		26.36	0.87	690	2.8×10^{59}	1.8×10^{47}	0.31	A1559
4C68.21	99.2, 28.0		26.03	0.57	633	1.5×10^{59}	9.4×10^{46}	0.19	
4C69.10	145.5, 26.1		24.53	0.75	451	2.3×10^{58}	1.4×10^{46}	0.06	A564*
4C74.20.1	109.9, 38.7		24.79	0.75	690	3.2×10^{58}	2.0×10^{46}	0.04	A2105

Source	l^{II}, b^{II}	S_s(5GHz) Jy	log P(408) W Hz^{-1}	α	r(Mpc)	W_{min} erg	L_γ(>100 MeV) ph s^{-1}	$F_\gamma \times 10^{-8}$ phcm^{-2}s^{-1}	Comments
3C305	103.2, 49.1	0.57		1.0	240	1.3×10^{59}	8.1×10^{46}	1.2	peculiar galaxy
3C433	74.5, -17.7	3.9		0.8	570	6.5×10^{59}	4.1×10^{47}	1.0	
3C430	99.7, 8.0	0.38		1.3	320	3.3×10^{59}	2.1×10^{47}	1.7	15^m elliptical galaxy
3C31	126.8, -30.3	0.14		1.4	100	7.2×10^{58}	4.5×10^{46}	3.7	NGC 383 DE3 galaxy
3C98	179.9, -31.1	2.9		0.8	180	1.6×10^{59}	1.0×10^{47}	2.5	ED3 galaxy
3C264	235.7, 73.0	0.4		1.3	120	1.0×10^{59}	6.3×10^{46}	3.7	NGC 3862 DE1 galaxy in A1367 (Coma)
3C272.1	278.2, 74.5	0.35		1.2	17	8.5×10^{57}	5.3×10^{45}	15.0	M84 E2 galaxy in Virgo
3C449	95.5, -15.9	0.05		1.6	110	7.7×10^{58}	4.8×10^{46}	3.3	
3C111	161.7, -8.8	3.3		0.9	290	3.2×10^{59}	2.0×10^{47}	2.0	19^m N galaxy
3C405.0	76.2, 5.8		27.62	0.77	316	1.3×10^{60}	8.1×10^{47}	7.0	Cygnus A
3C384	63.4, 18.0		26.39	1.0	398	3.4×10^{59}	2.1×10^{47}	1.1	Hercules A
4C12.76	74.1, -34.4		25.77	2.21	747	1.2×10^{60}	7.5×10^{47}	1.1	
4C26.64	103.5, -33.1		25.90	0.74	171	1.4×10^{59}	8.8×10^{46}	2.4	
4C39.45	62.9, 43.7		25.93	1.34	177	2.9×10^{59}	1.8×10^{47}	4.8	
4C41.07	150.4, -13.4		25.58	0.71	100	8.7×10^{58}	5.4×10^{46}	4.6	

TABLE A.6

The parameters of the Abell cluster sample used in the present analysis (l^{II}, b^{II}) are the Galactic coordinates of the cluster centres. The distance and richness classes are defined by Abell (1958) (see Table 7.2).

TABLE A6

Abell No.	l^{II} b^{II}	Distance class	Richness class
21	114.8, −34.7	4	1
260	137.2, −29.0	4	1
399	164.6, −40.5	3	1
400	170.2, −45.9	1	1
415	194.2, −59.9	4	1
426	150.4, −14.4	0	2
449	133.7, 16.2	4	1
496	209.6, −37.5	3	1
526	194.3, −22.8	4	1
539	195.7, −18.7	2	1
574	219.4, −37.0	3	2
592	210.2, 15.6	3	1
754	239.3, 24.8	3	2
787	137.9, 36.2	4	2
957	243.0, 42.9	4	1
978	250.0, 40.4	3	1
1020	232.7, 52.3	4	1
1035	179.4, 58.5	3	2
1126	227.5, 61.0	4	1
1185	203.0, 67.8	2	1
1187	175.6, 65.9	3	1
1213	201.5, 69.0	2	1
1216	263.8, 51.1	4	1
1228	186.9, 69.4	1	1
1238	260.0, 56.4	4	1
1254	132.4, 44.5	3	1
1364	270.8, 56.8	4	1
1365	194.5, 74.9	4	1
1367	234.8, 73.0	1	2
1377	140.6, 59.1	3	1
1382	129.9, 44.8	4	1
1399	274.9, 56.4	4	2
1436	136.9, 59.5	3	1
1468	139.5, 64.2	4	1
1474	261.0, 74.2	4	1
1496	131.9, 57.2	4	1

Abell No.	l^{II} b^{II}		Distance class	Richness class
1541	284.6,	70.9	4	1
1644	304.9,	45.3	4	1
1651	306.7,	58.6	4	1
1656	58.2,	88.0	1	2
1691	105.2,	77.2	3	1
1749	88.0,	76.8	4	1
1767	112.5,	57.0	4	1
1773	331.1,	62.3	3	1
1775	31.9,	78.7	4	2
1793	59.1,	76.6	4	1
1795	33.8,	77.2	4	2
1809	339.5,	63.6	4	1
1831	40.1,	75.0	3	1
1837	329.3,	48.1	4	1
1904	89.7,	62.3	3	2
1913	12.5,	65.6	4	1
1927	34.9,	67.7	4	1
1983	19.0,	60.1	3	1
1991	22.8,	60.5	3	1
1999	91.9,	54.8	4	1
2005	41.8,	61.8	4	2
2022	43.3,	60.7	3	1
2028	8.4,	51.9	4	1
2029	5.5,	50.6	4	2
2063	12.9,	49.7	3	1
2065	42.9,	56.6	3	2
2067	48.7,	56.8	4	1
2089	43.9,	54.4	4	1
2092	49.4,	54.6	4	1
2107	34.4,	51.5	4	1
2124	57.7,	52.3	3	1
2142	44.2,	48.7	4	1
2147	28.8,	44.5	1	1
2175	49.3,	44.4	4	1
2197	64.8,	43.8	1	1
2199	61.9	43.7	1	2
2255	94.0,	34.9	3	2
2256	111.1,	31.7	3	2
2312	99.0,	24.9	4	1

Abell No.	l^{II} b^{II}	Distance class	Richness class
2315	100.8, 25.6	4	1
2319	75.7, 13.6	3	1
2328	28.8, −34.6	4	2
2382	38.9, −47.9	4	1
2384	33.5, −49.4	4	1
2399	67.4, −35.3	3	1
2410	48.0, −47.6	4	1
2634	103.5, −34.1	1	1

REFERENCES

Abell, G.O., 1958, Astrophys. J. Suppl., 3, 211.

Abrampoulous, F., and Ku, W.H.M., 1983, Astrophys. J., 271, 446.

Allen, C.W., 1973, "Astrophysical Quantities", Athlone Press.

Arnaud, K., Li, T.P., Riley, P.A., Wolfendale, A.W., Dame T., Brock, J.E., and Thaddeus, P., 1982, Mon. Not. R. astr. Soc., 201, 745.

Austen, T.B., and Peach, J.V., 1974, Mon. Not. R. astr. Soc., 168, 591.

Ayre, C.A., Bhat, P.N., Owens, A., Summers, W.M., and Thompson, M.G., 1981, Phil. Trans. R. Soc. Lond., A301, 687.

Bachall, N.A., and Soneira, R.M., 1983, Astrophys. J., 270, 20.

Bartla, N.A., Wilson, T.L., Bastein, P., and Ruf, K., 1983, Astron. Astrophys., 128, 279.

Beck, R., and Grave, R., 1982, Astron. Astrophys., 105, 192.

Beckwith, S., Persson, S.E., and Neugebauer, G., Astrophys. J., 1979, 227, 436.

Beckwith, S., Evans, N.J., Gatley, I., Gull, G., and Russel, R.W., 1983, Astrophys. J., 264, 152.

Berger, M., Gehrz, R.D., and Hackwell, J.A., 1981, Astrophys. J., 248, 963.

Bertsch, D.L., and Kniffen, D.A., 1983, Astrophys. J., 270, 305.

Bhat, P.N., Gupta, S.K., Ramana Murthy, P.V., Sreekantan, B.V., Tonwar, S.C., and Viswanath, P.R., 1980a, Astron. Astrophys., 81, L3.

Bhat, C.L., Sparu, M., and Kaul, C., 1980b, Nature, 288, 136.

Bhat, C.L., Mayer, C.J., and Wolfendale, A.W., 1984a, Astron. Astrophys. (in the press).

Bhat, C.L., Issa, M.R., Houston, B.P., Mayer, C.J., and Wolfendale, A.W., 1984b, Nature (submitted).

Bhat, C.L., et al., 1984c (in preparation).

Bhat, C.L., Sapru, M.L., and Razdan, H., 1984d (in preparation).

Bignami, G,F., Fichtel, C.E., Kniffen, D.A., and Thompson, D.J., 1975, Astrophys. J., 199, 54.

Bignami, G.F., Bennett, K., Buccheri, R., Caraveo, P.A., Hermsen, W., Kanbach, G., Lichti, G.G., Masnou, J.L., Mayer-Hasselwander, H.A., Paul, J.A., Sacco, B., Scarsi, L., Swannenburg, B.N., and Wills, R.D., 1981, Astron. Astrophys., 93, 71.

Bignami, G.F., and Hermsen, W., 1983, Ann. Rev. Astron. Astrophys., 211, 67.

Bignami, G.F., Caraveo, P.A., and Lamb, R.C., 1983, Astrophys. J., 272, L13.

Bignami, G.F., 1984 (preprint).

Bignami, G.F., Caraveo, P.A., and Paul, J.A., 1984, Nature, 310, 464.

Blaauw, A., 1964, Ann. Rev. Astron. Astrophys., 2, 213.

Black, J.H., and Fazio, G.G., 1973, Astrophys. J., 185, L7.

Blitz, L., 1978, Ph.D. Thesis, Columbia University.

Blitz, L., and Shu, F.H., 1980, Astrophys. J., 238, 148.

Blitz, L., and Thaddeus, P., 1980, Astrophys. J., 241, 676.

Bloemen, J.B.G.M., Blitz, L., and Hermsen. W., 1984a, Astrophys. J., 279 , 136.

Bloemen, J.B.G.M., et al., 1984b, Astron. Astrophys. (submitted).

Bloemen, J.B.G.M., Caraveo, P.A., Hermsen, W., Lebrun, F., Maddalena, R.J., Strong, A.W., and Thaddeus, P., 1984c, Astron. Astrophys., 139, 37.

Bohlin, R.C., Savage, B.D., and Drake, J.F., 1978, Astrophys. J., 224, 132.

Bothe, W., and Kolhorster, W., 1929, Zeitschrift fur Physik, 56, 751.

Buccheri, R., Bennett, K., Bignami, G.F., Bloemen, J.B.G.M., Caraveo, P.A., Hermsen, W., Kanbach, G., Masnou, J.L., Mayer-Hasselwander, H.A., Ozel, M.E., Paul, J.A., Sacco, B., Scarsi, L., Strong, A.W., Boriakoff, V., and Manchester, R.N., 1983, Astron. Astrophys., 128, 245.

Buffington, A., Schindler, S.M., and Pennypacker, C.R., 1981, Astrophys. J., 248, 1179.

Caraveo, P.A., and Paul, J.A., 1979, Astron. Astrophys., 75, 340.

Caraveo, P.A., Bennett, K., Bignami, G.F., Hermsen, W., Kanbach, G., Lebrun, F., Masnou, J.L., Mayer-Hasselwander, H.A., Paul, J.A., Sacco, B., Scarsi, L., Strong, A.W., Swannenburg, B.N., and Wills, R.D., 1980, Astron. Astrophys., 91, L3.

Caraveo, P.A., Bignami, G.F., Vigroux, L., and Paul, J.A., 1984, Astrophys. J., 276, L45.

Cesarsky, C.J., and Volk, H.J., 1978, Astron. Astrophys., 70, 367.

Cesarsky, C.J., and Lagage, P.O., 1983, Astron. Astrophys., 125, 249.

Cline, T.L., and Desai, U.D., 1976, Astrophys. Space Sci., 42, 117.

Cohen, R.S., and Thaddeus, P., 1977, Astrophys. J., 217, L155.

Cohen, R.S., Tomasevitch, G.R., and Thaddeus, P., 1979, IAU Symp. 84, "The Large Scale Structure of the Galaxy", ed. W.B. Burton, Dordrecht : Reidel, p.53.

Cohen, R.S., Cong, H., Dame, T.M., and Thaddeus, P., 1980, Astrophys. J., 239, L59.

Colgate, S.A., 1968, Can. J. Phys., 46, 5476.

Dame, T.M., 1984, Ph.D. Thesis, Columbia University.

Danaher, S., Fegan,, D.J., Porter, N.A., and Weekes, T.C., 1981, Nature, 289, 568.

Dean, A.J., and Ramsden, D., 1981, Phil. Trans. R. Soc. Lond., A301, 577.

Dennison, B., 1980, Astrophys. J., 239 , L93.

Dewey, R.J., Uson, J.M., Weisberg, J.M., Wilkinson, D.T., and Stark, A.A., 1983, Astron. J., 88, 1832.

Dickey, J.M., 1983, Astrophys. J., 273, L71.

Dickman, R.L., 1978, Astrophys. J. Suppl., 37, 407.

Dodds, D., Strong, A.W., and Wolfendale, A.W., 1975, Mon. Not. R. astr. Soc., 171, 569.

Dogiel, V.A., Kiraly, P., Freedman, I., and Wolfendale, A.W., 1983, Proc. 18th ICRC, Bangalore, 2, 292.

Dowthwaite, J.C., Gibson, A.I., Harrison, A.B., Kirkman, I.W., Lotts, A.P., Macrae, J.H., Orford, K.J., Turver, K.E., and Walmsley, M., 1983, Astron. Astrophys., 126, 1.

Dowthwaite, J.C., Harrison, A.B., Kirkman, I.W., Macrae, J.H., Orford, K.J., Turver, K.E., and Walmsley, M., 1984, Astron. Astrophys., 136, L14.

Erikson, R.A., Fickle, R.K., and Lamb, R.C., 1976, Astrophys. J., 210, 539.

Felten, J.E., and Morrison, P., 1963, Phys. Rev. Lett., 10, 453.

Fichtel, C.E., Hartman, R.C., Kniffen, D.A., Thompson, D.J., and Bignami, G.F., 1975, Astrophys. J., 198, 163.

Fichtel, C.E., Kniffen, D.A., Thompson, D.J., Bignami, G.F., and Cheung, C.Y., 1976, Astrophys. J., 208, 211.

Fichtel, C.E., Hartman, R.C., Kniffen, D.A., and Thompson, D.J., 1977, Astrophys. J., 217, L9.

Fichtel, C.E., Simpson, G.A., and Thompson, D.J., 1978a, Astrophys. J., 222, 833.

Fichtel, C.E., Hartman, R.C., Kniffen, D.A., Thompson, D.J., Ogelman, H.B., Tumer, T., and Ozel, M.E., 1978b, NASA Tech. Memo. 79650.

Fichtel, C.E., and Kniffen, D.A., 1984, Astron. Astrophys., 134, 13.

Fomalont, E.B., and Rogstad, D.H., 1966, Astrophys. J., 146, 528.

Galper, A.M., Kirillov-Ugryumov, V.G., Kurochkin, A.V., Leikov, P.V., Luchkov, B.I., Yurkin, Uy. L., Fomin, V.P., Nespor, Yu. I., Stepanian, A.A., and Vladimirsky, B.M., 1977, Proc. 15th ICRC, Plovdiv, 1, 131.

Ginzburg, V.L., 1968, Astrophys. Space Sci., 1, 1.

Ginzburg, V.L., and Syrovatskii, S.I., 1964, "The Origin of Cosmic Rays", Pergamon Press.

Gordon, C.P., 1970, A.J., 75, 914.

Gordon, M.A., and Burton, W.B., 1976, Astrophys. J., 208, 346.

Grindlay, J.E., Helmken, H.F., Hanbury-Brown, R., Davis, J., and Allen, L.R., 1975, Astrophys. J., 201, 82.

Grindlay, J.E., Helmken, H.F., and Weekes, T.C., 1976, Astrophys. J., 209, 592.

Gursky, H., and Schwartz, D.A., 1977, Ann. Rev. Astron. Astrophys., 15, 541.

Gursky, H., Solinger, A., Kellog, E., Murray, S., Tananbaum,H., Giacconi, R., and Cavaliere, A., 1972, Astrophys. J., 173, L99.

Harding, A.K., 1981, Astrophys. J., 247, 639.

Hartman, R.C., Kniffen, D.A., Thompson, D.J., Fichtel, C.E., Ogelman, H.B., Tumer, T., and Ozel, M.E., 1979, Astrophys. J., 230, 597.

Haslam, C.G.T., Kearsey, S., Osborne, J.L., Phillips, S., and Stoffel, H., 1981, Nature, 289, 470.

Hawley, S.A., 1978, Astrophys. J., 224, 417.

Hayakawa, S., 1952, Prog. Theor. Phys., 8, 571.

Heiles, C., and Habing, H.J., 1974, Astron. Astrophys. Suppl., 14, 1.

Helmken, H.F., Fazio, G.G., O'Mongain, E., and Weekes, T.C., 1973, Astrophys. J., 184, 245.

Hermsen, W., 1980, Ph.D. Thesis, University of Leiden.

Hermsen, W., 1983, Space Sci. Rev., 36, 61.

Hess, V.F., 1912, Physk. Zeitchr., 13, 1804.

Houston, B.P., and Wolfendale, A.W., 1984a, J. Phys. G., 10, 1587.

Houston, B.P., and Wolfendale, A.W., 1984b, J. Phys. G. (in the press).

Hubble, E.P., 1933, Mt. W. Contr., 21, 139.

Hurley, K., 1983, Adv. Space Res., 3, 163.

Hutchinson, G.E., 1952, Phil. Mag., 43, 847.

Issa, M.R., and Wolfendale, A.W., 1981a, J. Phys. G., 7, L187.

Issa, M.R., and Wolfendale, A.W., 1981b, Nature, 292, 430.

Issa, M.R., Riley, P.A., Strong, A.W., and Wolfendale, A.W., 1981, J. Phys. G., 7, 973.

Jenkins, C.J., Pooley, G.C., and Riley, J.M., 1977, Mem. R. astr. Soc., 84, 61.

Jennings, M.C., 1982, Astrophys. J., 258, 110.

Johnson, W.N., and Hames, R.C., 1973, Astrophys. J., 250, 389.

Jones, C., and Forman, W., 1984, Astrophys. J., 276, 38.

Kellog, E.M., 1973, IAU Symp. 55, "X- and Gamma Ray Astronomy", eds. Bradt, H., and Giacconi, R., Dordrecht : Reidel, p.

Kinzer, R.L., Share, G.H., and Seeman, N., 1974, J. Geophys. Res., 79, 4567.

Kiraly, P., Szabelski, J., Wdowczyk, J., and Wolfendale, A.W., 1981, Nature, 293, 120.

Klebsadel, R., Evans, W.D., Larcos, J.G., Strong, I.B., Cline, T.L., Desai, U.D., Teegarden, B.J., Barat, C., Hurley, K., Niel, M., Vedrenne, G., Esttulin, I.V., Kuznetsov, A.V., and Zenchenko, V.M., 1982, Astrophys. J., 259, L51.

Kniffen, D.A., Hartman, R.C., Thompson, D.J., Bignami, G.F., Fichtel, C.E., Ogelman, H., and Tumer, T., 1974, Nature, 251, 397.

Kniffen, D.A., Fichtel, C.E., and Thompson, D.J., 1977, Astrophys. J., 215, 765.

Kodaira, K., 1974, Publ. Astron. Soc. Japan, 26, 255.

Kowalski, M.P., 1982, Ph.D. Thesis, Northwestern University.

Kraushaar, W.L., Clark,e G.E., Garmire, G.P., Helmken, H., Higbie, P., and Agogino, M., 1965, Astrophys. J., 141, 845.

Kraushaar, W.L., Clarke, G.E., Garmire, G.P., Borken, R., Higbie, P., Leong, V., and Thorsos, T., 1972, Astrophys. J., 177, 341.

Kutner, M., Tucker, K.D., Chin, G., and Thaddeus, P., 1977, Astrophys. J., 215, 521.

Kutner, M., and Mead, K., 1981, Astrophys. J., 249, L15.

Lamb, R.C., Fichtel, C.E., Hartman, R.C., Kniffen, D.A., and Thompson, D.J., 1977, Astrophys. J., 212, L63.

Lamb, R.C., 1978, Nature, 272, 429.

Lamb, R.C., Godfrey, C.P., Wheaton, W.A., and Tumer, T., 1982, Nature, 296, 543.

Lebrun, F., and Paul, J.A., 1980 (preprint).

Lebrun, F., Bignami, G.F., Buccheri, R., Caraveo, P.A., Hermsen, W., Kanbach, G., Mayer-Hasselwander, H.A., Paul, J.A., Strong, A.W., and Wills, R.D., 1982, Astron. Astrophys., 107, 390.

Lebrun, F., Bennett, K., Bignami, G.F., Bloemen, J.B.G.M., Buccheri, R., Caraveo, P.A., Gottwald, M., Hermsen, W., Kanbach, G., Mayer-Hasselwander, H.A., Montmerle, T., Paul, J.A., Sacco, B., Strong, A.W., Wills, R.D., Dame, T., Cohen, R.S., and Thaddeus, P., 1983, Astrophys. J., 274, 231.

Lebrun, F., and Paul, J.A., 1983, Astrophys. J., 266, 276.

Lebrun, F., and Huang, Y.L., 1984, Astrophys. J., 281, 634.

Leventhal, M., MacCallum, C.J., and Watts, A., 1977, Astrophys. J., 216, 491.

Leventhal, M., MacCallum, C.J., and Stang, P.D., 1978, Astrophys. J., 225, L19.

Li, T.P., and Wolfendale, A.W., 1981, Astron. Astrophys., 103, 19.

Li, T.P., Riley, P.A., and Wolfendale, A.W., 1982, J. Phys. G., 8, 1141.

Li, T.P., and Wolfendale, A.W., 1982, Astron. Astrophys., 116, 95.

Li, T.P., Riley, P.A., and Wolfendale, A.W., 1983, Mon. Not. R. astr. Soc., 203, 87.

Lilley, A.E., 1955, Astrophys. J., 121, 559.

Ling, J.C., Mahoney, W.A., Willett, J.B., and Jacobson, A.S., 1979, Astrophys. J., 231, 896.

List, H.S., Xiang, D., and Burton, W.B., 1981, Astrophys. J., 249, 532.

List, H.S., 1982, Astrophys. J., 262, 198.

Lloyd-Evans, J., Coy, R.M., Lambert, A., Lapikens, J., Patel, M., Reid, R.J.O., and Watson, A.A., 1983, Nature, 305, 784.

Longair, M.S., 1981, "High Energy Astrophysics", Cambridge University Press.

Loren, R.B., 1979, Astrophys. J., 234, L207.

Matteson, J.L., 1982, AIP Proc. No. 83, "The Galactic Centre", eds. G.R. Riegler, and R.D. Blandford, p.109.

Mayer-Hasselwander, H.A., Bennett, K., Bignami, G.F., Buccheri, R., D'Amico, N., Hermsen, W., Kanbach, G., Lebrun, F., Lichti, G.G., Masnou, J.L., Paul, J.A., Pinkau, K., Scarsi, L., Swannenburg, B.N., Wills, R.D., 1980, Ann. N.Y. Acad. Sci., 336, 211.

Mayer-Hasselwander, H.A., Bennett, K., Bignami, G.F., Buccheri, R., D'Amico, N., Hermsen, W., Kanbach, G., Lebrun, F., Lichti, G.G., Masnou, J.L., Paul, J.A., Pinkau, K., Scarsi, S., Swannenburg, B.N., and Wills, R.D., 1982, Astron. Astrophys., 105, 164.

Meegan, C.A., and Fishman, G.J., 1979, Astrophys. J., 234, L123.

Menon, T.K., 1958, Astrophys. J., 127, 28.

McHardy, I., 1978, Mon. Not. R. astr. Soc., 184, 783.

McHardy, I., 1979, Mon. Not. R. astr. Soc., 188, 495.

Millikan, R.A., and Cameron, G.H., 1926, Phys. Rev., 27, 645.

Montmerle, T., 1979, Astrophys. J., 231, 95.

Morello, C., and Navarra, G., 1983, Proc. 18th ICRC, Bangalore, 1, 127.

Morfill, G.E., 1982a, Mon. Not. R. astr. Soc., 198, 583.

Morfill, G.E., 1982b, Astrophys. J., 262, 749.

Morrison, P., 1958, Nuovo Cim., 7, 858.

Mukanov, J.B., and Fishman, G.J., 1979, Astrophys. J., 234, L123.

Murdoch, H.S., Crawford, D.F., and Jauncey, D.L., 1973, Astrophys. J., 183, 1.

Murray, S.S., 1981, "X-ray Astronomy with the Einstein Satellite", ed. R. Giacconi, p.281.

Omnes, R., 1969, Phys. Rev. Lett., 23, 38.

Pagel, B.E.J., and Edmunds, M.G., 1981, Ann. Rev. Astron. Astrophys., 19, 77.

Paul, J.A., Bennett, K., Bignami, G.F., Buccheri, R., Caraveo, P.A., Hermsen, W., Kanbach, G., Mayer-Hasselwander, H.A., Scarsi, L., Swannenburg, B.N., and Wills, R.D., 1978, Astron. Astrophys., 63, L31.

Peimbert, M., 1982, Ann. N.Y. Acad. Sci., 395, 24.

Pollock, A.M.T., Bignami, G.F., Hermsen, W., Kanbach, G., Lichti, G.G., Masnou, J.L., Swannenburg, B.N., and Wills, R.D., 1981,. Astron. Astrophys., 94, 116.

Pooley, G.G., and Henbest, S.N., 1984, Mon. Not. R. astr. Soc., 169, 477.

Protheroe, R.J., 1983, "Composition and Origin of Cosmic Rays", ed. M.M. Shapiro, Dordrecht:Reidel, p.351

Protheroe, R.J., Clay, R.W., and Gerhardy, P.R., 1984, Astrophys. J., 280, L47.

Puget, J.L., and Stecker, F.W., 1974, Astrophys. J., 191, 323.

Puget, J.L., Ryter, C., Serra, G., and Bignami, G.F., 1976, Astron. Astrophys., 50, 247.

Ramaty, R., and Lingenfelter, R.E., 1981, Phil. Trans. R. Soc. Lond., A301, 671.

Rana, N.C., Sadzinska, M., Wdowczyk, J., and Wolfendale, A.W., 1984, Astron. Astrophys. (in the press).

Riegler, G.R., Ling, J.C., Mahoney, W.A., Wheaton, W.A., Willett, J.B., Jacobson, A.S., and Prince, T.A., 1981, Astrophys. J., 248, L13.

Riley, J.M., 1975, Mon. Not. R. astr. Soc., 170, 53.

Riley, J.M., and Pooley, G.G., 1975, Mon. Not. R. astr. Soc., 180, 105.

Riley, P.A., Wolfendale, A.W., Chun-xian, Xu., Manchester, R.N., Robinson, B.J., and Whiteoak, J.B., 1984, Mon. Not. R. astr. Soc., 206, 423.

Riley, P.A., and Wolfendale, A.W., 1984, J. Phys. G., 10, 1149.

Robinson, B.J., McCutcheon, W.H., and Whiteoak, J.B., 1982, Internat. J. Infrared Millimetre Waves, 3, 63.

Said, S.S., Wolfendale, A.W., Giler, M., and Wdowczyk, J., 1982, J. Phys. G., 8, 383.

Samorski, M., and Stamm, W., 1983a, Astrophys. J., 268, L17.

Samorski, M., and Stamm, W., 1984b, Proc. 18th ICRC, Bangalore, 1, 135.

Sanders, D.B., 1981, Ph.D. Thesis, State University of New York at Stonybrook.

Sanders, D.B., Solomon, P.M., and Scoville, N.Z., 1984a, Astrophys. J., 276, 182.

Sanders, D.B., Scoville, N.Z., and Solomon, P.M., 1984b, Astrophys. J. (in the press).

Sastry, Ch.V., and Shevgaonkar, R.K., 1983, J. Astrophys. Astr., 4, 47.

Savage, B.D., Bohlin, R.C., Drake, J.F., and Budich, W., 1977, Astrophys. J., 216, 291.

Savage, B.D., and Mathis, J.S., 1979, Ann. Rev. Astron. Astrophys., 17, 73.

Schonfelder, V., Grasser, U., and Penninsfeld, F.P., 1980, Astrophys. J., 240, 350.

Scoville, N.Z., and Solomon, P.M., 1975, Astrophys. J., 199, L105.

Serlemitsos, P.J., Smith, B.W., Boldt, E.A., Holt, S.S., and Swank, J.H., 1977, Astrophys. J., 211, L63.

Shane, D.C., and Wirtanen, C.A., 1967, Publs. Lick Obs., 22, 1.

Share, G.H., Kinzer, R.L., and Seeman, N., 1974, Astrophys. J., 187, 511.

Silk, J., 1973, Ann. Rev. Astron. Astrophys., 11, 269.

Skilling, J., and Strong, A.W., 1976, Astron. Astrophys., 53, 253.

Solomon, P.M., Sanders, D.B., and Scoville, N.Z., 1979, IAU Symp. 84, "The Large Scale Structure of the Galaxy", ed. W.B. Burton, Dordrecht:Reidel, p.35.

Solomon, P.M., Scoville, N.Z., and Sanders, D.B., 1979, Astrophys. J., 232, L89.

Solomon, P.M., Stark, A.A., and Sanders, D.B., 1983, Astrophys. J., 267, L29.

Soltan, A., and Henry, J.P., 1983, Astrophys. J., 271, 442.

Stecker, F.W., 1969, Astrophys. J., 157, 507.

Stecker, F.W., 1975, "Origin of Cosmic Rays", eds. J.L. Osborne and A.W. Wolfendale, Dordrecht:Reidel, p.267.

Stecker, F.W., 1983, IAU Symp. 104, "Early Evolution of the Universe and Its Present Structure", eds. G.O. Abell and G. Chincarini, Dordrecht:Reidel, p.437.

Stecker, F.W., and Wolfendale, A.W., 1984, Nature, 309, 37.

Strickman, M.S., Kurfess, J.D., and Johnson, W.N., 1982, Astrophys. J., 253, L23.

Strong, A.W., and Worrall, D.M., 1976, J. Phys., A9, 823.

Strong, A.W., and Wolfendale, A.W., 1981, Phil. Trans. R. Soc. Lond., A301, 541.

Strong, A.W., Bignami, G.F., Bloemen, J.B.G.M., Buccheri, R., Caraveo, P.A., Hermsen, W., Kanbach, G., Lebrun, F., Mayer-Hasselwander, H.A., Paul, J.A., and Wills, R.D., 1982, Astron. Astrophys., 115, 404.

Strong, A.W., and Lebrun, F., 1982, Astron. Astrophys., 105, 159.

Strong, A.W., and Bignami, G.F., 1983, Astrophys. J., 274, 549.

Strong, A.W., 1984, Astron. Astrophys. (in the press).

Sturrock, P.A., and Baker, K.B., 1979, Astrophys. J., 234, 612.

Swannenburg, B.N., Bennett, K., Bignami, G.F., Buccheri, R., Caraveo, P.A., Hermsen, W., Kanbach, G., Lichti, G.G., Masnou, J.L., Mayer-Hasselwander, H.A., Paul, J.A., Sacco, B., Scarsi, L., and Wills, R.D., 1981, Astron. Astrophys., 243, L69.

Talent, D.L., and Dufor, R.J., 1979, Astrophys. J., 233, 888.

Thaddeus, P., 1982, Ann. N.Y. Acad. Sci., 895, 9.

Thompson, D.J., Fichtel, C.E., Kniffen, D.A., and Ogelman, H.B., 1975, Astrophys. J., 200, L79.

Thompson, D.J., and Fichtel, C.E., 1982, Astron. Astrophys., 109, 352.

Thompson, D.J., Bertsch, D.L., Hartman, R.C., and Hunter, S.D., 1983, Astron. Astrophys., 127, 220.

Trombka, J.I., Dyer, C.S., Evans, L.G., Bielefeld, M.J., Seltzer, S.M., and Metzger, A.E., 1977, Astrophys. J., 212, 925.

Tucker, K.D., Kutner, M., and Thaddeus, P., 1973, Astrophys. J., 186, L13.

Valtaoja, E., 1984, Astron. Astrophys., 135, 141.

van den Bergh, S., 1961, Astrophys. J., 134, 970.

van den Hulst, H.C., Muller, C.A., and Oort, J.H., 1954, B.A.N., 12, 117.

Verter, F., 1981, Phys. Rep., 81, 293.

Vladimirsky, B.M., Stepanian, A.A., and Fomin, V.P., 1973, Proc. 13th ICRC, Denver, 1, 456.

Wdowczyk, J., and Wolfendale, A.W., 1983, Nature, 305, 609.

Wdowczyk, J., and Wolfendale, A.W., 1984, J. Phys. G., 10, 1453.

Weaver, H., and Williams, D.R.W., 1973, Astrophys. J., 236, 448.

Weekes, T.C., and Helmken, H.F., 1977, Proc. 12th ESLAB Symp., Frascati, Italy (ESA SP-124, p.39).

Wolfendale, A.W., 1981, IAU SYmp. 94, "Origin of Cosmic Rays", eds. G. Setti, G. Spada, and A.W. Wolfendale, Dordrecht:Reidel, p.309.

Worrall, D.M., 1977, Ph.D. Thesis, University of Durham.

Worrall, D.M.,, and Strong, A.W., 1977, Astron. Astrophys., 57, 229.

Yoshimori, M., Watanake, H., Okudeira, K., Hirasima, Y., and Murakami, H., 1979, Aust. J. Phys., 32, 375.

Young, J.S., and Scoville, N.Z., 1982, Astrophys. J., 258, 467.

ACKNOWLEDGEMENTS